

NORTHWESTERN UNIVERSITY

The Glass Transition and Physical Aging Behavior of Polymer Nanocomposites

Studied via Fluorescence

A DISSERTATION

SUBMITTED TO THE GRADUATE SCHOOL

IN PARTIAL FULFILLMENT OF THE REQUIREMENTS

for the degree

DOCTOR OF PHILOSOPHY

Field of Chemical Engineering

By

Perla Rittigstein

EVANSTON, ILLINOIS

June 2008

ABSTRACT

The Glass Transition and Physical Aging Behavior of Polymer Nanocomposites Studied via Fluorescence

Perla Rittigstein

The average and local glass transition temperatures (T_g s) and physical aging behavior of various confined polymers were studied in order to gain an understanding of these surface/interface effects and their propagation into the polymer. Using a novel multilayer/fluorescence method, the T_g s of layers at the free surface, substrate-polymer interface, and at known distances away from the interfaces of poly(methyl methacrylate) (PMMA) films supported on silica were measured. Since attractive hydrogen-bonding interactions are present, it was shown that perturbations to T_g can propagate over length scales of several hundred nanometers and overwhelm the free surface effect, thereby leading to an increase in the average T_g across the film.

The effect of the addition of silica or alumina nanospheres to polystyrene, PMMA and poly(2-vinyl pyridine) (P2VP) on T_g was investigated using fluorescence. The results showed that the T_g and physical aging of polymer nanocomposites can be controlled by tuning the polymer-nanofiller interactions via choice of polymer, nanofiller, and the preparation procedure. The nanocomposite T_g may be either enhanced or depressed relative to bulk, depending on the presence of wetted interfaces with attractive interactions or free surfaces between the polymer and the nanofiller. In

addition, model PMMA- and P2VP-silica nanocomposites consisting of polymer films confined between silica slides were designed in order to provide a simple way to gain insight into the effect of interparticle spacing on T_g . The model and real nanocomposites with identical T_g deviations yield similar dramatic suppressions of physical aging. This study has also resulted in the first determination of the distribution of T_g s within polymer nanocomposites. Different functionalized single-wall carbon nanotubes (SWCNTs) were grafted to PMMA in order to identify their effect on the local and average T_g s of the system. The results indicate a relationship between the length and flexibility of the side groups in the SWCNT and the extent of the increase on T_g . Even more important from a technological standpoint is that the incorporation of nanofillers in the polymer dramatically suppresses the physical aging behavior of the matrix. This provides a new application for nanofillers creating glassy-state polymer nanocomposites with long-term stable properties.

Acknowledgments

I would like to acknowledge the many people that in different ways helped me during my time in graduate school. I will start by thanking my advisor, John M. Torkelson for his time, dedication guidance, support and enthusiasm. I enjoyed his advising style, as it stimulates individual thinking while still providing helpful and frequent advice. I would also like to thank the rest of my committee, Linda J. Broadbelt, Wesley R. Burghardt and L. Catherine Brinson, for their time and for the valuable feedback provided. In addition, it was a pleasure to work with Ramanathan Thillaiyan and Catherine Brinson in the Mechanical Engineering Department, as well as with Jun-Hyun Kim and SonBinh T. Nguyen in the Chemistry Department.

I would like to thank the members of the Torkelson research group. I appreciate the helpful discussions with Chris Ellison, Ross Behling, Rodney Priestley, Manish Mundra, Connie Roth, Sheldon Hewlett, Soyong Kim, Philip Brunner and Moustafa Kharaouta. Special thanks as well to Jungki Kim, Amanda Walker, Michelle Mok, Chris Wong, Cynthia Pierre, Robert Sandoval, Kat Wakabayashi, Ying Tao, Laura Dykes, Maisha Gray, Jun'ichi Masuda and Harley. Thank you for your advices and laughter over the years.

My time at Northwestern was made much more pleasant by the great friends we have found here. Alberto López, Catalina Curet-Arana, Lissette Ruberté, Stan Rendón, Monica Canalizo, Stephen Smith, Luis Mier y Terán, Genya Takeda, Hamsell Alvarez,

Jimena Sandoval, thanks for your friendship and all the good times shared. I am also very grateful to Jim and Jill Pfaendtner for their exceptional friendship.

I am very thankful to my parents Leo y Beatriz and my sister Jenny, for their support, love, encouragement and constant motivation, even from far away during all these years. I also thank my in-laws Miguel y Blanca and Angel y Ester Albo, and the rest of my family for being a great source of encouragement.

Finally, I want to dedicate this work to my husband Simon, your love, support and dedication are infinite. No tengo palabras para agradecerte por tu inmenso e incondicional amor, apoyo, cariño y ayuda, sin ti esto nunca hubiera sido posible.

Table of contents

ABSTRACT	2
Acknowledgments	4
Table of contents.....	6
List of tables	11
List of figures.....	12
1 Introduction	22
2 Physics of the Glass Transition for Amorphous Polymers.....	29
2.1 Glass Transition Behavior of Bulk Amorphous Polymers.....	29
2.2 The Alpha Relaxation Dynamics	31
2.3 The Kauzmann Paradox	36
2.4 Models of the Glass Transition.....	37
2.4.1 Gibbs-DiMarzio Theory	37
2.4.2 Free Volume Theory	38
2.4.3 Adam-Gibbs Theory.....	39
2.5 Dynamic Heterogeneity.....	41
2.6 Physical Aging of Bulk Amorphous Polymers	42
3 Confinement Effect on the Physical Properties of Amorphous Polymers.....	47

3.1	The Effect of Confinement on the Glass Transition Temperature of Amorphous Polymers	48
3.1.1	T_g in Supported Polymer Films	49
3.1.2	T_g in Freely Standing/Unsupported Polymer Films	55
3.1.3	T_g in Polymer Nanocomposites.....	57
3.2	Discussion of the Effect of Confinement on T_g	62
3.2.1	Origin of Deviations from Bulk T_g in Confined Polymers	62
3.2.2	Models and Hypotheses Explaining T_g -nanoconfinement Effects.....	67
3.3	Confinement Effect on the Physical Aging Behavior of Amorphous Polymers	70
3.3.1	Physical Aging Behavior in Supported Polymer Films	70
3.3.2	Physical Aging Behavior in Freely Standing/Unsupported Polymer Films	72
3.3.3	Physical Aging Behavior in Polymer Nanocomposites.....	73
3.4	Other Polymer Properties Impacted by Confinement.....	75
4	Novel Fluorescence Technique as a Characterization Tool.....	76
4.1	Phenomenon of Fluorescence	76
4.2	Polymer Characterization by Fluorescence	80
4.2.1	Fluorescence Technique for Characterizing T_g	80
4.2.2	Fluorescence Technique for Characterizing Physical Aging.....	83
4.2.3	Fluorescence Technique for Characterizing Local Polarity.....	85
5	Distribution of T_gs in Thin and Ultrathin PMMA films.....	92
5.1	Introduction	92
5.2	Experimental.....	95

5.3	Results and Discussion.....	98
5.4	Conclusions	114
6	Model Polymer Nanocomposites Provide Understanding of Confinement Effects in Real Nanocomposites	116
6.1	Introduction	116
6.2	Experimental	120
6.3	Results and Discussion.....	122
6.4	Conclusions	132
7	Polymer-Nanoparticle Interfacial Interactions in Polymer Nanocomposites: Confinement Effects on Glass Transition Temperature and Suppression of Physical Aging	134
7.1	Introduction	134
7.2	Experimental	138
7.3	Glass Transition Effects in Polymer Nanocomposites.....	141
7.4	Physical Aging Effects in Polymer Nanocomposites	151
7.5	Conclusions	157
8	Suppression of Physical Aging in Polymer Nanocomposites with Attractive Polymer-Nanofiller Interactions	159
8.1	Introduction	159
8.2	Experimental	165
8.3	Results and Discussion.....	167

8.4	Conclusions	180
-----	-------------------	-----

9 Controlling the Average and Local Glass Transition Temperatures of PMMA-SWCNT Nanocomposites 181

9.1	Introduction	181
-----	--------------------	-----

9.2	Experimental	185
-----	--------------------	-----

9.3	Results and Discussion.....	188
-----	-----------------------------	-----

9.4	Conclusions	202
-----	-------------------	-----

10 Dramatic Reduction of Physical Aging Behavior of PMMA-SWCNT Nanocomposites Studied by Fluorescence 204

10.1	Introduction	204
------	--------------------	-----

10.2	Experimental	208
------	--------------------	-----

10.3	Results and Discussion.....	211
------	-----------------------------	-----

10.4	Conclusions	218
------	-------------------	-----

11 Long-Term Reduction of Enthalpy Relaxation of PMMA-SWCNT Nanocomposites Studied by DSC..... 220

11.1	Introduction	220
------	--------------------	-----

11.2	Experimental	223
------	--------------------	-----

11.3	Results and Discussion.....	225
------	-----------------------------	-----

11.4	Conclusions	230
------	-------------------	-----

12 Conclusions and Recommendations..... 231

12.1	Conclusions	231
------	-------------------	-----

	10
12.2 Recommendations for Future Work	237
References	245

List of tables

Table 9-1: Polymer nanocomposite systems studied.	191
--	-----

List of figures

- Figure 2-1: Temperature dependence of specific volume or specific enthalpy for a general amorphous polymer. The vertical lines denote the glass transition temperatures determined using a fast cooling rate (T_g^1) and a slow cooling rate (T_g^2)..... 30
- Figure 2-2: The temperature dependence of the average α -relaxation time ($\langle \tau \rangle$) for a typical amorphous polymer. The arrows and lines show that for the same deviation in temperature around T_g , huge differences in relaxation dynamics are seen in the rubbery and the glassy states. The fragility index (m) is defined as the slope of the WLF curve at T_g , which is depicted as the dotted line. 34
- Figure 2-3: Physical aging of an amorphous polymer. With time there is a reduction in specific volume during physical aging. 44
- Figure 4-1: Simplified Jablonski diagram. The processes that lead to a photon being emitted as fluorescence include absorbance of a photon that promotes an electron to an excited singlet vibrational state, internal energy conversion and fluorescence emission. 77
- Figure 4-2: Fluorescence emission spectra of pyrene dopant (< 0.2wt%) in a bulk PS film at 418K (bold curve) and in a thick 0.5 vol% silica-PS nanocomposite film at 418K (thin curve). Data have been normalized to unity using the intensity at 374 nm. Inset shows the molecular structure of pyrene..... 89
- Figure 4-3: Temperature dependence of the intensity ratio of pyrene dopant (< 0.2wt%) in PS films and nanocomposites : a) bulk PS (squares), 0.3 vol% silica-PS

nanocomposite (circles), and 0.5 vol% silica-PS nanocomposite (triangles). (All sample thicknesses exceed 1000 nm.) b) 500-nm-thick PS film (open squares) and a 24-nm-thick PS film (closed squares). (Note: Different emission slits were used to take data in Figure 4-3a and Figure 4-3b, which prevents comparison of absolute ratio values between figures.)..... 90

Figure 5-1: T_g data from bulk PMMA and PMMA confined films determined via fluorescence. a) Temperature dependence of the normalized integrated fluorescence intensity of 250-nm-thick (open squares) and 50-nm-thick (open circles) pyrene-labeled PMMA films. The solid lines are fits of the data in both the rubbery and glassy states, with the intersections of the lines defining T_g . (Insets: Emission spectra of pyrene at 423 K (solid line) and 358 K (dotted line) of the 250-nm-thick film and the molecular structure of pyrene.) b) Temperature dependence of the normalized integrated fluorescence intensity of 200-nm-thick (open squares) and 35-nm-thick (open circles) TC1-labeled PMMA films. The solid lines are fits of the data in both the rubbery and glassy states, with the intersection of the lines defining T_g . (Insets: Emission spectra of TC1 at 423 K (solid line) and 358 K (dotted line) of the 200-nm-thick film and the molecular structure of TC1.)..... 99

Figure 5-2: $T_g(\text{film}) - T_g(\text{bulk})$ of pyrene-labeled PMMA (open square) and TC1-labeled PMMA (open circles) single layer films as a function of film thickness (d). Within experimental error, both chromophores detect identical increases in T_g as a function of film thickness. (Inset: Film geometry used in experiments.)..... 102

Figure 5-3: Measurement of substrate- and free-surface layer T_g values using bilayer films in which one layer is labeled with either pyrene (open squares) or TC1 (open circles). a) $T_g(\text{substrate layer}) - T_g(\text{bulk})$ of labeled substrate layer film as a function of the labeled substrate layer film thickness (h). Film thickness of bulk overlayer film is 240 nm. (Inset: Film geometry used in experiments.) b) $T_g(\text{free surface}) - T_g(\text{bulk})$ of label free-surface layer film as a function of free-surface layer film thickness (h).

Thickness of bulk underlayer is 240 nm. Pyrene-labeled PS data (open triangles) are from Ellison and Torkelson (2003). (Inset: Film geometry used in experiments.)..... 104

Figure 5-4: Determination of the distribution of T_g s as a function of depth displaced from either the free surface or substrate-polymer interface using trilayer films in which the middle layer is labeled with either pyrene or TC1. Labeled middle layer is 12-nm-thick, while bulk overlayer/ underlayer film thickness is 240 nm. Free surface/ substrate layer film thickness (h) is varied in trilayer film studies..... 107

Figure 5-5: $T_g(\text{free surface}) - T_g(\text{bulk})$ of pyrene-labeled (open square) or TC1-labeled (open circles) free surface layer as a function of overall film thickness (h'). The labeled-free surface layer thickness is held constant at 12 nm while the underlayer thickness is varied. 109

Figure 5-6: Influence of overall film thickness on $T_g(\text{substrate layer}) - T_g(\text{bulk})$ of a 12-nm-thick substrate layer within a bilayer film. The overall film thickness is (a) 250-260 nm, (b) 50-60 nm and (c) 35-40 nm..... 111

Figure 6-1: T_g data from bulk polymer and polymer nanocomposites determined via fluorescence. a) Temperature dependence of the normalized fluorescence integrated

intensity of BPD dopant (< 0.2 wt%) in a bulk PMMA film (open squares) and in 0.4 vol% silica-PMMA nanocomposite film (open circles). Inset: The molecular structure of BPD. (The data have been normalized to 1 relative to the intensity at $T_{g,bulk}$ and arbitrarily shifted vertically.) b) Deviations from $T_{g,bulk}$ as a function of silica nanofiller content in three polymer nanocomposites: P2VP (open squares), PMMA (open circles) and PS (open triangles). The error bars ($\pm 1K$) represent the inherent error due to the fitting of the data required to obtain T_g 124

Figure 6-2: Representative TEM micrograph of 0.4 vol% silica-PS nanocomposite. (The film thickness is ~ 50 nm.) 125

Figure 6-3: Deviations of T_g from $T_{g,bulk}$ of ultrathin films supported on silica and 'model' nanocomposites. a) Thickness dependence of the T_g deviation of P2VP supported films (open circles: data from van Zanten et al. (1996); filled circles: data from Park et al. (2004)) and pyrene-doped P2VP 'model' nanocomposites (open squares). (In the case of the P2VP supported films, the error bars are from van Zanten et al. (1996) and Park et al. (2004), and in the case of the P2VP 'model' nanocomposites, the error ($\pm 1K$) in the data is due to the fitting required to obtain T_g and is smaller than the symbol size.) b) Thickness dependence of the T_g deviation of TC1-labelled PMMA supported films (open circles) and 'model' nanocomposites (open squares). The error bars ($\pm 1K$) represent the inherent error due to the fitting of the data required to obtain T_g 127

Figure 6-4: Interlayer spacing (film thickness) in 'model' nanocomposites that yield the same T_g deviation as 0.4 vol% silica-PMMA and silica-P2VP nanocomposites. T_g deviations of P2VP 'model' nanocomposites (open squares) and PMMA 'model'

nanocomposites (open circles). Right and Left: Transmission electron microscopy images of 0.4 vol% silica-P2VP (right) and 0.4 vol% silica-PMMA (left) nanocomposites (scale bars = 100 nm). The error bars (± 1 K) represent the inherent error due to the fitting of the data required to obtain T_g 130

Figure 6-5: Physical aging of bulk polymer and polymer nanocomposites monitored by fluorescence. Normalized fluorescence intensity of TCJ dopant (<0.2 wt%) as a function of logarithmic physical aging time after a quench from above T_g (413 K) to below T_g (303 K): bulk P2VP film (open squares), 0.4 vol% silica-P2VP nanocomposite (open circles), and 300-nm-thick P2VP 'model' nanocomposite (open triangles). The physical aging rates are related to the slopes of the data sets..... 131

Figure 7-1: Fluorescence emission spectra of pyrene dopant (< 0.2 wt%) in a bulk P2VP film taken at temperatures of 333 and 418 K..... 142

Figure 7-2: Temperature dependence of the normalized integrated intensity of pyrene dopant (< 0.2 wt%) in a bulk P2VP film and in a 4 vol% alumina/P2VP nanocomposite film. (The integrated intensity has been normalized to one at T_g)..... 143

Figure 7-3: Deviations in T_g from neat, bulk polymer T_g as a function of alumina nanofiller content in three polymer nanocomposites: P2VP (closed squares), PS (closed triangles), PMMA (closed circles). (Error bars represent the inherent error due to the line fitting required to obtain T_g , which are similar to the obtained variation in T_g (± 1 K or less) from sample to sample.) 145

Figure 7-4: Representative TEM micrographs of 4 vol% alumina-polymer nanocomposites: a) PS, b) PMMA, c) P2VP. (The film thickness in the three samples is ~70 nm.).....	148
Figure 7-5: Deviations in T_g from neat, bulk PMMA T_g as a function of silica nanofiller content and solvent used to make solutions employed in spin coating the nanocomposite films: methyl ethyl ketone (closed circles), acetic acid (open squares). (Inherent errors associated with the measurements are equal to or smaller than the symbol size.)	150
Figure 7-6: Fluorescence emission spectrum of a TCJ-doped (< 0.2 wt %) bulk P2VP film at two physical aging times after quenching from 140 °C to 30 °C. Inset: Molecular structure of TCJ.....	152
Figure 7-7: Normalized fluorescence intensity of TCJ dopant (< 0.2 wt %) as a function of logarithmic physical aging time after quenching from above T_g (140 °C) to below T_g (30 °C): bulk P2VP film (squares), 0.4 vol % silica/P2VP nanocomposite (circles), 4 vol % alumina/P2VP nanocomposite (triangles). (Lines represent best fits to the physical aging data. Note: y represents normalized intensity, and Log(t) represents logarithmic aging time.)	154
Figure 8-1: a) Fluorescence emission spectrum of a TCJ-doped (< 0.2 wt%) bulk PMMA film at two physical aging times after quenching from above $T_{g,bulk}$ to $T_{g,bulk} - 86$ K. Inset: molecular structure of TCJ. b) Fluorescence emission spectrum of a bulk TC1-labeled PMMA film at two physical aging times after quenching from above $T_{g,bulk}$ to $T_{g,bulk} - 88$ K. Inset: molecular structure of TC1-labeled methacrylate monomer.	168

- Figure 8-2: a) Normalized fluorescence intensity of TCJ dopant (< 0.2 wt%) as a function of logarithmic physical aging time after quenching from above $T_{g,bulk}$ to 305 K: PMMA ($T_g - 86$ K) (squares), 4 vol% alumina-PMMA nanocomposite ($T_g - 83$ K) (triangles) and 0.4 vol% silica-PMMA nanocomposite (MEK) ($T_g - 91$ K) (circles). b) Normalized fluorescence intensity of TCJ dopant (< 0.2 wt%) as a function of logarithmic physical aging after quenching from above $T_{g,bulk}$ (413 K) to 358 K: PMMA ($T_g - 33$ K) (squares), 4 vol% alumina-PMMA nanocomposite ($T_g - 30$ K) (triangles) and 0.4 vol% silica-PMMA nanocomposite (MEK) ($T_g - 38$ K) (circles)..... 170
- Figure 8-3: Fluorescence aging rate, r_f , as a function of physical aging temperature for: PMMA (squares), PMMA 4 vol% alumina (triangles) and PMMA 0.4 vol% silica (MEK) (circles). (Fluorescence aging rate is calculated over a physical aging time scale from 10 to 480 min. TCJ-doped PMMA was used in all systems.) 172
- Figure 8-4: Normalized fluorescence intensity of TCJ dopant (< 0.2 wt%) as a function of logarithmic physical aging time after quenching from above $T_{g,bulk}$ to: 333 K: PS (open triangles) and 0.4 vol% silica-PS nanocomposite (closed triangles), 363 K: PS (open squares), 0.4 vol% silica-PS nanocomposite (closed squares) and 4 vol% alumina-PS nanocomposite (gray squares), 303 K: PS (open circles) and 0.4 vol% silica-PS nanocomposite (closed circles). 174
- Figure 8-5: a) Normalized fluorescence intensity of TC1-label as a function of logarithmic physical aging after quenching from above $T_{g,bulk}$ to 305 K: PMMA ($T_g - 86$ K) (squares), 0.4 vol% silica-PMMA nanocomposite (MEK) ($T_g - 91$ K) (open circles) and 0.4 vol% silica-PMMA nanocomposite (AA) ($T_g - 71$ K) (closed circles). b)

Normalized fluorescence intensity of TC1-label as a function of logarithmic physical aging after quenching from above $T_{g,bulk}$ to 363 K: PMMA ($T_g - 28$ K) (squares), 0.4 vol% silica-PMMA nanocomposite (MEK) ($T_g - 33$ K) (open circles) and 0.4 vol% silica-PMMA nanocomposite (AA) ($T_g - 13$ K) (closed circles).	176
Figure 8-6: Fluorescence aging rate, r_f , as a function of physical aging temperature for: PMMA (squares), PMMA 0.4 vol% silica (MEK) (open circles) and PMMA 0.4 vol% silica (AA) (closed circles). (Fluorescence aging rate is calculated over a physical aging time scale from 10 to 420 min. TC1-labeled PMMA was used in all systems.)	178
Figure 9-1: PMMA-SWCNT structures. SWCNTs functionalized with different side groups: A) $(CH_2)_{12}$, B) phenyl, and C) $(CH_2)_2$	190
Figure 9-2: Temperature dependence of fluorescence emission spectra: a) TC1 label in System B1 taken at temperatures of 366 K and 456 K and b) BPD dopant in System B1 taken at temperatures of 353 K and 433 K.	192
Figure 9-3: Temperature dependence of normalized fluorescence intensity of a) TC1 label and b) BPD dopant: System A1 (circles), System B1 (square) and System C1 (triangles). (The average intensity peak has been normalized to one at T_g and vertically shifted to aid the reader.)	193
Figure 9-4: T_g as a function of the level of PMMA-SWCNT (1 wt% SWCNT) in blends with neat PMMA and the side group in the functionalized SWCNT (Systems A, B, and C in Table 9-1): average T_g (open squares) and local T_g (closed circles).	197
Figure 9-5: Diagram of the different types of interfaces hypothesized to be present between PMMA and SWCNT.	200

Figure 9-6: T_g as a function of the amount of PMMA-SWCNT (3 wt% SWCNT with $(\text{CH}_2)_2$ as the side group) in blends with PMMA (Systems D1-D5 in Table 9-1): average T_g (open squares) and local T_g (closed circles). 201

Figure 10-1: Schematic of the studied nanocomposites. All nanocomposites have 70 wt% of neat PMMA and 30 wt% of PMMA grafted to functionalized SWCNT. In this 30 wt%, 1 wt% corresponds to the SWCNT and the rest to PMMA. The total weight % of the functionalized SWCNT in the nanocomposites is just 0.3 %. Three types of sides groups were used to functionalize the SWCNT: A) $(\text{CH}_2)_{12}$, B) Phenyl and C) $(\text{CH}_2)_2$. 207

Figure 10-2: Fluorescence emission spectrum of a bulk TC1-labeled PMMA film as a function of physical aging time after a temperature quench from above $T_{g,bulk}$ to $T_{g,bulk} - 88$ K: 10 min (solid line) and 420 min (dashed line). Inset: Molecular structure of TC1-labeled methacrylate monomer. 213

Figure 10-3: a) Normalized fluorescence intensity of TC1 as a function of logarithmic physical aging after quenching from above $T_{g,bulk}$ to 323 K: PMMA ($T_g - 68$ K) (closed squares), system A ($T_g - 71$ K) (open squares), system B ($T_g - 73$ K) (triangles) and system C ($T_g - 76$ K) (circles). b) Normalized fluorescence intensity of TC1 as a function of logarithmic physical aging after quenching from above $T_{g,bulk}$ to 295 K: PMMA ($T_g - 96$ K) (closed squares), system A ($T_g - 99$ K) (open squares), system B ($T_g - 101$ K) (triangles) and system C ($T_g - 104$ K) (circles). 214

Figure 10-4: Fluorescence aging rate, r_f , as a function of physical aging temperature for PMMA (closed squares), system A (open squares), system B (triangles) and system C (circles). (Fluorescence aging rate is calculated over a physical aging time scale from

10 to 420 min and is based on changes occurring with logarithmic aging time. TC1 was used as the fluorescence label in all systems.) 217

Figure 11-1: Enthalpy recovery curves for: a) neat PMMA and b) PMMA-SWCNT nanocomposite as a function of physical aging time at ambient temperature (20-22 °C): 0 h (extra bold line), 48 h (bold line), 17 days (regular line) and 100 days (dashed line).
..... 226

Figure 11-2: Enthalpy recovery as a function of logarithmic physical aging time at environmental temperature for neat PMMA (closed circles) and PMMA-SWCNT nanocomposite (open squares). 229

1 Introduction

Nanotechnology is a field of research at the crossroads of biology, chemistry, physics, engineering, and medicine. It plays a key role in many areas including material processing, mechanical engineering, optics and electronics. However, properties of materials at nanoscale dimensions may deviate from bulk-like behavior. Understanding the mechanism of property changes associated with nanoconfinement is essential for basic science and nanotechnology. Therefore, in the last decade, research focused on studying the properties of materials on the nanoscale has gained significant importance. This interest includes studies of properties of metals, ceramics and polymers at the nanoscale (Quake and Scherer, 2000).

The physical properties of dimensionally constrained polymer systems deviate significantly from those observed in the bulk state. Polymer confined in nanopores, polymer thin films and polymer nanocomposites have different properties than bulk polymer, e.g., the glass transition temperature (T_g) (Forrest and Dalnoki-Veress, 2001; Kawana and Jones, 2001; Ash et al., 2002b; Berriot et al., 2002; Liu et al., 2006), physical aging (Lee and Lichtenhan, 1998; Fukao et al., 2002; Kawana and Jones, 2003; Lu and Nutt, 2003a, 2003b), modulus (Ash et al., 2002a; Van Workum and De Pablo, 2003), compliance (O'Connell and McKenna, 2006; Ganss et al., 2007), crystallization behavior (Frank et al., 1996b; Al-Mulla et al., 2008), and diffusion coefficients (Frank et al., 1996a; Peter et al., 2008). Nanoconfined polymers are systems that open the door to novel applications in numerous areas including chemical sensing (Krasteva et al., 2002; Sarantopoulou et al., 2008), catalysis (Galow et al.,

2002; Esumi et al., 2004; Zampieri et al., 2004), drug delivery (Brigger et al., 2002; Wood et al., 2008), energy devices (Croce et al., 1998; Xi et al., 2005; Olivetti et al., 2006; Yildirim et al., 2008), membranes (Merkel et al., 2002; Song et al., 2007), lithographic patterning (Suh and Lee, 2002; Damean et al., 2005), tissue engineering (Griffith and Naughton, 2002; Shi et al., 2007), molecular electronics (Huang et al., 2001; Wang and Park, 2007), microfluidic devices (Therriault et al., 2003; Zhang et al., 2008), and photonic materials (Lin et al., 1998; Andriesh et al., 2007), among others.

This study of polymer confinement was stimulated by the early work of Jackson and McKenna (1991), who found that low molecular weight glass formers confined to nanopores exhibit reduced T_g s as compared with bulk values. In addition, Keddie et al. (1994b) observed a reduction of T_g relative to bulk values in polystyrene (PS) ultrathin films. Later, Ash et al. (2002b) showed that adding alumina nanospheres to PMMA reduced the T_g of the matrix. Since these influential and seminal studies, several hundred research articles focused on understanding the effect of polymer confinement in different geometries have answered a number of fundamental questions, as well as raised many more new and challenging questions that are still unanswered.

The current fundamental understanding of the property changes associated with polymer nanocomposites is still quite primitive. It has been noted that a better understanding of the properties of polymer nanocomposites may be possible by utilizing new techniques to characterize structure-property relationships (Krishnamoorti and Vaia, 2002). This study will address the consequences of the addition of nanofillers in the polymeric matrix by employing fluorescence spectroscopy, a technique that has

been successfully used to characterize physical properties in other nanoconfined systems (Ellison et al., 2002; Ellison and Torkelson, 2002, 2003; Ellison et al., 2005; Priestley et al., 2005a; Priestley et al., 2005b; Mundra et al., 2006; Mundra et al., 2007a; Mundra et al., 2007b; Roth et al., 2007; Roth and Torkelson, 2007). In the case of the characterization of T_g on thin polymer films, Ellison and Torkelson (2003) provided the first direct evidence of the distribution of T_g s by placing labels that are covalently attached to PS at particular locations in a multilayer film. Utilizing this technique, it is possible to measure directly the influence of interfaces on T_g and quantify how far these effects penetrate away from the interface. Later, Priestley et al. (2005b) employed this fluorescence multilayer method to understand the distribution of physical aging behavior in confined PMMA films. Therefore, fluorescence has an advantage over other techniques employed to measure T_g and physical aging in confined systems.

The research discussed in this dissertation is focused specifically on taking advantage of fluorescence spectroscopy to understand the T_g and physical aging behavior of various polymer nanocomposite systems. In particular, this study has led to a better understanding of how the effects of confinement on T_g and physical aging can be controlled by tuning the polymer-nanofiller interactions via choice of polymer, nanofiller species and content, and preparation procedure. In addition, the characterization of the distribution of T_g s and related relaxation behaviors in grafted polymer on the nanofiller surfaces was studied. This research also addressed poly(methyl methacrylate) (PMMA) multilayer studies using fluorescence labels at specific locations to measure the distribution of T_g s, thus characterizing the impacts of

free surfaces and polymer-substrate interfaces in thin supported films. The current understanding of confinement-induced property changes in thin and ultrathin polymer films was used to obtain a better understanding of confinement in polymer nanocomposites.

A major outcome from this dissertation is the development of model polymer nanocomposites that provides a simple way to gain insight into the effect of interparticle spacing on T_g and to predict the approximate aging response of real nanocomposites (Rittigstein et al., 2007). Another key outcome from this dissertation is the first determination of the distribution of T_g values within polymer nanocomposites through fluorescence. This allows direct characterization of local and average T_g s of the polymer and critical examination of the role of the interface in modifying the T_g of the nanocomposites. This research also provides the first determination of the distributions of T_g s in a polymer thin film with attractive interactions with the substrate.

The next chapter presents an overview of classical bulk polymer physics. Included in chapter 2 are important concepts related to T_g and physical aging, such as the alpha relaxation, dynamic heterogeneity, cooperativity, cooperatively rearranging regions (CRRs) and fragility.

Chapter 3 presents a review of the impact of T_g and physical aging due to confinement of polymers in different geometries including thin films, either substrate supported or freely standing, and polymer nanocomposites. The current understanding of the origins of the effect of nanoconfinement is also discussed.

Chapter 4 describes the phenomenon of fluorescence. It also introduces the use of fluorescence spectroscopy for characterizing T_g , physical aging and local polarity in polymeric bulk and confined systems.

The T_g -nanoconfinement effect of PMMA thin films is addressed in chapter 5. The use of the fluorescence multilayer technique to measure directly the effects of substrates and surfaces on the T_g of confined PMMA films is described. This chapter shows how the distribution of T_g s is highly dependent on the type of interface (free surface or attractive substrate interaction) and the degree of nanoconfinement. The measurements also reveal that the substrate effects on polymer dynamics can, in certain circumstances, be very long range.

Chapter 6 introduces the development of model PMMA and poly (2-vinyl pyridine) (P2VP) nanocomposites. A comparison of the T_g behavior of model nanocomposites with that of real nanocomposites yields a simple determination of an 'effective average' interparticle distance in real nanocomposites, providing a good prediction of the reduction in physical aging in real polymer nanocomposites. This indicates that model nanocomposites can be broadly useful in studying amorphous polymer nanocomposites with wetted interfaces.

Chapter 7 describes the effects on T_g and physical aging of tuning the polymer-nanofiller interactions via choice of polymer, nanofiller, or solvent used in nanocomposite preparation. Here, it is demonstrated that T_g values may be either enhanced or depressed substantially relative to bulk T_g values depending on the interfacial interactions. Physical aging is also studied using fluorescence, and it is

shown that, by making the appropriate choice of nanofiller dispersed in the polymer, it is possible to substantially suppress physical aging in glassy polymer nanocomposites.

The determination of the impact of addition of silica and alumina nanospheres on the physical aging behavior of PMMA and PS is presented on chapter 8. Adding alumina and silica nanospheres to PMMA reduces and even suppresses the initial (8-hr) physical aging response at different temperatures below T_g . In this chapter, it is shown how the extent of the reduction of physical aging of PMMA-silica nanocomposites is affected by the choice of spin coating solvent used to make the polymer nanocomposites. However, no reduction in physical aging rate is observed upon addition of these nanofillers to PS.

Chapter 9 provides the first determination of the distribution of T_g within polymer nanocomposites through fluorescence. In this chapter, the direct characterization of local and average T_g s of PMMA-SWCNT nanocomposites is presented. Also, the role of the interface in modifying the T_g of the nanocomposites is critically examined.

Chapter 10 shows the use of fluorescence spectroscopy to determine the impact of grafting functionalized SWCNT to PMMA on the physical aging behavior of the polymer. Here, it is demonstrated that a small modification in the structure of the functionalized SWCNT may tailor the PMMA-SWCNT interface strength and tune the physical aging behavior of the nanocomposite. On the other hand, chapter 11 explores the long-term structural relaxation of PMMA chains grafted to functionalized SWCNT using DSC. This chapter provides understanding that may contribute to identifying ways to control and even arrest physical aging. The effect of nanofillers in reducing physical aging suggests

a new application for polymer nanocomposites as substitutes for glassy polymers in long-term uses.

Finally, chapter 12 summarizes the results obtained and presents recommendations for future related studies. Each chapter is written to be self-contained. Therefore, each chapter includes an introduction reviewing the related literature, a description of the experimental procedure followed, and the results and conclusions relevant to that chapter.

2 Physics of the Glass Transition for Amorphous Polymers

2.1 Glass Transition Behavior of Bulk Amorphous Polymers

The glass transition temperature (T_g) is the temperature at which the properties of a polymer change from an equilibrium rubbery state to a non-equilibrium glassy state as the material is cooled. Figure 2-1 shows the specific volume or specific enthalpy as a function of temperature for a general amorphous polymer. When the polymer is cooled from temperatures above T_g , the viscosity of the liquid increases and the molecules that comprise it move more slowly. At some temperature the molecules will be moving so slowly that they do not have a chance to rearrange significantly before the temperature is lowered further. Since these rearrangements are necessary for the polymer to find the equilibrium state for that temperature, the experimentally observed properties will deviate from the equilibrium values. This falling out of equilibrium occurs across a narrow transformation range, where the characteristic molecular relaxation time becomes of the order of 10^2 seconds, the shear viscosity reaches 10^{13} poise and the rate of change of volume or enthalpy decreases abruptly (but continuously) compared to the liquid (Debenedetti and Stillinger, 2001). At subsequent cooling, the time scale for molecular rearrangements becomes long compared to the time scale of the experimental observations, resulting in the formation of a non-equilibrium glass. As indicated in Figure 2-1, T_g is identified by the intersection of the temperature dependence of specific volume or specific enthalpy in the glassy and liquid states. Also, Figure 2-1 demonstrates the kinetic nature of T_g that is observed experimentally,

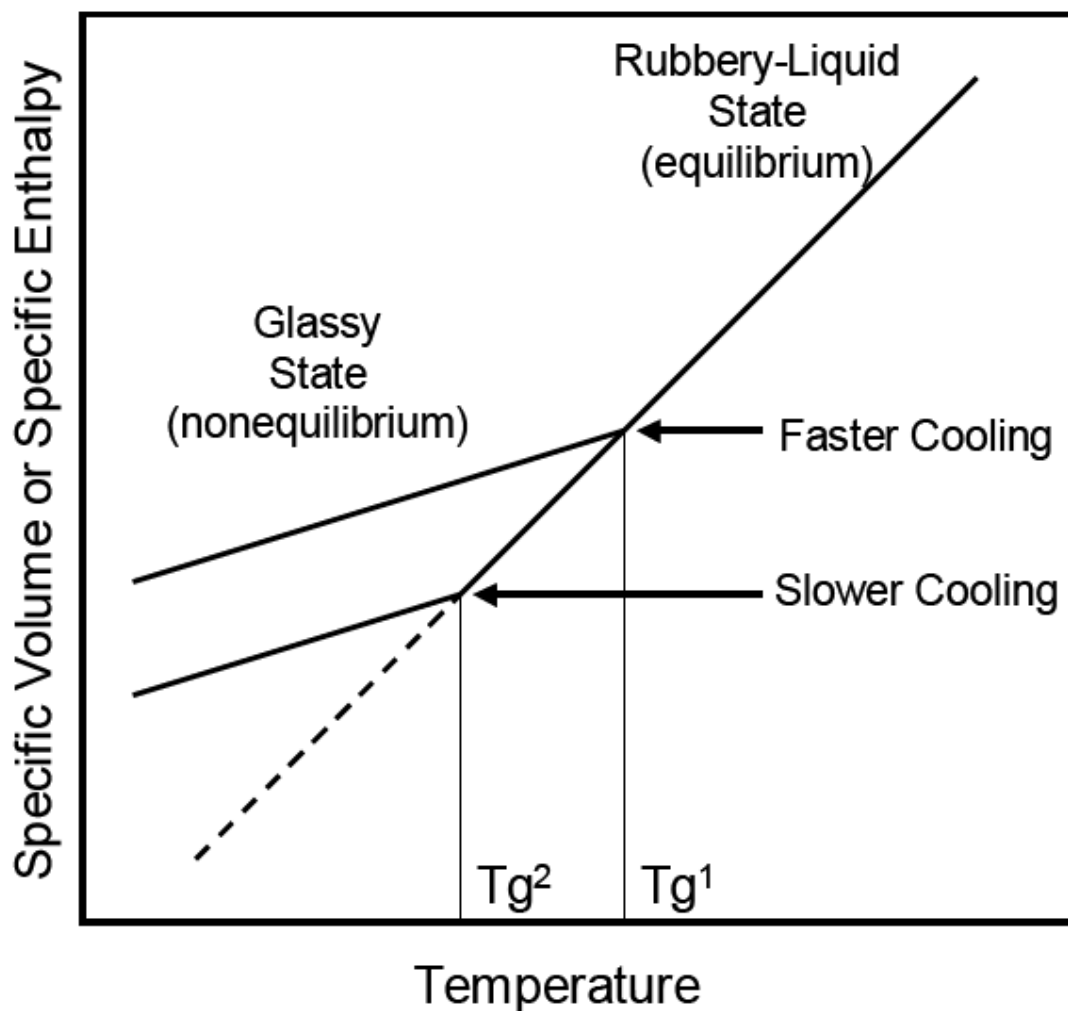


Figure 2-1: Temperature dependence of specific volume or specific enthalpy for a general amorphous polymer. The vertical lines denote the glass transition temperatures determined using a fast cooling rate (T_g^1) and a slow cooling rate (T_g^2).

where a slower cooling rate remaining in equilibrium at lower temperatures, resulting in a lower T_g (T_g^2), while a faster cooling rate results in a higher T_g (T_g^1). Normally, the dependence of T_g upon cooling rate is relatively weak; a change of one order of magnitude in the cooling rate may change T_g by 3-5 K (Ediger et al., 1996). Therefore, the glass transition is not a second-order thermodynamic phase transition; it is rather a kinetic transition and the properties of the glass that is formed depend on how the process was carried out (McKenna, 1989; Debenedetti and Stillinger, 2001; McKenna and Simon, 2002).

2.2 The Alpha Relaxation Dynamics

The alpha relaxation (α -relaxation) is a molecular relaxation process of the cooperative segmental motion of repeat units along the chain backbone. The α -relaxation is the most prominent relaxation process observed in polymers; therefore, it is also called the primary relaxation. Near T_g , the α -relaxation has been associated with the cooperative segmental motion of 30-300 chain segments (Schmidt-Rohr and Spiess, 1991; Sperling, 1992; Hempel et al., 2000; Reinsberg et al., 2001; Merabia et al., 2004). On the other hand, secondary relaxation processes such as beta (β), gamma (γ) and delta (δ) relaxations are related to localized motions of a side group attached to a single repeat unit or to rotational movements of a portion of a side group (Mark et al., 2004). These primary and secondary relaxation processes have also been observed and studied in low molecular weight glass formers (Gotze and Sjogren, 1992).

The α -relaxation is a non-exponential relaxation and is best described by a distribution of relaxation times and a “stretched exponential” relaxation function. This empirical relaxation function ($\varphi(t)$) is known as the Kohlrausch-Williams-Watts (KWW) “stretched exponential” function (Kohlrausch, 1847; Williams and Watts, 1970; Williams et al., 1971):

$$\varphi(t) = \exp\left[-\left(\frac{t}{\tau}\right)^\beta\right] \quad (2-1)$$

where t is time, τ is a characteristic relaxation time, and β is the stretching exponent which varies between 0 and 1 to describe the width of the distribution of the α -relaxation times. It has been shown that at temperatures far above T_g , β approaches 1, indicating almost purely single exponential relaxation and narrow α -relaxation times. Then upon cooling towards T_g , β becomes a decreasing function of temperature. A β value of less than 1 indicates that, as T_g is approached, the relaxation behavior cannot be described in terms of a single exponential relaxation time; instead, the distribution of α -relaxation times is very broad. Dhinojwala et al. (1993; 1994) showed that β remains relatively constant in polymers quenched to temperatures below T_g , having a much weaker dependence in the non-equilibrium glassy state than in the equilibrium liquid state.

Even though the KWW equation is empirical in nature, the form of the equation has been said to be “a consequence of cooperative motion” (Williams and Watts, 1970; Williams et al., 1971). The coupling model shows that below a critical temperature, cooperative motions begin to emerge and predicts the onset of non-exponential

relaxation. This model illustrates how the β value governs the relaxation properties or correlates with them; as a result β is a measure of the extent of cooperative motion of the α -relaxation. Therefore, upon cooling, the cooperative motion increases, and the β value decreases, indicative of a broad distribution of relaxation times (Ngai and Roland, 1993; Ngai, 1998, 2007).

The distribution of relaxation times can be characterized by fitting various parameters in the relaxation function to data taken using different techniques, such as dielectric relaxation spectroscopy (Dixon et al., 1990; McCrum et al., 1991; Stickel et al., 1996), light scattering (Li et al., 1992; Sidebottom et al., 1993), nuclear magnetic resonance (Spiess, 1983), second harmonic generation (Dhinojwala et al., 1993, 1994) and others. The average distribution time $\langle \tau \rangle$ can be determined from the fitting parameters of the KWW function by the following equation:

$$\langle \tau \rangle = \int_0^{\infty} \exp\left[-\left(\frac{t}{\tau}\right)^{\beta}\right] dt = \left(\frac{\tau}{\beta}\right) \Gamma\left(\frac{\tau}{\beta}\right) \quad (2-2)$$

where Γ is the gamma function (Williams and Watts, 1970; Williams et al., 1971).

Figure 2-2 shows the temperature dependence of the average α -relaxation time ($\langle \tau \rangle$). For the same magnitude change in temperature, cooling the polymer from above T_g to T_g in the equilibrium rubbery state results in a change of $\langle \tau \rangle$ by many more orders of magnitude as compared to cooling from T_g in the glassy state. The slope of the curve in Figure 2-2 in the limit when $T \rightarrow T_g$ from elevated temperature is known as the

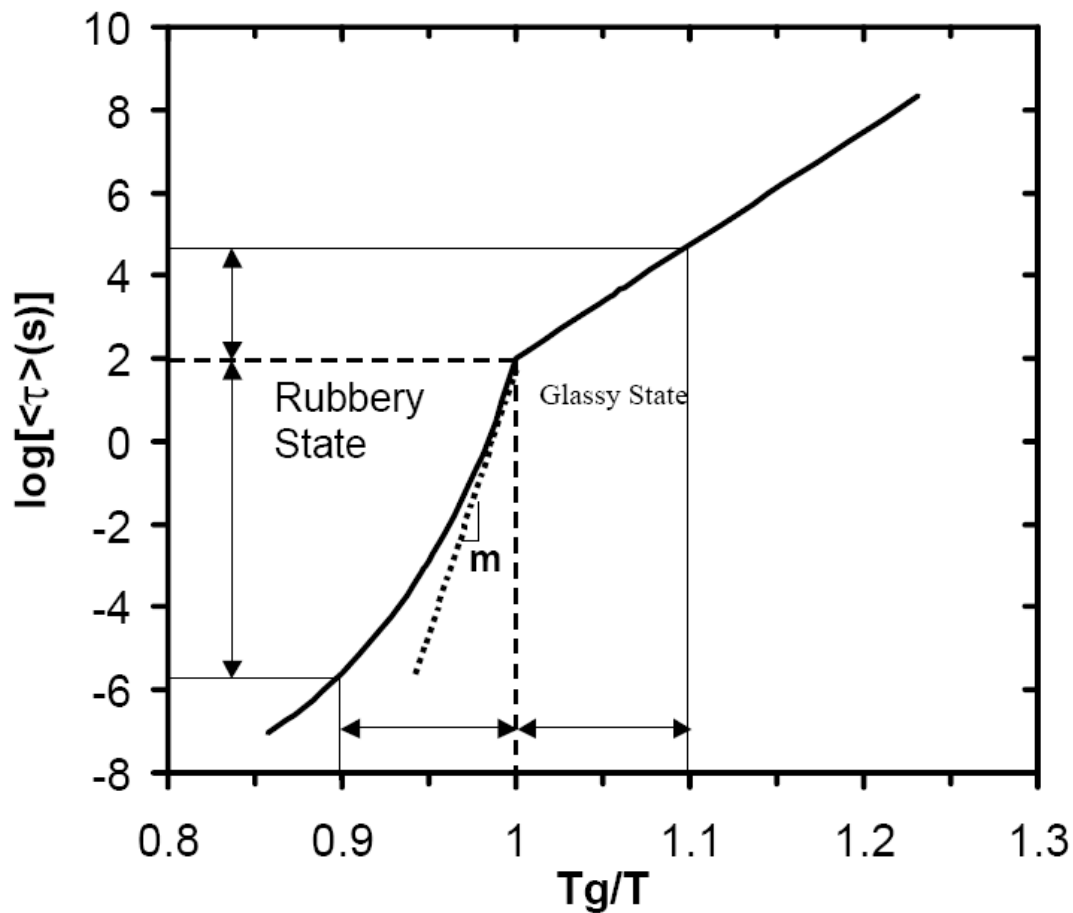


Figure 2-2: The temperature dependence of the average α -relaxation time ($\langle \tau \rangle$) for a typical amorphous polymer. The arrows and lines show that for the same deviation in temperature around T_g , huge differences in relaxation dynamics are seen in the rubbery and the glassy states. The fragility index (m) is defined as the slope of the WLF curve at T_g , which is depicted as the dotted line.

fragility or steepness index (m) (Angell, 1991; Bohmer and Angell, 1993; Bohmer et al., 1993; Angell, 1995a, 1997). The fragility concept is important because it provides a fair comparison of the different systems with widely varying T_g s and temperature dependencies of relaxation dynamics. This classification system includes “fragile” glass formers which have a strong temperature dependence just above T_g (large m) and “strong” glass formers which have a weak temperature dependence (nearly Arrhenius) just above T_g (small m) (Angell, 1991; Bohmer and Angell, 1993; Bohmer et al., 1993; Angell, 1995a, 1997).

The fragility index can be related to the chemical structure of the polymers: compact and symmetrical chains have smaller values of m , while larger m values are associated with polymers presenting more rigid backbones or sterically-hindering pendant groups (Roland and Ngai, 1991; Roland, 1992, 1994). Fragility has also been connected to a variety of other fundamental parameters defining T_g , including the degree of intermolecular cooperativity (Roland and Casalini, 2003) and the β parameter of the KWW expression (Bohmer et al., 1993). A β value close to zero correlates to more cooperative motion and a larger m , both associated with a more fragile glass former.

Below T_g , in the glassy state, the temperature dependence of the average α -relaxation time is best fitted by an Arrhenius expression:

$$\frac{\langle \tau \rangle}{\langle \tau_{T_g} \rangle} = A \exp \left[\frac{E_A}{kT} \right] \quad (2-3)$$

where A is a pre-exponential factor, k is the Boltzman constant and E_A is the apparent activation energy. E_A typically falls in the range of 20-60 kcal/mol for a number of polymeric systems, and it depends on the chain aromaticity and chain rigidity (Solunov, 1999).

On the other hand, above T_g , the dramatic changes in $\langle \tau \rangle$ with temperature can be described by the Williams-Landel-Ferry (WLF) equation (Williams et al., 1955):

$$\text{Log}(a_T) = \text{Log}\left(\frac{\eta_T}{\eta_{T_R}}\right) = \text{Log}\left[\frac{\langle \tau(T) \rangle}{\langle \tau(T_R) \rangle}\right] = \frac{-C_1(T - T_R)}{C_2 + T - T_R} \quad (2-4)$$

where a_T is a shift factor, η is the viscosity, C_1 and C_2 are constants and $\langle \tau(T_R) \rangle$ is the average relaxation time at the reference temperature T_R , often taken to be T_g , in which case $\langle \tau(T_g) \rangle \sim 100$ sec. Near the glass transition, the temperature dependence of viscosity is much stronger than that of density, so a_T is typically expressed as a ratio of viscosities. This equation is valid for temperature ranges of approximately T_g to $T_g + 100$ °C (Ferry, 1980). It has been observed that values of $C_1 = 17.44$ and $C_2 = 51.6$ K approximately predict the temperature dependence of the average distribution of relaxation times of a large number of glass formers; thus, they are called “universal” parameters (Williams et al., 1955; Angell, 1997; Bower, 2002).

2.3 The Kauzmann Paradox

Kauzmann (1948) showed that if the entropy of a liquid is extrapolated to low temperatures, at a point above 0 K, the amorphous, disordered liquid achieves a lower

value of entropy than the crystalline polymer. Furthermore, the entropy of the liquid becomes negative before reaching 0 K, violating the third law of thermodynamics. This is known as the Kauzmann paradox and will be used in the following discussion about the glass transition.

2.4 Models of the Glass Transition

The glass transition of glass-forming materials, including amorphous polymers, has been well characterized but not completely understood. At present no single theory or model exists that can describe all aspects of the glass transition. Theories based on thermodynamic and kinetic arguments will be briefly described in order to discuss this phenomenon.

2.4.1 Gibbs-DiMarzio Theory

Gibbs and DiMarzio (1958) formulated a configurational entropy model where polymer units are placed on a Flory-Huggins (Flory, 1953) lattice along with vacant sites. The internal energy of the system is calculated from the configurational entropy, or the number of ways in which the polymer chains may be arranged on the lattice. As the temperature is lowered, the system densifies, reducing the conformational freedom of the polymer chains. At a temperature (T_2) greater than 0 K, Gibbs and DiMarzio found that the configurational entropy went to zero, thus showing that an amorphous solid could be the lowest energy state of the system, successfully circumventing the Kauzmann paradox. The theory considers the glass transition to be a true thermodynamic transition, suggesting that the experimentally observed T_g would equal

T_2 if it were measured at an infinitely slow rate. This model is able to describe the effects of molecular weight and structure on T_g but does not address the dynamics near the glass transition.

2.4.2 Free Volume Theory

Resolutions of the Kauzmann paradox based on kinetic arguments inevitably invoke the concept of free volume (Cohen and Turnbull, 1959). Free volume (V_f) is defined as the amount of free space in an amorphous polymer arising from inefficient packing of the disordered chain segments in the amorphous regions of the material and is defined as the difference between the actual volume (V) and the theoretical volume (V_0), based on actual chemical structure and van der Waals radii. As the temperature decreases, free volume decreases and, as a consequence, polymer mobility decreases as well. Eventually, mobility of the polymer chain segments will not allow the sample to maintain equilibrium properties as seen experimentally.

Doolittle (Doolittle, 1951; Doolittle and Doolittle, 1957) used the concept of free volume to empirically describe the non-Arrhenius temperature dependence of viscosity (η), near the glass transition:

$$\eta = A \exp\left(B \frac{(V - V_f)}{V_f}\right) \quad (2-5)$$

where A and B are constant for a particular polymer. One difficulty in the application of this equation lies in quantifying V_0 . It is possible to circumvent this problem by describing changes in viscoelastic properties in terms of free volume relative to a

reference state. By assuming that the free volume increases linearly with temperature and taking T_g to be the reference state, Williams, Landel and Ferry (1955) restated the Doolittle expression in a more useful, mathematically identical form, the WLF equation (2-4). Extending the WLF equation to temperatures below T_g , the viscosity is predicted to go to infinity at a temperature greater than 0 K (~50 K below T_g using the “universal” parameters). Correspondingly, the time scale for α -relaxation goes to infinity, and the Kauzmann paradox is avoided. Free volume concepts allow for the description of molecular mobility of polymers. However, the inability of this argument to determine fractional free volume a priori (McKenna, 1989) and to predict the heat capacities and the heat capacity change at T_g (McKenna, 1989) has led to the development of arguments against this theory. In addition, when the glass forming liquid is cooled at a constant volume, a glass transition can still be observed (Colucci et al., 1997).

2.4.3 Adam-Gibbs Theory

Adam and Gibbs (1965) presented a molecular-kinetic theory, in which the temperature dependence of the relaxation process is related to the temperature dependence of the size of a cooperative rearranging region (CRR). The polymer or low molecular weight glass former is defined as an ensemble of cooperative regions. Upon sufficient fluctuations in energy (enthalpy), each CRR can rearrange into different configurations independently of neighboring regions. In other words, the mobility of molecules in low molecular weight glass formers or of segments in a polymer is tied to the mobility of other molecules or chain segments in a cooperative way. As the temperature decreases, the length scale of this cooperative dynamics region will increase (Greiner

and Schwarzl, 1984; Rizos and Ngai, 1999), and eventually at T_2 the size of these regions will equal the sample size. The relaxation time of the system is given by

$$\frac{1}{\tau(T)} = A \exp\left(\frac{-\Delta\mu Sc^*}{kTSc}\right) \quad (2-6)$$

where $\Delta\mu$ is the potential energy for cooperative rearrangement per monomer segment, k is the Boltzmann constant, Sc^* is the critical configurational entropy for the smallest size capable of having two configurations and Sc is the macroscopic configurational entropy. It can be observed that as the size of CRRs is increased, greater cooperativity is needed, and the system will have a longer relaxation time.

The WLF equation (2-4) was derived using free volume arguments, but it can also be obtained from the Adam and Gibbs theory (Adam and Gibbs, 1965):

$$C_1 = \frac{2.303\Delta\mu Sc^*}{k\Delta C_p T_R \ln\left(\frac{T_R}{T_2}\right)} \quad (2-7)$$

$$C_2 = \frac{T_R \ln\left(\frac{T_R}{T_2}\right)}{1 + \ln\left(\frac{T_R}{T_2}\right)} \quad (2-8)$$

where ΔC_p is the change in heat capacity between the liquid-state and the glassy-state. Since the kinetic and the thermodynamic approaches lead to the WLF equation, both theories are compatible.

2.5 Dynamic Heterogeneity

When a glass former is cooled toward its glass transition, the relaxation dynamics become spatially heterogeneous. The relaxation time scales can vary by orders of magnitude over distances of several nanometers, defining different individual regions in the system. If each homogeneous domain relaxes exponentially, then dynamic heterogeneity can result from the different relaxation times in each homogenous region (Ediger, 2000).

The spatially heterogeneous dynamics in glass formers has been studied experimentally using different techniques, including the following: differential scanning calorimetry (Donth, 1982, 1996; Korus et al., 1997; Hempel et al., 2000), nuclear magnetic resonance (NMR) (Schmidt-Rohr and Spiess, 1991; Tracht et al., 1998; Reinsberg et al., 2001; Qiu and Ediger, 2003), fluorescence recovery after photobleaching (FRAP) (Cicerone et al., 1995; Wang and Ediger, 1997; Hwang et al., 2000; Wang and Ediger, 2000), translational and rotational probe diffusion (Chang et al., 1994; Cicerone et al., 1995; Hall et al., 1997a; Wang and Ediger, 1997; Hall et al., 1998a; Wang and Ediger, 2000), dielectric hole-burning (Schiener et al., 1996), solvation dynamics (Richert, 1996, 2000), 3-D imaging (Weeks et al., 2000) and second harmonic generation measurements (Dhinojwala et al., 1993, 1994; Jerome and Commandeur, 1997). Dynamic heterogeneity has also been observed through molecular dynamics simulation and theoretical studies (Glotzer, 2000; Smith et al., 2003; Baljon et al., 2004; Merabia et al., 2004). These studies have shown that the size scale of dynamic heterogeneous regions is approximate 1-5 nm (Schmidt-Rohr and

Spiess, 1991; Tracht et al., 1998; Sillescu, 1999; Ediger, 2000; Hempel et al., 2000; Reinsberg et al., 2001; Berthier et al., 2005). Originally, Adam and Gibbs (1965) proposed that the shape of these heterogeneous domains was spherical; however, recent studies have found that the shape of these regions is string-like (Donati et al., 1998; Glotzer, 2000; Weeks et al., 2000).

The origin of spatially heterogeneous dynamics is unknown. Nevertheless, they must be understood in order to predict transport and relaxation properties of glass forming materials (Ediger, 2000). These dynamics can potentially affect a wide range of polymer properties at the nanoscale, impacting future applications of polymers in a wide range of areas, including information storage and photocromic switches (Ediger, 2000).

2.6 Physical Aging of Bulk Amorphous Polymers

A consequence of the experimentally observed kinetic glass transition is the formation of the non-equilibrium glass. Upon cooling, the molecules experience a substantial reduction in their mobility, losing their ability to reach their equilibrium conformational state, remaining semi-frozen into a non-equilibrium glassy state. An effect of the non-equilibrium characteristic of the glassy state is the relaxation process known as physical aging or structural recovery (Struik, 1978; Tant and Wilkes, 1981; Greiner and Schwarzl, 1984, 1989). In this process, the material continuously evolves towards equilibrium through spontaneous but very slow molecular rearrangements. The result is time dependent properties such as specific volume, enthalpy, entropy, yield stress, modulus, fracture energy, and ultimate elongation at break (Struik, 1978; Kovacs

et al., 1979; Kovacs, 1981; Tant and Wilkes, 1981; Greiner and Schwarzl, 1984, 1989; McKenna, 1989; Hodge, 1995; Hutchinson, 1995). Physical aging involves only thermoreversible changes in properties with no permanent modification of the structure of the material.

Figure 2-3 shows the graphical description of the densification process associated with physical aging. When a glass forming material is quenched below T_g to an aging temperature T_a , at a constant pressure, the formed glass has an excess of thermodynamic quantities, such as specific volume and specific enthalpy. Annealing the glass at T_a results in the relaxation of the excess thermodynamic quantities toward equilibrium until it is reached. Below T_g , the individual particle or segmental motion is almost suppressed; the only structural rearrangements that may occur involve the collective movement of many particles. The length scale of these regions of cooperative dynamics is temperature and time dependent, increasing as the temperature is lowered and aging time proceeds. Therefore, only at aging temperatures very close to T_g can equilibrium be achieved on reasonable experimental time scales (Greiner and Schwarzl, 1984).

When a glass forming material is annealed below its T_g , there are three distinct features that can be observed by plotting an isotherm in a volume vs. logarithmic time diagram: an initial plateau, a linear region and an equilibrium plateau. The exact cause of the initial plateau is unknown, but it has been observed that it depends on temperature and thermal history (Greiner and Schwarzl, 1984). The equilibrium plateau

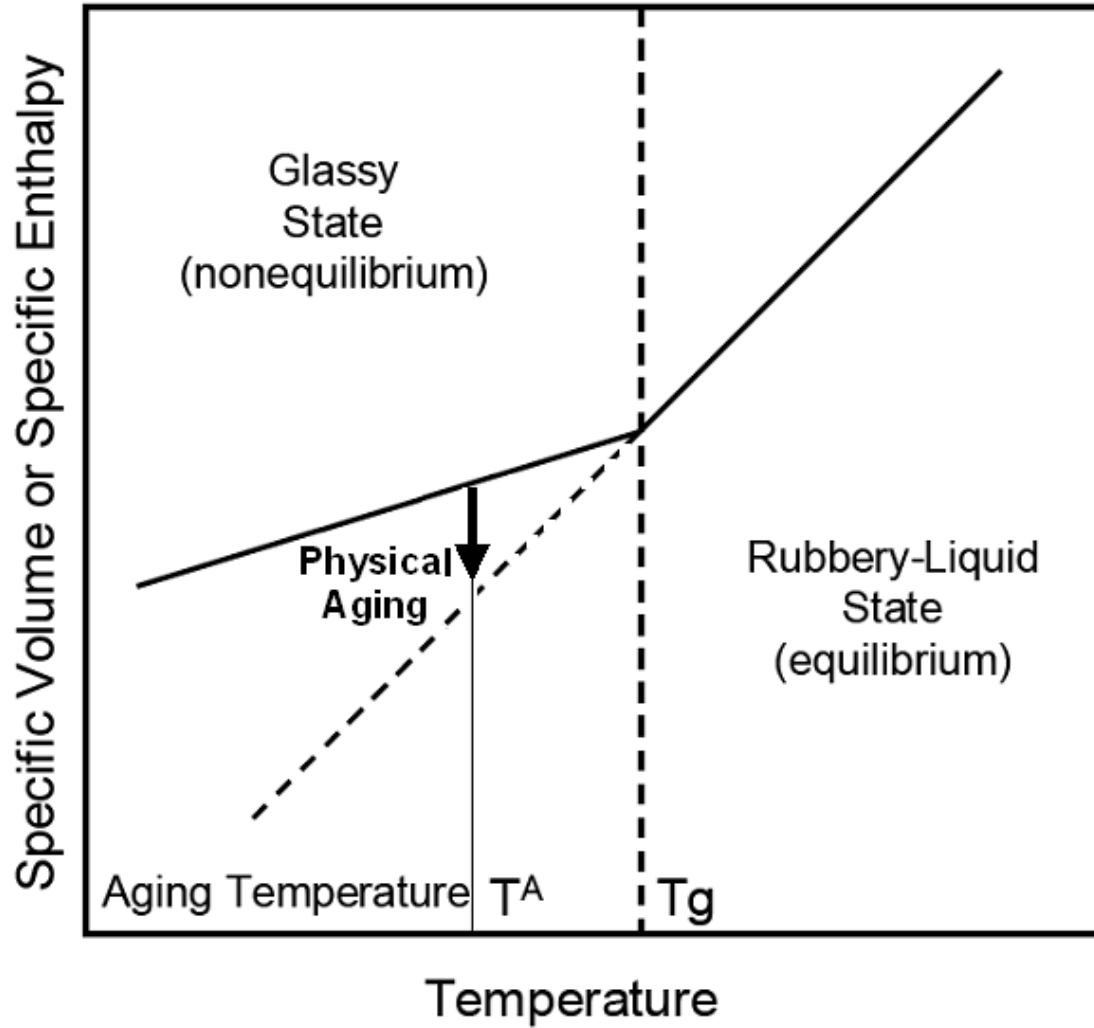


Figure 2-3: Physical aging of an amorphous polymer. With time there is a reduction in specific volume during physical aging.

is only observed when equilibrium is achieved. The linear region of the isotherm can be used to characterize the rate of volume relaxation during the aging process (Struik, 1978; Kovacs et al., 1979; Greiner and Schwarzl, 1984). The slope of the linear portion of the aging isotherm is defined as the volume relaxation aging rate (r_v):

$$r_v = -\frac{1}{v} \frac{dv}{d\text{Log}(t_a)} \quad (2-9)$$

where v is the specific volume, and t_a is aging time (Kovacs, 1981; Greiner and Schwarzl, 1984, 1989; Hodge, 1995; Hutchinson, 1995). The volume relaxation rate is temperature dependent and generally presents one maximum. The position of the maximum is highly material dependent; for example, for polystyrene (PS) the maximum aging rate is at $\sim T_g - 20$ °C while for poly(methyl methacrylate) (PMMA) the maximum aging rate is at $\sim T_g - 80$ °C (Greiner and Schwarzl, 1984). The existence of the maximum aging rate is due to the competition between the thermodynamic driving forces that promote physical aging and the molecular mobility of the system. The greater the departure from equilibrium is, the greater the thermodynamic driving forces for aging will be and the lesser the molecular mobility.

Thureau and Ediger (2002a; 2002b) studied physical aging of PS performing an optical photobleaching technique. They reported that the rotational and translational diffusion measurements of the dilute tetracene probe dispersed in the polymer matrix respond differently to the physical aging. The time required to reach equilibrium was shorter for the translational relaxation time than for the rotational relaxation time. This result indicates that the dynamics responsible for physical aging are spatially

heterogeneous. The difference in the time required for the translational and rotational relaxation times to reach equilibrium arises because the two variables average over heterogeneous dynamics in different ways. Therefore, the heterogeneous dynamics are important for the accurate description of physical aging and may be the reason why specific volume, specific enthalpy, stress relaxation and dielectric properties evolve differently during aging (Struik, 1978; Matsuoka et al., 1985; Matsuoka, 1986; McKenna, 1989; Simon, 2002; Badrinarayanan and Simon, 2007).

Any technology that requires the use of polymer glasses for long-term applications needs to take into account physical aging. The changes in material properties caused by the densification associated with the relaxation toward equilibrium can, in many cases, negatively impact the performance and useful lifetime of the polymer. As a result, physical aging affects the design, manufacture and use of amorphous polymers in diverse applications.

3 Confinement Effect on the Physical Properties of Amorphous Polymers

Deviations from bulk properties have been observed when a polymer sample is confined to the extent that the interface or surface to volume ratio becomes increasingly important. As the confinement dimension is decreased, a greater portion of the material is in immediate contact with an interface, suggesting that interfacial interactions play a crucial role in the observed properties. These deviations from bulk properties have implications in a broad range of technological applications such as photoresists for the production of microelectronics, disk drive lubricants, asymmetric membranes for gas separation, nanostructured blends and foams, and nanocomposites (Huang et al., 2005; Buriak, 2006; Du et al., 2006; Ferry et al., 2006; Chen et al., 2007; Marsh et al., 2007). It is important to note that confinement effects have also been observed for low molecular weight glass formers (Jackson and McKenna, 1991; Melnichenko et al., 1995; Arndt et al., 1997; Barut et al., 1998; Schonhals et al., 2002; Wang et al., 2004); therefore, such effects are a universal phenomenon for all glass formers. A review of the effect of confinement on the glass transition temperature and physical aging of polymers is presented below.

3.1 The Effect of Confinement on the Glass Transition Temperature of Amorphous Polymers

The first report on the effect of confinement on T_g was provided by Jackson and McKenna (1991), who found that the T_g values of low molecular weight glass formers in nanopores of Vycor glass were reduced as compared to the bulk values, with a maximum 18 K reduction for o-terphenyl in a 4 nm diameter porous glass. This original work has led to extensive experimental and theoretical studies of the effect of confinement on T_g using different sample materials and geometries.

A variety of methods have been used to characterize T_g and alpha relaxation behavior including dielectric relaxation spectroscopy (Fukao and Miyamoto, 1999, 2000; Fukao et al., 2002; Sharp and Forrest, 2003a, 2003b, 2003c; Wubbenhorst et al., 2003; Priestley et al., 2007a), fluorescence spectroscopy (White et al., 2001; Ellison et al., 2002; Ellison and Torkelson, 2002, 2003; Ellison et al., 2004; Ellison et al., 2005; Mundra et al., 2006; Rittigstein and Torkelson, 2006; van den Berg et al., 2006; Mundra et al., 2007a; Mundra et al., 2007b; Priestley et al., 2007b; Rittigstein et al., 2007; Roth et al., 2007; Roth and Torkelson, 2007), Brillouin scattering (Forrest et al., 1996; Forrest et al., 1997, 1998; Forrest and Mattsson, 2000), ellipsometry (Beaucage et al., 1993; Keddie et al., 1994a, 1994b; Forrest et al., 1997; Dalnoki-Veress et al., 2001; Fryer et al., 2001; Kawana and Jones, 2001; Kim et al., 2001; Tsui and Zhang, 2001; Grohens et al., 2002; Pham and Green, 2003; Pham et al., 2003; Sharp and Forrest, 2003b; D'Amour et al., 2004; Park et al., 2004; Singh et al., 2004), X-ray reflectivity (van Zanten et al., 1996; Fryer et al., 2001; Miyazaki et al., 2004; Soles et al., 2004b), positron

annihilation spectroscopy (DeMaggio et al., 1997; Jean et al., 1997) and nonlinear optics (Hall et al., 1997b). These methods identify T_g either by following the temperature dependence of specific volume, density, film thickness, or by characterizing the alpha relaxation dynamics directly. Most reports in this area involve investigations of linear amorphous polymers, but several studies (Grohens et al., 2001; Lenhart and Wu, 2002, 2003) have considered cross-linked or network polymers.

Thin and ultrathin films have dominated research in the area of confined polymer behavior due to the ease with which the confining dimension (film thickness) can be varied, and only recently have much more complex systems such as polymer nanocomposites been studied. In the case of a thin film geometry, it can involve either substrate-supported thin films or freely standing thin films. Substrate supported films are very important in characterizing the impact of a solid-polymer interface on the T_g in confined films. They also represent a pragmatic case, as many thin film applications are substrate based. Freely standing films have a symmetric geometry with a polymer-air interface on both sides. A brief review of the effects of confinement on T_g in different geometries is presented in the following sections.

3.1.1 T_g in Supported Polymer Films

Confinement effects on the T_g of supported polymer films have been studied for numerous polymer-substrate combinations using different techniques (Keddie et al., 1994a, 1994b; van Zanten et al., 1996; Forrest et al., 1997; Fukao and Miyamoto, 1999, 2000; Kim et al., 2000; Kawana and Jones, 2001; Kim et al., 2001; Ellison et al., 2002; Ellison and Torkelson, 2002, 2003; Park et al., 2004; Soles et al., 2004b; Ellison et al.,

2005). Keddie et al. (1994b) provided the first direct evidence of a reduction relative to bulk in T_g of ultrathin polystyrene (PS) films supported on single crystal (111) silicon wafers. Relative to bulk PS, a 25 K reduction in T_g was observed for a 10-nm-thick film. Three molecular weights (MWs) were investigated ranging from 120,000 g/mol to 2,900,000 g/mol, and no impact of MW was observed on the thickness dependence of T_g . Their results were fitted to the following empirical relation:

$$T_g(d) = T_g(\infty) \left[1 - \left(\frac{A}{d} \right)^\delta \right] \quad (3-1)$$

where A and δ are fitting parameters, d is the thickness of the film, and $T_g(\infty)$ is the bulk T_g . The onset of the deviation of the bulk T_g was seen at a thickness of ~ 40 nm. This effect was explained by Keddie et al. (1994a; 1994b) by suggesting the presence of a liquid-like layer at the free surface of high mobility and reduced T_g . Later studies have confirmed this trend in PS films using a variety of techniques (DeMaggio et al., 1997; Forrest et al., 1997; Fukao and Miyamoto, 1999, 2000; Forrest and Dalnoki-Veress, 2001; Kawana and Jones, 2001; Ellison et al., 2002; Ellison and Torkelson, 2002, 2003; Ellison et al., 2005). Polystyrene has been the most widely studied system; there are only scattered reports on a few other polymers which exhibit a reduction of T_g with decreasing film thickness. In addition to PS, this behavior has been observed for poly(methyl methacrylate) (PMMA) (Keddie et al., 1994a; Prucker et al., 1998; Fryer et al., 2001; Grohens et al., 2002; Yamamoto et al., 2002; Sharp and Forrest, 2003a), bisphenol-A-polysulfone (BPAPS) ((Kim et al., 2000), poly(alpha-methylstyrene) (PAMS) (Kim et al., 2000, 2001), poly(4-methyl styrene) (P4MS) (Ellison et al., 2005),

poly(*tert*-butyl styrene) (PTBS) (Ellison et al., 2005), bisphenol-A polycarbonate (BPAPC) (Soles et al., 2004b), poly(2,6-dimethyl-1,4-phenyleneoxide) (PPO)/PS blends (Kim and Jang, 2002), and polycarbonate/PS blends (Pham and Green, 2002). The need to expand the number of systems studied still remains.

It is clear that the impact of nanoconfinement is not restricted to a particular material. The systems that behave similarly to PS upon confinement, which exhibits a T_g reduction with decreasing film thickness, exhibit no particular interaction (e.g., hydrogen bonding) beyond van der Waals forces with the substrate. The first proof of this came from the study by Sharp and Forrest (2003b) where supported PS films “properly” capped with a 5 nm thick evaporated gold layer exhibited a bulk T_g value at a thickness as small as 8 nm. Therefore, the effect of confinement on T_g in supported PS films is due to the presence of the free surface. Using a multilayer/fluorescence method, Ellison and Torkelson (2003) performed the first direct measurement of the T_g of an ultrathin 14-nm-thick layer in contact with a free surface. They found a decrease in T_g at the free surface of a PS film, which extends several tens of nanometers into the film. Since a 12-nm-thick substrate interface layer showed a bulk T_g , their investigation demonstrated that the free surface was the cause of the T_g confinement effect in PS.

In contrast to PS, systems such as PMMA (Keddie et al., 1994a; Prucker et al., 1998; Fryer et al., 2000; Grohens et al., 2002; Yamamoto et al., 2002; Sharp and Forrest, 2003a) and poly(2-vinyl pyridine) (P2VP) (van Zanten et al., 1996; Ellison et al., 2002; Ellison and Torkelson, 2002; Park et al., 2004; Roth et al., 2007) experience attraction to hydroxyl group on a native oxide substrate (due to the presence of

hydrogen bonding) which result in increasing T_g with decreasing film thickness. (The surface of ordinary unmodified silicon or glass is comprised of silicon oxide and an equilibrium level of hydroxyl units at room temperature and ambient conditions in the concentration range of 7-9 OH/nm² (McCafferty and Wightman, 1998) and an adsorbed layer of water that is 1 or 2 monolayers in thickness (Weldon et al., 1996).)

Keddie et al. (1994a) studied the effect of the substrate on the T_g -nanoconfinement effect in poly(methyl methacrylate) (PMMA). In the case of PMMA on a gold substrate, it was found that T_g decreases as the film thickness decreases in a qualitatively similar way to that seen with PS film. In contrast, in the case of PMMA on silica, T_g increased slightly with film thickness, where the onset of the increase in T_g with nanoconfinement was observed at a thickness of ~ 80 nm. For the case of PMMA or P2VP on silica, the attractive polymer-substrate interaction (hydrogen bonding with hydroxyl groups naturally on the native oxide silicon surface) has been hypothesized to overcome the effects of the free surface and cause an overall increase in T_g (Keddie et al., 1994a; van Zanten et al., 1996). Prucker et al. (1998) carried out similar studies on PMMA and measured T_g reductions in thin films supported on a hydrophobic glass substrate. Grohens et al. (2002) studied the effects of tacticity on the T_g of thin films of isotactic, syndiotactic and atactic PMMA on silicon substrates with native oxide. They found that the observed T_g of PMMA films of similar thickness but different tacticity were significantly different. Isotactic PMMA exhibited the most extreme T_g increases with decreasing thickness (~ 39 K increase from bulk in a 20 nm film) on substrates where an attractive interaction exists. This result is in agreement with the study of isotactic

PMMA of Sharp and Forrest (2003a). In contrast, atactic PMMA exhibited no change (within error) in T_g for nearly identical films. Interestingly, syndiotactic PMMA exhibited decreases in T_g with decreasing thickness, even though there is the potential for an attractive interaction with the substrate. These results were explained in terms of a correlation that was found between the tacticity and the density of repeat unit and substrate interactions and the observed T_g . These studies showed that the response of T_g to thickness could be tuned to various degrees by changing the polymer-substrate interaction.

The most extreme increase in T_g has been observed with decreasing thickness for P2VP films on silicon oxide substrates (van Zanten et al., 1996). The interaction of P2VP through the nitrogen in the ring structure of the repeat unit with the substrate is so strong that a 50 K increase from bulk T_g is observed for an 8 nm thick film. Other polymers that exhibit T_g increases with decreasing film thickness include polycarbonate (Pham and Green, 2002; Soles et al., 2004b) and polyhydroxystyrene (Tate et al., 2001).

There have been studies of T_g -nanoconfinement effects in thin polymer blend films (Kim and Jang, 2002; Pham and Green, 2002). They found that these effects are tunable by simply varying the blend composition. Tsui et al. (2001) presented a study of T_g in thin PS films as a function of thickness and interaction by grafting a random copolymer of poly(styrene-co-methyl methacrylate) (PS-co-PMMA) to the substrate. The interfacial energy was tuned by varying the styrene mole fraction in the random copolymer influencing the T_g of PS. Using ellipsometry, Park et al. (2004) studied the T_g

of thin PS-co-PMMA and random copolymer of poly(2-vinyl pyridine-co-styrene) (P2VP-co-PS) films coated on a native oxide surface of Si wafer (100). The choice of the systems was supported by the fact that methyl methacrylate units are moderately attractive to the substrate, while 2-vinyl pyridine units are strongly attractive to it and styrene units do not interact with the substrate. Depending on the composition of the comonomer units in the copolymer, T_g can be tuned as a function of thickness from nearly invariant, increases and decreases compared with bulk behavior (Hall et al., 1997b; Park et al., 2004; Mundra et al., 2006).

Ellison et al. (2004) showed that by adding a high concentration of small diluent molecules to PS thin films, the T_g -nanoconfinement effect can be tunable. They found that by adding 9 wt% of pyrene or 4 wt% of dioctyl phthalate (DOP) to a 13-nm-thick PS film, the T_g of the system is within error equivalent to that of bulk PS containing the same amount of pyrene or DOP. The reduction or complete elimination of the confinement effect is due to the plasticizers alleviating the polymer requirement of cooperativity (Roland et al., 1993; Santangelo et al., 1994a; Santangelo et al., 1994b; Casalini et al., 2000), reducing the size scale of an average CRR and the length scale needed to encompass the breadth of cooperative segmental dynamics over which confinement effects are observed.

Only a few studies have investigated the effect of confinement on T_g of surface grafted polymers. Using ellipsometry, Keddie and Jones (1995) studied the T_g confinement effect of PS grafted onto a native oxide substrate. They determined that, down to a thickness of 8 nm, the effect of thickness on T_g was similar to that observed

on PS spin coated onto the substrate. Prucker et al. (1998) examined PMMA grafted onto a treated silica substrate (the silica substrate presented trimethylsilyl groups on the surface). Their results indicated a decrease in T_g with decreasing thickness that is quantitatively comparable to their results in PMMA films formed by spin coating on the same substrate. Tate et al. (2001), using local thermal analysis and ellipsometry, studied the T_g of grafted thin films of poly(4-hydroxystyrene) (PHS) and hydroxy terminated polystyrene (PS-OH) onto silicon oxide substrates. In the case of PHS, the T_g of films 100 nm thick or less were elevated by more than 50 °C above the bulk value. For PS-OH, the T_g elevations were not as large as for PHS. In this study, the film dependence of T_g for PHS and PS-OH were described with a “dual-mechanism” model. Yamamoto et al. (2002) studied PMMA surface-grafted at high density onto silicon wafers by a controlled radical polymerization technique. The grafted chains were highly extended along the film thickness direction due to the high graft density (as high as 0.7 chains/nm²). Their ellipsometry results revealed an increasing T_g with decreasing brush thickness. This was explained as being a consequence for steric constraints arising from the extended chain conformation resulting in limited cooperative segmental mobility. In contrast, their results for free PMMA spin coated on a hydrophobically treated silicon wafer showed a decrease in T_g with decreasing film thickness.

3.1.2 T_g in Freely Standing/Unsupported Polymer Films

Several studies have considered the effect of confinement on the T_g of freely standing polymer films (Forrest et al., 1996; Forrest et al., 1997, 1998; Mattsson et al., 2000; Dalnoki-Veress et al., 2001; Roth and Dutcher, 2003; Liem et al., 2004; Roth and

Dutcher, 2005; Miyazaki et al., 2007). The first T_g measurements for freely standing thin polymer films were provided by Forrest and coworkers (1996; 1997; 1998). These studies used different techniques such as Brillouin light scattering (Forrest et al., 1996; Forrest et al., 1997, 1998) and transmission ellipsometry (Forrest et al., 1997). Later, Roth and Dutcher (2003) reproduced these measurements which are summarized in a recent review article (Roth and Dutcher, 2005). A much greater reduction in T_g with confinement was observed in freely standing films as compared to substrate-supported films, sustaining the idea of Keddie et al. (Keddie et al., 1994a, 1994b) that the free surface has a liquid-like layer with a reduced T_g . Mattsson et al. (2000) reported an astonishing reduction of 70 K from bulk T_g in a freely standing 20-nm-thick PS film.

Interestingly, in freely standing films a strong effect of MW has been observed on the T_g -nanoconfinement effect. Apparently, in freely standing PS films there exist two MW regimes for the thickness dependence of T_g (Forrest and Dalnoki-Veress, 2001). In the low MW regime ($M_n \leq \sim 380$ kg/mol), the thickness dependence of T_g is MW independent (Forrest and Dalnoki-Veress, 2001). In the high MW regime ($M_n \geq \sim 580$ kg/mol) there is substantial MW dependence, where higher MW samples exhibit a stronger T_g thickness dependence. It is not known at this time why this MW dependence is observed in freely standing PS films, but no MW dependence is observed in the supported PS films (Forrest and Dalnoki-Veress, 2001; Ellison et al., 2005). Recently reported studies on freely standing PMMA films (Roth and Dutcher, 2003) showed the same qualitative dependence of T_g on thickness as PS, but the extent of T_g reduction was smaller in the PMMA films. Obviously, the impact of the

repeat unit structure on the T_g -confinement effect can be very important and needs further study. Recently, Miyazaki et al. (Miyazaki et al., 2007) studied thermal expansion of freely standing PS films using X-ray reflectivity to elucidate T_g . They found a decrease in T_g with film thickness. Also, their results indicate a MW dependence. They suggest that some segmental motions are activated due to free surfaces on both sides in the freely standing films and not in supported films.

3.1.3 T_g in Polymer Nanocomposites

The effect of confinement on the T_g response of polymer nanocomposites (Starr et al., 2001; Ash et al., 2002b; Berriot et al., 2002; Savin et al., 2002; Starr et al., 2002; Arrighi et al., 2003; Berriot et al., 2003; Blum et al., 2003; Liu et al., 2003; Mbhele et al., 2003; Wang et al., 2003; Ash et al., 2004; Sun et al., 2004; Bansal et al., 2005; Kotsilkova et al., 2005; Ramanathan et al., 2005b; Bansal et al., 2006; Blum et al., 2006; Chen et al., 2006; Hong et al., 2006; Rittigstein and Torkelson, 2006; Ding et al., 2007; Hub et al., 2007; Kropka et al., 2007; Lee et al., 2007a; Lee et al., 2007b; Rittigstein et al., 2007; Sargsyan et al., 2007; Sen et al., 2007; Srivastava and Basu, 2007a, 2007b; Theneau et al., 2007; Wang et al., 2007) has received relatively little attention in the research literature compared with this effect in thin polymer films. As such, there remain many opportunities for important studies in this area.

Molecular dynamic simulations of an idealized polymer surrounding a nanofiller were performed by Starr et al. (2001). They showed that T_g can be shifted to higher or lower temperatures by tuning the polymer-nanofiller interactions and that the effects are similar to those resulting from free surfaces and polymer-substrate interactions in

ultrathin polymer films. Also, using Monte Carlo simulations, Papakonstantopoulos et al. (2005) showed that the inclusion of a nanoparticle into a polymer matrix results in structural changes that depend strongly on the polymer attraction to the surface of the filler. Simulations of local properties reveal that a glassy layer is formed in the vicinity of the attractive filler, increasing its T_g , while a region of negative moduli emerges around repulsive fillers, lowering the T_g of the system. Berriot et al. (2002; 2003) used the idea of a distribution of T_g s to understand the behavior of polymer nanocomposites. Providing a new understanding of complex mechanical behavior, they invoked a gradient in T_g associated with a gradient in mechanical properties in the vicinity of silica particles in filled elastomers (Berriot et al., 2002). By comparing NMR and mechanical data, this gradient of the polymer matrix T_g in the vicinity of silica particles has been reported to be as large as 20 nm at temperatures of $T_g + 6$ K for poly(ethyl acrylate) nanocomposites, demonstrating that segmental dynamics can be impacted locally near the interfaces (Berriot et al., 2003). Using modulated differential scanning calorimetry (MDSC), Blum and coworkers (Porter and Blum, 2000, 2002; Blum et al., 2003; Zhang and Blum, 2003; Blum et al., 2006) quantified the T_g of very small adsorbed amounts of different polymers on silica. They found a broader two-component transitions for the adsorbed PMMA on silica nanospheres (Blum et al., 2003; Blum et al., 2006). The thermograms for the adsorbed PMMA showed two distinct transitions, one being close to bulk T_g , representing the part of the polymer that is loosely bound, and the other transition about 30 °C higher than bulk T_g , representing the part of the polymer that is tightly bound.

Ash and co-workers (2002b; 2004) observed a 25 K reduction in T_g of PMMA with the incorporation of 0.5 wt% of alumina nanospheres (diameter = 17 nm) or 1 wt% of alumina nanospheres (diameter = 39 nm) via *in situ* polymerization of methyl methacrylate in the presence of alumina nanofiller. This T_g behavior suggests that the PMMA is not wetting the alumina surface and that some free surface is present between the filler and the polymer. Mbhele et al. (2003) observed a 21 K increase in T_g for a poly(vinyl alcohol) (PVA) nanocomposite containing only 0.73 wt% of silver nanospheres (diameter = 5 nm). Also, a broadening of the melting peak in the heat capacity curves with an increase of the content of the inorganic phase was reported. They claimed that the observed behavior is a consequence of the attachment of the PVA chains to the surface of the Ag-nanofiller reducing mobility of the polymer chains in the nanocomposite and affecting the chain density packing in the vicinity of the surface of the nanofillers. Arrighi et al. (2003) studied the thermomechanical behavior of a styrene-butadiene rubber containing 23.5% styrene and filled with up to 55 wt% with silica nanoparticles. The plot of $\tan \delta$ as a function of temperature for the composites showed a second relaxation, whose intensity increases with filler content, at temperatures about 40 °C above bulk T_g . This was attributed to an interfacial layer of polymer whose chain relaxation dynamics have been altered by interaction with the filler surface. On the other hand, when the filler surface is organophilic instead of hydrophilic, a displacement of T_g to lower temperatures was observed. The T_g s of epoxy composites with micrometer-sized fillers and nanofillers, including silver, silica, aluminum and carbon black, were investigated using DSC by Sun et al. (2004). They

found that the nanocomposites showed a significant reduction in T_g in comparison with their counterparts with micrometer-sized fillers. The T_g depression observed in the different epoxy nanocomposites is related to the enhanced polymer dynamics due to the extra free volume at the resin-filler interface. Bansal et al. (2005) observed that mixing high levels of nanosized untreated silica particles into a PS matrix suppressed T_g . On the other hand, if the surface of the silica nanospheres were modified, there was no change in T_g . They demonstrated an approximate equivalence between ultrathin film thickness and average interparticle spacing in nanocomposites for two surface treatments, resulting in either non-wetting or wetting polymer-nanofiller interfaces.

Liu et al. (2003) presented a method to prepare spherical PMMA-gold hybrid nanocomposites via synthesis of gold nanospheres in the presence of a PMMA matrix. Using DSC, they found a ~ 30 °C decrease in T_g compared with bulk in the nanocomposite. This result is in agreement with Keddie et al. (1994a) who found a decrease in T_g upon confinement in a PMMA supported thin film on a gold substrate. However, Srivastava and Basu (2007a), following the same procedure as that used by Liu et al. (2003) to make PMMA-gold nanoparticles, showed that relative to the T_g of neat, bulk PMMA, the T_g of the PMMA-gold system can be either increased or decreased by varying the nanoparticle-polymer interface width (σ).

Ramanathan et al. (2005a) described a procedure to prepare single-walled carbon nanotubes (SWCNT) functionalized with amino groups (amide and amine-moieties) via chemical modification of carboxyl groups introduced on the carbon nanotube surface. The amino-termination allows further chemistry of the functionalized SWCNT and

makes possible covalent bonding to polymers. Later, Ramanathan et al. (2005b) presented results for PMMA covalently bonded to amine-functionalized SWCNT. The results demonstrate that even with low SWCNT loadings (1 wt%), the thermal, mechanical and electrical properties are significantly improved when compared to those in the neat polymer. In the case of the glass transition behavior, they observed a 33 K increase in T_g of PMMA with 1 wt% of amine-functionalized SWCNT covalently bonded to PMMA. These results suggest the formation of an interfacial region of reduced molecular mobility in the vicinity of the nanotubes that penetrates throughout the composite, leaving very little bulk polymer response. They addressed the need for more detailed experiments to provide understanding of the changes in local polymer dynamics near nanoparticles and the percolation of these effects in the systems.

By surface-initiated ATRP, Savin et al. (2002) prepared high-density PS brushes on silica nanospheres (diameter = 20 nm). The T_g of annealed bulk films of the hybrid nanoparticles was elevated with respect neat, bulk PS. The enhancement ranged from 13 K to 2 K for low and high MW, respectively. Bansal et al. (2006) demonstrated that the thermomechanical properties of polymer nanocomposites are critically affected by polymer-particle wetting behavior. They studied the T_g of nanocomposites formed of dense PS brushes grafted on silica nanoparticles blended to PS melts. Depending on the MW of the PS matrix, they found that T_g could increase, decrease or remain equal to neat, bulk T_g with increasing silica nanosphere concentration. When low MW PS melt is used, the matrix wets the nanospheres, and the T_g of the system increases with

nanofiller content. On the other hand, when high MW melt is used, dewetting is observed in the system, and the T_g decreases with nanofiller content.

3.2 Discussion of the Effect of Confinement on T_g

This section will provide a review and a critical discussion of the T_g nanoconfinement effect based on the literature.

3.2.1 Origin of Deviations from Bulk T_g in Confined Polymers

Many postulates have been proposed in order to explain the origin of the effect of nanoconfinement on the T_g (Forrest and Dalnoki-Veress, 2001) of systems lacking attractive polymer-substrate interactions, including the following: internal stresses caused by film preparation methods (e.g. spin coating) (McKenna, 2000; Bernazzani et al., 2002); a “finite size effect” due to the thickness approaching a fundamental length scale associated with glass formers (Keddie et al., 1994b), e.g. the cooperatively rearranging region (CRR) introduced by Adam and Gibbs (1965); interfacial effects involving a reduced entanglement concentration (Brown and Russell, 1996; McKenna, 2000; Tsui and Zhang, 2001; Bernazzani et al., 2002) or a segregation of chain ends to the free surface (air-polymer interface) (Mayes, 1994; Tsui and Zhang, 2001); and a radius of gyration (R_g) value that is on the order or a small multiple of the film thickness (Dalnoki-Veress et al., 2001; Singh et al., 2004).

Agreement among many studies of supported PS films (Forrest and Dalnoki-Veress, 2001; Kawana and Jones, 2001) in which samples of similar thickness were prepared using different solutions (solvent type and polymer concentration) and

preparation conditions (spin coating speed) refute the idea that internal stresses may cause the T_g -nanoconfinement effect. However, related studies of ultrathin PS (Orts et al., 1993; Kanaya et al., 2003) and polycarbonate (Soles et al., 2004a) films have shown the existence of a negative thermal expansivity in the glassy state, which has been attributed to a non-relaxed structure that is set in during spin coating (Kanaya et al., 2003; Miyazaki et al., 2004). This effect, which exhibits little impact on T_g (Kanaya et al., 2003), can be removed by annealing above bulk T_g (Kanaya et al., 2003; Miyazaki et al., 2004; Mundra et al., 2006; Mundra et al., 2007b).

Attempts have been made to connect the size scale at which nanoconfinement effects are observed to the size scale of a CRR (Forrest and Dalnoki-Veress, 2001). The length scale of a CRR near T_g has been investigated by differential scanning calorimetry (Donth, 1982, 1984, 1996; Korus et al., 1997; Donth, 1999; Hempel et al., 2000; Donth, 2001; Robertson and Wang, 2004; Vyazovkin and Dranca, 2004), 4D-NMR (Barut et al., 1998; Tracht et al., 1998; Reinsberg et al., 2001) and other techniques (Arndt et al., 1996; Richert, 1996; Arndt et al., 1997; Erwin and Colby, 2002; Hong et al., 2002) and has been reported to lie in the range of ~ 1 -5 nm for low MW and polymeric glass formers. However, the length scale at which nanoconfinement effects are observed is ~ 10 nm or less for low MW glass formers (Jackson and McKenna, 1991; Melnichenko et al., 1995; Arndt et al., 1997; Barut et al., 1998; Schonhals et al., 2002; Wang et al., 2004) and ranges from several tens to hundreds of nanometers for polymers (Keddie et al., 1994a, 1994b; van Zanten et al., 1996; DeMaggio et al., 1997; Forrest et al., 1997; Fryer et al., 2000; Fukao and Miyamoto, 2000; Dalnoki-Veress et

al., 2001; Forrest and Dalnoki-Veress, 2001; Fryer et al., 2001; Kawana and Jones, 2001; Kim et al., 2001; Tsui and Zhang, 2001; Grohens et al., 2002; Pham and Green, 2002; Pham et al., 2003; Sharp and Forrest, 2003a, 2003b; D'Amour et al., 2004; Miyazaki et al., 2004; Park et al., 2004; Singh et al., 2004; Soles et al., 2004a; Soles et al., 2004b; Mundra et al., 2006; Rittigstein and Torkelson, 2006; Miyazaki et al., 2007; Mundra et al., 2007a; Mundra et al., 2007b; Priestley et al., 2007a; Priestley et al., 2007b; Rittigstein et al., 2007; Roth et al., 2007; Roth and Torkelson, 2007). This indicates that the length scale of a single CRR is far less than the thickness at which T_g -nanoconfinement effects are observed; therefore, it is not the origin of this effect.

Many studies (Keddie et al., 1994a; Jean et al., 1997; Kajiyama et al., 1997; Schwab et al., 2000; Torres et al., 2000; Forrest and Dalnoki-Veress, 2001; Pochan et al., 2001; Wallace et al., 2001; Ellison and Torkelson, 2003; Sharp and Forrest, 2003b; Wang et al., 2004; Ellison et al., 2005; Mundra et al., 2007a; Roth et al., 2007; Roth and Torkelson, 2007) have indicated that interfacial effects are the most logical explanation for the underlying cause of the T_g -nanoconfinement effect. Sharp and Forrest (2003b) showed that removing the free-surface interface by placement of a gold layer onto the film results in a T_g that is independent of thickness down to 8 nm, thus supporting the importance of free-surface effects for PS. Recent understanding gained from fluorescence experiments (Ellison and Torkelson, 2003) has reiterated this point. The multilayer fluorescence experiments have revealed that the free-surface effect causes a T_g reduction that persists several tens of nanometers into the film interior (much larger than a single CRR). Furthermore, it was observed (Ellison and Torkelson, 2003) that a

region of reduced T_g near the free surface exists as a continuous distribution of T_g s that depends on the degree of nanoconfinement. These results have shown directly that two-layer and three-layer models (van Zanten et al., 1996; DeMaggio et al., 1997; Forrest and Mattsson, 2000; Fukao and Miyamoto, 2000; Forrest and Dalnoki-Veress, 2001; Kawana and Jones, 2001; McCoy and Curro, 2002) are inadequate to explain T_g -nanoconfinement behavior and that a model that incorporates a continuous distribution of T_g s across the thickness of a film is needed (Priestley et al., 2005a; Priestley et al., 2007a; Roth et al., 2007; Roth and Torkelson, 2007). This picture is consistent with recent simulations (Jain and De Pablo, 2004) and predictions from theoretical studies (Berriot et al., 2002, 2003; Herminghaus et al., 2004; Merabia et al., 2004).

The key role of interfacial effects is also supported by studies of the thickness dependence of T_g for polymers with attractive substrate interactions (Keddie et al., 1994a; van Zanten et al., 1996; Forrest and Dalnoki-Veress, 2001; Fryer et al., 2001; Ellison et al., 2002; Ellison and Torkelson, 2002; Grohens et al., 2002; Pham and Green, 2002; Mundra et al., 2006; Rittigstein and Torkelson, 2006; Mundra et al., 2007a; Mundra et al., 2007b; Priestley et al., 2007b; Rittigstein et al., 2007), e.g. poly(2-vinylpyridine) and poly(methyl methacrylate) on silicon (with native oxide) or glass substrates which exhibit increases in T_g with decreasing thickness due to the attractive substrate interactions. Simulations have confirmed this point by verifying that changing the interaction potential between substrate and polymer results in a T_g deviation (decrease or increase based on the nature of interaction between the substrate and the polymer) as a function of film thickness (Torres et al., 2000; Starr et al., 2001).

Although there is substantial evidence supporting a free-surface effect as the origin of T_g reductions in nanoconfined PS films, there is not yet a detailed understanding of the free-surface effect. A simple explanation is that polymer segments that lie at the free surface possess fewer conformational restrictions than those in the bulk; this results in a higher degree of cooperative segmental mobility and an associated lower T_g . While this explanation is logical, it lacks details regarding the extent to which interfaces may be expected to modify cooperative segmental mobility or T_g from that of bulk. Others have offered the explanation that the free surface results in a reduced entanglement concentration (Brown and Russell, 1996; McKenna, 2000; Tsui et al., 2001; Bernazzani et al., 2002), which may yield enhanced mobility and reduced T_g near the free surface. However, this explanation can be criticized because a thickness dependent T_g has been observed for both entangled and unentangled PS (DeMaggio et al., 1997; Fukao and Miyamoto, 2000; Forrest and Dalnoki-Veress, 2001; Kawana and Jones, 2001; Tsui et al., 2001) (M_c , the critical entanglement MW, is $\sim 35,000 - 38,000$ g/mol (Sperling, 1992; Majeste et al., 1998) for PS) and because bulk T_g does not depend on chain entanglements (Sperling, 1992). Another potential explanation involves the segregation of chain ends to the free surface, reducing the local T_g at the free surface (Mayes, 1994; Tsui et al., 2001). However, if chain ends were the origin of this effect, it would be expected that the thickness dependence of T_g could be significantly altered by varying the surface chain-end concentration by modification of the polymer MW (Mayes, 1994), which is not supported by experimental data. Variation of polymer MW also greatly alters the R_g of the bulk polymer, which may affect the film

thickness at which overall chain conformation would be expected to differ substantially from bulk. Some have argued that such effects may yield a MW dependence of the T_g -nanoconfinement effect (Fukao and Miyamoto, 1999; Singh et al., 2004). There is a large body of evidence in opposition to this picture (DeMaggio et al., 1997; Fukao and Miyamoto, 2000; Forrest and Dalnoki-Veress, 2001; Kawana and Jones, 2001; Tsui et al., 2001; Ellison et al., 2005) indicating that the T_g -nanoconfinement effect for supported PS films is approximately independent of MW, indicating that neither chain ends nor bulk R_g plays a significant role in defining this effect.

3.2.2 Models and Hypotheses Explaining T_g -nanoconfinement Effects

Attempts to understand polymer confinement have led to the development of phenomenological descriptions known as layer models. Layer models have been able to provide some insight into the observed properties by segmenting the cross section of the film into layers of different properties. The first model proposed to explain the T_g -nanoconfinement effect was an empirical bilayer model by Keddie et al. (1994b), who introduced the idea of an air-polymer surface layer with enhanced mobility and lower T_g than for bulk PS. Further, it was shown that the substrate had little effect on the mobility of PS thin films, consistent with what had been seen in molecular dynamic simulations (Bitsanis and Hadziioannou, 1990) of a polymer melt near a wall. Freely standing films have two air-polymer interfaces; therefore, they are expected to exhibit behavior similar to that of a supported film of half the thickness, which was later shown experimentally (Forrest and Mattsson, 2000; Mattsson et al., 2000; Roth and Dutcher, 2003). Later, more models were proposed that were in essence a modified version of the bilayer

model (DeMaggio et al., 1997; Kawana and Jones, 2001; Park et al., 2004). Another layer model (Forrest and Mattsson, 2000), with dynamic heterogeneities at the free surface, was proposed to describe T_g in low to moderate MW polymeric freely standing films. It was suggested that the mobile surface layer had a width determined by the length scale of cooperative dynamics. The model incorporated the idea of Adam and Gibbs (1965) of a fundamental length scale coupled with the dynamics of the T_g . Later, Ellison and Torkelson (2003) showed that bilayer and trilayer models are inadequate to explain T_g -nanoconfinement effects and that a model with gradients in dynamics accounting for a distribution of T_g s across the film thickness is required.

Hypothesis-driven models have also been proposed to explain the effect of confinement on T_g . Ngai and coworkers (Ngai et al., 1998; Ngai, 2000) proposed the coupling model, which is focused on the cooperative motions associated with T_g (Adam and Gibbs, 1965). The model characterizes the impact of local structure on the steric constraints from the neighboring nonbonded segments or simply the intermolecular coupling. This intermolecular coupling is linked to the size scale of CRRs, which is believed by some to be connected to T_g -nanoconfinement effects. Supporting evidence came from a recent study (Ellison et al., 2004) in which the addition of a small amount of plasticizer in PS reduced the requirement for the intermolecular coupling and the size scale of CRRs at T_g . Nevertheless, a connection between the size scale of CRRs and the T_g -nanoconfinement effects was not established. Several other models have also been proposed to describe the effect of confinement on T_g in thin and ultrathin films (Jiang et al., 1999; De Gennes, 2000).

Long and Lequeux (Long and Lequeux, 2001; Merabia et al., 2004) proposed a model based on the idea that thermally induced density fluctuations play a critical role in determining T_g in bulk. These fluctuations lead to regions of faster and slower dynamics. The total number of regions with slower dynamics increases with decreasing temperature. They defined the T_g as the temperature at which these slow moving regions are interconnected throughout the bulk of the sample. The deviation from bulk T_g in confined systems is explained by a shift in the percolation of regions of fast and slow dynamics from a 3-dimensional (3-D) to a 2-dimensional (2-D) geometry. In the case of ultrathin supported films with little or no attractive substrate interaction, the T_g occurs when the slow regions percolate in the direction parallel to the film. This requires a larger fraction of slow domains and results in a decrease of T_g relative to ultrathin films with attractive substrate interactions. In the case of substrate-supported films with strong attractive interactions with the substrate, the transition occurs when both interfaces are connected with continuous paths of slow regions. This requires that the correlation length of the 3-D percolation (ζ) is comparable to the thickness of the film, which may require a smaller fraction of slow subunits as compared to the bulk glass transition. Then, the T_g -nanoconfinement effects are seen when the thickness of the sample becomes comparable to ζ . This model (Long and Lequeux, 2001; Merabia et al., 2004) explains many attributes of the T_g -nanoconfinement effect satisfactorily as well as addresses the issues of interactions with the substrate. In addition, the model is free of any fitting parameters used in various other models to describe at least

qualitatively the behavior in bulk and in thin films. However, because it has been applied to only a couple of systems (Merabia et al., 2004), it merits further investigation.

3.3 Confinement Effect on the Physical Aging Behavior of Amorphous Polymers

Compared to the T_g -nanoconfinement effect, few studies of physical aging in confined polymer have been reported (Pfromm and Koros, 1995; Lee and Lichtenhan, 1998; Dorkenoo and Pfromm, 1999, 2000; McCaig and Paul, 2000; McCaig et al., 2000; Ellison et al., 2002; Kawana and Jones, 2003; Lu and Nutt, 2003a, 2003b; Huang and Paul, 2004; Zhou et al., 2004; Fukao and Sakamoto, 2005; Huang and Paul, 2005; Priestley et al., 2005a; Priestley et al., 2005b; Vlasveld et al., 2005; Kim et al., 2006; Rittigstein and Torkelson, 2006; Huang and Paul, 2007a, 2007b; Priestley et al., 2007c; Rittigstein et al., 2007; Theneau et al., 2007). A brief review of the effects of confinement on physical aging in different geometries is presented below.

3.3.1 Physical Aging Behavior in Supported Polymer Films

Ellison et al. (2002) conducted the first study to address the impact of confinement on physical aging of supported polymer films. They reported little change in the physical aging rate of poly(isobutyl methacrylate) films supported on quartz over a range of thicknesses from 10 nm to 800 nm. Later, the effect of confinement on the physical aging response of PS films with thickness between 10-200 nm was studied by Kawana and Jones (2003). They showed that a 10 nm thick film was still in an equilibrium state at 30 °C below bulk T_g , consistent with the notion that the T_g of the 10 nm thick film is reduced relative to bulk by at least 30 °C. A recent study by Priestley et

al. (2005a) provided the first characterization of physical aging as a function of polymer-substrate interactions. Physical aging in ultrathin PS films was shown to be dependent on thickness and absent when the aging temperature was above the T_g of the confined film but below that of bulk polymer. In contrast, the presence of structural relaxation was observed 6 °C above the bulk T_g for an ultrathin PMMA film supported on a silica substrate. This result was obtained because confinement leads to an increase of T_g due to the attractive interaction between the polymer and the substrate. Using dielectric measurements, Fukao and Sakamoto (2005) reported physical aging results of PMMA thin films. They observed a decrease of the aging rate as the film thickness decreases. Recently, using fluorescence multilayer techniques, Priestley et al. (2005b) studied the structural relaxation of PMMA at interfaces and between them. They showed that physical aging is almost totally suppressed next to the substrate because the hydrogen bonds restrain small motions associated with structural relaxation. At the free surface the physical aging is diminished but to a lesser extent than at the substrate. The free surface effects were rationalized as being due to the reduced thermodynamic driving force for structural relaxation. Interestingly, the substrate and free surface layers affect the structural relaxation rate over similar distances into the film interiors. Also, this study suggested that T_g and physical aging may be affected over different length scales by perturbations caused by surfaces and interfaces.

3.3.2 Physical Aging Behavior in Freely Standing/Unsupported Polymer Films

Using permeability measurements, Pfromm and Koros (1995) reported significantly accelerated physical aging with decreasing thickness, from 2.5 μm to 0.5 μm , for free-standing polyimide and polysulfone films. Such a large length scale for a confinement effect had not been previously reported for either T_g or physical aging. Using permeability measurements, Dorkenoo and Pfromm (1999) later observed an accelerated physical aging process with decreasing thickness (800 nm to 100 nm) free-standing polynorbornene films.

Recently, Huang and Paul (2004) also reported accelerated physical aging with decreasing thickness for thin (900 nm to 400 nm) free-standing polysulfone, polyamide and poly(phenylene oxide) films using permeability measurements. In contrast to their physical aging results, Huang and Paul (2004) observed no significant T_g confinement effect for films over the same thickness range. However, Kim et al. (2000) showed that thin supported polysulfone films exhibit decreasing T_g with decreasing film thickness, with T_g beginning to deviate from its bulk value at ~ 80 nm. These results suggest that the length scale at which confinement effects alter T_g and physical aging may be different. Huang and Paul (2005) reported similar qualitative trends of aging rate by permeability and refractive index measurements for free-standing polysulfone and poly(2,6-dimethyl-1,4-phenylene oxide) films. They observed an accelerated physical aging for thin films compared to thick films. All the permeability studies (Pfromm and Koros, 1995; Dorkenoo and Pfromm, 1999, 2000; McCaig and Paul, 2000; McCaig et

al., 2000; Huang and Paul, 2004, 2005; Kim et al., 2006; Huang and Paul, 2007a, 2007b) observed an accelerated physical aging response of free-standing polymer films as the film thickness is reduced. These contrast with the multilayer fluorescence results of Priestley et al. (2005b) in the case of the diminished physical aging rate at the free surface. It is noteworthy that the permeability studies used polymers with significantly more rigid backbones than in the multilayer fluorescence studies (which were done in supported, not free-standing, films). Whether this difference in polymer backbone rigidity is the origin of the difference in the effect of confinement in physical aging rate is as yet unclear. Additional studies of physical aging rates and T_g in thin and ultrathin films for polymer lacking C-C backbones are warranted to resolve this issue.

3.3.3 Physical Aging Behavior in Polymer Nanocomposites

Very little work has been done to study the effect of confinement on physical aging in polymer nanocomposites. A few studies have aimed at identifying the impact of the addition of nanofillers in the polymeric matrix on the structural relaxation (Lee and Lichtenhan, 1998; Lu and Nutt, 2003a, 2003b; Vlasveld et al., 2005; Rittigstein and Torkelson, 2006; Priestley et al., 2007c; Rittigstein et al., 2007; Theneau et al., 2007). The first study of the physical aging behavior of polymer impacted by the presence of a nanofiller was done by Lee and Lichtenhan (1998). They reported that the inclusion of polyhedral oligomeric silsesquioxane (POSS) nanoreinforcements in epoxy by *in situ* polymerization retarded the physical aging rate and the time to reach equilibrium. They proposed that the presence of POSS cages attached to the network chains provides topological constraints to the network junctions, which prevents or severely retards the

process of the matrix reaching structural equilibrium. More recently, Lu and Nutt (2003a; 2003b) observed that inclusion of intercalated clay nanofillers into an epoxy network had a significant effect on the segmental relaxation of the matrix. They found a restricted relaxation behavior with slower overall relaxation rates and a broader distribution of relaxation times in intercalated silicate-epoxy nanocomposites relative to the neat epoxy resin. They concluded that this behavior depends on the extent of exfoliation of the layered silicates and the strength of interaction between the silicate surface and the polymer.

Vlasveld et al. (2005) used creep measurements to study the physical aging phenomena of polyamide 6 (PA6) nanocomposites containing exfoliated layered silicate particles at environmental moisture conditions. They showed that the shape of the creep curves of the nanocomposites is similar to unfilled polyamide 6 and time-aging time superposition is possible with all materials. The shift rate is in the same range, but a little higher for nanocomposites, indicating a slightly faster aging rate in the nanocomposites. Very recently, Theneau et al. (2007) used a phenomenological model based on the evolution of the configurational entropy and DSC measurements to study the influence of silica on the kinetics of the structural relaxation process of the poly(2-hydroxyethyl methacrylate) (PHEMA) nanocomposites. They showed a reduction of structural relaxation of PHEMA with different silica content. In addition, the silica presence leads to a broadening of temperature interval in which conformational motions in the glassy state take place in 200 min. The distribution of the relaxation times also

broadens as the silica content increases, as characterized by the decrease of the KWW parameter β and the increase of the fragility of the polymer (see chapter 2).

Given the importance of physical aging in determining long-term material properties, it is unfortunate that so few studies have focused on the effects of physical aging in polymer nanocomposites. Clearly, there are many opportunities for fundamental investigations in this area.

3.4 Other Polymer Properties Impacted by Confinement

It has been observed that a variety of other key polymer properties are impacted by confinement. These include polymer chain diffusion (Frank et al., 1996a; Zheng et al., 1997; Kuhlmann et al., 1998; Pu et al., 2001a; Pu et al., 2001b; Kawaguchi et al., 2003), small-molecule probe diffusion (Hall and Torkelson, 1998; Pu et al., 2001b), dewetting behavior (Reiter, 1992, 1993), viscosity (Masson and Green, 2002), hole growth (Dalnoki-Veress et al., 1999; Masson and Green, 2002), phase separation behavior (Krausch et al., 1993; Tanaka et al., 1995; Sung et al., 1996), crystallization (Despotopoulou et al., 1996; Frank et al., 1996b; Jackson and McKenna, 1996; Srivatsan et al., 1997; Sutton et al., 1997), chain conformations (Despotopoulou et al., 1995; Grohens et al., 1997; Jones et al., 1999; Kraus et al., 2000; Muller, 2002) and rheology (Hu and Granick, 1992; Granick and Hu, 1994).

4 Novel Fluorescence Technique as a Characterization Tool

Fluorescence is a powerful tool for investigating the structure and dynamics of matter. In particular, this technique can be very useful in studying physical properties of polymers. The success of fluorescence arises from its high sensitivity, specificity and its ability to provide spatial and temporal information (Valeur, 2002). A brief review on the phenomenon of fluorescence and its use to characterize T_g , physical aging and local polarity of polymers is presented below.

4.1 Phenomenon of Fluorescence

When a fluorescent molecule or fluorophore absorbs energy, the promotion of an electron to an excited singlet state occurs. A subsequent return of the excited state electron to the ground state can take place by many mechanisms, one of which is the emission of a photon (fluorescence). This process is illustrated pictorially in the simplified Jablonski diagram shown in Figure 4-1 (Lakowicz, 1999). Upon absorption of a photon on time scales of 10^{-15} sec, an electron is promoted to one of several vibrational levels in an excited singlet state (S_1, S_2, \dots, S_n); this is followed by an internal conversion relaxation process (spontaneous non-radiative transition between two electronic states of the same spin multiplicity) in which the electron decays to the lowest excited singlet vibrational level (S_1) on the time scale of 10^{-12} sec (Lakowicz, 1999; Sharma and Schulman, 1999; Valeur, 2002). Fluorescence emission occurs as the electron in the lowest singlet vibrational level returns to one of the ground state on the time scale of 10^{-8} sec (Lakowicz, 1999; Sharma and Schulman, 1999; Valeur, 2002).

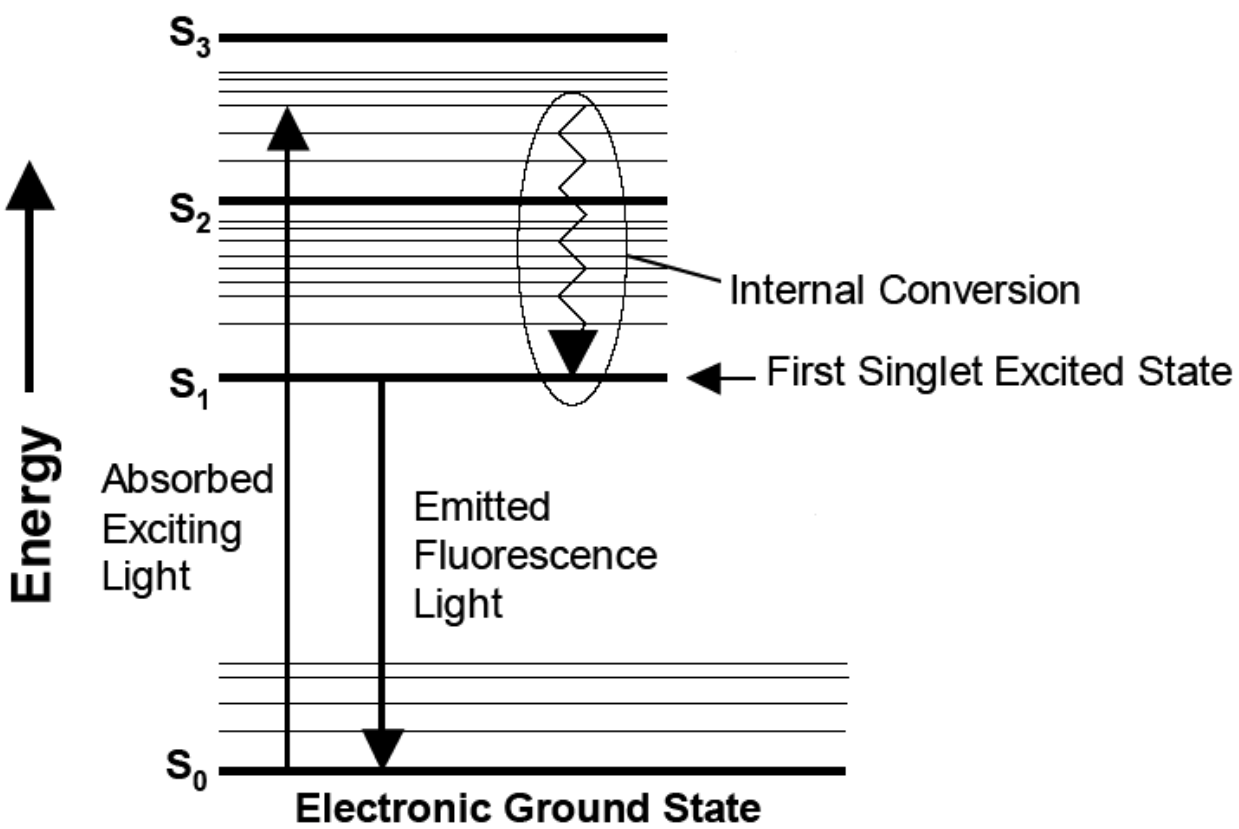


Figure 4-1: Simplified Jablonski diagram. The processes that lead to a photon being emitted as fluorescence include absorbance of a photon that promotes an electron to an excited singlet vibrational state, internal energy conversion and fluorescence emission.

Since energy is lost in the internal conversion, fluorescence emission is observed at longer wavelengths or lower energy than the absorption spectrum. This difference in the spectrum is called the Stokes shift. However, emission and excitation spectra often are mirror images because the differences between vibrational levels are similar in the ground state and the excited state (Lakowicz, 1999; Valeur, 2002). The quantum yield, defined as the ratio of the number of photons emitted to the number of photons absorbed, is used to quantify the fluorescence process efficiency, as it represents the fraction of excited molecules that fluoresce. It is almost never unity because there are other energy dissipation mechanisms, such as collisional deactivation, bond vibration, bond rotation, internal system crossing, intramolecular charge transfer, energy transfer, and conformational changes, that suppress the emission of a photon by releasing the energy of the excited state electron through non-radiative pathways (Schulman, 1977; Lakowicz, 1999; Valeur, 2002).

Experimentally, fluorescence can be classified into two types of measurements: steady state and time-resolved (Lakowicz, 1999). Steady state measurements are performed under constant illumination. The chromophore is excited at an appropriate wavelength to efficiently promote the electrons to an excited electronic state. The fluorescence emission spectrum is obtained by monitoring the emission intensity as a function of wavelength. The excitation spectrum is recorded by monitoring the emission intensity at a single wavelength while scanning the excitation wavelength. On the other hand, time-resolved spectroscopy measures fluorescence intensity decays. Experimentally, the sample is exposed to a pulse of light that is shorter than the decay

time. Intensity decay measurements are recorded with a rapid detection system. The steady state emission intensity is a time average of the fluorescence intensity decay. These two types of fluorescence measurements are related by the following equation:

$$I_{SS} = \int_0^{\infty} I_0 \exp\left(\frac{-t}{\tau}\right) dt = I_0 \tau \quad (4-1)$$

where a single exponential intensity decay is assumed, and I_{SS} is the steady state emission intensity, t is the decay time, τ is the average excited state lifetime, and I_0 is a parameter that depends on the fluorophore concentration and a number of instrumental parameters (Lakowicz, 1999). This relation shows that the steady state intensity I_{SS} is proportional to the average excited state lifetime τ (typically 1-100 ns) (Lakowicz, 1999). A longer fluorescence decay lifetime allows more time for the excited state fluorophore to interact with the surrounding environment before emitting a photon, which may provide more information of the microenvironment compared to a shorter decay lifetime (Lakowicz, 1999). There are several benefits associated with measuring fluorescence lifetime instead of steady state emission. First, the fluorescence decay may be multi-exponential if there are different molecular environments, e.g., in a confined polymer the existence of mobile surface regions and less mobile bulk regions. Secondly, although time-resolved measurements are more complex experiments, the results are independent of sample geometry, refractive index changes and excitation source fluctuations that may affect steady state emission (Lakowicz, 1999).

The pathway by which a probe de-excites depends on various parameters such as polarity, pressure, temperature and viscosity. Therefore, the fluorescence of a

chromophore depends on its surrounding environment (Lakowicz, 1999; Valeur, 2002).

4.2 Polymer Characterization by Fluorescence

Fluorescence is widely used to investigate the properties of chemical, biological and biochemical systems due to the strong influence of the surrounding environment on the fluorescence emission spectrum of the probe molecules (Lakowicz, 1999; Valeur, 2002). In the case of polymers, fluorescence has been used to characterize polymer dynamics in solution and melts, polymer in the glassy state and polymer blends (Winnik, 1986). Here, an overview of fluorescence as a tool to characterize the glass transition temperature, physical aging and local polarity is presented.

4.2.1 Fluorescence Technique for Characterizing T_g

The use of fluorescence in conjunction with molecular rotor probes to measure T_g of polymers was first suggested by Loutfy et al. (Loutfy, 1981; Law and Loutfy, 1983; Loutfy, 1986) more than twenty years ago. Molecular rotor probes provide sensitivity to free volume due to their non-radiative mechanism for dissipation of absorbed energy by bond rotations (Law and Loutfy, 1983). Specifically, Loutfy et al. (Law and Loutfy, 1983; Loutfy, 1986) showed that the fluorescence intensity of a p-N,N-dialkylaminobenzylidene malonitrile rotor probe doped into poly(methyl methacrylate) decreased with increasing temperature and exhibited different temperature dependences above and below the calorimetric T_g with the transition occurring near the calorimetric T_g . Brady and Charlesworth (1993) monitored the intrinsic fluorescence response of an epoxy resin to characterize T_g at the discontinuity in the temperature

dependence of peak intensity. Later, Lenhart et al. (2001) showed a similar sensitivity to T_g in epoxy resins using fluorescence intensity of a 4,4'-dimethylaminonitrostilbene (DANS) probe. In the study, DANS was either doped into the matrix or labeled to a triethoxysilane coupling agent that was grafted to the glass substrate. It was shown that at the epoxy-glass interface, T_g could be higher or lower than the bulk T_g depending on the structure of the silane coupling agent. They suggested that a gradient in properties may be present near the interface and that their interfacial measurements were just an average of the gradient in properties. Also, Hofstraat et al. (1998) reported that T_g could be obtained using the temperature dependence of extrinsic fluorescence in a polyether-polyester block copolymer.

Since 2002, Torkelson and coworkers have used fluorescence spectroscopy to measure T_g of polymeric systems (Ellison et al., 2002; Ellison and Torkelson, 2002, 2003; Ellison et al., 2004; Ellison et al., 2005; Mundra et al., 2006; Rittigstein and Torkelson, 2006; Mundra et al., 2007a; Mundra et al., 2007b; Priestley et al., 2007b; Rittigstein et al., 2007; Roth et al., 2007; Roth and Torkelson, 2007). In these studies, T_g was determined by monitoring the emission intensity as a function of temperature. The determination of T_g was done by fitting lines to the temperature dependences of intensity in both the rubbery and the glassy states, with the intersection of the lines defining T_g . Taking into account the appropriate selection of the probe, the sample preparation and the experimental setup, the T_g determined by fluorescence is nearly identical to the value determined by differential scanning calorimetry (DSC) for all the systems studied by Torkelson and coworkers. The importance of fluorescence as a tool

to characterized T_g in polymers is the potential of the technique to monitor T_g of nanoconfined systems (Ellison et al., 2002; Ellison and Torkelson, 2002).

Ellison et al. (Ellison et al., 2002; Ellison and Torkelson, 2002) presented the first demonstration of the utility of fluorescence probe methods to characterize T_g values in confined polymer films. The T_g s of ultrathin polystyrene films determined by fluorescence were nearly identical to the T_g s obtained using ellipsometry. Later, Ellison and Torkelson developed a fluorescence/multilayer approach that allowed the first determination of a distribution of T_g in a supported polystyrene film, quantifying the impact of different interfaces (Ellison and Torkelson, 2003). In the study, a pyrene-labeled polystyrene film of known thickness was placed atop of a neat polystyrene film of known thickness using a water transfer technique. Fluorescence measurements only provided T_g of the labeled layer. Therefore, fluorescence spectroscopy is a powerful tool to characterize T_g and is the only method currently employed that can be used to measure discrete distributions of T_g (Ellison and Torkelson, 2003).

Recently, Jager et al. (2005) showed that a mobility sensitive color-shifting fluorescent probe could be employed to determine T_g of poly(methyl methacrylate) and polystyrene. In order to obtain T_g , the wavelength of the peak maximum was plotted as a function of temperature. Fitting lines to the fluorescence peak maximum wavelength in the rubbery and the glassy state provides the T_g of the material. The T_g s of poly(methyl methacrylate) and polystyrene measured using the color-shifting probe were consistent with those obtained using DSC.

Also, several studies have plotted the full width half maximum of the fluorescence emission spectrum (de Deus et al., 2004; Martins et al., 2006) or the first moment of the fluorescence intensity (Turrion et al., 2005) as a function of temperature to study the glass transition and secondary relaxation processes. A slope change in the temperature dependence of the parameter as a function of temperature provided a measure of the transition temperature. In addition, these approaches have been used (not convincingly) to monitor different secondary relaxation processes (de Deus et al., 2004; Martins et al., 2006).

4.2.2 Fluorescence Technique for Characterizing Physical Aging

The use of fluorescence spectroscopy to measure physical aging of polymers was first conducted by Meyer et al. (1990) and Schwab and Levy (1990). Meyer et al. (1990) used Auramine O dispersed randomly in poly(vinylacetate) (PVA) to study isothermal physical aging by measuring the time-dependent change in the emission intensity of the probe. During isothermal aging, after a quench from the equilibrium melt, the emission intensity increases as the physical aging proceeds. This result is consistent with measurements of momentary stress relaxation of PVA with time. Schwab and Levy (1990) studied the physical aging response of poly(methyl methacrylate) and amine cured diglycidyl ether of bisphenol A epoxy by monitoring isothermally the emission intensity of [p-(N,N-dialkylamino)benzylidene malononitrile] (DABM) and 4-(N,N-dimethylamino)-4-nitrostilbene (DANS) with time. They found that the emission intensity of the probes increased linearly with logarithmic physical aging time.

Royal and Torkelson studied physical aging in PS, PMMA, poly(vinyl acetate), polycarbonate and poly(isobutyl methacrylate) using rotor fluorophores (Royal and Torkelson, 1990, 1992, 1993). They determined physical aging rates of various glassy polymers by fluorescence methods using the probe julolidenemalononitrile (JMN) (Royal and Torkelson, 1992, 1993). They showed that the dependence of physical aging rates by fluorescence methods agree well with those from specific volume relaxation experiments, demonstrating the free-volume sensitivity of JMN (Royal and Torkelson, 1993). Also, they showed that the times required to reach equilibrium for the enthalpy relaxation experiments are similar to the fluorescence equilibrium times (Royal and Torkelson, 1992). In analogy with the definition of physical aging rate obtained in volumetric relaxation studies (see equation 2-9), a fluorescence physical aging rate r_f may be defined (Royal and Torkelson, 1993; Priestley et al., 2005a; Priestley et al., 2005b) as

$$r_f = -\frac{1}{f_0} \frac{df}{d\text{Log}(t_a)} \quad (4-2)$$

where f_0 is the initial fluorescence intensity and f is the fluorescence intensity at aging time t_a . (The fact that f increases when v decreases accounts for the different sign in equations 2-9 and 4-2.)

Fluorescence spectroscopy presents the same unique advantages for the characterization of physical aging as in the case of T_g . Priestley et al. (2005b) showed that it can be used to measure the distribution of aging rates across a film and the effect of different interfaces on aging.

Recently, van den Berg et al. (2006) employed a wavelength-shifting mobility sensitive fluorescent probe to investigate physical aging of polycarbonate and poly(methyl methacrylate). A linear correlation was found between the emission wavelength of the probe and the specific volume of the polymers. As the physical aging time increases, a blue shift occurs for the peak maximum of the fluorescence emission spectrum. This shift in the emission wavelength was used to determine an effective relaxation time by fitting the relaxation curves to the KWW function (equation 2-1). The aging response of the polymers determined by fluorescence using wavelength-shifting probes was comparable to that observed with other techniques, such as positron annihilation spectroscopy. Therefore, fluorescence employing a color-shifting probe is a reliable method to study physical aging (van den Berg et al., 2006).

4.2.3 Fluorescence Technique for Characterizing Local Polarity

Polarity plays a major role in many physical, chemical, biochemical and biological phenomena. Since the fluorescence of a chromophore depends on its surrounding environment, this technique provides unique opportunities to characterize local polarity in different systems.

In some aromatic molecules that have a high degree of symmetry, such as benzene, triphenylene, naphthalene, pyrene and coronene, the first singlet absorption ($S_0 \rightarrow S_1$) may be symmetry forbidden and the corresponding oscillator strength is weak. The intensities of the various forbidden vibronic bands are highly sensitive to polarity (Valeur, 2002). Nakajima (1971; 1974; 1976a; 1976b) found that the intensities of various vibronic bands of pyrene depend strongly on the solvent environment. In the

presence of polar solvents there is an enhancement in the intensity of the 0-0 band (first peak) at the expenses of others. Dipole-induced dipole interactions between the solvent and pyrene play a major role. The polarity of the solvent determines the extent to which an induced dipole moment is formed by vibrational distortions of the nuclear coordinates of pyrene (Karpovich and Blanchard, 1995). Kalyanasundaram and Thomas (1977) showed that the polarity of an environment can be estimated by measuring the ratio of the fluorescence intensities of the third and first vibronic bands (ratio of the third and first intensity peaks of the spectrum) of pyrene. This ratio ranges from ~1.7 in hydrocarbon media to ~0.5 in dimethyl sulfoxide (Kalyanasundaram and Thomas, 1977). These values provide a polarity scale called the Py scale that correlates with dielectric data (Valeur, 2002).

Pyrene has been used to investigate the extent of water penetration into micelles and to accurately determine micellar concentrations (Kalyanasundaram, 1987). Also, polarity studies of silica and alumina surfaces have been reported using fluorescence (Stahlberg and Almgren, 1985; Hayashi et al., 1995; Imans et al., 1996; Spange et al., 2000).

Gonzalez-Benito et al. (2000) used fluorescence of pyrene-sulfonamide conjugates probe to study the coating microstructure of polyorganosiloxane layer on glass fibers by estimating the interaction of the coating with different solvents (solvent accessibility to the chromophore). The ratio of the intensity peaks was correlated with polarity parameters. They found favorable interactions between the polymer and apolar solvents.

In the rest of this section, we will extend this approach to demonstrate that fluorescence methods using pyrene dye doped into polymers may be useful in indicating how the polarity of a polymeric medium can be affected by interfaces with substrates (in the case of films) or nanoparticles (in the case of nanocomposites).

4.2.3.1 Experimental

Polystyrene (Pressure Chemical, $M_n = 290,000$ g/mol, $M_w/M_n = 1.06$) was used as received. Poly(methyl methacrylate) was synthesized by free radical polymerization ($M_n = 355,000$ g/mol, $M_w/M_n = 1.54$, by gel permeation chromatography (GPC) using universal calibration with PS standards). Poly(2-vinyl pyridine) (Scientific Polymer Products, reported value of $M_v = 200,000$ g/mol) was used after drying the as received material in a vacuum oven at ~ 110 °C to remove residual monomer. Pyrene (Aldrich) and silica nanospheres (colloidal silica in methyl ethyl ketone, Nissan Chemical Industries, reported diameter of 10–15 nm) were used as received.

Thin films of polymers or polymer nanocomposites were prepared by spin coating (Hall et al., 1998b) dilute solutions of polymer, with or without pyrene dye and with or without silica nanofiller, onto quartz slides. Solutions containing nanofiller were sonicated (Branson 1200 sonicator) for 40 min prior to spin coating. Film thicknesses were determined using a Tencor P10 profilometer. Films with thickness less than 500 nm were dried in a fume hood overnight while films with thickness exceeding 500 nm were dried for 48 h in vacuum oven at room temperature. Nanocomposite films were dried for 48 h in a fume hood prior to performing fluorescence measurements. Fluorescence was measured using a SPEX Fluorolog-2DM1B fluorimeter or a Photon

Technology International fluorimeter following procedures described in Ellison et al. (2002), Ellison and Torkelson (2002), Ellison and Torkelson (2003), Ellison et al. (2004), Ellison et al. (2005), Rittigstein and Torkelson (2006), and Rittigstein et al. (2007).

4.2.3.2 Results and Discussion

Taking advantage of the influence of polarity environment on the emission spectrum of pyrene, the impact of nanoconfinement on polymer systems has been studied using fluorescence. Figure 4-2 illustrates the difference in emission intensity of pyrene doped at trace levels in neat polystyrene (PS) and in PS containing 0.5 vol% silica nanoparticles. (The silica nanoparticles have hydroxyl groups on their surfaces which account for a shift in microenvironment polarity.) The spectrum obtained with the PS-silica nanocomposite shows the signature of enhanced medium polarity as defined by Kalyanasundaram and Thomas (Kalyanasundaram and Thomas, 1977).

The impact of silica nanoparticles on PS polarity can be summarized by plotting the temperature dependence of the ratio of fluorescence intensity at 386 nm to that at 374 nm. Figure 4-3a shows the impact on local polarity of different concentrations of silica nanospheres in PS at different temperatures. A reduction in the ratio of intensity at 386 nm to that at 374 nm (I_{386}/I_{374}) means that the microenvironment in the polymer is more polar. While the presence of 0.5 vol% silica nanoparticles reduces this ratio relative to that of neat PS, the data obtained in 0.3 vol% silica-PS nanocomposites are identical to the data for neat PS. Apparently, a critical level of dispersed silica nanoparticles is required before the pyrene fluorescence can sense a shift in medium micropolarity. Figure 4-3b shows results obtained in 24-nm-thick and 500-nm-thick PS

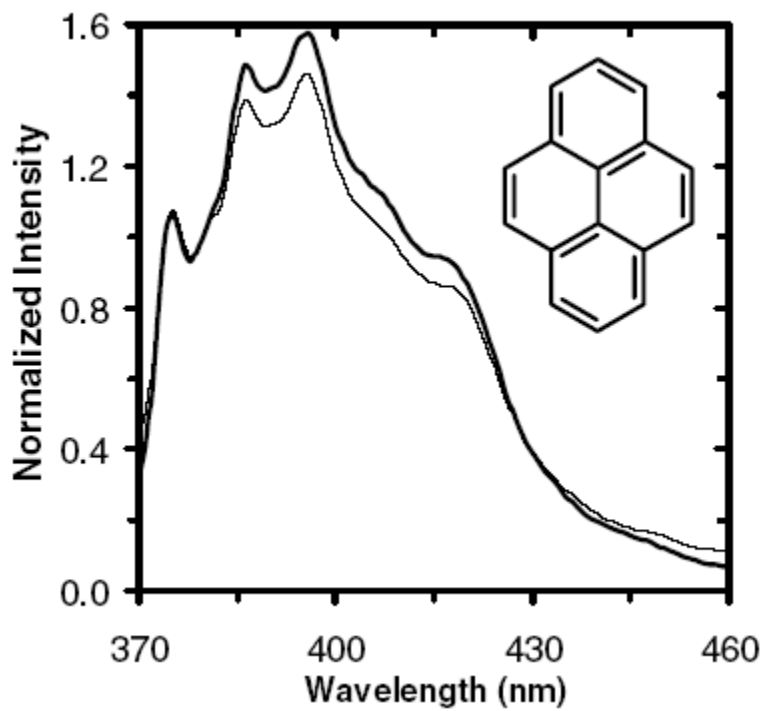


Figure 4-2: Fluorescence emission spectra of pyrene dopant (< 0.2wt%) in a bulk PS film at 418K (bold curve) and in a thick 0.5 vol% silica-PS nanocomposite film at 418K (thin curve). Data have been normalized to unity using the intensity at 374 nm. Inset shows the molecular structure of pyrene.

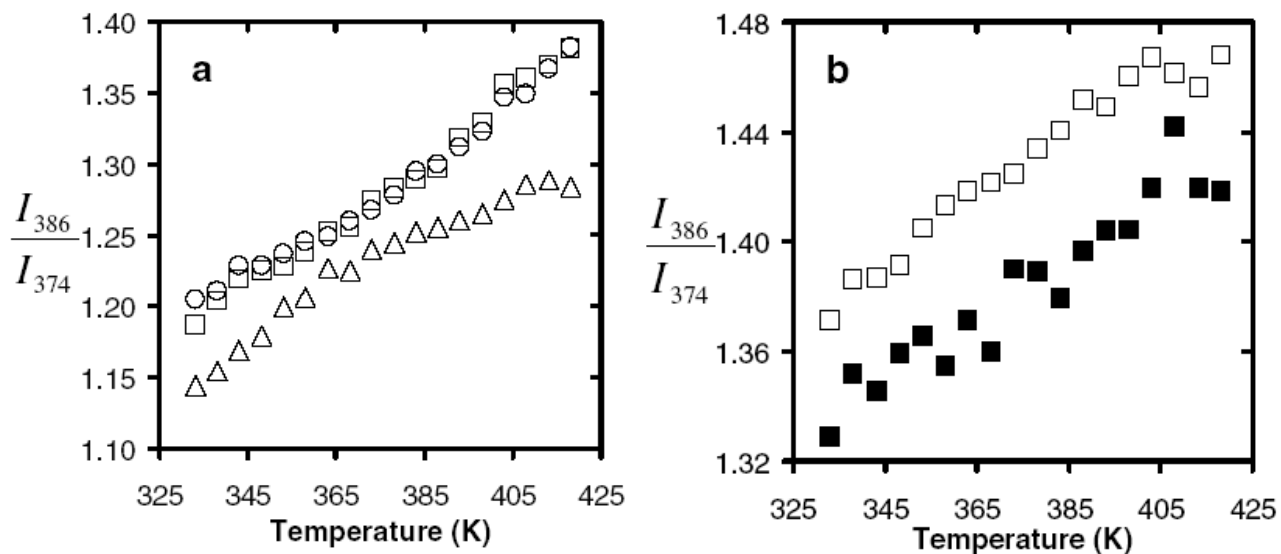


Figure 4-3: Temperature dependence of the intensity ratio of pyrene dopant (< 0.2wt%) in PS films and nanocomposites : a) bulk PS (squares), 0.3 vol% silica-PS nanocomposite (circles), and 0.5 vol% silica-PS nanocomposite (triangles). (All sample thicknesses exceed 1000 nm.) b) 500-nm-thick PS film (open squares) and a 24-nm-thick PS film (closed squares). (Note: Different emission slits were used to take data in Figure 4-3a and Figure 4-3b, which prevents comparison of absolute ratio values between figures.)

films on a silica substrate (with hydroxyl groups on the substrate surface). The fluorescence ratio is smaller in the ultrathin film, indicating a significant increase in medium polarity being sensed by the pyrene dyes. (Different emission slits were used to obtain spectra in the nanocomposites and films; thus, the quantitative values of ratios in Figure 4-3a cannot be compared meaningfully to those in Figure 4-3b. However, comparisons within a figure are meaningful.) Thus, confinement either by nanocomposite formation with silica nanoparticles or by formation of ultrathin films on silica can lead to measurable modifications of effective polarity in PS systems. When similar experiments were done using PMMA and poly(2-vinyl pyridine) (P2VP), no changes in the shape of the pyrene dye emission spectrum were observed within experimental error. The lack of effect in PMMA and P2VP with addition of silica nanospheres is likely associated with the intrinsically polar nature of those two polymers in comparison with the non-polar nature of PS. The P2VP-silica and PMMA-silica interactions block the access of pyrene to the adsorption sites on the nanofiller surface. However, PS does not interact with the nanofiller; thus, the pyrene can interact with the surface of the polar nanoparticle.

5 Distribution of T_g s in Thin and Ultrathin PMMA films

5.1 Introduction

A major intellectual challenge in condensed matter physics is the achievement of a complete understanding of the nature of the glass transition in amorphous materials (1995; Angell, 1995b; Angell et al., 2000; Debenedetti and Stillinger, 2001; Merolle et al., 2005). The cooperatively rearranging region (CRR), a central tenet of the physics of the glass transition (Adam and Gibbs, 1965; Sillescu, 1999; Ediger, 2000; Donth, 2001; Stevenson et al., 2006), is “the smallest region that can undergo a requisite transition to a new configuration without a requisite simultaneous configurational change on and outside its boundary” as defined by Adam and Gibbs (1965). Experimental studies show that the size of a CRR is approximately 1-4 nm (Richert, 1996; Arndt et al., 1997; Tracht et al., 1998; Hempel et al., 2000; Berthier et al., 2005; Ellison et al., 2005) and may be considered as the lower limit for the size of a dynamic heterogeneous region (Ediger, 2000).

Many experimental studies (Forrest et al., 1996; van Zanten et al., 1996; DeMaggio et al., 1997; Fukao and Miyamoto, 2000; Dalnoki-Veress et al., 2001; Fryer et al., 2001; Fukao et al., 2001; Grohens et al., 2002; Ellison and Torkelson, 2003; Ellison et al., 2004; Park et al., 2004; Ellison et al., 2005; Mundra et al., 2006) and simulations (Torres et al., 2000; Varnik et al., 2002; Baljon et al., 2004; Peter et al., 2006; Riggleman et al., 2006) have been carried out in order to characterize and understand the deviations in T_g compared to the bulk state when polymer films are confined to the nanoscale. Two prominent explanations about the impact of

nanoconfinement on T_g are finite size effects and interfacial effects. Finite size effects are hypothesized to occur when the length scale of the system, i.e., film thickness, and the length scale governing T_g , i.e., a CRR, coincide (Fukao and Miyamoto, 2000; Fukao et al., 2001). On the other hand, interfacial effects are expected to increase in significance with an increase in the ratio of interfacial area to volume, altering the segmental mobility of the polymer and therefore the T_g of the nanoconfined system (Keddie et al., 1994a, 1994b; Forrest et al., 1996; Ellison and Torkelson, 2003).

The definition of a CRR has been used to justify two- and three-layer models that offer explanations of the deviation from $T_{g,bulk}$ in nanoscopically confined polymer films (Keddie et al., 1994b; Forrest and Mattsson, 2000). These models assume that perturbations to T_g at the free surface (air-polymer interface) or the polymer-substrate interface are limited to length scales roughly the size of a CRR. (By some interpretations, CRRs are always independent of one another and should not impact the dynamics of adjacent CRRs; with these interpretations, perturbations to T_g at the free surface or substrate interface are believed to be limited to a layer thickness of one CRR and unable to propagate from the interface into the film interior.) However, reductions in T_g from $T_{g,bulk}$ have been reported for films as thick as 300-400 nm when the films lack attractive interactions with the substrate on which they are supported (Ellison et al., 2005). Because of the large difference in the length scale at which T_g -confinement effects have been observed in polymer films and the accepted length scale of a CRR, it can be concluded that deviations in T_g are not directly related to the size scale of a CRR (Forrest et al., 1996). In addition, it is unclear how perturbations limited to the very

small length scale of a CRR can lead to significant changes in the average T_g of polymer films with thicknesses that are one or even two orders of magnitude larger than a CRR.

The picture that T_g dynamics are perturbed by interfacial effects only over the length scale of a CRR has been experimentally refuted by a recent study employing a fluorescence/multilayer technique that found that perturbations to T_g at the free surface of a film are able to propagate into the film interior (Ellison and Torkelson, 2003). In particular, this study showed that the perturbed T_g dynamics at the free surface of polystyrene (PS) led to T_g s differing from $T_{g,\text{bulk}}$ at distances of several tens of nanometers from the PS free surface. This behavior was explained to result from the strongly perturbed CRRs in the free-surface layer affecting the average cooperative dynamics in adjoining layers of CRRs, and to a lesser extent the CRRs of the next layer, and so on.

This chapter reports the first study to characterize the distribution of T_g s for polymer films that possess strong attractive interactions with the substrate. The results demonstrate not only that strongly perturbed T_g behavior in an interfacial layer of a polymer film propagates over length scales equivalent to a number of layers of CRRs but that perturbations to T_g caused by attractive interactions with the substrate can be observed over length scales of several hundred nanometers. This was accomplished using a fluorescence/multilayer method (Ellison and Torkelson, 2003; Ellison et al., 2004; Ellison et al., 2005; Priestley et al., 2005a; Priestley et al., 2005b) to measure T_g in layers at the free surface, substrate-polymer interface, and known distances away

from the interfaces of poly(methyl methacrylate) (PMMA) films supported on silica. It is observed that the free surface and substrate act in opposition to one another in modifying T_g dynamics. For example, the T_g of a 12-nm-thick free-surface layer of a bulk PMMA film is reduced by 7-8 K compared with $T_{g,bulk}$ while the T_g of a 12-nm-thick substrate layer of a bulk PMMA film is increased by 10 K compared with $T_{g,bulk}$. Using a bilayer film geometry in which the T_g of a 12-nm-thick free-surface layer is measured as a function of confinement of the overall film, it is demonstrated that perturbed T_g dynamics at the substrate interface can percolate across a 200-nm-thick PMMA film to affect the T_g dynamics at the free surface. Furthermore, when the overall PMMA film thickness is less than 90 nm, the T_g in the free-surface layer actually exceeds $T_{g,bulk}$. This behavior can occur only if perturbations to T_g dynamics propagate over many layers of CRRs. These results disallow the simple layer models as explanations of T_g -confinement effects and, more importantly, require re-evaluation of the interpretation of the CRR.

5.2 Experimental

Poly(methyl methacrylate) is synthesized by free radical polymerization, with $M_n = 355,000$ g/mol and $PDI = 1.54$ obtained by gel permeation chromatography (universal calibration relative to PS standards). The onset $T_g = 394$ K, as determined by DSC (Mettler Toledo DSC822e) on second heating with a heating rate of 10 K/min. The chromophore 4-tricyanovinyl-[N-(2-hydroxyethyl)-N-ethyl]aniline (TC1) is synthesized by reaction with tetracyanoethylene (TC1 America) and 2-(N-ethylaniline)ethanol (TC1

America) dissolved in dimethyl formamide (Fisher) at 55 °C for 15 min and then recrystallized from glacial acetic acid. The 1-pyrenyl butanol-labeled (Aldrich) and TC1-labeled methacrylate monomers are synthesized through an esterification reaction with methacryloyl chloride (Aldrich) in the presence of triethylamine (Aldrich) and dichloromethane (Aldrich) at 0 °C for 2 h. Labeled PMMA is synthesized by reaction of MMA monomer (Aldrich) in the presence of a trace amount of either pyrene-labeled or TC1-labeled methacrylate monomer. The pyrene-labeled PMMA contains 1.22 mol % (1 in 82 repeat units) of pyrene-labeled monomer and the TC1-labeled PMMA contains 1.37 mol% (1 in 73 repeat units) of the TC1-labeled monomer determined by UV-Vis absorbance spectroscopy (Perkin Elmer Lambda 35). For pyrene-labeled PMMA, $M_n = 456,000$ g/mol, $PDI = 2.0$, and the onset $T_g = 395$ K. For TC1-labeled PMMA, $M_n = 509,000$ g/mol, $PDI = 1.67$, and the onset $T_g = 394$ K. All polymer is washed by dissolving in toluene (Fisher) and precipitating in methanol (Fisher) at least five times to remove residual solvent and then dried in a vacuum oven at $T_g + 15$ K for 24 h.

Single-layer films are prepared by spin casting polymer/toluene solutions onto quartz slides (Hall et al., 1998b). The films are allowed to dry in vacuum at $T_g + 5$ K for 8 h. Multilayer films are prepared by spin casting polymer/toluene solutions onto either a quartz slide or a NaCl salt disk. Films spun cast onto NaCl salt disks are floated on top of films spun cast onto quartz slides by submersing the salt disk in a water bath. After preparation of the multilayer film, it is dried in vacuum at room temperature for 12 h and then annealed at $T_g + 25$ K for 10 min to ensure a completely consolidated film. Film thicknesses are measured with a Tencor P10 profilometer.

All polymers were of sufficiently high molecular weight to ensure that interlayer diffusion is at most several nanometers during the experimental time, which includes the time to create a consolidated film. The estimated interlayer diffusion can be determined from nuclear reaction analysis data (Shearmur et al., 1998). For the conditions employed in this study, the total diffusion time of 40 min is much less than the polymer disentanglement time. The disentanglement time can be calculated by the following equation: $\tau_D = (2R_g^2)/(\pi^2 D_s)$, where R_g is the radius of gyration of the polymer and D_s is the bulk self-diffusion coefficient. For PMMA (lowest molecular weight and fastest diffusing component used in these studies) at $T_g + 25$ K, the disentanglement time is 3850 min using $D_s = \sim 3 \times 10^{-18}$ cm²/s from nuclear reaction analysis diffusion data (Shearmur et al., 1998). Since the total experimental time above T_g is substantially smaller than the disentanglement time (experimental time above T_g is only 1% of disentanglement time), the maximum interlayer penetration distance is substantially less than the PMMA R_g (~ 18.5 nm), with a reasonable estimate of a few nanometers. It is important to note that the above estimate is an upper limit as the polymer used in the study (355,000 g/mol, 456,000 g/mol and 509,000 g/mol) is of higher molecular weight than that used in the interlayer diffusion study (100,000 g/mol and 127,000 g/mol) (Shearmur et al., 1998).

Steady-state fluorescence emission spectra are taken as a function of temperature (on cooling) using a Photon Technology International fluorimeter in a front-face geometry (with emission at 90° relative to excitation and the film at an angle of 28° relative to excitation) with 3.0 mm excitation and emission slits (12 nm bandpass) used

for TC1-labeled PMMA experiments and 1.25 mm excitation and emission slits (5 nm bandpass) used for pyrene-labeled PMMA experiments. The wavelength used to excite the TC1 and pyrene is 480 nm and 254 nm, respectively. The emission spectrum of TC1 and pyrene is measured at 540-690 nm and 360-460 nm, respectively. The T_g values of the labeled films are determined by fitting the temperature dependence of the integrated fluorescence intensity to linear correlations in both the rubbery and glassy states. In fitting the data to linear correlations, only data well outside T_g are used in the fitting procedure. (Additional information on the fluorescence technique used to monitor T_g is found in chapters 4, 6, 7 and 9.)

5.3 Results and Discussion

The fluorescence of chromophores covalently attached (labeled) to the polymer at trace levels was used to measure T_g in single-layer and multilayer PMMA films supported on silica substrates. Multilayer films consist of a single, labeled PMMA layer and one or two unlabeled PMMA layers of known thickness. Heating the multilayer films for a short time above T_g produces a consolidated film. The polymer is of sufficiently high molecular weight to ensure that labeled PMMA diffuses, at most, a few nanometers during the measurements. (See section 5.2 for further detail.)

Figure 5-1 shows the normalized integrated fluorescence intensity as a function of temperature for pyrene-labeled and 4-tricyanovinyl-[N-(2-hydroxyethyl)-N-ethyl]aniline (TC1)-labeled PMMA films. Data points were obtained by taking the integrated intensity of the fluorescence emission spectrum of the labeled polymer as a function of

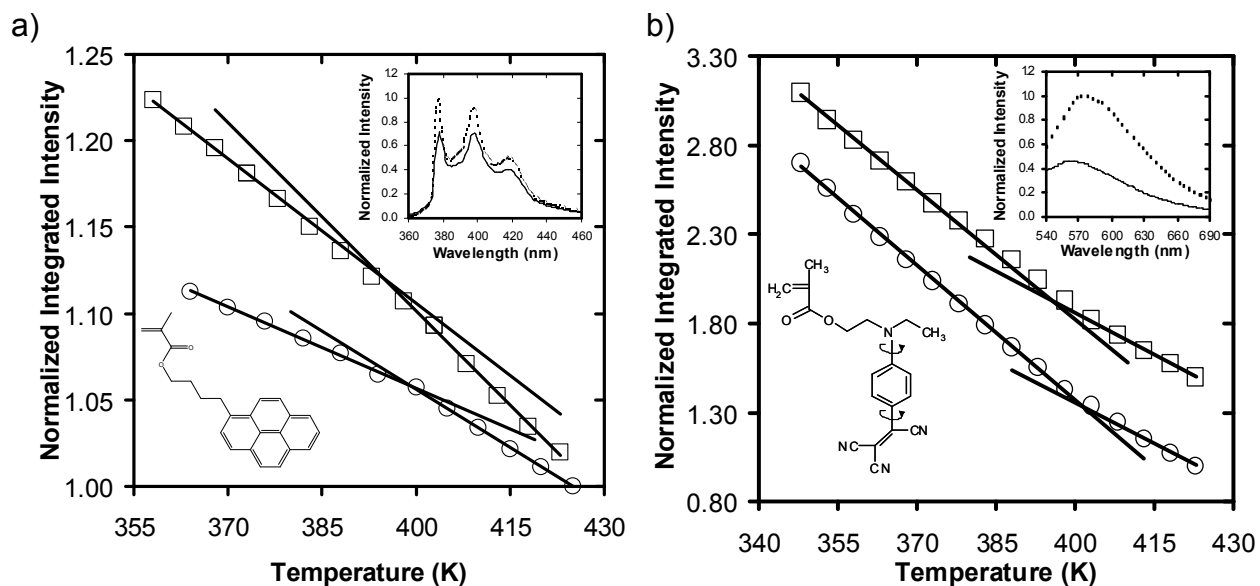


Figure 5-1: T_g data from bulk PMMA and PMMA confined films determined via fluorescence. a) Temperature dependence of the normalized integrated fluorescence intensity of 250-nm-thick (open squares) and 50-nm-thick (open circles) pyrene-labeled PMMA films. The solid lines are fits of the data in both the rubbery and glassy states, with the intersections of the lines defining T_g . (Insets: Emission spectra of pyrene at 423 K (solid line) and 358 K (dotted line) of the 250-nm-thick film and the molecular structure of pyrene.) b) Temperature dependence of the normalized integrated fluorescence intensity of 200-nm-thick (open squares) and 35-nm-thick (open circles) TC1-labeled PMMA films. The solid lines are fits of the data in both the rubbery and glassy states, with the intersection of the lines defining T_g . (Insets: Emission spectra of TC1 at 423 K (solid line) and 358 K (dotted line) of the 200-nm-thick film and the molecular structure of TC1.)

temperature. (See insets in Figure 5-1.) Linear correlations were fit to data points in both the rubbery and glassy states, with the intersection providing a measure of T_g . The T_g values of the 250-nm-thick pyrene-labeled PMMA and 200-nm-thick TC1-labeled PMMA films are 394 K and 395 K, respectively, and are within 1 K of $T_{g,bulk}$ determined by differential scanning calorimetry (DSC) of the labeled PMMA.

While the values of T_g obtained using pyrene- and TC1-labeled PMMA are consistent, the temperature dependence of the fluorescence intensity exhibited by both chromophores are opposite. This difference is related to the dissimilar mechanism by which each chromophore undergoes non-radiative decay from its excited state. Pyrene, a band definition chromophore, undergoes non-radiative decay by vibrational motions (Lakowicz, 1999; Valeur, 2002); thus, the emission intensity follows the density of the polymer and the temperature dependence of the emission intensity is smaller below T_g than above T_g . Numerous band definition chromophores have been used to determine T_g in bulk polymeric glass formers (Meyer et al., 1990; Ellison and Torkelson, 2002, 2003; de Deus et al., 2004; Ellison et al., 2004; Ellison et al., 2005; Priestley et al., 2005a; Priestley et al., 2005b; Turrion et al., 2005). The TC1 dye, a “rotor” chromophore, undergoes non-radiative decay by rotational motion as depicted by the inset in Figure 5-1b (Valeur, 2002). To facilitate the rotational motion of the chromophore, a certain amount of free volume is required (Loutfy and Arnold, 1982); thus, it is believed that changes in polymer density impede the rotational motion to a greater extent in the glassy state than in the liquid state. As a result, the temperature dependence of the emission intensity is greater in the glassy state than in the rubbery

state. Because of the enhanced sensitivity of “rotor” chromophores to density changes that occur in the glassy state, they have been widely used to monitor physical aging of polymeric glass formers (Meyer et al., 1990; Royal and Torkelson, 1992, 1993; Ellison et al., 2002; Ellison and Torkelson, 2002; Priestley et al., 2005a; Priestley et al., 2005b; Rittigstein and Torkelson, 2006; Rittigstein et al., 2007).

According to Figure 5-1, the T_g s of a 50-nm-thick pyrene-labeled PMMA film and a 35-nm-thick TC1-labeled-PMMA film are 399 K and 402 K, respectively. This indicates that there is an increase in T_g with decreasing film thickness for PMMA films supported on silica. The increase in T_g with decreasing thickness is related to hydrogen bond formation that can occur between the ester groups on PMMA and the hydroxyl groups on the silica substrate (Keddie et al., 1994a; Grohens et al., 2002; Priestley et al., 2005a; Priestley et al., 2005b; Rittigstein et al., 2007). The formation of hydrogen bonds is believed to reduce the cooperative segmental mobility of the polymer at and near the silica interface, thus resulting in an increase in T_g with decreasing film thickness as the ratio of interfacial area to volume becomes increasingly large.

Figure 5-2 shows the effect of film thickness (d) on $T_g(\text{film}) - T_g(\text{bulk})$ obtained by fluorescence of pyrene- and TC1-labeled PMMA films. The increase in T_g with decreasing film thickness is identical for pyrene- and TC1-labeled PMMA films and is qualitatively consistent with other studies of single-layer PMMA films supported on silica substrates (Keddie et al., 1994a; Fryer et al., 2001; Park et al., 2004). For $d > \sim 90$ nm, T_g is independent of thickness. For $d < \sim 90$ nm, T_g increases roughly linearly on a

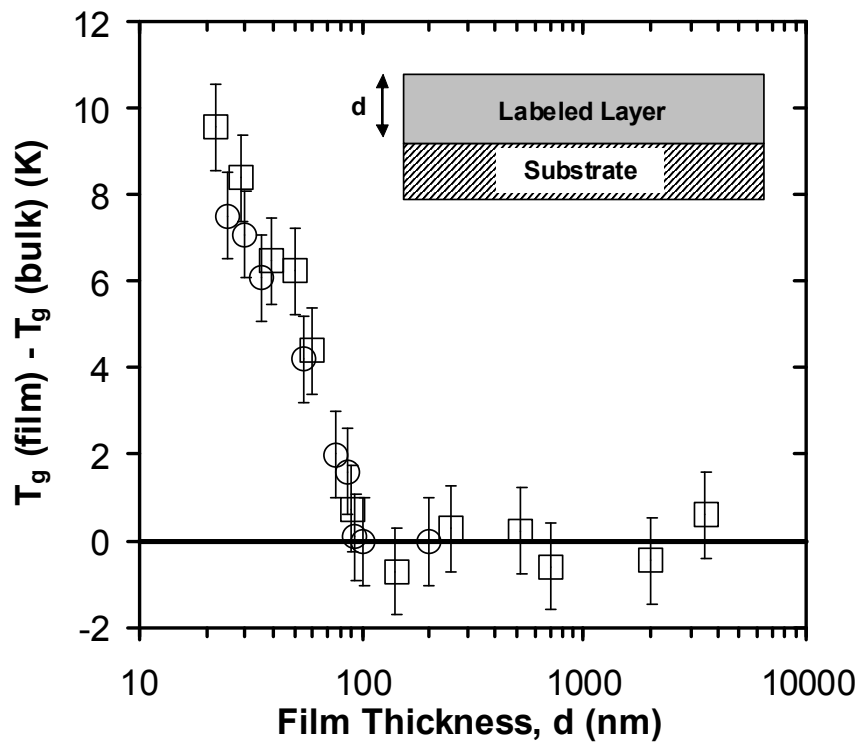


Figure 5-2: $T_g(\text{film}) - T_g(\text{bulk})$ of pyrene-labeled PMMA (open square) and TC1-labeled PMMA (open circles) single layer films as a function of film thickness (d). Within experimental error, both chromophores detect identical increases in T_g as a function of film thickness. (Inset: Film geometry used in experiments.)

logarithmic scale with decreasing thickness. For a 20-nm-thick film, $T_g(\text{film}) - T_g(\text{bulk}) = 9 \text{ K}$.

The direct impact of the substrate on the local T_g near the polymer-substrate interface of a bulk PMMA film is determined using a bilayer film geometry (see Figure 5-3a inset) in which a labeled PMMA layer of known thickness (h) is sandwiched between the substrate and an unlabeled PMMA layer which is 240 nm thick. The overall bilayer film thickness is sufficiently large that $T_g(\text{film}) = T_g(\text{bulk})$. Figure 5-3a shows that $T_g(\text{substrate layer}) - T_g(\text{bulk}) = 10 \text{ K}$ for a 12-nm-thick substrate layer. When the thickness of the substrate layer is increased, the value of $T_g(\text{substrate layer}) - T_g(\text{bulk})$ gradually approaches zero at $h = 70\text{-}80 \text{ nm}$. In a similar experiment with a 14-nm-thick substrate layer in a bulk PS bilayer film, Ellison and Torkelson (2003) found that $T_g(\text{substrate layer}) - T_g(\text{bulk}) = 0 \text{ K}$. The difference in the T_g behavior of the PS and PMMA substrate layers can be explained by hydrogen bonding effects that are present at the PMMA/silica substrate interface (Keddie et al., 1994a; Grohens et al., 2002; Park et al., 2004; Priestley et al., 2005a; Priestley et al., 2005b; Rittigstein et al., 2007) but absent at the PS/silica substrate interface (Keddie et al., 1994a, 1994b; Ellison and Torkelson, 2003; Ellison et al., 2005; Rittigstein et al., 2007).

Placement of a labeled PMMA layer atop a bulk film allows for local T_g measurements at the free surface of PMMA. Labeled PMMA layers of known h are floated onto the surface of a 240-nm-thick PMMA film supported on silica. The overall bilayer film thickness is sufficiently large that $T_g(\text{film}) = T_g(\text{bulk})$. The impact of the free surface on modifying T_g dynamics is opposite that of the silica substrate. Figure 5-3b

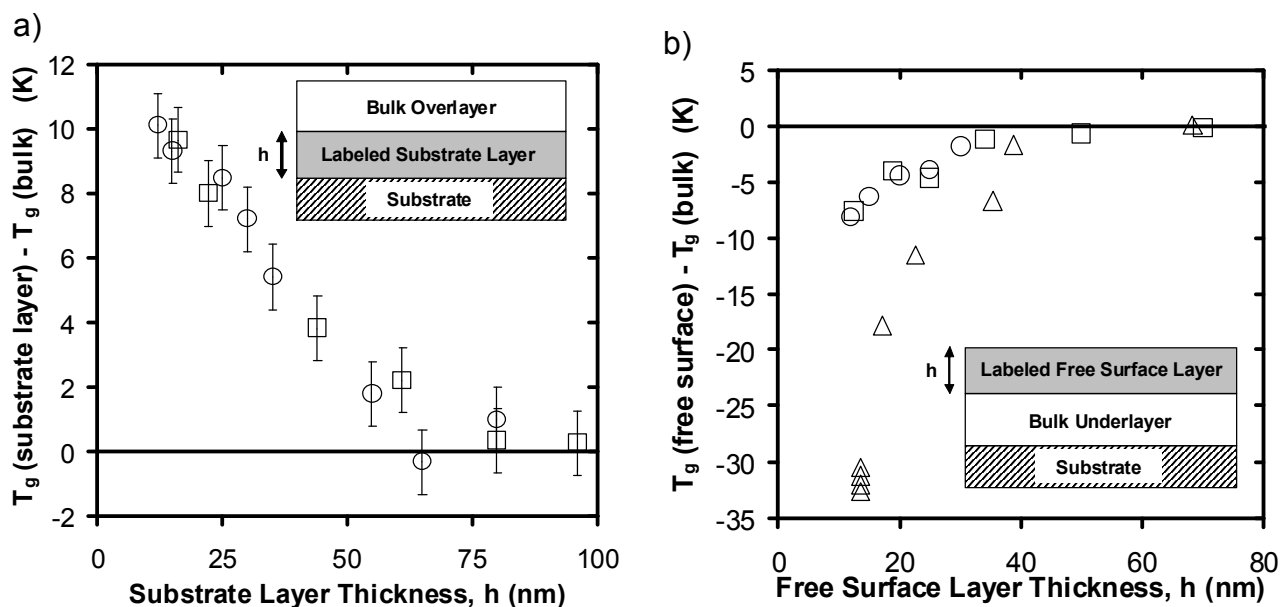


Figure 5-3: Measurement of substrate- and free-surface layer T_g values using bilayer films in which one layer is labeled with either pyrene (open squares) or TC1 (open circles). a) $T_g(\text{substrate layer}) - T_g(\text{bulk})$ of labeled substrate layer film as a function of the labeled substrate layer film thickness (h). Film thickness of bulk overlayer film is 240 nm. (Inset: Film geometry used in experiments.) b) $T_g(\text{free surface}) - T_g(\text{bulk})$ of label free-surface layer film as a function of free-surface layer film thickness (h). Thickness of bulk underlayer is 240 nm. Pyrene-labeled PS data (open triangles) are from Ellison and Torkelson (2003). (Inset: Film geometry used in experiments.)

shows that $T_g(\text{free surface}) - T_g(\text{bulk}) = -7-8 \text{ K}$ for a 12-nm-thick free-surface layer. When the thickness of the labeled free-surface layer is increased, the value of $T_g(\text{free surface}) - T_g(\text{bulk})$ gradually approaches zero at $h = 40 \text{ nm}$. For purposes of comparison, the free-surface layer T_g measurements of PS from Ellison and Torkelson (2003) are replotted in Figure 5-3b. As seen in Figure 5-3b, the free-surface layer thicknesses at which PMMA and PS begin to exhibit reductions in T_g are approximately the same. However, the magnitude of the reduction in T_g at the free surface is much weaker in PMMA than in PS. These results demonstrate that the ability of a free surface to perturb T_g dynamics is strongly dependent on chemical structure of the polymer. This observation is in accord with T_g measurements done on 40-nm-thick freely standing (two free surfaces) PMMA ($M_n = 718,000 \text{ g/mol}$) and PS ($M_n = 690,000 \text{ g/mol}$) films, for which the values of T_g were reduced by $\sim 15 \text{ K}$ and $\sim 52 \text{ K}$, respectively, compared to $T_{g,\text{bulk}}$ (Roth and Dutcher, 2003).

Regarding the effects of surfaces and interfaces on T_g shown in Figure 5-3, the increase in T_g near the silica substrate is understood qualitatively to arise from hydrogen bonding interactions between the ester side groups of PMMA and the hydroxyl groups on the silica substrate. In the absence of hydrogen bonding interactions, as in the case of PS films supported on silica substrates, no change in T_g is expected or observed. In contrast, the underlying cause of the large difference in the magnitude of the free surface effects in PMMA and PS films is not yet understood even at a qualitative level. There is no molecular-scale mechanism or theory by which to

explain the observations. Further study of the effect of repeat unit structure on perturbations to T_g at free surfaces of films is warranted.

Employing a 12-nm-thick labeled middle layer, trilayer films are used to determine the length scale over which the free surface and substrate modify T_g dynamics within bulk PMMA films. As illustrated in Figure 5-4, when an 8-nm-thick unlabeled free-surface layer is placed on top of a 12-nm-thick labeled middle layer (meaning that the labeled-layer depth within the film is 8-20 nm), the T_g of the labeled layer is reduced by only 2 K compared to $T_{g,bulk}$. When the unlabeled free-surface layer thickness is 12 nm, the labeled middle layer reports $T_{g,bulk}$. In the opposite case, when a 12-nm-thick labeled middle layer is displaced 12 nm from the substrate interface, its T_g is increased by 5 K compared to $T_{g,bulk}$. As shown in Figure 5-4, it is not until the labeled middle layer is displaced ~ 50 -70 nm from the substrate interface that it reports a T_g value that is within experimental error equal to $T_{g,bulk}$.

These experiments demonstrate several key points. First, there is a distribution of T_g s near the free surface and substrate interface of bulk PMMA films supported on silica substrates. Second, the results disallow the concept of simple two- and three-layer models to explain the T_g -confinement effect (Keddie et al., 1994b; Forrest and Mattsson, 2000) and instead imply that a distribution of T_g s should be incorporated into any model being used to explain T_g -confinement behavior (Ellison and Torkelson, 2003). Third, the length scale over which the substrate interactions modify T_g dynamics within a bulk PMMA film is greater than that associated with free-surface effects,

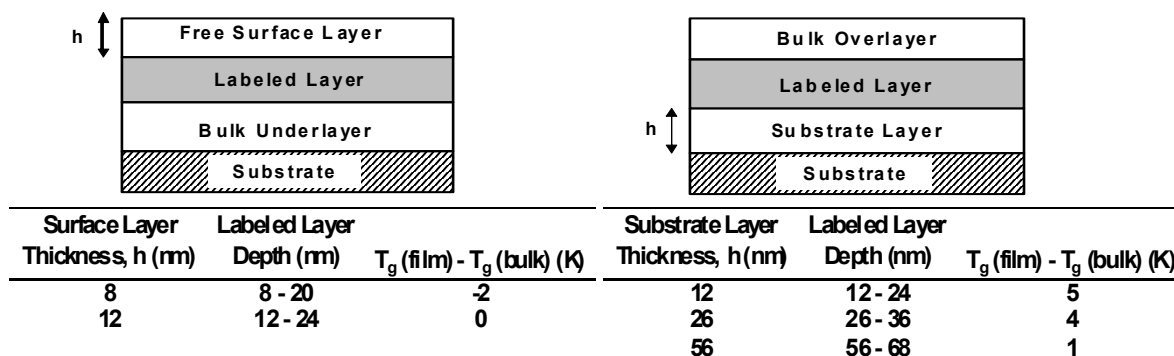


Figure 5-4: Determination of the distribution of T_g s as a function of depth displaced from either the free surface or substrate-polymer interface using trilayer films in which the middle layer is labeled with either pyrene or TC1. Labeled middle layer is 12-nm-thick, while bulk overlayer/ underlayer film thickness is 240 nm. Free surface/ substrate layer film thickness (h) is varied in trilayer film studies.

consistent with the notion that perturbations to T_g caused by substrate effects are stronger than those caused by free-surface effects for PMMA supported on silica.

Figure 5-5 allows us to quantify the relative strengths of the competing free-surface and substrate effects and the length scales over which the stronger substrate effects modify T_g dynamics in confined PMMA films. Specifically, the impact of the substrate on the T_g of a 12-nm-thick labeled free-surface layer is measured as a function of overall film thickness (h'). The length scale separating the 12-nm-thick free-surface layer from the substrate is adjusted by controlling the underlayer thickness. As shown in Figure 5-5, when $h' > 250$ nm (I), the T_g within the free-surface layer is reduced by 7-8 K from $T_{g,\text{bulk}}$. At these thicknesses, the free-surface T_g dynamics are unaffected by the increased T_g at the polymer-substrate interface. When 90 nm $< h' < 250$ nm (II), the free-surface layer T_g increases with decreasing h' but remains below $T_{g,\text{bulk}}$. At these thicknesses, the effects of the strongly reduced cooperative segmental mobility at the polymer-substrate interface percolate across the film, increasing the free-surface layer T_g . When $h' < 90$ nm (III), the T_g within the free-surface layer actually exceeds $T_{g,\text{bulk}}$ and continues to increase with decreasing h' ; this means that the perturbed T_g dynamics at the substrate that percolate across the film are sufficiently strong within the free-surface layer to dominate the perturbations to T_g caused by the free surface. Thus, under certain circumstances of confinement with attractive polymer-substrate interactions, the T_g of an ultrathin free-surface layer may exceed $T_{g,\text{bulk}}$. This is the first report of such an effect.

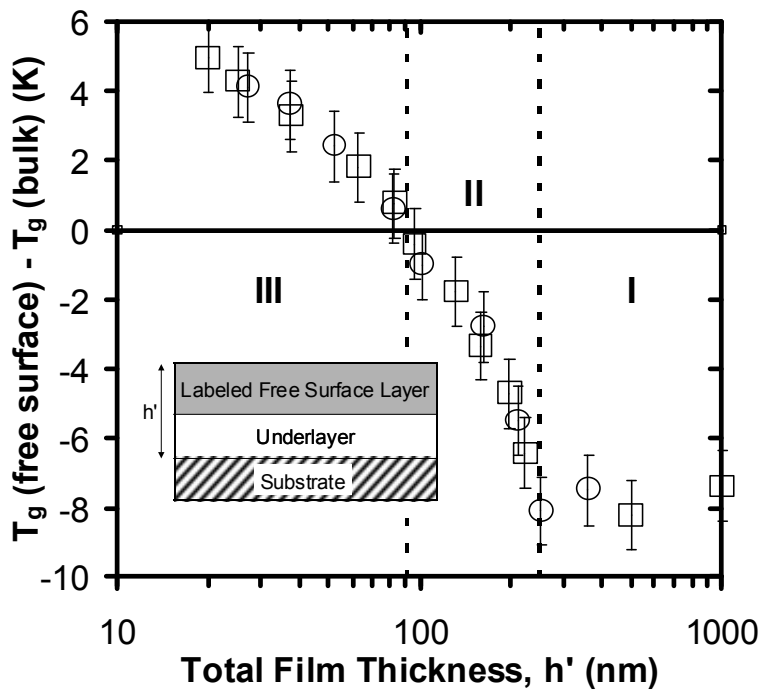


Figure 5-5: $T_g(\text{free surface}) - T_g(\text{bulk})$ of pyrene-labeled (open square) or TC1-labeled (open circles) free surface layer as a function of overall film thickness (h'). The labeled-free surface layer thickness is held constant at 12 nm while the underlayer thickness is varied.

Figure 5-6 illustrates the effect of overall film thickness on $T_g(\text{substrate layer}) - T_g(\text{bulk})$ of a 12-nm-thick substrate layer within a PMMA bilayer film. When the overall film thickness is 250-260 nm, $T_g(\text{substrate layer}) - T_g(\text{bulk}) = 9-10$ K. As shown in Figure 5-6, decreasing the overall thickness results in a decrease in the substrate layer T_g . When the overall thickness of the bilayer film is reduced to 50-60 nm, $T_g(\text{substrate layer}) - T_g(\text{bulk}) = 7$ K. Further reduction of the overall thickness to 35-40 nm leads to $T_g(\text{substrate layer}) - T_g(\text{bulk}) = 3-4$ K.

According to Figure 5-5 and Figure 5-6, when the overall bilayer film thickness exceeds 250 nm, $T_g(\text{free surface}) - T_g(\text{bulk}) = - (7-8)$ K for a 12-nm-thick free-surface layer and $T_g(\text{substrate layer}) - T_g(\text{bulk}) = 9-10$ K for a 12-nm-thick substrate layer. The difference between the T_g s at the free surface and substrate is 16-18 K. When the overall bilayer film thickness is reduced to 35-40 nm, $T_g(\text{free surface}) - T_g(\text{bulk}) = 3-4$ K for a 12-nm-thick free-surface layer as well as for a 12-nm-thick substrate layer. The difference between the T_g s at the free surface and substrate is 0 K. We also note that in 35- to 40-nm-thick bilayer films, the T_g s of the free-surface and substrate layers are identical within experimental error to the T_g of a 35- to 40-nm-thick single-layer PMMA film (see Figure 5-2). Thus, with increasing nanoscale confinement, the gradient in T_g across a PMMA film is reduced and, within the experimental uncertainty of our multilayer method, can be eliminated under circumstances of extreme confinement. The observation that confinement leads to a reduction in the gradient in T_g across a PMMA film is consistent with similar measurements conducted on PS films (Ellison and Torkelson, 2003). The results associated with both PS and PMMA films indicate that

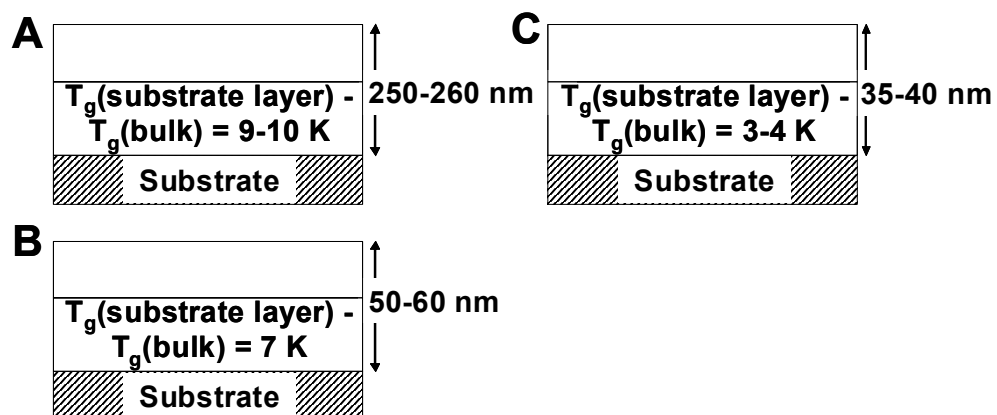


Figure 5-6: Influence of overall film thickness on $T_g(\text{substrate layer}) - T_g(\text{bulk})$ of a 12-nm-thick substrate layer within a bilayer film. The overall film thickness is (a) 250-260 nm, (b) 50-60 nm and (c) 35-40 nm.

below a certain overall thickness the T_g dynamics adjust to satisfy the constraint that the gradient in T_g dynamics across an ultrathin polymer film cannot be too sharp and abrupt (Ellison and Torkelson, 2003).

A comparison of Figure 5-2 and Figure 5-3a reveals that $T_g(\text{film}) - T_g(\text{bulk}) = 6$ K for a 50-nm-thick single-layer PMMA film and $T_g(\text{substrate layer}) - T_g(\text{bulk}) = 2$ K for a 50-nm-thick substrate-layer in a bulk bilayer PMMA film. This indicates that placing a layer with bulk T_g dynamics over a 50-nm-thick substrate layer can lead to faster cooperative dynamics and a lower T_g in the substrate layer. The observation that the T_g dynamics of a layer is affected by the dynamics of an adjacent layer has been previously reported for PS films (Ellison and Torkelson, 2003). For example, the T_g of a 14-nm-thick labeled PS free-surface layer in a bulk bilayer film is ~ 5 K higher than the T_g of a 14-nm-thick single-layer film. This indicates that placing a PS layer with average bulk T_g dynamics underneath a 14-nm-thick PS layer results in slower cooperative dynamics and a higher T_g in the free-surface layer.

This latter observation has recently been explained in the context of the coupling model (Ngai, 2006), which recognizes the importance of many-molecule or many-segment relaxation dynamics associated with the glass transition. The placement of a bulk layer with slower dynamics underneath a 14-nm-thick surface layer imposes intersegmental constraints on the surface layer. These constraints result in slower dynamics and a higher T_g in the 14-nm-thick free surface layer than in the 14-nm-thick film (Ngai, 2006). A similar explanation can be given for some of the PMMA results. Placement of a layer with bulk T_g dynamics atop a 50-nm-thick substrate layer imposes

intersegmental interactions on the substrate layer, resulting in faster dynamics and a lower T_g . However, it is worth mentioning that $T_g - T_{g,bulk} = 9$ K for both 20-nm-thick single-layer film and 20-nm-thick substrate layer in a bulk bilayer film. Thus, for a 20-nm-thick film in which it is possible for most of the PMMA chains to be pinned at the substrate interface (Baschnagel et al., 2003) via hydrogen bonds, placing a thick layer atop it has no measurable impact on its T_g . This means that the substrate effects are strong enough to dominate any effects of intermolecular interactions imposed by the bulk overlayer film.

The results reported in Figure 5-3 and Figure 5-6 can occur only if perturbations caused by surfaces or interfaces to T_g dynamics propagate many layers of CRRs within the films. That is, if on average the cooperative dynamics in a layer are perturbed substantially relative to bulk, then, on average, many adjoining layers must also have their dynamics perturbed, although to lesser extents. This idea is consistent with simulations (Donati et al., 1998; Glotzer, 2000) and experiments (Weeks et al., 2000; Ellison and Torkelson, 2003) indicating that glass-formers do not typically have abrupt transitions in neighboring regions of local dynamic heterogeneity from very fast dynamics to slow dynamics and is consistent with dielectric noise studies (Russell and Israeloff, 2000) suggesting that a minimum length scale (> 40 nm) is required to obtain the full breadth of the distribution of cooperative relaxation dynamics in polymers near T_g .

From a scientific point of view, the results in Figure 5-3 to Figure 5-6, associated with T_g behavior that is strongly perturbed by interfacial effects, stand in opposition to

the simple definition of a CRR offered more than forty years ago (Adam and Gibbs, 1965) in which configurational changes within a CRR are assumed to occur independently of neighboring CRRs. Instead, the results highlight the long-range effects of substrate interactions on T_g dynamics and are qualitatively consistent with recent models (Long and Lequeux, 2001; Merabia et al., 2004) and simulations (Baljon et al., 2004) suggesting that percolation of slow-relaxing regions associated with attractive polymer-substrate interactions can explain enhancements in average T_g s in confined films.

5.4 Conclusions

The study in this chapter employs an innovative fluorescence/multilayer method to investigate the impact of confinement and interfacial effects on the T_g of PMMA films supported on silica substrates. With single-layer PMMA films that are less than 90-nm-thick, T_g increases roughly linearly with decreasing logarithmic thickness. The use of bilayer films reveals that compared to $T_{g,bulk}$, T_g is reduced at the free surface by 7-8 K for a 12-nm-thick free-surface layer and increased at the substrate interface by 10 K for a 12-nm-thick substrate layer of a bulk film, resulting in a T_g -gradient across the film. Measurements of confined bilayer films reveal that the stronger substrate effects percolate across the film to modify the T_g dynamics at the free surface. Thus, with nanoconfinement, the stronger substrate effects dominate the free-surface effects, providing an explanation for the increase in average T_g with decreasing single-layer PMMA film thickness. With extreme confinement, the T_g -gradient across the film

thickness is suppressed, with both substrate layer and free-surface layer T_g s exceeding $T_{g,\text{bulk}}$. These results demonstrate that strongly perturbed T_g dynamics at the interfaces propagate across many layers of CRRs within the films, meaning that configurational changes associated with cooperative segmental dynamics within a CRR do not occur independently of neighboring CRRs. Thus, insight into the fundamental nature of the glass transition may be gained by measuring the nanoscale distributions of T_g s in confined polymers.

6 Model Polymer Nanocomposites Provide Understanding of Confinement Effects in Real Nanocomposites

6.1 Introduction

The effect of nanoscale confinement on T_g has been studied in polymers since the mid-1990's (Keddie et al., 1994b; Forrest et al., 1996; van Zanten et al., 1996; Fryer et al., 2001; Ellison et al., 2002; Grohens et al., 2002; Ellison and Torkelson, 2003; Sharp and Forrest, 2003b; Park et al., 2004; Alcoutlabi and McKenna, 2005; Ellison et al., 2005; Roth and Dutcher, 2005; Mundra et al., 2006). Deviations from bulk behavior in T_g due to nanoconfinement effects have implications in a broad range of technological applications. These include polymer based photoresists used in the production of microelectronic devices, disk drive lubricants, nanocomposites and asymmetric membranes used for gas separation. With ultrathin films, deviations from bulk T_g ($T_{g,bulk}$) have been reported as large as 45-50 K in supported films (van Zanten et al., 1996; Ellison et al., 2005) and 70 K in freely standing films (Forrest et al., 1996). In supported films, the thickness dependence of T_g is affected by polymer-substrate interactions (Keddie et al., 1994b; van Zanten et al., 1996; Fryer et al., 2001; Grohens et al., 2002; Park et al., 2004; Mundra et al., 2006) and the free surface (Keddie et al., 1994b; Forrest et al., 1996; Ellison and Torkelson, 2003; Sharp and Forrest, 2003b; Ellison et al., 2005), the impact of which increases as the ratio of interfacial area to volume increases. At the free surface, T_g is reduced compared to $T_{g,bulk}$, as revealed by fluorescence measurements (Ellison and Torkelson, 2003). This effect propagates into

the film (Ellison and Torkelson, 2003), reducing the T_g of ultrathin free-standing films and supported films lacking attractive polymer-substrate interactions. Thus, the T_g reduction originates with the free-surface effect; as shown by Ellison and Torkelson (2003), nanoconfinement itself only affects the magnitude of the T_g -gradient within the film. With moderate-to-strong attractive polymer-substrate interactions, for example, hydrogen bonds between hydroxyl groups on silica surfaces and oxygen atoms in poly(methyl methacrylate) (PMMA) or nitrogen atoms in poly(2-vinyl pyridine) (P2VP), T_g increases with decreasing thickness (van Zanten et al., 1996; Fryer et al., 2001; Ellison et al., 2002; Grohens et al., 2002; Park et al., 2004; Mundra et al., 2006).

Due to improvement of properties including conductivity, toughness and permeability, polymer nanocomposites are slated for applications ranging from membranes to fuel cells (Vaia and Giannelis, 2001; Sanchez et al., 2005). In nanocomposites with well-dispersed nanofiller, T_g can exhibit substantial deviations relative to bulk polymer (Ash et al., 2002b; Berriot et al., 2002; Arrighi et al., 2003; Sun et al., 2004; Blum et al., 2006; Rittigstein and Torkelson, 2006), decreasing when polymer-nanofiller interfaces yield free surfaces (Ash et al., 2002b; Rittigstein and Torkelson, 2006) and increasing when wetted interfaces with attractive interactions result (Rittigstein and Torkelson, 2006). These outcomes in nanocomposites were predicted via simulation (Starr et al., 2001) prior to their experimental demonstration (Ash et al., 2002b; Rittigstein and Torkelson, 2006). These results are due to the extremely large surface-to-volume ratio created by the nanoparticles modifying the dynamics of the chains in the polymer matrix, resulting in bulk properties that are

defined almost entirely by nanoscopically confined materials (Vaia and Giannelis, 2001). The enhancement of polymer properties by the addition of inorganic nanoparticles is a complex function of interfacial interactions, interfacial area, and the distribution of inter-nanofiller distances. The latter two factors depend on nanofiller dispersion, making it difficult to develop a fundamental understanding of their effects on nanocomposite properties.

The T_g changes due to nanoconfinement effects in ultrathin polymer films are qualitatively similar to those observed in polymer nanocomposites (Starr et al., 2001). In a recent study, Bansal et al. (2005) have reported a direct analogy between film thickness and average interparticle spacing in polystyrene-silica nanocomposites using two surface treatments, corresponding to non-wetted or wetted interfaces with no polymer surface interaction.

In contrast to the many studies of the T_g -confinement effect (Keddie et al., 1994b; Forrest et al., 1996; van Zanten et al., 1996; Fryer et al., 2001; Ellison et al., 2002; Grohens et al., 2002; Ellison and Torkelson, 2003; Sharp and Forrest, 2003b; Park et al., 2004; Alcoutlabi and McKenna, 2005; Ellison et al., 2005; Roth and Dutcher, 2005; Mundra et al., 2006), fewer studies have addressed the effect of confinement on physical aging of neat polymers (Ellison et al., 2002; Kawana and Jones, 2003; Huang and Paul, 2004, 2005; Priestley et al., 2005a; Priestley et al., 2005b; Huang and Paul, 2006) or polymer nanocomposites at low nanoparticle loadings (Lu and Nutt, 2003a, 2003b; Rittigstein and Torkelson, 2006). (Physical aging is the change in properties as a function of annealing time below T_g that accompanies the spontaneous relaxation of a

non-equilibrium glass toward equilibrium.) In films or nanocomposites without attractive interfacial interactions, for example, polystyrene (PS)-silica systems, there is in general no significant effect of confinement on aging at a constant quench depth below T_g (Priestley et al., 2005a). An exception occurs at temperatures near but below $T_{g,bulk}$, where bulk polymer ages but ultrathin films with reduced T_g s are at equilibrium (Kawana and Jones, 2003; Priestley et al., 2005a). In contrast, aging is suppressed in confined films or nanocomposites with attractive interfacial interactions (Lu and Nutt, 2003a, 2003b; Priestley et al., 2005a; Priestley et al., 2005b; Rittigstein and Torkelson, 2006).

Here we design model PMMA- and P2VP-silica nanocomposites consisting of polymer films confined between silica slides. Model nanocomposites are made from doubly supported films lacking a free surface. This structure is achieved by spin coating two films supported on silica slides, laying one atop the other, and annealing to heal the interface. This yields a consolidated film with a constant interlayer distance between silica surfaces. We compare the dependence of T_g and physical aging on the interlayer distance in model nanocomposites to the dependence of silica nanoparticle content in real nanocomposites. These provide a simple way to gain insight into the effect of interparticle spacing on T_g and to predict the approximate aging response of real nanocomposites. We find that model and real nanocomposites with identical T_g deviations yield similar dramatic suppressions of physical aging. This indicates that model nanocomposites can be broadly useful in studying amorphous polymer nanocomposites with wetted interfaces.

6.2 Experimental

Polystyrene (Pressure Chemical, $M_n = 290,000$ g/mol, $M_w/M_n = 1.06$) was used as received. Poly(methyl methacrylate) was synthesized by free radical polymerization ($M_n = 355,000$ g/mol, $M_w/M_n = 1.54$, by gel permeation chromatography (GPC) using universal calibration with PS standards). 4-tricyanovinyl-[N-(2-hydroxyethyl)-N-ethyl]aniline (TC1)-labeled PMMA ($M_n = 509,000$ g/mol, $M_w/M_n = 1.67$ by GPC using universal calibration with PS standards) was synthesized by reacting methyl methacrylate monomer in the presence of a trace amount of TC1-labeled methacrylate monomer. The TC1-labeled monomer was synthesized following the description of Priestley et al. (2005b). TC1-labeled PMMA contained 1.37 mol% labeled monomer as determined by UV absorbance. After synthesis, PMMA and TC1-labeled PMMA were washed by multiple dissolving/precipitating steps in toluene/methanol and dried in vacuo at 410 K for 24 hr. Poly(2-vinyl pyridine) (Scientific Polymer Products, $M_v = 200,000$ g/mol) was used after drying in a vacuum oven at ~ 383 K to remove residual monomer. The $T_{g,bulk}$ values measured by differential scanning calorimetry (DSC) (Mettler-Toledo, second heat, onset method, 10 K/min) and by fluorescence agreed within experimental error: PS $T_{g,bulk} = 375$ K by DSC and 374 K by fluorescence; PMMA $T_{g,bulk} = 393$ K by DSC and 391 K by fluorescence; TC1-labeled PMMA $T_{g,bulk} = 394$ K by DSC and 395 K by fluorescence; and P2VP $T_{g,bulk} = 373$ K by DSC and fluorescence. Three fluorescence dyes, pyrene (Aldrich Chemical, 99+% purity), 1,10-bis-(1-pyrene)decane (BPD) (Molecular Probes), and 4-tricyanovinyljulolidene (TCJ) (Molecular Probes), were used as received, while TC1 was synthesized following the description of Priestley et al.

(2005b). Silica nanospheres (colloidal silica in methyl ethyl ketone, Nissan Chemical Industries, reported diameter of 10-15 nm) were used as received.

Films of neat, bulk polymers and real polymer nanocomposites were prepared by spin-coating dilute solutions of polymer and dye in methyl ethyl ketone (MEK), with or without nanofiller, onto quartz slides. Solutions containing nanofiller were sonicated (Branson 1200 sonicator) for 40 min prior to spin coating. Resulting films contained less than 0.2 wt% dye relative to polymer and were at least 1 μm in thickness (Tencor P10 profilometer). Films were dried for at least 2 days in a chemical fume hood prior to performing fluorescence measurements.

Spin-coating a dilute solution is necessary to obtain the differences observed in T_g with the addition of nanoparticles to the polymer matrix. The changes in T_g reported in this study are not observed when nanocomposite films are made by solvent casting instead of spin coating. Solvent casting results in much less nanoparticle dispersion in the nanocomposite film due to the aggregation that accompanies the slow drying process associated with solvent casting.

Ultrathin PMMA films were prepared by spin-coating toluene solutions onto quartz slides. The films were then dried in vacuum at $T_g + 5 \text{ K}$ for 8 hr. To prepare model polymer nanocomposites, two films of identical thickness were spin-coated from dilute solution (PMMA in toluene or P2VP in MEK) onto quartz substrates and dried as described above. These films were brought into contact at $T_g + 25 \text{ K}$ for 3 hr and allowed to anneal, healing a portion of the interface.

Fluorescence was measured using a Spex Fluorlog-2DM1B fluorimeter and a Photon Technology International fluorimeter. Values of T_g were measured using pyrene as the dye in the PS and P2VP nanocomposites, both real and model. The BPD dye was used to measure T_g in the real PMMA nanocomposites; the TC1 label was used to characterize T_g in the PMMA model nanocomposites and ultrathin films. The T_g values were determined following a procedure explained by Ellison et al. (2005) and Rittigstein and Torkelson (2006). Physical aging was characterized as described by Priestley et al. (2005a; 2005b) using TCJ as the fluorescence dye in neat polymer and polymer nanocomposite films. The maximum emission intensity of TCJ (at 597-602 nm for P2VP, at 598-602 nm for P2VP-silica nanocomposites, and at 590-594 nm for the model nanocomposites) was measured as a function of aging time after quenching from the rubbery state above T_g to 303 K.

For transmission electron microscopy (TEM) (JEOL 100CX) images, dilute solutions of polymer and nanofiller were spin-coated onto grids to make films that were 50-70 nm thick. Otherwise, the preparation procedure was identical to that used for preparing the real polymer nanocomposites samples employed in fluorescence measurements.

6.3 Results and Discussion

Fluorescence has been used to characterize T_g and aging in confined polymer (Ellison et al., 2002; Ellison and Torkelson, 2003; Ellison et al., 2005; Priestley et al., 2005a; Priestley et al., 2005b; Mundra et al., 2006; Rittigstein and Torkelson, 2006) and

is employed here to characterize these properties in model and real nanocomposites. Figure 6-1a shows the temperature dependence of the fluorescence of 1,10-bis-(1-pyrene)decane (BPD) doped at trace levels into bulk PMMA and a 0.4 vol% silica-PMMA nanocomposite. The T_g is identified by the intersection of linear fits in the liquid and glassy states. The T_g of the nanocomposite is increased by 5 K relative to bulk PMMA.

Figure 6-1b summarizes the effect of nanoparticle loading on the T_g s of P2VP-, PMMA- and PS-silica nanocomposites. Within experimental uncertainty, adding 0.5 vol% silica (10- to 15-nm-diameter nanoparticles) has no effect on the T_g of PS. This agrees with the reported $T_{g,bulk}$ observed in a 14-nm-thick layer at the silica substrate interface in a bulk PS bilayer film (Ellison and Torkelson, 2003). Figure 6-2 presents a TEM image that illustrates the good dispersion of 0.4 vol% silica in PS matrix. It should be noted that a recent study (Bansal et al., 2005) reported a decrease in T_g of ~11 K when 40 wt% (~18 vol%) silica nanoparticles identical to those employed here were added to PS; this T_g reduction was ascribed to the presence of free surfaces at the non-wetted interfaces of the PS and silica nanoparticles that were not well-dispersed. However, when they reduced the nanoparticle loading to 2 wt% (~0.9 vol%), near the concentrations employed here, there was no change in T_g from that of bulk PS, in good agreement with our results.

On the other hand, Figure 6-1b shows that the P2VP- and PMMA-silica nanocomposites exhibit enhancements in T_g at silica loadings as low as 0.1-0.3 vol%. The apparent maximum 5 K and 10 K enhancements in the T_g s obtained with 0.4-0.5

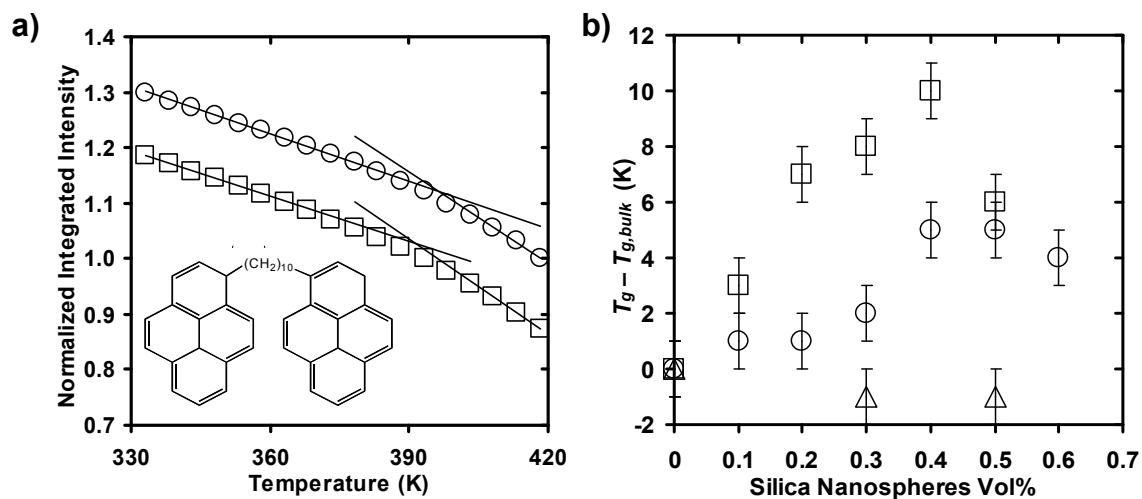


Figure 6-1: T_g data from bulk polymer and polymer nanocomposites determined via fluorescence. a) Temperature dependence of the normalized fluorescence integrated intensity of BPD dopant (< 0.2 wt%) in a bulk PMMA film (open squares) and in 0.4 vol% silica-PMMA nanocomposite film (open circles). Inset: The molecular structure of BPD. (The data have been normalized to 1 relative to the intensity at $T_{g,bulk}$ and arbitrarily shifted vertically.) b) Deviations from $T_{g,bulk}$ as a function of silica nanofiller content in three polymer nanocomposites: P2VP (open squares), PMMA (open circles) and PS (open triangles). The error bars (± 1 K) represent the inherent error due to the fitting of the data required to obtain T_g .

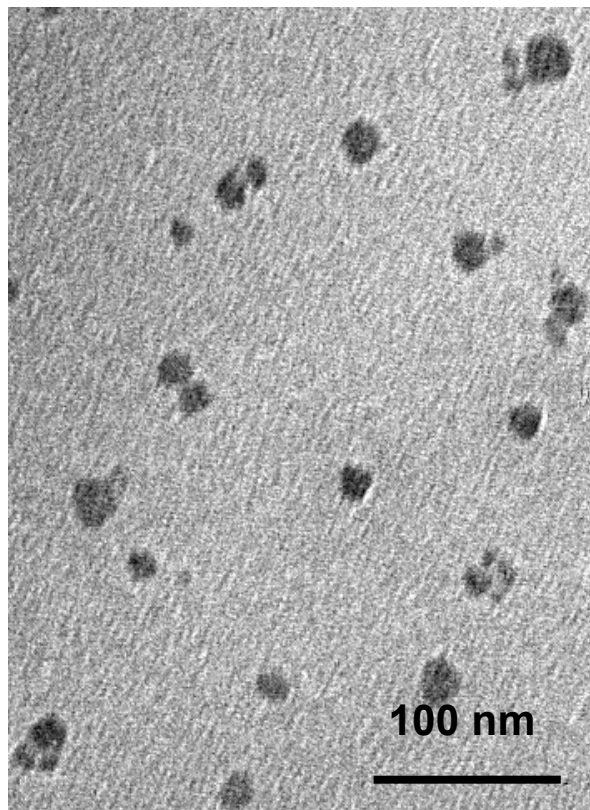


Figure 6-2: Representative TEM micrograph of 0.4 vol% silica-PS nanocomposite. (The film thickness is ~50 nm.)

vol% silica in the PMMA and P2VP nanocomposites, respectively, are hypothesized to result from decreases in nanoparticle dispersion achieved at higher loadings.

It is well known that PMMA and P2VP experience hydrogen-bonding interactions with silica surfaces containing hydroxyl groups (van Zanten et al., 1996; Ellison et al., 2002; Grohens et al., 2002; Priestley et al., 2005b) while PS does not. The enhanced T_g s observed in the PMMA-silica nanocomposites in Figure 6-1b arise from these attractive polymer-nanoparticle interfacial interactions that reduce cooperative segmental mobility. Similar effects are expected in P2VP-silica nanocomposites. However, it should be noted that nanoparticle-polymer interactions may lead to internal stresses within polymer nanocomposites (Papakonstantopoulos et al., 2005; Narayanan et al., 2006); these stresses could affect the relaxation dynamics in nanocomposites, including those associated with T_g .

There are two complications in developing a fundamental understanding of the effects of nanoparticle loading and interparticle distance on T_g in well-dispersed nanocomposites. First, there is a wide distribution of interparticle distances, and, second, the T_g dynamics of polymer segments may be impacted by any number of nanoparticles located within a radius of tens to even hundreds of nanometers. In order to eliminate these complications, a model nanocomposite with a known constant interlayer spacing was developed by confining polymer films between silica slides. Figure 6-3 shows $T_g - T_{g,bulk}$ as a function of thickness for both ultrathin films supported on silica and model nanocomposites of P2VP and PMMA. As illustrated in Figure 6-3,

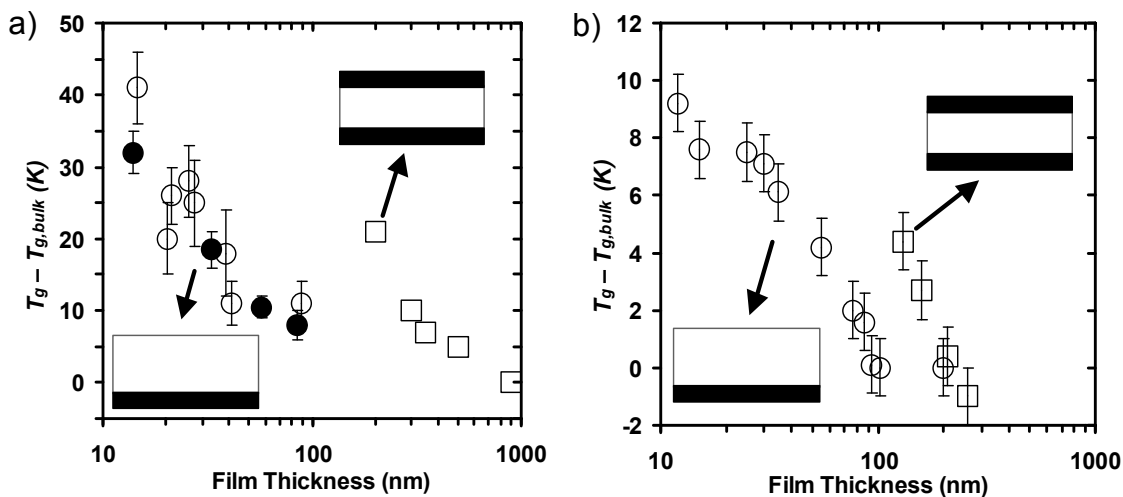


Figure 6-3: Deviations of T_g from $T_{g,bulk}$ of ultrathin films supported on silica and 'model' nanocomposites. a) Thickness dependence of the T_g deviation of P2VP supported films (open circles: data from van Zanten et al. (1996); filled circles: data from Park et al. (2004)) and pyrene-doped P2VP 'model' nanocomposites (open squares). (In the case of the P2VP supported films, the error bars are from van Zanten et al. (1996) and Park et al. (2004), and in the case of the P2VP 'model' nanocomposites, the error (± 1 K) in the data is due to the fitting required to obtain T_g and is smaller than the symbol size.) b) Thickness dependence of the T_g deviation of TC1-labelled PMMA supported films (open circles) and 'model' nanocomposites (open squares). The error bars (± 1 K) represent the inherent error due to the fitting of the data required to obtain T_g .

replacement of the free surface in the films by a silica interface (model nanocomposites) with attractive interfacial interactions leads to an increase in the length scale at which T_g -confinement effects are observed. For example, a 21 K enhancement of T_g is observed in both a 200-nm-thick P2VP-silica model nanocomposite and a 30-nm-thick P2VP film supported on silica (one free surface). Similarly, a 4-5 K enhancement of T_g is observed in both a 130-nm-thick PMMA-silica model nanocomposite and a 55-nm-thick PMMA film supported on silica (one free surface). Sharp and Forrest (2003b) observed that 'properly' capped supported PS films with a 5 nm thick evaporated gold layer exhibited a bulk T_g value at film thicknesses as thin as 8 nm. The results showed that free surfaces are crucial for observing T_g reductions in ultrathin PS films. Conversely, Forrest, Dalnoki-Veress, Dutcher and co-workers (Forrest et al., 1996; Forrest et al., 1997; Dalnoki-Veress et al., 2001) measured T_g values of free-standing (unsupported) ultrathin films and demonstrated an enhancement in the T_g -nanoconfinement effect with two free surfaces, further alluding to the importance of free surfaces on the reduction in T_g . Figure 6-3 shows that doubly supported PMMA and P2VP films yield major increases in T_g with confinement at much greater length scales than those observed in films supported by a single substrate. Thus, removing the free surface results in a dramatic increase in the T_g -nanoconfinement effect of polymer that possesses attractive substrate-polymer interactions.

Remarkably, the length scale at which confinement effects are observed in model nanocomposites can be hundreds of nanometers. In particular, P2VP model nanocomposites show a 5 K enhancement of T_g relative to bulk at a thickness

(interlayer spacing) of 500 nm. This is the largest length scale for which an effect of confinement on T_g has been reported and indicates that these effects can be observed in the microscale when strong attractive interactions are present.

Figure 6-4 shows micrographs of 0.4 vol% silica nanocomposites indicating good nanoparticle dispersion. Assuming that the geometry (curvature) does not play an important role in the dependence of the T_g -nanoconfinement effect, the T_g values of the 'model' nanocomposites can be compared to the T_g values of the real nanocomposites to determine their approximate 'effective average' interparticle distance. From the T_g comparison between real and model nanocomposites presented in Figure 6-4, the T_g enhancement in the real P2VP nanocomposite is equal to that of a model nanocomposite with a ~300 nm interlayer spacing while the T_g enhancement in the real PMMA nanocomposite is equal to that of a model nanocomposite with a ~130 nm interlayer spacing. Consistent with the fact that the nanoparticles have diverse interparticle spacings, the 130 and 300 nm 'effective average' interlayer spacings are greater than the ~50 nm theoretical interparticle distance (silica surface to silica surface) determined assuming an ideal cubic dispersion of nanoparticles. These 'effective average' interlayer spacings determined by comparison with model nanocomposites provide a simple approach for quantifying the extent to which confinement effects involving attractive interactions at nanofiller interfaces modify polymer T_g behavior.

Likewise, model nanocomposites can also be useful in roughly predicting the physical aging behavior of real nanocomposites. Figure 6-5 shows results of

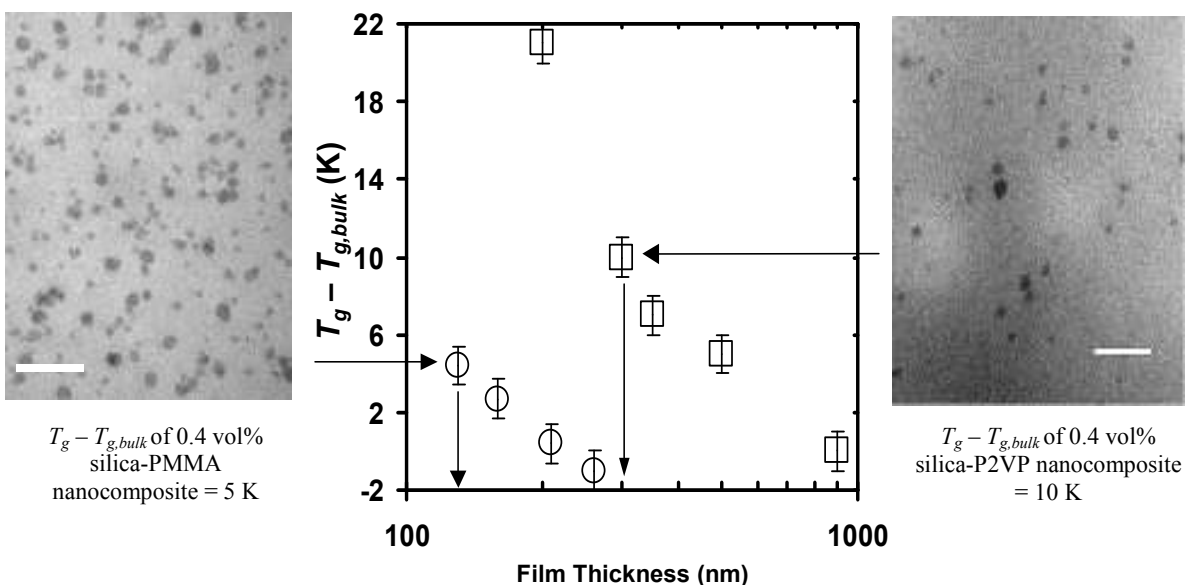


Figure 6-4: Interlayer spacing (film thickness) in 'model' nanocomposites that yield the same T_g deviation as 0.4 vol% silica-PMMA and silica-P2VP nanocomposites. T_g deviations of P2VP 'model' nanocomposites (open squares) and PMMA 'model' nanocomposites (open circles). Right and Left: Transmission electron microscopy images of 0.4 vol% silica-P2VP (right) and 0.4 vol% silica-PMMA (left) nanocomposites (scale bars = 100 nm). The error bars (± 1 K) represent the inherent error due to the fitting of the data required to obtain T_g .

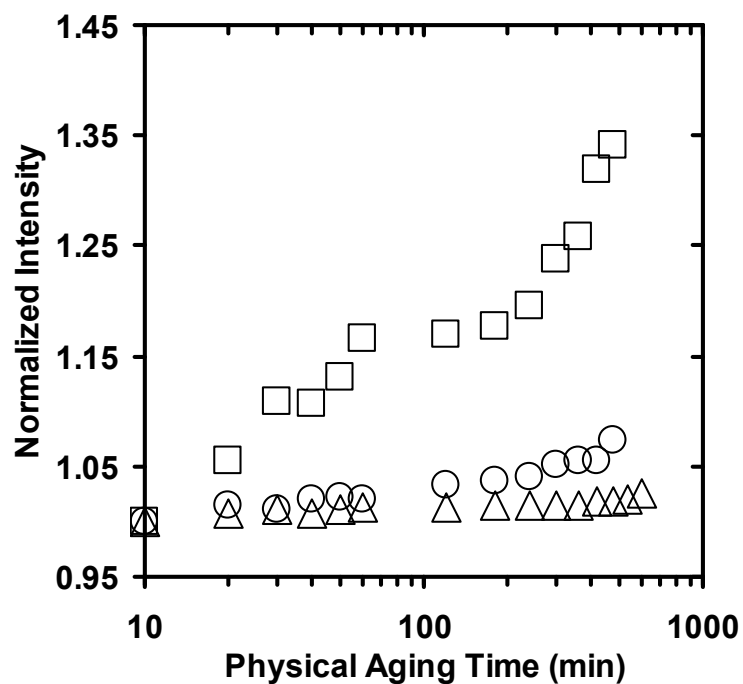


Figure 6-5: Physical aging of bulk polymer and polymer nanocomposites monitored by fluorescence. Normalized fluorescence intensity of TCJ dopant (<0.2 wt%) as a function of logarithmic physical aging time after a quench from above T_g (413 K) to below T_g (303 K): bulk P2VP film (open squares), 0.4 vol% silica-P2VP nanocomposite (open circles), and 300-nm-thick P2VP 'model' nanocomposite (open triangles). The physical aging rates are related to the slopes of the data sets.

fluorescence studies characterizing aging in bulk P2VP and real and model nanocomposites, the latter two exhibiting the same 10 K confinement-induced T_g enhancement. During aging, an increase in fluorescence intensity correlates with an order-of-magnitude smaller increase in density (Priestley et al., 2005a; Priestley et al., 2005b; Rittigstein and Torkelson, 2006). The roughly linear increase in intensity with logarithmic aging time in bulk P2VP is consistent with the manner in which physical aging leads to changes in properties, including density. When aged at 303 K, bulk P2VP exhibits a 35% increase in fluorescence intensity over 8 hr. However, both model and real P2VP-silica nanocomposites exhibit dramatically suppressed physical aging, meaning that model nanocomposites can serve as an appropriate system for studying a range of glassy state behavior in real nanocomposites. These results are consistent with a study showing a near elimination of aging in interfacial layers of a bulk PMMA film supported on silica (Priestley et al., 2005b). These results also indicate that interfacial interactions that yield significant increases in T_g in nanocomposites may have more significant effects on other glassy behavior such as physical aging. This suggests that nanocomposites may lead to the production of glassy-state polymeric systems with properties that are nearly stable during long-term use.

6.4 Conclusions

In this chapter, fluorescence was used to reveal a major impact of nanoconfinement on T_g in polymer-silica nanocomposites possessing attractive interfacial interactions. It was shown that the comparison of the T_g behavior of 'model'

nanocomposites with that of real nanocomposites yields a simple determination of an 'effective average' interparticle distance in real nanocomposites, providing a good prediction of the reduction in physical aging in real polymer nanocomposites.

The technological importance and significant scientific questions associated with the very long-range, confinement-related enhancements in T_g and the suppression of physical aging observed in polymers undergoing attractive interfacial interactions provide further impetus to study confinement effects in polymer nanocomposites. Model nanocomposites with silica and other substrates yield well-designed systems for such investigations.

7 Polymer-Nanoparticle Interfacial Interactions in Polymer Nanocomposites: Confinement Effects on Glass Transition Temperature and Suppression of Physical Aging

7.1 Introduction

It has been known for more than a decade that nanoconfinement can lead to significant changes in the glass transition temperature (T_g) behavior of polymer films (Keddie et al., 1994a, 1994b; Forrest et al., 1996; van Zanten et al., 1996; Hall et al., 1997b; Grohens et al., 1998; Fryer et al., 2001; Ellison et al., 2002; Grohens et al., 2002; Hartmann et al., 2002; Ellison and Torkelson, 2003; Roth and Dutcher, 2003; Ellison et al., 2004; Park et al., 2004; Soles et al., 2004b; Akabori et al., 2005; Ellison et al., 2005). Seminal studies by Keddie et al. (1994b) and Forrest et al. (1996) reported reductions in T_g from the bulk value by ~ 23 K in 15-nm-thick polystyrene (PS) films supported on a silica substrate and by ~ 70 K in 29-nm-thick freestanding PS films (two free surfaces), respectively. The reductions in T_g observed in ultrathin films were hypothesized to result from reductions in T_g (or enhancement in cooperative segmental mobility) in regions close to the free surface (air-polymer interface). Ellison and Torkelson (2003) employed a novel multilayer/fluorescence method to determine T_g s at specific locations within thin and ultrathin films, including the free surface. They observed a 32 K reduction in T_g relative to $T_{g,bulk}$ in a 14-nm-thick free-surface layer located at the top of bulk, bilayer film. Using trilayer films, they also found that a

reduction in T_g extended from the free surface several tens of nanometers into the film interior. Other recent studies have found that T_g s can be depressed from bulk values in films exceeding 100 nm in thickness. Soles et al. (2004b) reported T_g depressions in 140 Å thick supported polycarbonate films while Ellison et al. (2005) found T_g depressions in 300-400 nm thick supported poly(*t*-butyl styrene) films.

When attractive interactions, for example, hydrogen bonds, are present at a polymer-substrate interface, confinement effects can lead to enhancements rather than depressions in T_g relative to bulk values (Keddie et al., 1994a; van Zanten et al., 1996; Grohens et al., 1998; Fryer et al., 2001; Grohens et al., 2002; Hartmann et al., 2002; Park et al., 2004). Keddie et al. (1994a) and van Zanten et al. (1996) found enhancements in T_g from $T_{g,bulk}$ by 4-5 K in 15-nm-thick poly(methyl methacrylate) (PMMA) films and by as much as 50 K in 8-nm-thick poly(2-vinyl pyridine) (P2VP) films, respectively, when attractive polymer-substrate interactions are present. The attractive interactions are believed to result from hydrogen bonds between the hydroxyl groups naturally on the silica substrate surfaces and the ester side group in PMMA or the nitrogen atom in P2VP.

Recently, important connections between the deviations of T_g values or related dynamics in polymer nanocomposites from those of neat, bulk polymers have been made to the many studies of the effects of confinement on T_g in polymer films. Molecular dynamics simulations, experiments and models (Starr et al., 2001; Ash et al., 2002b; Berriot et al., 2002; Arrighi et al., 2003; Berriot et al., 2003; Liu et al., 2003; Sun et al., 2004; Bansal et al., 2005) have lent support to the concept that the T_g s of

polymer nanocomposites can be enhanced or depressed by tuning the polymer-nanofiller interactions and that the effects are similar to those resulting from free surfaces and polymer-substrate interactions in ultrathin polymer films. Via experimental studies, Bansal et al. (2005) have argued for an approximate equivalence between ultrathin film thickness and an average interparticle spacing in nanocomposites for two nanofiller surface treatments, resulting in either non-wetting or wetting polymer-nanofiller interfaces.

In contrast to the many studies on the T_g -nanoconfinement effect (for relevant reviews, see Forrest and Dalnoki-Veress (2001); Alcoutlabi and McKenna (2005); Baschnagel and Varnik (2005); Roth and Dutcher (2005)), much less work (Pfromm and Koros, 1995; Lee and Lichtenhan, 1998; Ellison et al., 2002; Kawana and Jones, 2003; Lu and Nutt, 2003a, 2003b; Huang and Paul, 2004; Fukao and Sakamoto, 2005; Huang and Paul, 2005; Priestley et al., 2005a; 2005b) has been devoted to the effect of confinement on physical aging or structural relaxation in polymer films and nanocomposites. This is unfortunate because physical aging, which is a relaxation process in which a non-equilibrium glass spontaneously evolves toward thermodynamic and structural equilibrium, often results in deleterious changes in properties ranging from brittleness and ultimate elongation to permeability. Ellison et al. (2002) reported little change within error in physical aging rate of poly(isobutyl methacrylate) films supported on quartz over a range of thicknesses from 10 nm to 800 nm. Kawana and Jones (2003) monitored PS physical aging at $T_{g,bulk} - 30$ K and found that physical aging is absent in a 10-nm-thick film, consistent with the notion that the T_g of the 10-nm-

thick film is reduced relative to bulk by at least 30 K. Priestley et al. (2005a; 2005b) employed single layer/ and multilayer/fluorescence methods to demonstrate that confinement in PMMA ultrathin films can significantly reduce the physical aging rate, a point also made by Fukao and Sakamoto (2005), and that the physical aging response in PMMA films is affected by confinement over a larger length scale than is the T_g response. Priestley et al. (2005a) further found that physical aging is present in supported ultrathin PMMA films at temperatures above $T_{g,bulk}$; this is associated with the enhancement of T_g due to hydrogen bond effects at the polymer-silica substrate interface. It is interesting to note that Pfromm and Koros (1995) and Huang and Paul (2004; 2005) have measured permeation across free-standing films of several high T_g polymers as a function of aging time and have found an accelerated reduction in permeability with decreasing thickness below $\sim 1 \mu\text{m}$.

Regarding physical aging of nanocomposites, Lee and Lichtenhan (1998) reported that inclusion of polyhedral oligomeric silsesquioxane (POSS) nanoreinforcements in epoxy retarded the physical aging rate and the time to reach equilibrium. More recently, Lu and Nutt (2003a; 2003b) also found reduced relaxation rates and a broader distribution of relaxation times in intercalated silicate-epoxy nanocomposites relative to physical aging rate in neat epoxy.

In this chapter, the effects of confinement on T_g and physical aging are studied by tuning the polymer-nanofiller interactions in nanocomposites via choice of polymer, nanofiller, or solvent used in nanocomposite preparation. Using nanocomposites containing low levels of nanofiller together with fluorescence, it is demonstrated that T_g

values may be either enhanced or depressed substantially relative to bulk T_g values. The trend will depend on the solvent used in preparing the nanocomposites by spin coating. Physical aging is also studied using fluorescence and it is shown that, by making the appropriate choice of nanofiller dispersed in the polymer, it is possible to substantially suppress physical aging in glassy polymer nanocomposites.

7.2 Experimental

Polystyrene (Pressure Chemical, reported values of $M_n = 290,000$ g/mol, $M_w/M_n < 1.06$) was used as received. Poly(methyl methacrylate) was synthesized by free radical polymerization ($M_n = 355,000$ g/mol, $M_w/M_n = 1.54$, by gel permeation chromatography using universal calibration with PS standards). Poly(2-vinyl pyridine) (Scientific Polymer Products, reported value of $M_v = 200,000$ g/mol) was used after drying the as received material in a vacuum oven at ~ 110 °C to remove residual monomer. Bulk T_g ($T_{g,bulk}$) values were measured by differential scanning calorimetry (DSC) (Mettler-Toledo DSC822, second heat, onset method, 10 K/min) and also via fluorescence methods and were found to agree within experimental error: PS $T_{g,bulk} = 102$ °C by DSC and 101 °C by fluorescence; PMMA $T_{g,bulk} = 120$ °C by DSC and 118 °C by fluorescence; and P2VP $T_{g,bulk} = 100$ °C by DSC and fluorescence. Three fluorescence dyes, pyrene (Aldrich Chemical, 99+% purity), 1.10-bis-(1-pyrene)decane (BPD) (Molecular Probes), and 4-tricyanovinyljulolidene (TCJ) (Molecular Probes), were used as received. Alumina nanospheres (alumina oxide nanopowder, Sigma-Aldrich, reported diameter of 47 nm)

and silica nanospheres (colloidal silica in methyl ethyl ketone, Nissan Chemical Industries, reported diameter of 10-15 nm) were used as received.

Thin films of neat polymers and polymer nanocomposites were prepared by spin-coating (Spangler et al., 1990; Hall et al., 1998b) dilute solutions of polymer and dye, with or without nanofiller, onto quartz slides. All solutions were made using methyl ethyl ketone (MEK) as solvent except for a series of PMMA-silica nanocomposites that were made using acetic acid (AA) as solvent. (The colloidal silica in methyl ethyl ketone was diluted in acetic acid.) Solutions containing nanofiller were sonicated (Branson 1200 sonicator) for 40 min prior to spin coating. Resulting films contained less than 0.2 wt% dye relative to polymer and were at least 1 μm in thickness as determined using a Tencor P10 profilometer. Films were dried for at least 2 days in a chemical fume hood prior to performing fluorescence measurements.

Fluorescence was measured using a Spex Fluorlog-2DM1B fluorimeter for T_g characterization and a Photon Technology International fluorimeter for physical aging characterization. Values of T_g were measured using pyrene as the dye in the PS and P2VP films (neat and nanocomposite) and BPD as the dye in the PMMA films (neat and nanocomposite). Typically, fluorescence spectra were recorded upon cooling from the rubbery state after having annealed samples at $\sim T_g + 40$ K for 15 min. In a few cases, samples were annealed at $\sim T_g + 30$ K for 15 min. The cooling protocol involved measuring the fluorescence spectrum at a given temperature followed by reducing the film temperature by 5 $^{\circ}\text{C}$, holding at that temperature for 5 min, and then measuring the fluorescence spectrum, and so forth. In fitting the temperature dependence of

fluorescence in the rubbery and glassy states, only data points well outside T_g were used for the linear fits, and typical correlation coefficients (R^2) were better than 0.990. To initiate the fitting procedure, data points were added to the rubbery- and glassy-state linear regressions at the extrema in the temperature range of the data. The correlation coefficient was monitored as more data points were added (approaching T_g from the extrema in the temperature range of the data) to each of the linear regressions. If the R^2 value began to steadily decrease below a threshold value (i.e., 0.990) as more data points were added, then these data points were removed to produce a value of R^2 higher than the threshold value, and the linear regressions were considered acceptable. The linear fits in both the rubbery and glassy states included a minimum of four fluorescence data points (usually more), spanning a minimum of 15 K in temperature. Spectra were taken over a sufficient range of wavelengths that integration could be done from instrument baseline at the lowest wavelengths to the same instrument baseline at the highest wavelengths.

When a deviation in T_g from $T_{g,bulk}$ was apparent, several repeat experiments were performed to confirm the shift in T_g . In all cases, for a given system the repeated result values were identical within experimental error, ± 1 K.

Physical aging was characterized as described by Priestley et al. (2005a; 2005b). TCJ was used as the fluorescence dye in all neat polymer and polymer nanocomposite films. Physical aging was monitored by measuring the maximum emission intensity of TCJ (at 597 - 602 nm for P2VP, at 598-602 nm for P2VP-silica nanocomposites, and at

601- 605 nm for P2VP-alumina nanocomposites) as a function of aging time after quenching the films from the rubbery state above T_g to 30 °C.

7.3 Glass Transition Effects in Polymer Nanocomposites

The T_g s of polymer nanocomposites were measured as a function of nanofiller concentration, nanofiller type, and polymer species using the temperature dependence of the integrated intensity of pyrene doped as low levels (0.2 wt% or less) in the polymers. Figure 7-1 illustrates a significant increase in the pyrene fluorescence intensity with decreasing temperature in a neat P2VP film. Similar results are obtained in BPD-doped PMMA and pyrene-doped PS films with and without nanofiller. (It should be noted that many fluorescence dyes are capable of providing measurements of T_g in polymer films via a break in the temperature dependence of fluorescence intensity (Loutfy and Teegarden, 1983; Strehmel et al., 1999; Lenhart et al., 2001; Ellison and Torkelson, 2002). However, pyrenyl-type dyes have an advantage in such applications due to their strong absorbance of excitation light and high fluorescence quantum yield.)

Figure 7-2 shows the normalized integrated fluorescence intensity as a function of temperature for a neat P2VP film and a P2VP-alumina nanocomposite film; in each case, the fluorescence is associated with pyrene dyes doped at trace levels in the polymers. Both systems exhibit stronger temperature dependences at higher temperature and weaker temperature dependences at lower temperature. The intersection of the high and low temperature dependences is T_g . (Note: All T_g

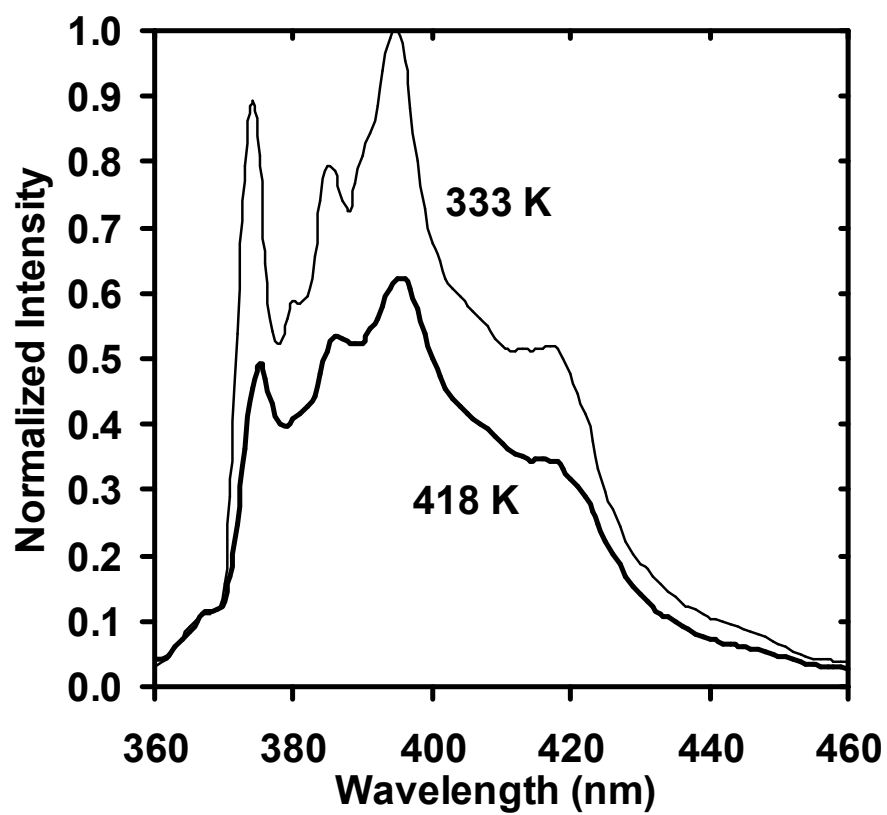


Figure 7-1: Fluorescence emission spectra of pyrene dopant (< 0.2 wt%) in a bulk P2VP film taken at temperatures of 333 and 418 K.

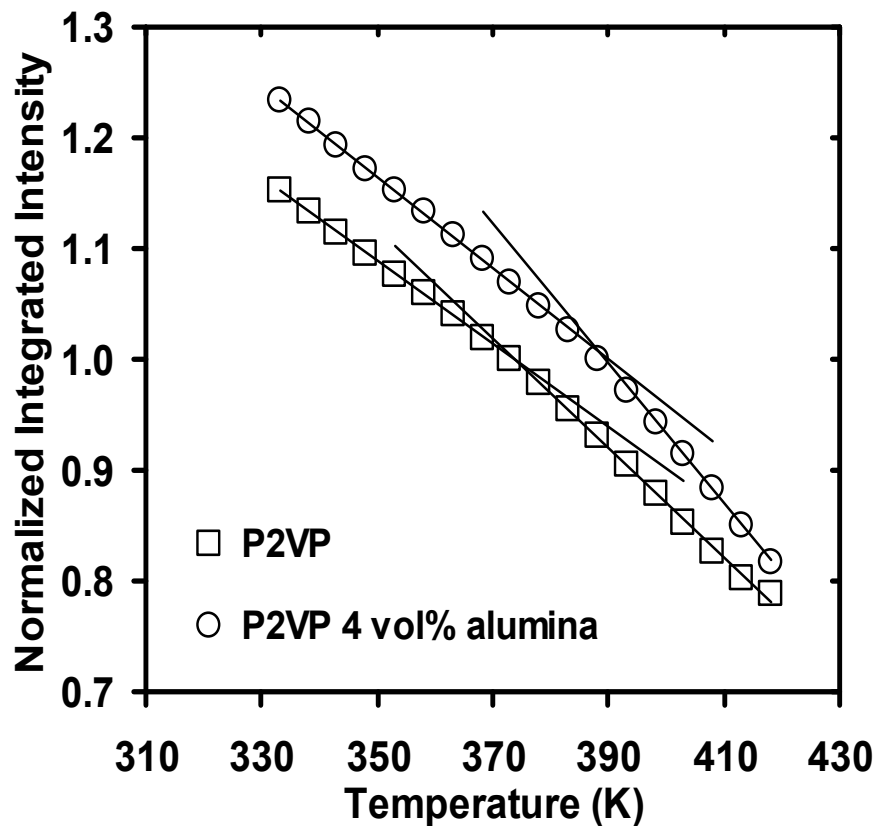


Figure 7-2: Temperature dependence of the normalized integrated intensity of pyrene dopant (< 0.2 wt%) in a bulk P2VP film and in a 4 vol% alumina/P2VP nanocomposite film. (The integrated intensity has been normalized to one at T_g).

measurements in this study are made by cooling from the rubbery state above T_g , in accord with the protocol typically used in volumetric measurements of T_g .) Figure 7-2 makes evident a substantial, 16 K increase in T_g of the P2VP/4 vol% alumina nanocomposite relative to neat, bulk P2VP. (It should be noted that this 16 K increase in T_g is not observed when a nanocomposite film is made by solvent casting instead of spin coating. This is because solvent casting the sonicated solutions results in much less dispersion of nanoparticles in the final nanocomposite film due to the aggregation that occurs during the slow drying process accompanying solvent casting.)

Figure 7-3 shows the effect of nanofiller concentration on the T_g values of polymer-alumina nanocomposites made using PS, PMMA, and P2VP. Polystyrene-alumina nanocomposites exhibit no change in T_g within error when nanofiller is present up to 10 vol%. In contrast, PMMA-alumina nanocomposites exhibit a reduction in T_g by 3-5 K at 3-10 vol% nanofiller while the P2VP-alumina nanocomposites exhibit a 12-16 K enhancement in T_g at 3.5-6 vol% nanofiller. The reduction in the PMMA T_g with addition of alumina nanofiller is qualitatively consistent with results of Ash et al. (2002b) who previously reported T_g reductions in nanocomposites made by *in situ* polymerization of PMMA in the presence of alumina nanofiller. This T_g behavior has been rationalized as resulting from the presence of a free surface (free space) between the PMMA and the alumina nanofiller surface, i.e., PMMA is not wetting the alumina surface. (Recall that T_g reductions at a free surface have been inferred from the T_g -nanoconfinement behavior of many polymers and have been experimentally determined via

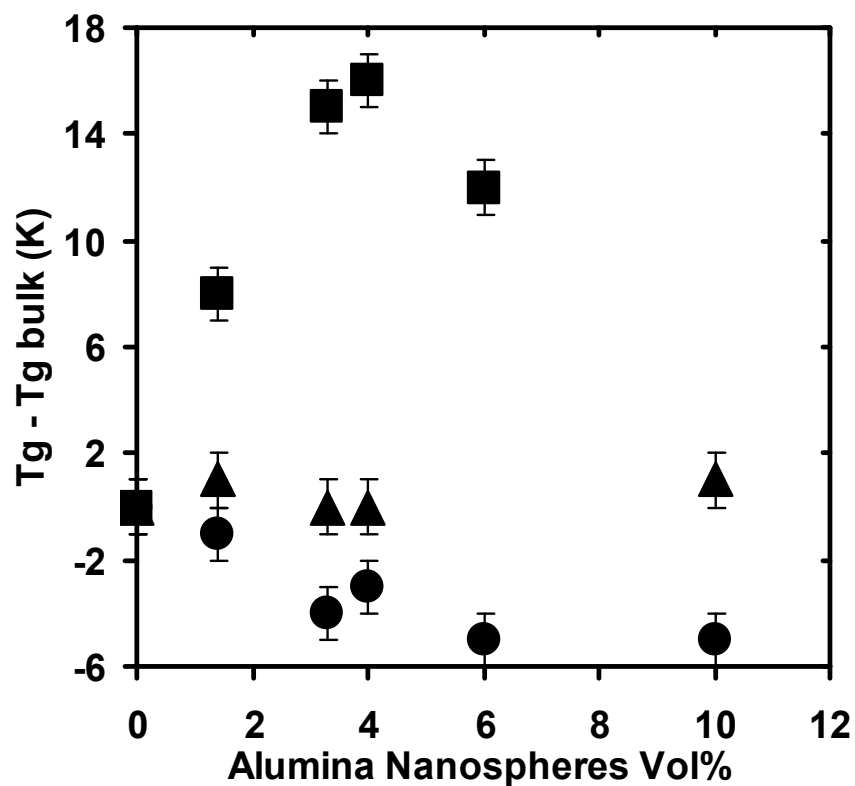


Figure 7-3: Deviations in T_g from neat, bulk polymer T_g as a function of alumina nanofiller content in three polymer nanocomposites: P2VP (closed squares), PS (closed triangles), PMMA (closed circles). (Error bars represent the inherent error due to the line fitting required to obtain T_g , which are similar to the obtained variation in T_g (± 1 K or less) from sample to sample.)

multilayer/fluorescence methods for PS films (Ellison and Torkelson, 2003).) The T_g reductions obtained in the current study can be explained in a manner similar to those obtained by Ash et al. (2002b) and are consistent with the modest T_g reductions reported by Roth and Dutcher (2003) in freely standing PMMA films.

No previous report has been made regarding the effect of alumina nanofiller on the T_g values of either PS or P2VP. However, Xie and Blum (1996) have noted similarity in the interactions of styrene/2-vinyl pyridine block copolymers with silica and alumina. As the P2VP block is well known to undergo strong attractive interactions with silica via hydrogen bonding (Parsonage et al., 1991; Huguenard and Pefferkorn, 1994) while the PS block does not, it is reasonable to assume that a similar behavior applies in the case of alumina nanofiller. The invariance of T_g with alumina nanofiller in PS nanocomposites is consistent with the notion that wetted PS-alumina interfaces are present. A previous study (Ellison and Torkelson, 2003) has shown that in a bulk PS film, the T_g value in an ultrathin layer next to a silica substrate is identical within error to bulk T_g ; it was also shown in chapter 4 that adding up to 0.5 vol% silica to PS does not change the T_g of the matrix. If the interfacial interaction between PS and alumina is similar to that of PS and silica (where there is no attractive interaction), then the presence of alumina nanofiller should have little or no effect on the PS T_g . In contrast, the origins of the major enhancement of T_g with alumina nanofiller in P2VP-alumina nanocomposites are presumably due to wetted P2VP-alumina interfaces possessing strong attractive interactions, leading to reductions in cooperative segmental mobility in the polymer and an increase in T_g .

This explanation of the enhanced T_g values in P2VP-alumina nanocomposites is reinforced by noting that P2VP-silica nanocomposites, which by the nature of interfacial hydrogen bonds have strong attractive polymer-substrate interactions, yield T_g enhancements relative to bulk P2VP (see Figure 6-1b). When a P2VP nanocomposite is made with 0.4 vol% silica (reported nanosphere diameter of 10-15 nm), its T_g value exceeds the T_g of neat P2VP by 10 K (see chapter 6). The surface areas at equal volumes of silica nanofiller and alumina nanofiller (reported nanosphere diameter of 47 nm) differ by a factor of ~ 3.8 . This means that if the nanofiller dispersion and the strength of interfacial interactions are comparable in the P2VP-silica and P2VP-alumina nanocomposites, then a T_g enhancement of roughly 10 K relative to neat P2VP may be expected in a P2VP nanocomposite made with 1.5 vol% alumina. Figure 7-3 indicates that the T_g enhancement in such a nanocomposite is ~ 8 K, in reasonable agreement with expectations.

Figure 7-4 shows three TEM images of PS/, PMMA/ and P2VP/4 vol% alumina nanocomposites. Alumina nanospheres have a reported diameter of 47 nm. However, the TEM images reveal that the nanoparticles have a broad distribution of diameters. In the case of PS-alumina nanocomposite, the nanoparticles are not well dispersed in the matrix. On the other hand, in PMMA, the alumina nanospheres have better dispersion, and their dispersion is even more improved in P2VP. These results suggest that while the dispersion of the nanoparticles is an important parameter, it is not the only one that should be taken into account in order to understand the changes in T_g of the matrix with the addition of the alumina nanoparticles.

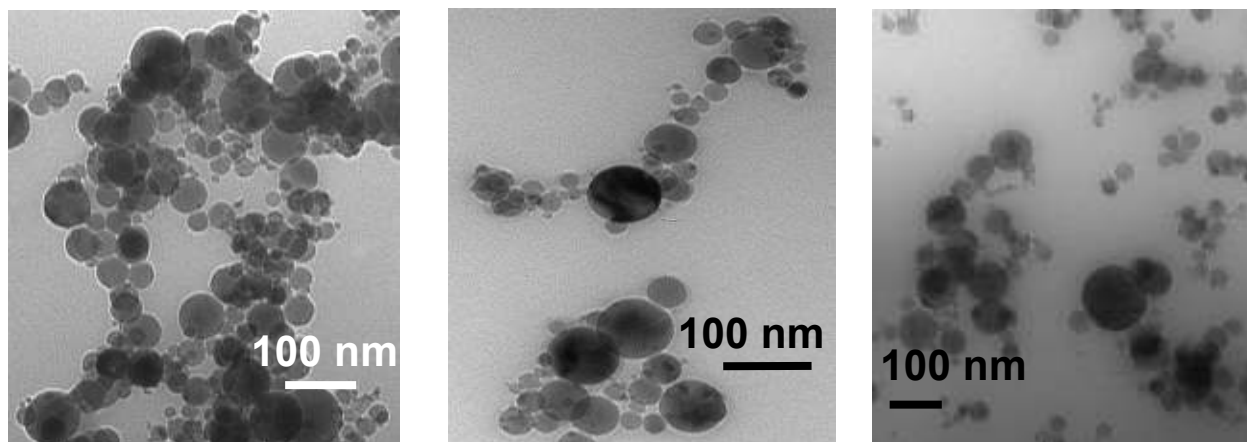


Figure 7-4: Representative TEM micrographs of 4 vol% alumina-polymer nanocomposites: a) PS, b) PMMA, c) P2VP. (The film thickness in the three samples is ~70 nm.)

While it is obvious that polymer-nanofiller interactions may be tuned by choice of polymer and nanofiller, it should also be noted that the choice of solvent used to prepare the nanocomposites via spin coating can lead to major differences in polymer-nanofiller interactions and thereby effects on T_g . Figure 7-5 compares the impact on T_g of silica nanofiller addition to PMMA when the nanocomposite is prepared in different solvents. When the nanocomposite is made using MEK, an increase in T_g is observed relative to $T_{g,bulk}$, with an increase in T_g by 5-6 K in the presence of 0.4-0.5 vol% silica. These results are consistent with the presence of wetted interfaces between PMMA and the silica nanofillers, leading to hydrogen bonds that are the underlying cause of the T_g enhancement. In stark contrast, when the nanocomposites are made using acetic acid, there is a sharp decrease in T_g with increasing nanofiller content, with the PMMA T_g being depressed from $T_{g,bulk}$ by as much as 17 K in the presence of 0.6 vol% silica. This effect can be understood by the development of free surfaces (free space) between the PMMA and the silica nanofiller. A recent study by Roth and Dutcher (2003) has reported that a 17 K reduction in T_g relative to $T_{g,bulk}$ was observed in 30-nm-thick freely standing PMMA films. We believe that the acid group of acetic group prevents or severely reduces the interaction between PMMA and the hydroxyl groups on the surface of silica; this is because the acid group interacts strongly with the PMMA ester side group (Bobiak and Koenig, 2004). (The sharply contrasting T_g results obtained in the PMMA-silica nanocomposites made using MEK and acetic acid cannot be explained by a segregation of dye to the nanofiller interface in a nanocomposite made in one solvent but not when made in the other solvent. It is well known that the vibrational

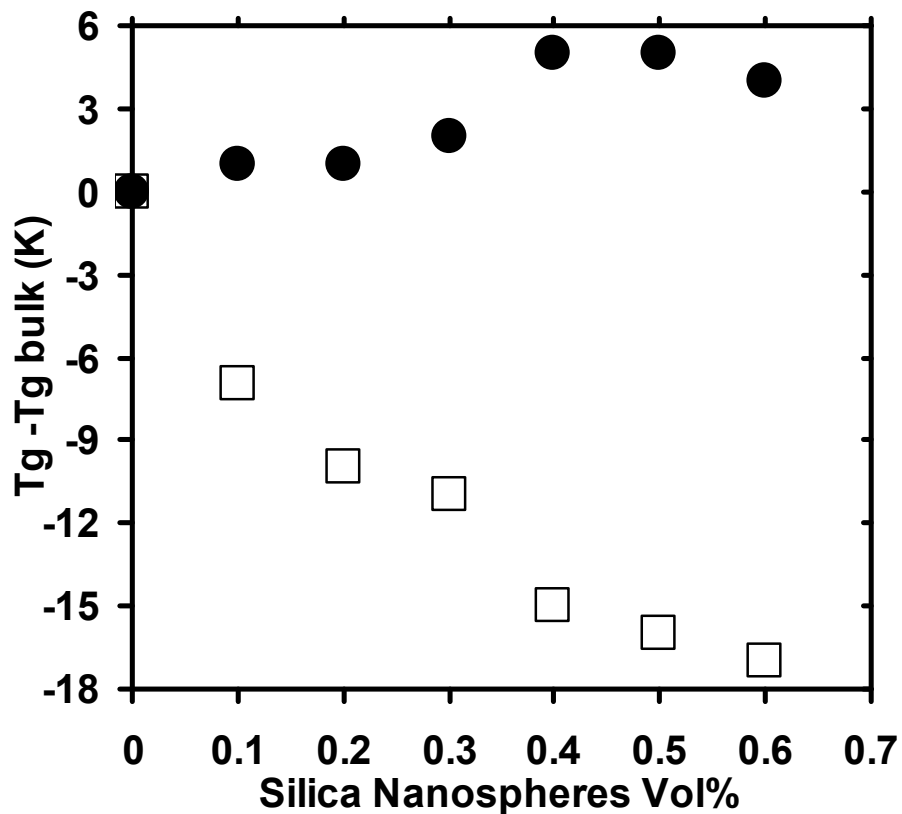


Figure 7-5: Deviations in T_g from neat, bulk PMMA T_g as a function of silica nanofiller content and solvent used to make solutions employed in spin coating the nanocomposite films: methyl ethyl ketone (closed circles), acetic acid (open squares). (Inherent errors associated with the measurements are equal to or smaller than the symbol size.)

structure of pyrenyl dye monomer fluorescence is dependent on local polarity (Kalyanasundaram and Thomas, 1977), which would be substantially different if the BPD dye were segregated at a nanofiller interface as compared to being dispersed in the polymer. However, careful inspection revealed an identical nature, within error, of the vibrational structures of the BPD emission spectra for the PMMA-silica nanocomposites made using the two solvents.)

7.4 Physical Aging Effects in Polymer Nanocomposites

The physical aging behaviors of P2VP-silica and P2VP-alumina nanocomposites were measured using the increase in fluorescence intensity of an intramolecular charge transfer probe, TCJ, as a function of logarithmic aging time to quantify aging rate. This approach takes advantage of the fact that the fluorescence intensity of TCJ (inset of Figure 7-6), which is also called a “rotor” probe, is very sensitive to local density near T_g . This excellent sensitivity originates from the fact that when the TCJ dye is in its electronic excited state, it can return to the ground by means of non-radiative decay pathways, for example, bond rotation or vibration, or by fluorescence. With minute increases in local density near T_g , the likelihood of achieving these non-radiative decay pathways during the excited state lifetime of the TCJ dye (in the order of nanoseconds) decreases, resulting in an increase in fluorescence intensity. (The much greater sensitivity of rotor probes to local density near T_g makes them better choices for monitoring physical aging than pyrenyl dyes.) Royal and Torkelson (1990; 1992; 1993) found that rotor probes provided quantitative measures of local physical aging rates and

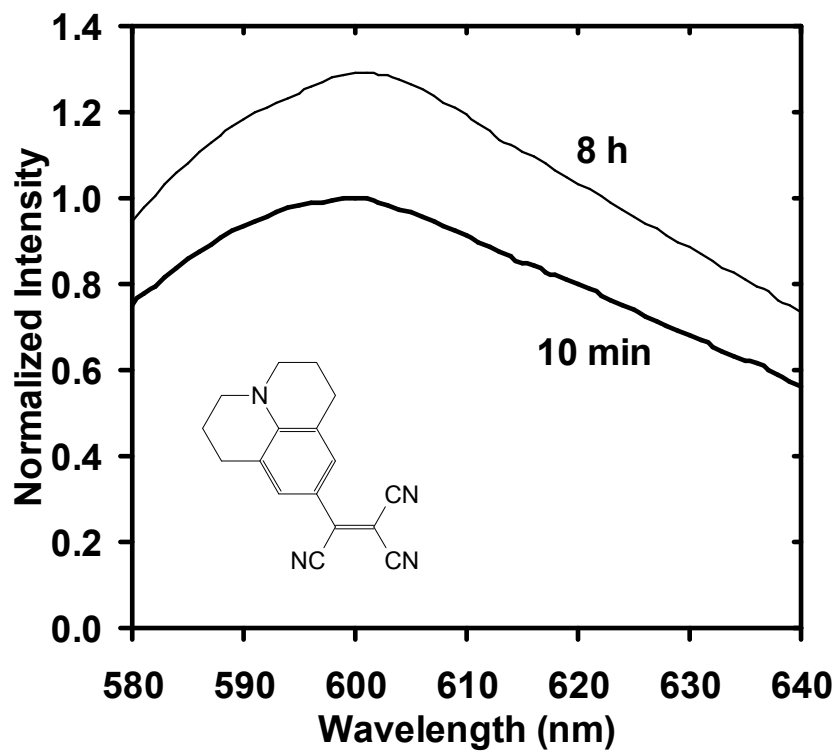


Figure 7-6: Fluorescence emission spectrum of a TCJ-doped (< 0.2 wt %) bulk P2VP film at two physical aging times after quenching from 140 °C to 30 °C. Inset: Molecular structure of TCJ.

complex relaxation behavior such as asymmetry and “memory” effects in a range of bulk polymers (PS, PMMA, poly(vinyl acetate), poly(isobutyl methacrylate), and polycarbonate). They also showed (Royal and Torkelson, 1992, 1993) that the data obtained via fluorescence regarding the temperature dependence of physical aging rate and the time to reach equilibrium during aging very near T_g agreed with results obtained by volumetric relaxation and enthalpy relaxation measurements. This fluorescence method was recently adapted by Priestley et al. (2005a; 2005b) for monitoring physical aging rate (both average and distributions) in thin and ultrathin polymer films. Here we employ this method to characterize physical aging in polymer nanocomposites. (A related fluorescence approach to monitor physical aging in bulk polymer films was recently reported by van den Berg et al. (2006).)

Figure 7-6 illustrates the change in the fluorescence spectrum of the TCJ dye during physical aging of a neat P2VP film after quenching the temperature from 140 °C to the aging temperature of 30 °C, deep in the glassy state. In 8 h of physical aging, there is a nearly 35% increase in the fluorescence intensity of the TCJ dyes doped in the P2VP film.

Figure 7-7 compares the change in fluorescence intensity during physical aging of neat P2VP to the changes observed in two P2VP nanocomposites, one with 0.4 vol% silica and the second with 4 vol% alumina. In the case of the neat P2VP film, the fluorescence intensity increases roughly linearly with logarithmic physical aging time. (The classic response in physical aging studies is a roughly linear change of the

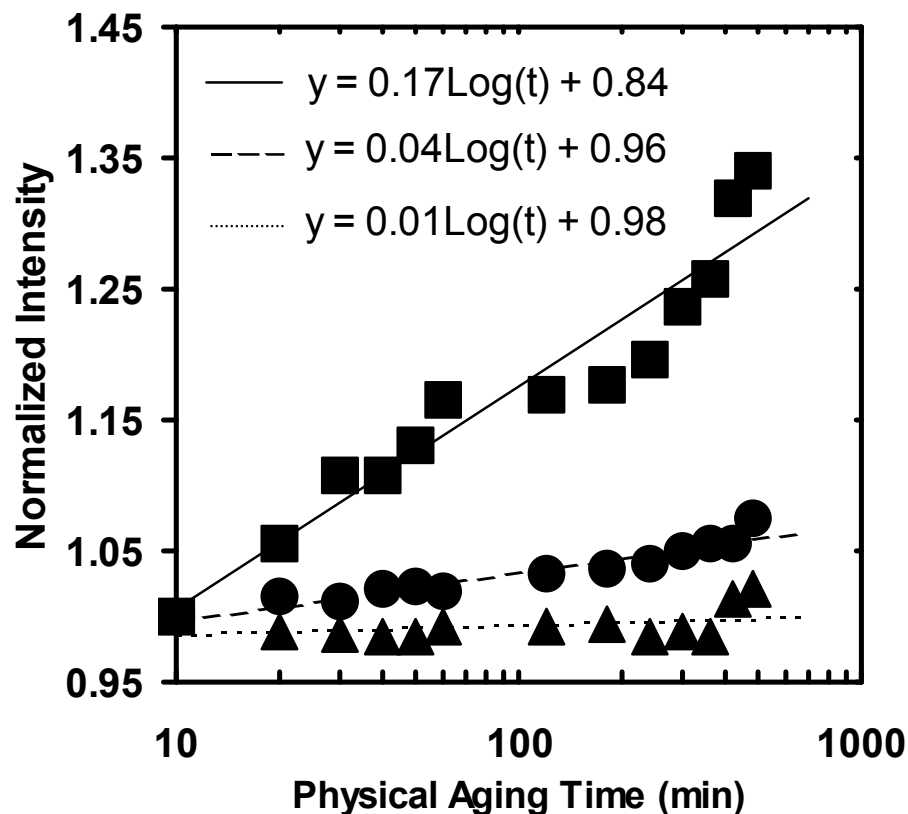


Figure 7-7: Normalized fluorescence intensity of TCJ dopant (< 0.2 wt %) as a function of logarithmic physical aging time after quenching from above T_g (140 °C) to below T_g (30 °C): bulk P2VP film (squares), 0.4 vol % silica/P2VP nanocomposite (circles), 4 vol % alumina/P2VP nanocomposite (triangles). (Lines represent best fits to the physical aging data. Note: y represents normalized intensity, and $\text{Log}(t)$ represents logarithmic aging time.)

measurable with logarithmic aging time (Struik, 1978; Greiner and Schwarzl, 1984; Royal and Torkelson, 1990, 1993; Hutchinson, 1995).) However, there is a much reduced effect of physical aging time on fluorescence intensity in the P2VP nanocomposite made with 0.4 vol% silica and a nearly invariant fluorescence intensity in the P2VP nanocomposites made with 4 vol% alumina.

In analogy with a definition of physical aging rate obtained in volumetric relaxation studies (Struik, 1978; Greiner and Schwarzl, 1984) [rate = $-(1/V_0)(dV/d\log t_a)$ where V (V_0) is the specific volume at aging time t_a (t_0)], a fluorescence physical aging rate, r_f , may be defined (Royal and Torkelson, 1993; Priestley et al., 2005a; 2005b) as follows:

$$r_f = \frac{1}{f_0} \frac{df}{d\text{Log}(t_a)} \quad (7-1)$$

where f (f_0) is the fluorescence intensity at aging time t_a (t_0). (The fact that f increases when V decreases accounts for the different sign, positive versus negative, in the equations for fluorescence physical aging rate and volumetric physical aging rate.) When equation (7-1) is applied to the data in Figure 7-7, it is seen that fluorescence physical aging rate (calculated with t_a in units of minutes) decreases in the following manner: $r_f = 0.17$ for neat P2VP, $r_f = 0.04$ for 0.4 vol% silica/P2VP nanocomposites, and $r_f = 0.01$ for 4 vol% alumina/P2VP nanocomposites. It is interesting to note that both suppression of physical aging and the T_g enhancement are greater in the 4 vol% alumina nanocomposite than in the 0.4 vol% silica nanocomposite. As the T_g enhancement is strongly correlated to the level of attractive interfacial interactions in the

nanocomposite, this suggests that the suppression of physical aging may be similarly correlated.

The factor of 4 to 17 reduction in physical aging rate of the nanocomposites relative to neat P2VP is consistent with recent measurements by Priestley et al. (2005b) of the distribution of physical aging rates in PMMA films supported on silica substrates. Relative to the bulk PMMA physical aging rate, a factor of 15 reduction in physical aging rate was observed deep in the glassy state of the 25-nm-thick layer next to the silica substrate in a supported bulk PMMA film. Furthermore, the physical aging rate was reduced from the bulk PMMA rate at length scales at least 100 nm away from the substrate interface in the film interior. This near elimination of physical aging in the region of the bulk film closest to the silica substrate and the suppression of aging rate well into the film were rationalized by the effect of hydrogen bonds at the substrate interface in suppressing the conformational relaxation processes associated with physical aging. It is not yet understood why these attractive substrate interactions have such large effects on physical aging rate deep in the glassy state, especially in comparison with their measurable but more modest impact on T_g . This issue deserves further experimental and theoretical study.

The order of magnitude reduction of physical aging rate of the P2VP/alumina nanocomposite relative to that of bulk P2VP as well as the results of Priestley et al. (2005b) suggest that a potential strategy to suppress or nearly eliminate physical aging of non-equilibrium polymer glasses is via the incorporation of well-dispersed nanofillers that undergo attractive interactions with the polymer matrix. While the underlying origin

of the very significant effect of nanofillers in suppressing physical aging is not fully understood, the effect nevertheless indicates that there may be a major advantage associated with polymer nanocomposites related to the long-term stability of certain properties of glassy polymer systems. The potential achievement of a non-equilibrium amorphous polymer nanocomposite that is stable or nearly stable to physical aging has many important technological implications.

7.5 Conclusions

The effect of the addition of alumina nanospheres to PS, PMMA and P2VP matrices on T_g was investigated using fluorescence. It was found that when wetted interfaces and attractive polymer-nanofiller interactions are both present, for example in the case of P2VP-alumina nanocomposites, the T_g is increased relative to neat, bulk polymer. When there are wetted interfaces but no significant attractive interfacial interaction, for example in the case of PS-alumina nanocomposites, the T_g is equal to neat, bulk T_g . Finally, when the interfaces are non-wetted, that is, when a free surface is present between the polymer and the nanofiller as in the case of PMMA-alumina nanocomposites, there is a reduction in T_g relative to neat, bulk T_g . These results are well understood by making analogies to studies on confined, ultrathin polymer films (see chapter 3).

Also, in this chapter it was shown how the choice of solvent used to prepare the PMMA-silica nanocomposites can lead to major differences in polymer-nanofiller interactions and thereby to major differences in effects on T_g . It was observed that

when the PMMA nanocomposites are prepared using MEK, T_g increases with the nanofiller content. For example, adding 0.4 vol% of silica resulted in a 5 K increase in T_g compared with $T_{g,Bulk}$. However when the polymer nanocomposites are made using AA, there is a sharp decrease in T_g with increasing nanofiller content, with the PMMA T_g being depressed from $T_{g,bulk}$ by 15 K in the presence of 0.4 vol% silica nanofiller. Methyl ethyl ketone allows hydrogen bonding between the ester side groups of the PMMA and the hydroxyl groups on the surface of the silica, resulting in a subtle increase in T_g . On the other hand, the acid group of AA prevents or severely reduces this interaction (because the acid group interacts strongly with the PMMA ester side group) leading to the development of free surfaces (free space) between the PMMA and the silica nanofiller. Consequently, a major decrease in T_g is observed.

Using fluorescence, the physical aging response of P2VP upon the addition of 0.4 vol% silica nanospheres or 4 vol% alumina nanospheres was investigated. This study showed that the extent of the reduction of physical aging that can be obtained depends on the strength of the interaction between the polymer and the nanofiller. For example, in the case of the P2VP-alumina nanocomposite, a nearly totally suppression of physical aging was observed, while in the case of the P2VP-silica nanocomposite physical aging was reduced but to a lesser extent. Our results suggest that surface and interface effects in polymer nanocomposites may be tailored to control the structural relaxation of high performance polymeric materials. The effect of nanofillers in reducing and suppressing physical aging may indicate a possible advantage of using polymer nanocomposites in long-term applications requiring a glassy-state material.

8 Suppression of Physical Aging in Polymer Nanocomposites with Attractive Polymer-Nanofiller Interactions

8.1 Introduction

When an amorphous polymer is cooled through its glass transition temperature, the material goes from its equilibrium rubbery state to its non-equilibrium glassy state. An effect of the non-equilibrium characteristic of the glassy state is the relaxation process known as physical aging (Greiner and Schwarzl, 1984, 1989). In this process, the material continuously evolves towards equilibrium through spontaneous, but very slow molecular rearrangements. The result is time dependent properties such as specific volume, enthalpy, entropy and mechanical response (Struik, 1978; Kovacs, 1981; Greiner and Schwarzl, 1984, 1989; McKenna, 1989; Hodge, 1995; Hutchinson, 1995). The specific volume decreases roughly linearly with logarithmic aging time (Struik, 1978; Kovacs, 1981; Greiner and Schwarzl, 1984, 1989; Hutchinson, 1995); the slope of the linear portion of this relation is defined as the volume relaxation aging rate r_v (see equation 2-9). The volume relaxation aging rate is temperature dependent and generally presents one maximum.

The importance of physical aging lies in the changes in the material properties that are caused by the densification associated with the relaxation toward equilibrium. These changes can, in many cases, negatively affect the performance and useful lifetime of the materials (Simon, 2002). Consequently, physical aging impacts the

design, manufacture and use of amorphous polymers in diverse applications (Hodge, 1995). There are significant technological and economic implications for controlling and minimizing the effects of aging on the physical properties of polymers derived from the obvious need to obtain materials with superior long-term behavior. Many techniques have been used to monitor relaxations or their manifestations including dilatometry (Kovacs et al., 1979; Kovacs, 1981; Adachi and Kotaka, 1982; Greiner and Schwarzl, 1984, 1989) which measures the specific volume, differential scanning calorimetry (Petrie, 1972; Marshall and Petrie, 1975; Bair et al., 1981; Tribone et al., 1986; Hodge, 1987; Echeverria et al., 1995) which measures enthalpy, dielectric relaxation (Bair et al., 1981; Matsuoka et al., 1985; Pathmanathan et al., 1986), positron annihilation spectroscopy (Kobayashi et al., 1989), Brillouin scattering (Patterson et al., 1990), X-ray scattering (Roe and Curro, 1983; Curro and Roe, 1984; Roe and Song, 1985; Song and Roe, 1987), tensile modulus and stress relaxation (Cizmecioglu et al., 1981; Vleeshouwers et al., 1989; Cowie et al., 1998), permeation (Levita and Smith, 1981; Coll and Searles, 1988), and probe techniques, including electron spin resonance (Tsay et al., 1982; Tsay and Gupta, 1987), photochromic (Lamarre and Sung, 1983; Victor and Torkelson, 1988; Yu et al., 1988; Royal et al., 1992), second-order nonlinear optical (Hampsch et al., 1990; Hayden et al., 1990) and fluorescence (Meyer et al., 1990; Royal and Torkelson, 1990; Schwab and Levy, 1990; Royal and Torkelson, 1992, 1993; van den Berg et al., 2006).

Fluorescence is a powerful tool for investigating the structure and dynamics of matter. In particular, this technique can be very useful in studying physical properties of

polymers. The success of fluorescence arises from its high sensitivity, specificity and its ability to provide spatial and temporal information (Valeur, 2002). In analogy with the definition of the physical aging rate obtained in volumetric relaxation studies (equation 2-9), a fluorescence physical aging rate r_f may be defined (Royal and Torkelson, 1993; Priestley et al., 2005a; Priestley et al., 2005b) (equation 4-2).

Royal and Torkelson (1990; 1992; 1993) studied physical aging in polystyrene (PS), poly(methyl methacrylate) (PMMA), poly(vinyl acetate), polycarbonate and poly(isobutyl methacrylate) using rotor fluorophores. They determined physical aging rates of various glassy polymers by fluorescence methods using the probe julolidenemalononitrile (JMN) (Royal and Torkelson, 1992, 1993). They showed that the dependence of physical aging rates by fluorescence methods agree well with those from specific volume relaxation experiments, demonstrating the free-volume sensitivity of JMN (Royal and Torkelson, 1993). In addition, they showed that the times required to reach equilibrium for the enthalpy relaxation experiments are similar to the fluorescence equilibrium times (Royal and Torkelson, 1992).

When a polymer is confined to the extent where the surface (or interface) to volume ratio exceeds a particular value, its properties may deviate dramatically from those observed in bulk. As the confining dimension is decreased, a greater portion of material is in immediate contact with an interface, leading to interfacial interactions playing a substantial role in the observed properties. This behavior has implications in a broad range of technological applications such as photoresists, membranes and nanocomposites, among others. Thin and ultrathin films have dominated research in

the area of confined polymer behavior due to the ease with which the confinement dimension (film thickness) can be varied, and only recently have much more complex systems such as polymer nanocomposites been studied. The next paragraphs attempt to shortly summarize the efforts to study physical aging in thin and thick films.

Ellison et al. (2002) studied poly(isobutyl methacrylate) films supported on quartz over a range of thicknesses from 10 nm to 800 nm; they found an almost invariable physical aging rate. The effect of confinement on the physical aging response of PS films with thicknesses between 10-200 nm was studied by Kawana and Jones (2003). They showed that a 10 nm film was still in an equilibrium state at 30 °C below bulk T_g , consistent with the notion that the T_g of the 10 nm thick film is reduced relative to the bulk value by at least 30 °C. Priestley et al. (2005a) provided the first characterization of physical aging as a function of polymer-substrate interactions. Physical aging in ultrathin PS films was shown to be dependent on thickness and absent when the aging temperature was above the T_g of the confined film but below that of bulk polymer. In contrast, the presence of structural relaxation was observed 6 °C above the bulk T_g for an ultrathin PMMA film supported on a silica substrate. This result is a consequence of the attractive interactions between the polymer and the substrate which lead to an increase of T_g . Using dielectric measurements, Fukao and Sakamoto (2005) reported physical aging results of PMMA thin films. They observed a decrease of the aging rate as the film thickness decreases. Priestley et al. (2005b) studied the structural relaxation of PMMA at interfaces and between them, using fluorescence multilayer techniques. They showed that physical aging is almost totally suppressed in a 25-nm-thick layer

adjacent to the substrate due to formation of hydrogen bonds that restrain small motions associated with structural relaxation. At the free surface, the physical aging rate is also diminished, but to a lesser extent than at the substrate. The free surface effects were explained as a consequence of the reduced thermodynamic driving force for structural relaxation. Interestingly, the substrate and free surface layers affect the structural relaxation rate over similar distances into the film interior.

Permeability measurements on numerous polymers have shown accelerated physical aging in thin free-standing films compared with much thicker bulk films (Pfromm and Koros, 1995; Dorkenoo and Pfromm, 1999, 2000; McCaig and Paul, 2000; McCaig et al., 2000; Huang and Paul, 2004, 2005; Kim et al., 2006; Huang and Paul, 2007a, 2007b). All these results contrast with the multilayer fluorescence results of Priestley et al. (2005b) which present diminished physical aging rates at the free surface. The differences between these studies are twofold: the permeability studies used higher free volume polymers with significantly more rigid backbones than the PMMA employed in the multilayer fluorescence studies, and the permeability studies were done on free-standing films while the multilayer fluorescence measurements were performed on supported films. However, the diminished aging observed by fluorescence was measured in the free surface layer, and therefore, should be unaffected by the substrate. Whether the origin of the difference in the effect of confinement on physical aging rate is due to the differences in polymer free volume and backbone rigidity between these polymers remains unclear.

Only a few studies have aimed at identifying the impact of the addition of nanofillers in the polymeric matrix on the structural relaxation (Lee and Lichtenhan, 1998; Lu and Nutt, 2003a, 2003b; Rittigstein and Torkelson, 2006). Lee and Lichtenhan (1998) reported that the inclusion of polyhedral oligomeric silsesquioxane (POSS) nanoreinforcements in epoxy by *in situ* polymerization retarded the physical aging rate and the time to reach equilibrium. They proposed that the presence of POSS cages attached to the network chains provide topological constraints to the network junctions, preventing or severely retarding the process of the matrix reaching structural equilibrium. More recently, Lu and Nutt (2003a; 2003b) observed that the inclusion of intercalated clay nanofillers into an epoxy network had a significant effect on the segmental relaxation of the matrix. They found a restricted relaxation behavior with slower overall relaxation rates and a broader distribution of relaxation times in intercalated silicate-epoxy nanocomposites relative to the neat epoxy resin. They concluded that this behavior depends on the extent of exfoliation of the layered silicates and the strength of interaction between the silicate surface and the polymer. Rittigstein and Torkelson (2006) showed reduction and suppression of fluorescence physical aging when 0.4 vol% silica and 4 vol% alumina nanospheres, respectively, are added to a poly(2-vinyl pyridine) matrix (see chapter 7).

In this chapter it is shown, through the use of fluorescence, that adding alumina and silica nanospheres to PMMA reduces and even suppresses the initial (8-hr) physical aging response at different temperatures below T_g . It will be demonstrated that and explained how the extent of the reduction of physical aging of PMMA-silica

nanocomposites is affected by the choice of spin coating solvent used to make the polymer nanocomposites. In addition, it will be shown that the inclusion of these nanofillers into PS does not affect its relaxation process due to the lack of interaction between them.

8.2 Experimental

Polystyrene (PS) (Pressure Chemical, reported values of $M_n = 290,000$ g/mol, $M_w/M_n < 1.06$) was used as received. Poly(methyl methacrylate) (PMMA) was synthesized by free radical polymerization ($M_n = 355,000$ g/mol, $M_w/M_n = 1.54$, by gel permeation chromatography using universal calibration with PS standards). The probe 4-tricyanovinyljulolidene (TCJ) (Molecular Probes) was used as received, and TC1 was synthesized using procedures reported by Hooker (1996) and McKusick et al. (1958). Following an approach used by Deppe et al. (1996), PMMA was synthesized incorporating a trace of TC1-labeled methacrylate monomer ($M_n = 350,000$ g/mol, $M_w/M_n = 1.60$, by gel permeation chromatography using universal calibration with PS standards). Bulk T_g ($T_{g,bulk}$) values were measured by differential scanning calorimetry (DSC) (Mettler-Toledo DSC822, second heat, onset method, 10 °C/min) and also via fluorescence methods and were found to agree within experimental error: PS $T_{g,bulk} = 102$ °C by DSC and 101 °C by fluorescence; PMMA $T_{g,bulk} = 120$ °C by DSC and 118 °C by fluorescence; and TC1-labeled PMMA $T_{g,bulk} = 120$ °C by DSC and fluorescence. Alumina nanospheres (alumina oxide nanopowder, Sigma-Aldrich, reported diameter of 47 nm) and silica nanospheres (colloidal silica in methyl ethyl ketone, Nissan Chemical

Industries, reported diameter of 10-15 nm) were used as received.

Thin films of neat polymers and polymer nanocomposites were prepared by spin-coating (Spangler et al., 1990; Hall et al., 1998b) dilute solutions of polymer and dye, with or without nanofiller, onto quartz slides. All solutions were made using methyl ethyl ketone (MEK) as solvent except for a sample of 0.4 vol% silica-PMMA nanocomposite that was made using acetic acid (AA) as solvent. (The colloidal silica in methyl ethyl ketone was diluted in AA.) Solutions containing nanofiller were sonicated (Branson 1200 sonicator) for 40 min prior to spin coating. TCJ-doped films contained less than 0.2 wt% dye relative to polymer and TC1-labeled PMMA had 0.24 mol% TC1 label (UV-vis absorbance). Resulting films were at least 1 μm in thickness as determined using a Tencor P10 profilometer. Films were dried for at least 2 days in a chemical fume hood prior to performing fluorescence measurements.

Prior to each aging experiment, the thermal history was erased by annealing at 150 °C for 1 h. Films were quenched using a temperature-controlled cell holder preset to the aging temperature. Fluorescence was measured using a Photon Technology International fluorimeter with 2.5 mm excitation and emission slits (10 nm and 5 nm band-pass, respectively). Physical aging was characterized using TCJ dopant and TC1 label as the fluorescence dyes in bulk polymer and polymer nanocomposite films. In the case of TCJ-doped films the excitation wavelength used was 520 nm, while in the case of TC1-labeled material was 480 nm. Physical aging was monitored by measuring the maximum emission intensity of TCJ-doped PMMA (at 586-590 nm for bulk PMMA and at 564-568 nm for bulk PS, at 584-588 nm for 0.4 vol% silica-PMMA nanocomposite

and at 571-575 nm for 0.4 vol% silica-PS nanocomposite, at 585-589 nm for 4 vol% alumina-PMMA nanocomposite and at 564-568 nm for 4 vol% alumina-PS nanocomposite) and of TC1-labeled PMMA (at 560-565 nm for bulk PMMA and at 584-588 nm for 0.4 vol% silica-PMMA nanocomposite). Measurements were made as a function of aging time after quenching the films from the rubbery state above T_g to different aging temperatures.

8.3 Results and Discussion

The physical aging behavior of PMMA-silica, PMMA-alumina, PS-silica and PS-alumina nanocomposites are studied in this chapter. The nanocomposites made with silica nanospheres (10-15 nm diameter) are well-dispersed systems as shown in the TEM micrographs presented in Figure 6-2 and Figure 6-4. On the other hand, the dispersion of the nanocomposites made with alumina nanospheres (nominally 47 nm diameter but with much polydispersity) depends on the polymer matrix, achieving a better dispersion in PMMA than in PS as shown in the TEM micrographs presented in Figure 7-4.

The increase in fluorescence intensity as a function of logarithmic aging time of an intramolecular charge probe, TCJ or TC1, was used to characterize the physical aging behavior at different temperatures of the polymer nanocomposites. Figure 8-1a illustrates the change in the fluorescence spectrum of TCJ dopant in a bulk PMMA film during physical aging after quenching the temperature from above $T_{g,Bulk}$ to $T_{g,Bulk} - 86$

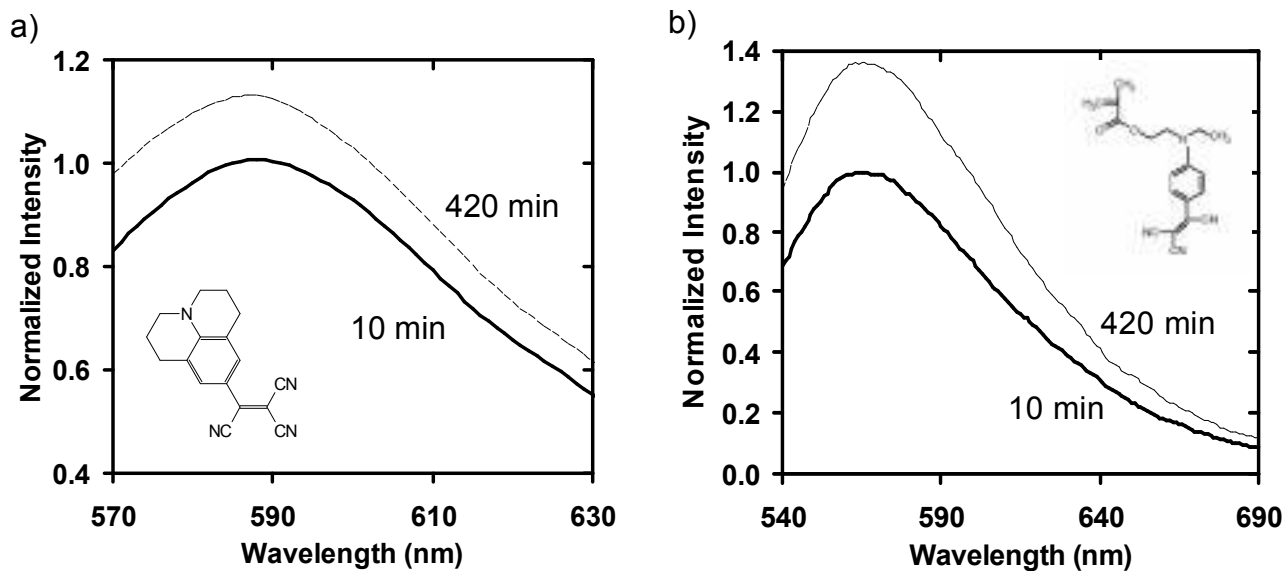


Figure 8-1: a) Fluorescence emission spectrum of a TCJ-doped (< 0.2 wt%) bulk PMMA film at two physical aging times after quenching from above $T_{g,bulk}$ to $T_{g,bulk} - 86$ K. Inset: molecular structure of TCJ. b) Fluorescence emission spectrum of a bulk TC1-labeled PMMA film at two physical aging times after quenching from above $T_{g,bulk}$ to $T_{g,bulk} - 88$ K. Inset: molecular structure of TC1-labeled methacrylate monomer.

K. Figure 8-1b shows the emission spectrum of a bulk TC1-labeled PMMA film at two physical aging times after quenching the temperature from above $T_{g,Bulk}$ to $T_{g,Bulk} - 88$ K. After absorption of light and promotion of an electron to an excited singlet state, both TCJ and TC1 'rotor' probes return to the ground state by internal conversion (energy loss by vibrational and rotor motions) or by fluorescence. Densification of the material upon aging occurs, suppressing the internal conversion and yielding an increase in fluorescence intensity. Figure 8-1 shows that TC1-labeled PMMA exhibits a higher sensitivity to physical aging than TCJ dopant in PMMA. Also, the increased intensity of TC1-labeled PMMA exceeds that observed in various JMN-doped polymers (Royal and Torkelson, 1992, 1993) as well as in TC1-doped PMMA (Priestley et al., 2005a). When a 'rotor' probe is labeled instead of doped, its quantum yield increases as a result of the more restricted mobility associated with covalent attachment, resulting in an excellent sensitivity to physical aging.

Figure 8-2 compares the change in TCJ dopant fluorescence intensity during physical aging of bulk PMMA to the changes observed in 4 vol% alumina-PMMA nanocomposite and 0.4 vol% silica-PMMA nanocomposite (made using MEK solvent) after quenching the temperature from above $T_{g,bulk}$ to aging temperatures of 305 K and 358 K. When aged at 305 K, the bulk PMMA film showed an approximately 13% increase in fluorescence intensity over 8 h. However, over the same 8 h physical aging time, there is a greatly reduced effect of aging in the PMMA nanocomposite made with 4 vol% alumina (~6% intensity increase), and the fluorescence intensity in the PMMA nanocomposite made with 0.4 vol% silica (MEK) is nearly invariant. At 358 K, the TCJ-

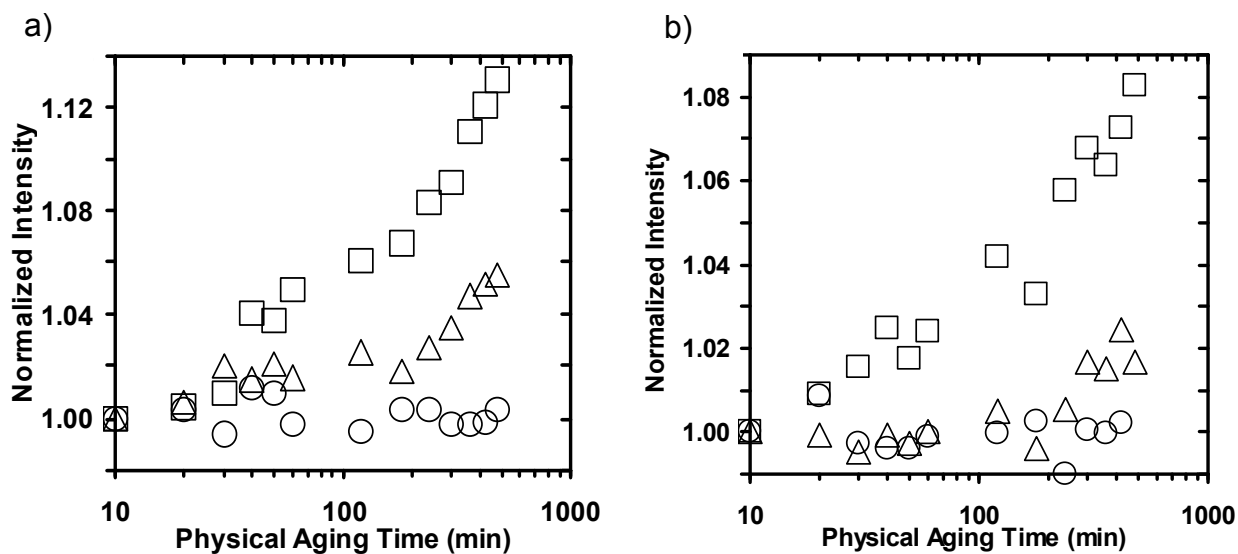


Figure 8-2: a) Normalized fluorescence intensity of TCJ dopant (< 0.2 wt%) as a function of logarithmic physical aging time after quenching from above $T_{g,bulk}$ to 305 K: PMMA ($T_g - 86$ K) (squares), 4 vol% alumina-PMMA nanocomposite ($T_g - 83$ K) (triangles) and 0.4 vol% silica-PMMA nanocomposite (MEK) ($T_g - 91$ K) (circles). b) Normalized fluorescence intensity of TCJ dopant (< 0.2 wt%) as a function of logarithmic physical aging after quenching from above $T_{g,bulk}$ (413 K) to 358 K: PMMA ($T_g - 33$ K) (squares), 4 vol% alumina-PMMA nanocomposite ($T_g - 30$ K) (triangles) and 0.4 vol% silica-PMMA nanocomposite (MEK) ($T_g - 38$ K) (circles).

doped bulk PMMA film exhibits an increase in fluorescence intensity of about 8% over an 8 h physical aging time, while the 4 vol% alumina-PMMA nanocomposite exhibits an intensity increase of only 2% and the 0.4 vol% silica-PMMA nanocomposite (MEK) exhibits, within error, no aging.

In order to compare the effect of aging temperature on the TCJ dopant fluorescence aging rate, r_f , in bulk PMMA and silica- and alumina-PMMA nanocomposites, equation 4-2 was applied to the fluorescence physical aging data. The calculated r_f values are presented in Figure 8-3. This figure shows that bulk PMMA has a maximum aging rate at 305 K. This agrees with the specific volume aging rate of bulk PMMA reported by Greiner and Schwarzl (1984) and the characterization of r_f using julolidenemalonitrile (JMN) performed by Royal and Torkelson (1993). The aging rate of 4 vol% alumina-PMMA nanocomposite is reduced dramatically in comparison to the bulk material. However, both materials appear to have the same trend of r_f with physical aging temperature. When 0.4 vol% silica is added to the PMMA matrix, there is no change in r_f over the temperature and time studied using TCJ-doped dye.

The differences in physical aging behavior in the PMMA nanocomposites made with silica and alumina may be due to the difference in the surface interaction between the fillers and PMMA. It was shown previously (Rittigstein and Torkelson, 2006) that 0.4 vol% silica-PMMA made using MEK exhibits an increase in T_g by 5 K relative to $T_{g,bulk}$ (see chapter 7). This T_g increase is consistent with the presence of hydrogen bonds between PMMA and the silica nanofillers. These hydrogen-bonding interactions between the ester side groups of PMMA and the hydroxyl groups on the surface of the

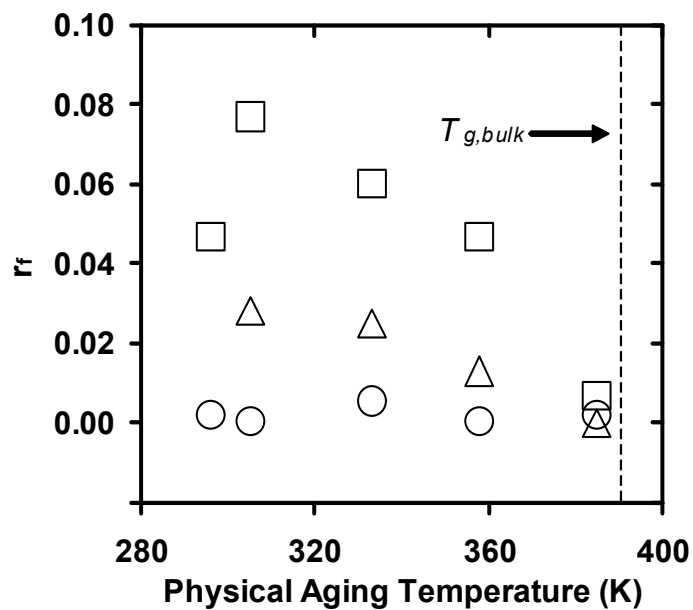


Figure 8-3: Fluorescence aging rate, r_f , as a function of physical aging temperature for: PMMA (squares), PMMA 4 vol% alumina (triangles) and PMMA 0.4 vol% silica (MEK) (circles). (Fluorescence aging rate is calculated over a physical aging time scale from 10 to 480 min. TCJ-doped PMMA was used in all systems.)

silica nanospheres significantly retard the conformational relaxation processes that are associated with physical aging. In the case of the alumina-PMMA nanocomposites, reductions in T_g relative to $T_{g,bulk}$ have been previously reported (Ash et al., 2002b; Rittigstein and Torkelson, 2006). This T_g behavior was rationalized as resulting from the presence of a free surface between the PMMA and the alumina nanofiller surface, i.e., PMMA does not form a wetted interface with alumina. The results in Figure 8-3 suggest that suppression of physical aging is strongly correlated to the presence of wetted interfaces or free surfaces between the polymer and the nanofiller, and they agree with the results of the multilayer fluorescence measurements by Priestley et al. (2005b).

Figure 8-4 shows the physical aging T_g response of bulk PS, 0.4 vol% silica-PS and 4 vol% alumina-PS nanocomposites at different temperatures over 8 h. In agreement with previous studies, the bulk PS film ages faster at 333 K than at 304 K and 363 K (Greiner and Schwarzl, 1984; Priestley et al., 2005a). Also, it can be observed that the nanocomposite films exhibit the same aging behavior within error as the bulk PS at those conditions; therefore, the addition of 0.4 vol% silica or 4 vol% alumina nanospheres does not affect the physical aging response of PS. Rittigstein and Torkelson (2006) showed that PS-silica and PS-alumina nanocomposites exhibit no change in T_g within error when silica or alumina nanofiller is present up to 0.5 vol% or 10 vol%, respectively (see chapter 7). The absence of changes on T_g and physical aging with the addition of alumina or silica nanospheres to PS is consistent with the notion that wetted PS-silica and PS-alumina interfaces are present with no interactions.

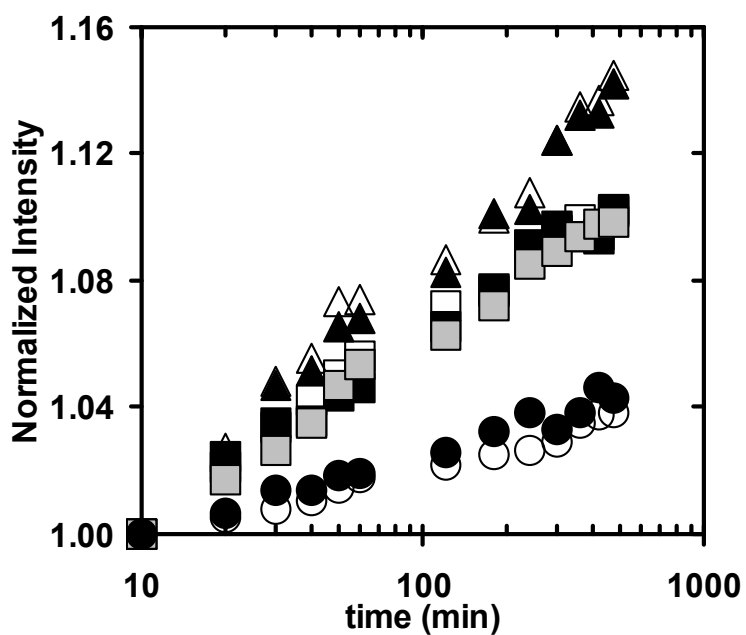


Figure 8-4: Normalized fluorescence intensity of TCJ dopant (< 0.2 wt%) as a function of logarithmic physical aging time after quenching from above $T_{g,bulk}$ to: 333 K: PS (open triangles) and 0.4 vol% silica-PS nanocomposite (closed triangles), 363 K: PS (open squares), 0.4 vol% silica-PS nanocomposite (closed squares) and 4 vol% alumina-PS nanocomposite (gray squares), 303 K: PS (open circles) and 0.4 vol% silica-PS nanocomposite (closed circles).

These results are in agreement with the study of physical aging in PS thin and ultrathin films supported on silica by Priestley et al. (2005a). Both studies showed that when the effect of nanoconfinement on T_g is accounted for, there is no effect of nanoconfinement on aging rate in PS.

Since no change of TCJ dopant fluorescence intensity was observed over the physical aging times and temperatures studied for the case of 0.4 vol% silica-PMMA nanocomposites (MEK), this system will also be examined using TC1-labeled PMMA. Employing a 'rotor' dye as a label instead of a dopant allows for a higher sensitivity to physical aging, thus permitting more critical differentiation of r_f with temperature and helping to understand its trend. Figure 8-5 compares the change in TC1-labeled PMMA fluorescence intensity during physical aging of bulk PMMA to the changes observed in 0.4 vol% silica-PMMA nanocomposites made using MEK and AA. In both cases, the measurements are made after quenching the temperature from above $T_{g,bulk}$ to aging temperatures of 305 K and 363 K. When aged at 305 K, the bulk PMMA film showed a 39% increase in fluorescence intensity over 8 h. However, with the same aging time and temperature the fluorescence intensity is nearly invariant (~ 2% increase) in the PMMA nanocomposites made with 0.4 vol% silica, regarding of solvent used in making the nanocomposites. At 363 K, the bulk PMMA film exhibits an increased intensity of about 32% over 8h, while the PMMA-silica nanocomposites showed a greatly reduced effect: the 0.4 vol% silica-PMMA nanocomposite made using AA exhibited a 10% increase in fluorescence intensity while the 0.4 vol% silica-PMMA nanocomposite made

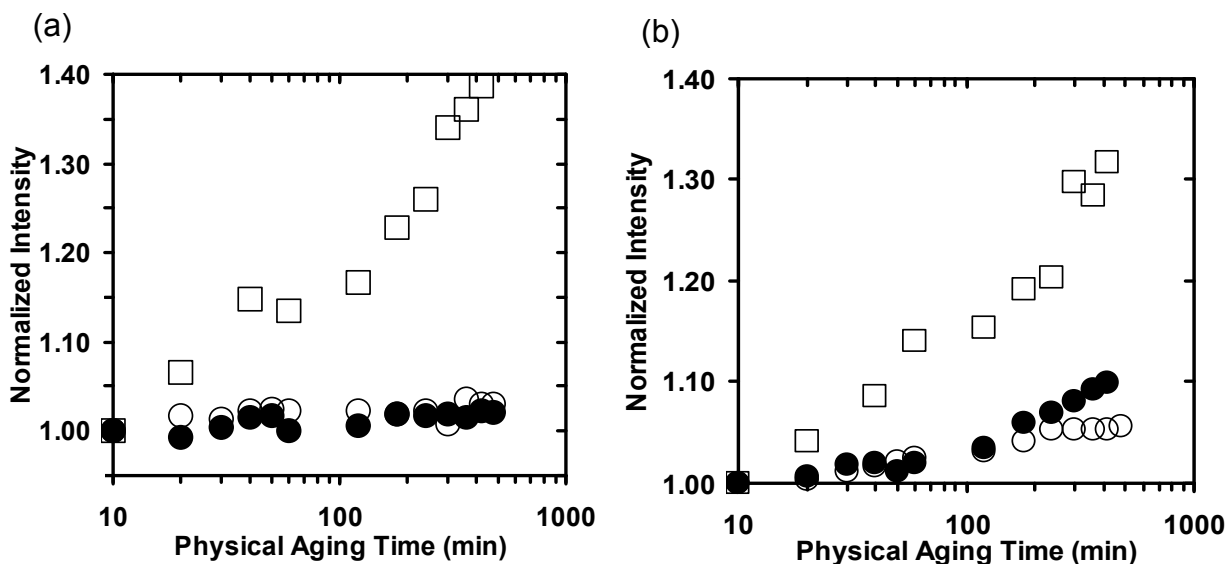


Figure 8-5: a) Normalized fluorescence intensity of TC1-label as a function of logarithmic physical aging after quenching from above $T_{g,bulk}$ to 305 K: PMMA ($T_g - 86$ K) (squares), 0.4 vol% silica-PMMA nanocomposite (MEK) ($T_g - 91$ K) (open circles) and 0.4 vol% silica-PMMA nanocomposite (AA) ($T_g - 71$ K) (closed circles). b) Normalized fluorescence intensity of TC1-label as a function of logarithmic physical aging after quenching from above $T_{g,bulk}$ to 363 K: PMMA ($T_g - 28$ K) (squares), 0.4 vol% silica-PMMA nanocomposite (MEK) ($T_g - 33$ K) (open circles) and 0.4 vol% silica-PMMA nanocomposite (AA) ($T_g - 13$ K) (closed circles).

using MEK exhibited a 6% increase. Thus, by using a label 'rotor' probe with enhanced sensitivity to physical aging, we can observe not only a strong reduction in physical aging rate upon addition of 0.4 vol% silica but also the influence of using different solvents to prepare the nanocomposites.

The fluorescence physical aging rates for TC1-labeled PMMA systems were obtained by applying equation 4-2 to the physical aging data. The results are presented in Figure 8-6. Comparison of Figure 8-3 and Figure 8-6 reveals that regardless of whether TCJ dopant or TC1 label was employed in the measurements, the physical aging rate of bulk PMMA exhibits a similar trend with temperature with a maximum at 305 K. Again in this case, the advantage of using the TC1-label dye instead of the TCJ-doped dye is that the former allows one to observe not only the suppression of physical aging with the addition of silica nanospheres, but also its trends with temperature and the choice of solvent used to prepare the nanocomposites. Over the physical aging temperatures and times studied, both nanocomposites made with 0.4 vol% silica (MEK and AA) exhibit the same trend with temperature, presenting a maximum aging rate around 360 K. Relative to bulk PMMA, the rate of structural relaxation of 0.4 vol% silica-PMMA nanocomposite at 323 K is reduced by a factor of 17 using MEK as solvent and a factor of 7 using AA as solvent. This extraordinary suppression in aging rate is consistent with a previous report of arrested physical aging in 0.4 vol% silica-P2VP nanocomposites (Rittigstein and Torkelson, 2006) and with studies examining the physical aging rates, both average values and their distributions, across thin PMMA

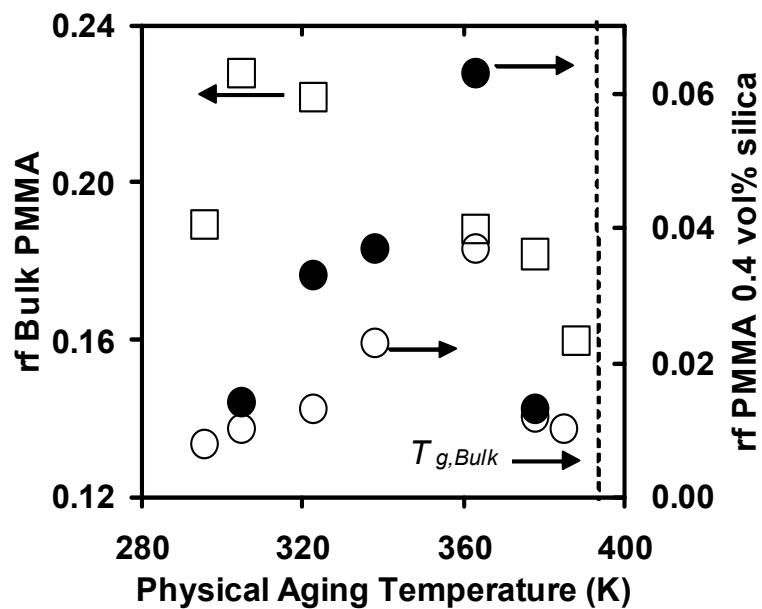


Figure 8-6: Fluorescence aging rate, r_f , as a function of physical aging temperature for: PMMA (squares), PMMA 0.4 vol% silica (MEK) (open circles) and PMMA 0.4 vol% silica (AA) (closed circles). (Fluorescence aging rate is calculated over a physical aging time scale from 10 to 420 min. TC1-labeled PMMA was used in all systems.)

films supported on one side by a silica (quartz) substrate (Priestley et al., 2005a; Priestley et al., 2005b).

The choice of solvent used to prepare the PMMA-silica nanocomposites can lead to major differences in polymer-nanofiller interactions and thereby major differences in T_g and physical aging rate. In a previous study, Rittigstein and Torkelson (2006) found that use of MEK to make 0.4 vol% silica-PMMA led to an increase in T_g of 5 K relative to neat bulk PMMA. In contrast, when 0.4 vol% silica-PMMA nanocomposites were made using AA, there was a decrease in T_g with increasing nanofiller content, with the PMMA T_g being depressed from $T_{g,bulk}$ by 15 K (see chapter 7). The use of MEK during nanocomposite preparation allowed hydrogen bonding between the ester side groups of the PMMA and the hydroxyl groups on the surface of the silica, resulting in a subtle increase in T_g and a nearly total suppression of physical aging. On the other hand, the acid group of AA apparently prevents or severely reduces this interaction (because the acid group interacts strongly with the PMMA ester side group (Bobiak and Koenig, 2004)) leading to development of free surfaces (free space) between the PMMA and the silica nanofiller. Consequently, a major decrease in T_g and arrested physical aging are observed. These results are consistent with the study of the distribution of physical aging rates in PMMA films supported on silica by Priestley et al. (2005b). Both studies showed that the presence of hydrogen bonds almost suppressed physical aging in PMMA, while the existence of free surfaces diminish physical aging but to a lesser extent.

8.4 Conclusions

Fluorescence spectroscopy has been used to determine the impact of the addition of low levels of well-dispersed silica and alumina nanospheres on the physical aging behavior of PMMA and PS. Following a temperature quench from above T_g into the glass, isothermal aging was monitored over 8 h at temperatures ranging from 296 K to 388 K. The addition of 4 vol% alumina nanospheres (nominally 47 nm diameter but with much polydispersity) or 0.4 vol% of silica nanospheres (10-15 nm diameter) to PMMA greatly reduces the physical aging response of the polymer. However, no reduction in physical aging rate was observed upon addition of these nanofillers to PS. In the case of PMMA-silica nanocomposite, we demonstrated that the extent of the reduction of physical aging is affected by the choice of spin coating solvent used to make the polymer nanocomposite.

Our results suggest that surface and interface effects may be tailored to control the structural relaxation of high performance materials using polymer nanocomposites. The effect of nanofillers in reducing and suppressing physical aging indicates a possible advantage of using polymer nanocomposites in long-term applications where physical aging can lead to deleterious effects on the properties of glassy polymers.

9 Controlling the Average and Local Glass Transition Temperatures of PMMA-SWCNT Nanocomposites

9.1 Introduction

Polymer nanocomposites are materials that open the door to novel applications in numerous areas including chemical sensing (Krasteva et al., 2002), catalysis (Galow et al., 2002; Esumi et al., 2004), drug delivery (Brigger et al., 2002), energy devices (Croce et al., 1998; Xi et al., 2005; Olivetti et al., 2006), membranes (Merkel et al., 2002) and lithographic patterning (Damean et al., 2005). Several benefits of these diverse, unique and versatile functional systems have been identified, providing the potential to compete commercially with more traditional materials. These improvements include efficient reinforcement with minimal loss of ductility and impact strength, reduced weight, thermal stability, flame resistance, improved abrasion resistance, and enhanced barrier, optical and electrical properties, among others (Kojima et al., 1993; Yano et al., 1993; Messersmith and Giannelis, 1995; Akelah and Moet, 1996; Giannelis, 1996; Ke et al., 1999). However, the current fundamental understanding of the mechanism of property changes associated with polymer nanocomposites is still quite primitive; advancing this knowledge is essential for basic science and technology.

In order to effectively understand the physics behind polymer nanocomposites, close attention must be given to properties that can provide key information about them. The glass transition temperature (T_g) is the temperature at which the properties of a polymer change from an equilibrium rubbery state to a non-equilibrium glassy state as

the material is cooled. The T_g value is widely used to characterize a material and determines the use and processing temperatures of polymers (McKenna and Simon, 2002). In polymer nanocomposites with well-dispersed nanofillers, T_g can exhibit substantial deviations relative to the bulk polymer (Starr et al., 2001; Ash et al., 2002b; Berriot et al., 2002; Arrighi et al., 2003; Berriot et al., 2003; Liu et al., 2003; Mbhele et al., 2003; Wang et al., 2003; Ash et al., 2004; Sun et al., 2004; Bansal et al., 2005; Kotsilkova et al., 2005; Ramanathan et al., 2005b; Bansal et al., 2006; Blum et al., 2006; Rittigstein and Torkelson, 2006; Kropka et al., 2007; Lee et al., 2007b; Rittigstein et al., 2007), decreasing when the polymer-nanofiller interfaces yield free surfaces (nonwetted interface) (Starr et al., 2001; Ash et al., 2002b; Arrighi et al., 2003; Liu et al., 2003; Wang et al., 2003; Ash et al., 2004; Sun et al., 2004; Bansal et al., 2005; Bansal et al., 2006; Rittigstein and Torkelson, 2006) and increasing when wetted interfaces with attractive interactions result (Starr et al., 2001; Berriot et al., 2002, 2003; Mbhele et al., 2003; Kotsilkova et al., 2005; Ramanathan et al., 2005b; Bansal et al., 2006; Blum et al., 2006; Rittigstein and Torkelson, 2006; Kropka et al., 2007; Rittigstein et al., 2007).

Simulations (Starr et al., 2001; Vacatello, 2001; Smith et al., 2002; Vacatello, 2002) suggest that the presence of nanoparticles change the monomer packing near the polymer-particle interface, leading to global and local perturbations of the segmental dynamics compared with the bulk polymer. The notion of polymer within the composites having different properties depending on whether it is located near a filler structure (interface region) or in the bulk polymer had been suggested long ago (Kaufman et al., 1971; Iisaka and Shibayama, 1978; Struik, 1978, 1987; Hergeth et al., 1989) but was

only used for qualitative understanding. In the mid-1990's, Tsagaropoulos and Eisenberg (1995) showed via dynamic mechanical analysis that some polymer nanocomposites can exhibit two different $\tan \delta$ peaks. This reflects the presence of two glass transitions; one is related to the bulk polymer and the other, occurring at higher temperatures, is assigned to the glass transition of polymer regions containing chains of reduced mobility within the nanoparticle agglomerations. More recently, efforts have focused on using the idea of a distribution in T_g s to understand the behavior of polymer nanocomposites (Berriot et al., 2002, 2003; Ash et al., 2004). Providing a new understanding of complex mechanical behavior, Berriot et al. (2002; 2003) invoked a gradient in T_g associated with a gradient in mechanical properties in the vicinity of silica particles in filled elastomers. By comparing NMR and mechanical data, they demonstrated that segmental dynamics can be impacted locally near the interfaces.

Ramanathan et al. (2005b) presented results for poly(methyl methacrylate) (PMMA) grafted to amide-functionalized single-walled carbon nanotubes (SWCNTs). They demonstrated that even with low SWCNT loadings (1 wt%), the thermal, mechanical and electrical properties are significantly improved when compared to those in the neat polymer. In the case of the glass transition behavior, they observed a 33 K increase in T_g of PMMA when covalently attached to 1 wt% amide-functionalized SWCNT. This result suggests the formation of an interfacial region of reduced molecular mobility in the vicinity of the nanotubes that penetrates throughout the composite, leaving very little bulk polymer response. They addressed the need for

more detailed experiments to provide understanding of the changes in local polymer dynamics near nanoparticles and the percolation of these effects in the systems.

A quantitative understanding of the structure and properties of the polymer-nanofiller interface is necessary to be able to design polymer nanocomposites with specific industrial applications (Ramanathan et al., 2005b; Schadler et al., 2007a; Schadler et al., 2007b). Various researchers have shown that the structure and properties of the interfacial region are different from bulk and are critical to control the properties of the overall nanocomposites (Tsagaropoulos and Eisenberg, 1995; Starr et al., 2001; Berriot et al., 2002, 2003; Bansal et al., 2006; Schadler et al., 2007a). It is well known that the interfacial region impacts the macroscopic response of the polymer nanocomposites; however, direct measurements of its properties are difficult but essential to comprehend how these effects propagate from the interface into the polymer (Starr et al., 2001; Berriot et al., 2002, 2003; Ramanathan et al., 2005b; Bansal et al., 2006; Rittigstein and Torkelson, 2006; Rittigstein et al., 2007; Schadler et al., 2007a).

Understanding the correlation between nanoscale interactions at the interface and changes in the glass transition temperature of the polymer nanocomposite is also important for designing nanocomposites (Schadler et al., 2007a). A possible approach for tuning polymer-filler interfaces to achieve specific properties is the covalent attachment of polymers to the filler surface; an important challenge associated with this approach is understanding the relationship between the chemical modifications of the filler and the resulting properties of the interfacial region and of the whole material

(Ramanathan et al., 2005b; Bansal et al., 2006; Schadler et al., 2007b). However, the current understanding is only qualitative and therefore is a limitation in designing nanocomposites with specific properties (Schadler et al., 2007b).

Fluorescence is the only method currently available that can be used to measure discrete distributions of T_g and also to quantify the impact of different interfaces on T_g (Ellison and Torkelson, 2003). In this chapter, the first determination of the distribution of T_g within polymer nanocomposites through fluorescence is reported, allowing direct characterization of local and average T_g s of the systems. Also, the role of the interface in modifying the T_g of the nanocomposites is critically examined. This research employs different types of functionalization of SWCNT, allowing both the tuning of the interface between PMMA and SWCNT and thus the glass transition behavior of the interface region. In turn, this affords control of the T_g of the whole system due to the percolation of the effects from the SWCNT-PMMA interface to the polymer some many tens of nanometers away from the SWCNT.

9.2 Experimental

Purified HiPCO SWCNTs (Bucky Pearls) were supplied by Carbon Nanotechnologies, Inc. (CNI, Houston, TX). Poly(methyl methacrylate) was synthesized by free radical polymerization ($M_n = 355,000$ g/mol, $M_w/M_n = 1.54$, by gel permeation chromatography using universal calibration with PS standards). The probe 1.10-bis-(1-pyrene)decane (BPD) (Molecular Probes) was used as received and 4-tricyanovinyl-[N-(2-hydroxyethyl)-N-ethyl]aniline (TC1) was synthesized using

procedures reported by Hooker (1996) and McKusick et al. (1958). As shown by Deppe et al. (1996), PMMA was synthesized incorporating a trace of TC1-labeled methacrylate monomer ($M_n = 350,000$ g/mol, $M_w/M_n = 1.60$, by gel permeation chromatography using universal calibration with PS standards and tetrahydrofuran as eluent). TC1-labeled PMMA contained 0.24 mol% labeled monomer as determined by UV absorbance. Bulk T_g ($T_{g,bulk}$) values were measured by differential scanning calorimetry (DSC) (Mettler-Toledo DSC822, second heat, onset method, 10 °C/min) and also via fluorescence methods and were found to agree within experimental error: PMMA $T_{g,bulk} = 393$ K by DSC and 391 K by fluorescence and TC1-labeled PMMA $T_{g,bulk} = 393$ K by DSC and fluorescence.

Amide-functionalized SWCNTs were prepared through carboxylic acid residues, which were introduced on SWCNT surfaces by a chemical oxidation method, followed by direct coupling of ethylenediamine to obtain SWCNTs functionalized with a $(CH_2)_2$ side group or 1,12- diaminododecane to obtain SWCNTs functionalized with a $(CH_2)_{12}$ side group or m-phenylenediamine to obtain SWCNTs functionalized with a phenyl side group. (The details of this method are described elsewhere (Ramanathan et al., 2005a).) A solution evaporation technique was used to graft PMMA to 1 and 3 wt% of the different amide-functionalized SWCNTs. With this technique, the PMMA was first dissolved in tetrahydrofuran (THF). In another vial, SWCNTs were dispersed in THF by bath sonication for 1 h, added to the polymer solution, and again bath-sonicated for 1 h to disperse the SWCNT in the polymer. The mixture was stirred at 60 °C for 5 h and then cooled to room temperature. The cooled mixture was subsequently poured into

stirred methanol and filtered through polytetrafluoroethylene filter paper with a 10 μm pore size. The product was dried at 80 $^{\circ}\text{C}$ under vacuum for 10 h (Ramanathan et al., 2005b). To verify that the PMMA was covalently bonded to the functionalized nanotubes, Fourier transform infrared (FTIR) spectra of the PMMA-SWCNT structures were examined before performing T_g measurements for all types of nanocomposites. The IR spectra of neat PMMA and functionalized SWCNTs were compared with the IR spectrum of PMMA-SWCNT structures. The comparison of these spectra provided evidence of the existence of the amide bonds (peak at 1662 cm^{-1}) in the PMMA-SWCNT structures. These bonds are present in the functionalized SWCNTs and are also formed between the free amine groups (NH_2) in the functionalized SWCNTs and the ester groups in PMMA. In addition, the existence of the ester group (peak at 1728 cm^{-1}) in the spectra of the structures confirmed the presence of PMMA (Ramanathan et al., 2005b).

Films of neat polymer and polymer nanocomposites were prepared by spin-coating (Spangler et al., 1990; Hall et al., 1998b) dilute solutions of polymer with or without nanofiller and dye onto quartz slides. All solutions were made using THF as solvent. Resulting films were at least 1 μm in thickness as determined using a Tencor P10 profilometer. Films were dried for at least 2 days in a chemical fume hood prior to performing fluorescence measurements.

The T_g was characterized by steady-state fluorescence emission spectra as a function of temperature (on cooling) using a Spex Fluorlog-2DM1B fluorimeter and a Photon Technology International fluorimeter with 2.5 mm excitation and emission slits

(10 nm and 5 nm band-pass, respectively). Values of average T_g were measured using BPD dopant (0.2 wt% or less) in PMMA films (neat and nanocomposites), and local T_g values were measured using TC1 label (covalently attached) in PMMA films (neat and nanocomposites). The wavelengths used to excite the TC1 and BPD dyes were 480 nm and 341 nm, respectively. The emission spectra of TC1 and BPD were measured at 530-700 nm and 360-460 nm, respectively. The T_g values of polymer films were determined by fitting the temperature dependence of the integrated fluorescence intensity (BPD dopant) or average fluorescence intensity peak (TC1 label) to linear correlations in both the rubbery and glassy states, with the intersection providing a measure of T_g . In fitting the data to linear correlations, only data well outside T_g are used in the fitting procedure. Additional information on the fluorescence technique used to monitor T_g is found in chapters 4, 5, 6 and 7.

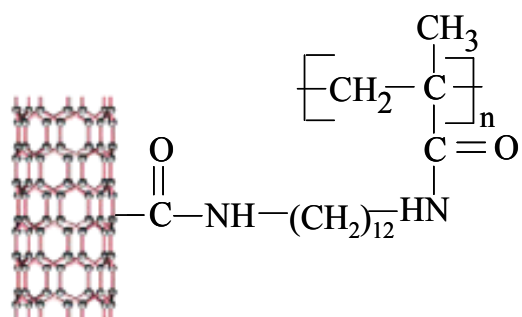
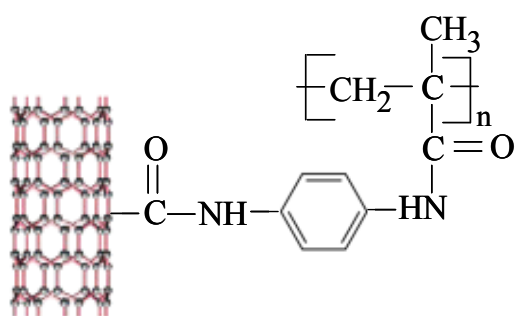
9.3 Results and Discussion

This study addresses the T_g characterization of different PMMA-SWCNT nanocomposites by employing fluorescence spectroscopy, a technique that has been successfully used to characterize physical properties in other systems (Loutfy, 1981, 1986; Lenhart et al., 2001; Ellison et al., 2002; Ellison and Torkelson, 2002, 2003; Ellison et al., 2004; Ellison et al., 2005; Priestley et al., 2005a; Priestley et al., 2005b; Mundra et al., 2006; Rittigstein and Torkelson, 2006; Mundra et al., 2007a; Mundra et al., 2007b; Priestley et al., 2007b; Rittigstein et al., 2007; Roth et al., 2007; Roth and Torkelson, 2007). PMMA was grafted to 1 wt % functionalized SWCNT to form PMMA-

SWCNT structures. Three PMMA-SWCNT structures were studied and are presented in Figure 9-1. The difference among them is the side group in the functionalized SWCNT. Here, the side groups are designated as follows: A) $(\text{CH}_2)_{12}$, B) phenyl and C) $(\text{CH}_2)_2$. Polymer nanocomposites were made by blending the PMMA-SWCNT structures with neat PMMA in different compositions; the resulting systems are presented in Table 9-1. Two types of measurements were done for all systems: local T_g and average T_g . The local T_g was measured using TC1-labeled PMMA (this PMMA is covalently attached to the SWCNT) and the average T_g was measured using BPD dopant in the entire system.

Systems A1, B1 and C1 as named in Table 9-1 correspond to the composites formed by the 99/1 wt% PMMA-SWCNT structures without any added PMMA. Figure 9-2 shows the effect of temperature on the fluorescence of the TC1 label and BPD dopant in System B1. In both cases, there is a significant increase in the fluorescence intensity with decreasing temperature. After absorption of light and promotion of an electron to an excited singlet state, both the TC1 label and BPD dopant return to the ground state by internal conversion (energy loss by rotor and vibrational motions) or by fluorescence. Densification of the material upon cooling occurs, suppressing the internal conversion and yielding an increase in fluorescence intensity. Similar results are obtained in Systems A1 and C1.

Figure 9-3a shows the normalized average fluorescence intensity peak as a function of temperature of the TC1 label in Systems A1, B1 and C1. Figure 9-3b shows the normalized integrated fluorescence intensity as a function of temperature of BPD

A) PMMA-SWCNT ((CH₂)₁₂)

B) PMMA-SWCNT (Ph)

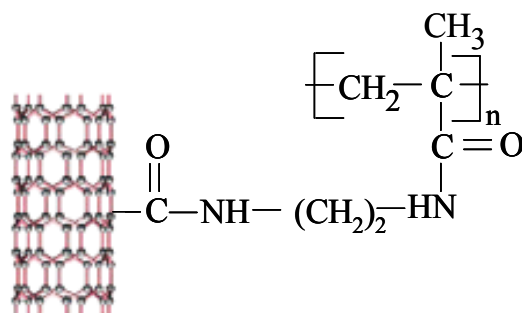
C) PMMA-SWCNT ((CH₂)₂)

Figure 9-1: PMMA-SWCNT structures. SWCNTs functionalized with different side groups: A) (CH₂)₁₂, B) phenyl, and C) (CH₂)₂.

Table 9-1: Polymer nanocomposite systems studied.

Structure	Side Group	System	99/1 PMMA-SWCNT wt %	Neat PMMA wt %	97/3 PMMA-SWCNT wt %
A	$(\text{CH}_2)_{12}$	A1	100	0	-
		A2	70	30	-
		A3	30	70	-
		A4	10	90	-
		A5	0	100	-
B	Phenyl	B1	100	0	-
		B2	30	70	-
		B3	0	100	-
C	$(\text{CH}_2)_2$	C1	100	0	-
		C2	70	30	-
		C3	30	70	-
		C4	0	100	-
D	$(\text{CH}_2)_2$	D1	-	0	100
		D2	-	30	70
		D3	-	70	30
		D4	-	90	10
		D5	-	100	0

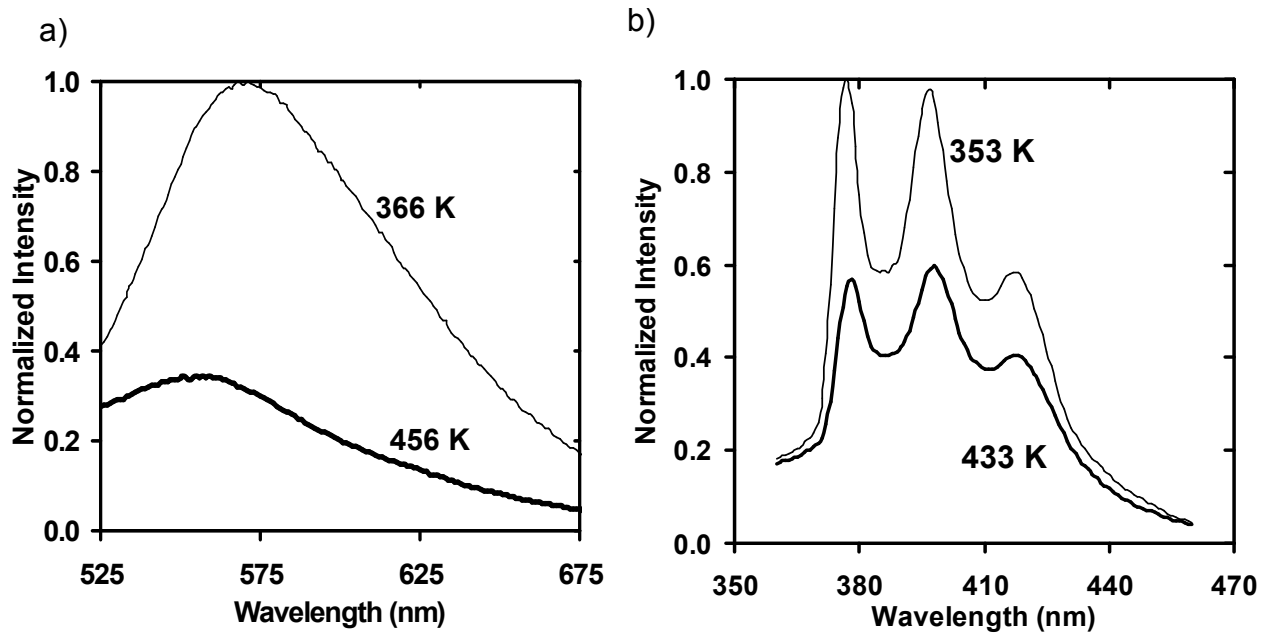


Figure 9-2: Temperature dependence of fluorescence emission spectra: a) TC1 label in System B1 taken at temperatures of 366 K and 456 K and b) BPD dopant in System B1 taken at temperatures of 353 K and 433 K.

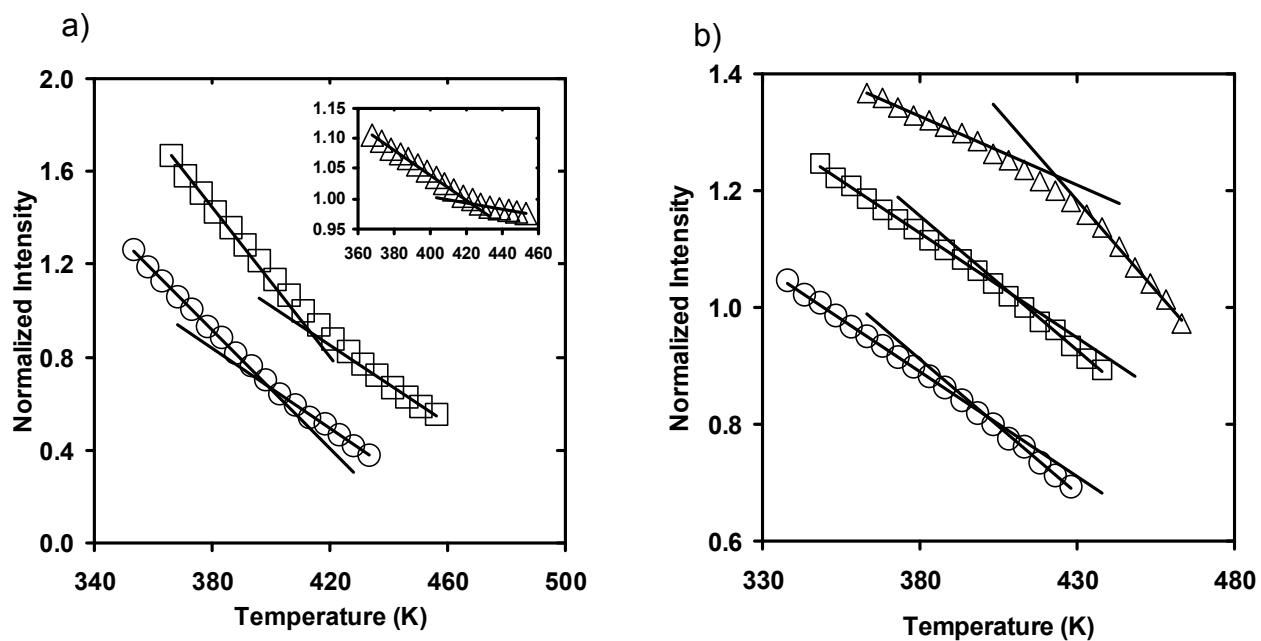


Figure 9-3: Temperature dependence of normalized fluorescence intensity of a) TC1 label and b) BPD dopant: System A1 (circles), System B1 (square) and System C1 (triangles). (The average intensity peak has been normalized to one at T_g and vertically shifted to aid the reader.)

dopant in Systems A1, B1 and C1. The same T_g value of 400 K is obtained for System A1 when it is measured using TC1 label or BPD dopant, showing an increase in T_g of ~8 K compared with bulk PMMA. (Recall that neat PMMA exhibited $T_g = 391$ K by BPD dopant fluorescence measurements and $T_g = 393$ K by TC1 label fluorescence measurements.) For System B1 the T_g obtained with both methods is 412 K, showing an increase in T_g compared with bulk PMMA of ~20 K. The T_g value of System C1 is 423 K as obtained by both BPD dopant and TC1 label fluorescence measurements, an increase in T_g compared with bulk PMMA of ~31 K. The results in System C1 are consistent with the 33 K increase observed via dynamic mechanical analysis (DMA) by Ramanathan et al. (2005b) in a similar system.

The agreement in the T_g values obtained using both BPD dopant and TC1 label fluorescence measurements shows that when 99/1 wt% PMMA-SWCNT structures (without any added PMMA) are used, the local and average T_g s are the same, as expected. Differential scanning calorimetry (DSC) results agree with the T_g values obtained by fluorescence. The increment in the T_g s obtained relative to neat, bulk PMMA suggests that the functionalization of the SWCNTs significantly improves the interfacial interaction with the polymer, resulting in a strong interface that restricts the chain segmental mobility. Therefore, by grafting just 1 wt% SWCNT to PMMA, an increment in T_g is achieved, the extent of which depends on the side group in the functionalized SWCNTs. By changing the type of functionalization in the SWCNT, the interface between the polymer and the SWCNT can be tuned, allowing control of the T_g of the system and impacting the ability to efficiently design polymer nanocomposites.

The difference in the temperature dependences of the fluorescence intensity exhibited by TC1-labeled PMMA and BPD-doped PMMA is related to the mechanism by which each chromophore undergoes non-radiative decay from its excited state. BPD, a band definition chromophore, undergoes non-radiative decay by vibrational motions (Lakowicz, 1999; Valeur, 2002); thus, the emission intensity follows the density of the polymer and the temperature dependence of the emission intensity is smaller below T_g than above T_g . Numerous band definition chromophores have been used to determine T_g in bulk polymeric glass formers (Ellison et al., 2002; Ellison and Torkelson, 2002, 2003; de Deus et al., 2004; Ellison et al., 2005; Turrion et al., 2005; Martins et al., 2006; Rittigstein and Torkelson, 2006; Rittigstein et al., 2007). The TC1 dye, a “rotor” chromophore, undergoes non-radiative decay by rotational motion (Valeur, 2002). To facilitate the rotational motion of the chromophore, a certain amount of free volume is required (Loutfy, 1986); thus, it is believed that changes in polymer density impede the rotational motion to a greater extent in the glassy state than in the liquid state. As a result, the temperature dependence of the emission intensity is greater in the glassy state than the rubbery state. Because of the enhanced sensitivity of “rotor” chromophores to density changes, they have been widely used to monitor T_g and physical aging of polymeric glass formers (Loutfy, 1986; Meyer et al., 1990; Royal and Torkelson, 1992; Brady and Charlesworth, 1993; Royal and Torkelson, 1993; Lenhart et al., 2001; Ellison et al., 2002; Priestley et al., 2005a; Priestley et al., 2005b; Rittigstein and Torkelson, 2006; Rittigstein et al., 2007).

Fluorescence was also used to characterize the average and local T_g s of different nanocomposite systems. PMMA-SWCNT structures were blended with PMMA, forming polymer nanocomposite systems of diverse compositions (see Table 9-1). When the PMMA that is grafted to SWCNT is labeled with TC1, the local T_g of the chains that are directly attached to the SWCNT and influenced by the matrix can be measured. However, if the PMMA that is grafted to SWCNT is unlabeled but the blend has been doped with BPD, the average T_g within the nanocomposites can be measured instead. Using a free dopant dye in the polymer nanocomposites allows determination of the relatively long-ranged effect of the nanofiller on T_g . On the other hand, employing a dye that is covalently attached to the polymer grafted to the SWCNT allows for understanding of the localized changes in the dynamics of polymer experiencing direct interfacial binding with the nanoparticles.

Figure 9-4 shows the average and local T_g of the polymer nanocomposite systems as a function of the amount of PMMA-SWCNT structures in the blend and the side groups in the functionalized SWCNT. In the case of all three side groups, the average T_g increases linearly with the amount of PMMA-SWCNT in the blend. However, the local T_g in the PMMA-SWCNT structures changes little upon addition of up to 70-90 wt% neat PMMA to the blend. In the case of $(\text{CH}_2)_{12}$ as the side group in the functionalized SWCNT, the average and local T_g s of the polymer nanocomposites increase subtly with the amount of PMMA-SWCNT in the blend. In the case of the phenyl ring as the side group in the functionalized SWCNT, the average and local T_g s of the polymer nanocomposites increase moderately as the amount of PMMA-SWCNT in the blend

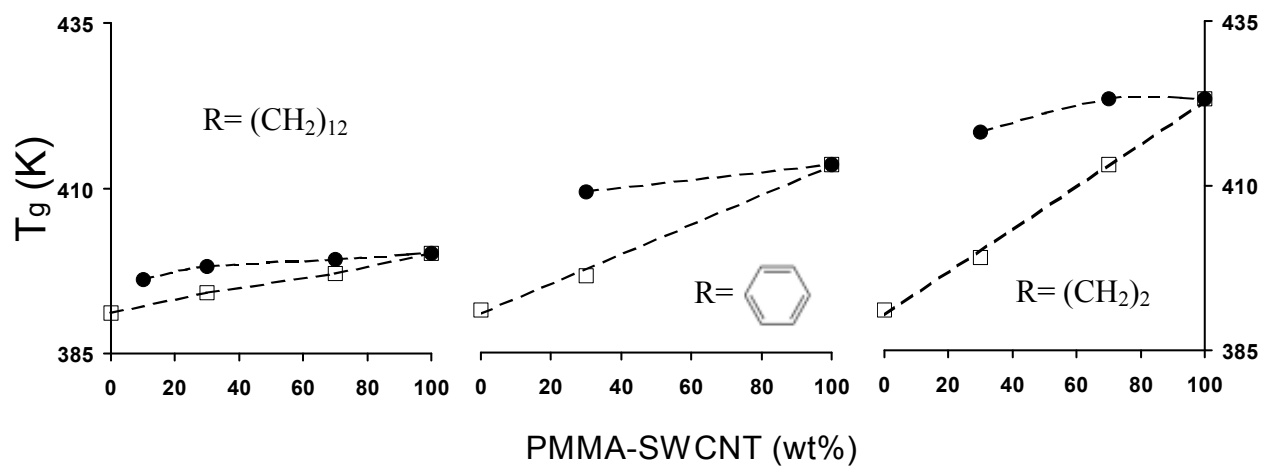


Figure 9-4: T_g as a function of the level of PMMA-SWCNT (1 wt% SWCNT) in blends with neat PMMA and the side group in the functionalized SWCNT (Systems A, B, and C in Table 9-1): average T_g (open squares) and local T_g (closed circles).

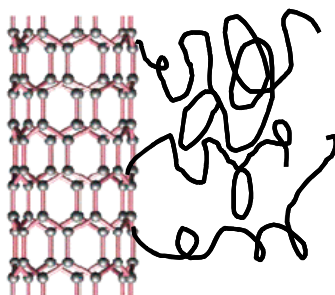
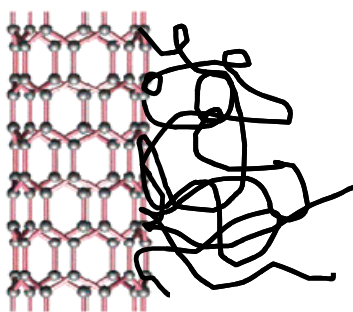
increases. However, when $(\text{CH}_2)_2$ is the side group in the functionalized SWCNT, the average and local T_g s of the polymer nanocomposites increase greatly as the PMMA-SWCNT amount in the blend increases.

This is the first time discrete distributions of T_g in polymer-nanofiller nanocomposites have been determined. These results show that functionalized SWCNTs perturb the dynamics of the polymer matrix increasing its T_g , consistent with the formation of a region of reduced molecular mobility in the vicinity of the nanotubes that perturbs the entire polymer nanocomposite. Also, depending of the type of functionalization (Figure 9-1) the effect on the T_g of the polymer is different. The particular details of the side group involved in polymer-filler covalent bonding and the bridging between particles may contribute to the variety of influence that nanoparticles have on the properties of the polymer.

The dependence of local and average T_g obtained on the side group of the functionalized SWCNT shows that there is a relation between the length and flexibility of the side groups and the changes on T_g of the polymer. The type of functionalized SWCNTs will determine the nature of the strength of the interface between the filler surface and the polymer chains grafted to it, thereby affecting differently the T_g of the diverse polymer nanocomposite systems. The $(\text{CH}_2)_2$ unit is short and rigid; therefore, we hypothesize that the PMMA chains that are grafted to the SWCNTs through the $(\text{CH}_2)_2$ unit can easily be attached multiple times to the SWCNT, creating a strong interface that causes the T_g of the system to increase greatly with the amount of PMMA-SWCNT $((\text{CH}_2)_2)$ in the blend. On the other hand, $(\text{CH}_2)_{12}$ is long and flexible;

consequently, the PMMA chains have difficulty attaching to the SWCNTs multiple times, making the interface weaker and causing the T_g of the system to increase subtly with the amount of PMMA-SWCNT ((CH₂)₁₂) in the blend. The case of the phenyl ring as the side group in the functionalized SWCNT falls between the other two extreme cases (see Figure 9-5).

Previous discussion in this chapter concerned the study of nanocomposites consisting totally or partially of PMMA covalently bonded to 1 wt% SWCNT. In order to investigate the impact on the local and average T_g s of the amount of SWCNT covalently attached to polymer, PMMA was also grafted to 3 wt% SWCNT functionalized with (CH₂)₂. These PMMA-SWCNT structures were blended with neat PMMA to form polymer nanocomposites of diverse compositions. Figure 9-6 shows the average and local T_g s of the polymer nanocomposites as a function of the amount of PMMA-SWCNT ((CH₂)₂) in the blend. As expected, the average T_g increases with the amount of PMMA-SWCNT in the blend. In contrast to the apparent linear dependence of average T_g in the blends containing 99/1 wt% PMMA-SWCNT (see Figure 9-4), the average T_g increases nonlinearly with the level of 97/3 wt% PMMA-SWCNT in the blends with PMMA. On the other hand, the local T_g in the PMMA-SWCNT structures changes little upon addition of up to 90 wt% neat PMMA to the blend, similar to that observed in Figure 9-4. In general, the average and local T_g s obtained for polymer nanocomposites that contain PMMA covalently attached to 3 wt% SWCNT (Figure 9-6) are higher than those obtained in polymer nanocomposites that contain PMMA covalently attached to 1 wt% SWCNT (Figure 9-4).

PMMA-SWCNT ((CH₂)₁₂)

PMMA-SWCNT (Ph)

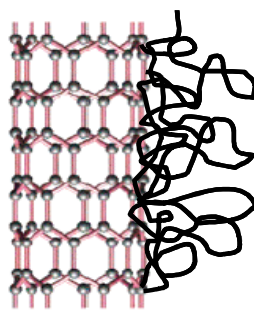
PMMA-SWCNT ((CH₂)₂)

Figure 9-5: Diagram of the different types of interfaces hypothesized to be present between PMMA and SWCNT.

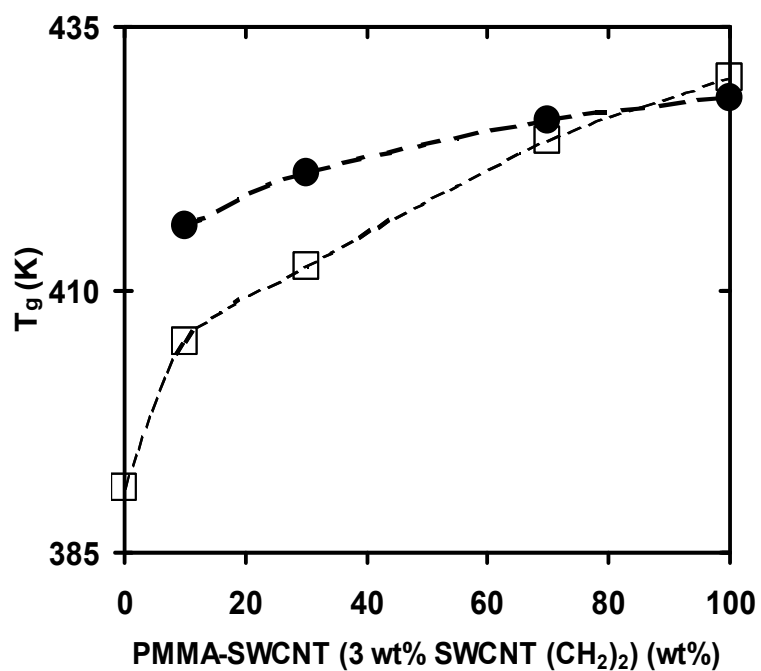


Figure 9-6: T_g as a function of the amount of PMMA-SWCNT (3 wt% SWCNT with $(CH_2)_2$ as the side group) in blends with PMMA (Systems D1-D5 in Table 9-1): average T_g (open squares) and local T_g (closed circles).

Long and coworkers (Long and Lequeux, 2001; Merabia et al., 2004) proposed a model that describes the mechanism of the glass transition characterizing it by the presence of slow and fast domains based on thermally induced density fluctuations. In their model, the total number of regions with slower dynamics increases with decreasing temperature. The glass transition is described in the model as the temperature at which these slow moving regions percolate throughout the bulk of the sample. In the present study, the mobility of the PMMA segments is reduced close to the polymer-nanotube interfaces. The strong interactions between the PMMA and the SWCNTs thereby lead to an increase of T_g in the vicinity of the interface. Since the change of the polymer dynamics induced by interfaces with interactions is long ranged (Long and Lequeux, 2001; Baljon et al., 2004; Merabia et al., 2004), the effect percolates across the sample, leading to an increase in the average T_g of the polymer nanocomposite. The extent of this increase depends on the amount of well-dispersed nanofillers in the system and on the strength of the interface.

9.4 Conclusions

In this chapter, the local and average T_g s of different PMMA-SWCNT nanocomposites were studied. It was shown that fluorescence can be used to measure directly the enhanced T_g of the polymer in the vicinity of the nanofiller and also to characterize the percolation of this effect through the whole polymer nanocomposite sample. Different polymer-nanofiller interfaces strengths were studied in order to identify their effect on the local and average T_g s of the system. As the side group in the

functionalized SWCNTs becomes shorter and more rigid, the interface between the PMMA and the SWCNT becomes stronger, causing more constraints to the PMMA cooperative segmental mobility and thereby increasing the local and average T_g s of the system. Higher SWCNT concentrations lead to more polymer-nanofiller interfacial area, increasing the magnitude of the observed effects.

10 Dramatic Reduction of Physical Aging Behavior of PMMA-SWCNT Nanocomposites Studied by Fluorescence

10.1 Introduction

Nanoscopically confined polymers often exhibit a deviation in glass transition temperature (T_g) from that of bulk material (Keddie et al., 1994b; Forrest et al., 1996; van Zanten et al., 1996; Kajiyama et al., 1997; Fukao and Miyamoto, 2000; Gonzalez-Benito et al., 2000; Schwab et al., 2000; Forrest and Dalnoki-Veress, 2001; Fryer et al., 2001; Ash et al., 2002b; Berriot et al., 2002; Ellison et al., 2002; Starr et al., 2002; Berriot et al., 2003; Ellison and Torkelson, 2003; Mbhele et al., 2003; Pham and Green, 2003; Roth and Dutcher, 2003; Sharp and Forrest, 2003b; Ash et al., 2004; Ellison et al., 2004; Park et al., 2004; Soles et al., 2004b; Bansal et al., 2005; Ellison et al., 2005; Ramanathan et al., 2005b; Roth and Dutcher, 2005; Mundra et al., 2006; Rittigstein and Torkelson, 2006; Mundra et al., 2007a; Mundra et al., 2007b; Priestley et al., 2007a; Priestley et al., 2007b; Rittigstein et al., 2007; Roth et al., 2007; Roth and Torkelson, 2007). There is evidence that enhanced mobility near the air-polymer interface in thin supported films, or in the non-wetted surface (free space) between the polymer and the nanofiller in polymer nanocomposites, causes a depression in T_g (Kajiyama et al., 1997; Schwab et al., 2000; Forrest and Dalnoki-Veress, 2001; Fryer et al., 2001; Ash et al., 2002b; Ellison et al., 2002; Ellison and Torkelson, 2003; Liu et al., 2003; Sharp and Forrest, 2003b; Sun et al., 2004; Bansal et al., 2005; Bansal et al., 2006; Rittigstein and Torkelson, 2006; Rittigstein et al., 2007; Srivastava and Basu, 2007b). On the other

hand, a reduced mobility due to attractive polymer-substrate or polymer-nanofiller interactions can cause an increase in T_g (Keddie et al., 1994a; van Zanten et al., 1996; Fryer et al., 2001; Tate et al., 2001; Berriot et al., 2002; Ellison et al., 2002; Grohens et al., 2002; Pham and Green, 2002; Savin et al., 2002; Berriot et al., 2003; Mbhele et al., 2003; Park et al., 2004; Ramanathan et al., 2005b; Bansal et al., 2006; Rittigstein and Torkelson, 2006; Rittigstein et al., 2007; Srivastava and Basu, 2007b).

As presented in chapter 9, different types of side groups in functionalized SWCNT alter the T_g of PMMA-SWCNT nanocomposites in which the PMMA is covalently attached to low levels of SWCNT. The results show that shorter and more rigid side groups create a stronger interface between the PMMA and the SWCNT, constraining to a greater extent the PMMA segmental mobility and thereby increasing the T_g of the system.

In addition to T_g , physical aging also has a large impact on the performance of amorphous polymers (Ellison et al., 2002; McKenna and Simon, 2002). Physical aging is the structural relaxation process below T_g associated with the transition from a nonequilibrium state to an equilibrium state characterized by nonlinearity and nonexponentiality (Struik, 1978; Greiner and Schwarzl, 1984; Andreatti et al., 2003; Lu and Nutt, 2003a). The result is time-dependent properties such as an increase in density, yield stress and modulus and a decrease in specific enthalpy, fracture energy, ultimate elongation, and impact strength (Struik, 1978; Tant and Wilkes, 1981; Ellison et al., 2002). Compared to the large number of research articles concerning the T_g -nanoconfinement effect, relatively few studies of physical aging in confined polymer

have been reported (Pfromm and Koros, 1995; Lee and Lichtenhan, 1998; Dorkenoo and Pfromm, 1999; Ellison et al., 2002; Simon et al., 2002; Kawana and Jones, 2003; Lu and Nutt, 2003a, 2003b; Huang and Paul, 2004; Fukao and Sakamoto, 2005; Huang and Paul, 2005; Priestley et al., 2005a; Priestley et al., 2005b; Rittigstein and Torkelson, 2006; Rittigstein et al., 2007; Theneau et al., 2007). The first study of the physical aging behavior of polymer impacted by the presence of a nanofiller was done by Lee and Lichtenhan (1998). They reported that the addition of polyhedral oligomeric silsesquioxane (POSS) nanoreinforcements in epoxy resin retarded the physical aging rate and the time to reach equilibrium of the polymer. Also, Lu and Nutt (2003a; 2003b) observed that the inclusion of intercalated clay nanofillers into an epoxy network restricts the relaxation behavior compared to the neat epoxy resin. Later, Rittigstein et al. (Rittigstein and Torkelson, 2006; Rittigstein et al., 2007) showed that the presence of low levels of well-dispersed silica and alumina nanospheres in PMMA and P2VP reduces or suppresses the glassy-state structural relaxation behavior of the matrix (see chapters 6, 7 and 8). Very recently, Theneau et al. (2007) showed a reduction of structural relaxation of poly(2-hydroxyethyl methacrylate) (PHEMA) with increasing silica nanosphere content.

Here, a fluorescence study of the physical aging behavior of different PMMA-SWCNT nanocomposites is presented. Figure 10-1 provides a schematic description of the studied systems. As shown in the figure, the nanocomposites in this chapter contain 70 wt% of neat PMMA and 30 wt% of PMMA grafted to functionalized SWCNT. The PMMA grafted to SWCNT contains 1 wt% SWCNT and 99 wt% grafted PMMA.

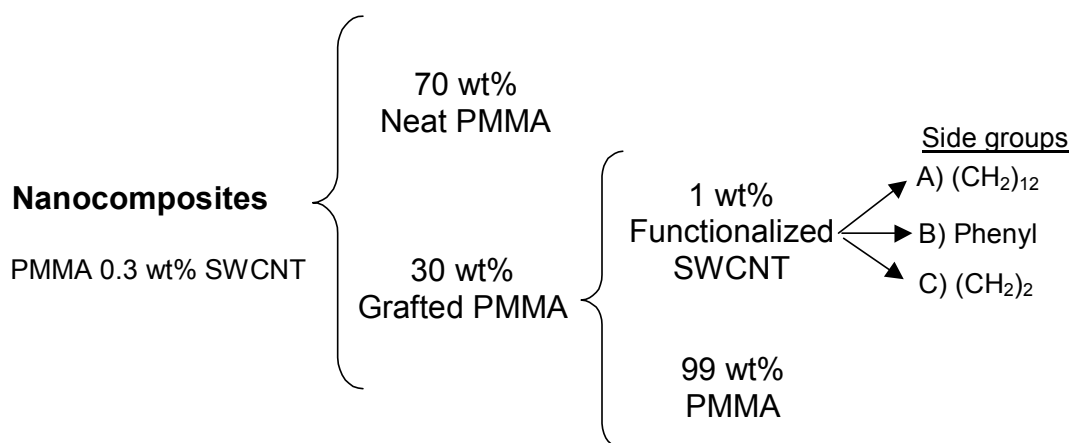


Figure 10-1: Schematic of the studied nanocomposites. All nanocomposites have 70 wt% of neat PMMA and 30 wt% of PMMA grafted to functionalized SWCNT. In this 30 wt%, 1 wt% corresponds to the SWCNT and the rest to PMMA. The total weight % of the functionalized SWCNT in the nanocomposites is just 0.3 %. Three types of sides groups were used to functionalize the SWCNT: A) $(\text{CH}_2)_{12}$, B) Phenyl and C) $(\text{CH}_2)_2$.

The total weight % of the functionalized SWCNT in the nanocomposites is therefore only 0.3 %. Three side groups were used to functionalize the SWCNT. In the remainder of the chapter, System A will refer to nanocomposites with $(\text{CH}_2)_{12}$ as the side group, System B to nanocomposites with a phenyl ring as the side group, and System C to those with $(\text{CH}_2)_2$ as the side group. (See Figure 9-1 and Figure 9-5 for indications of how the PMMA is covalently attached to the SWCNT via the side groups containing $(\text{CH}_2)_{12}$, a phenyl ring, or $(\text{CH}_2)_2$.) The different side groups allow tuning of the interface between PMMA and SWCNT to control the structural relaxation behavior of the system. The results demonstrated a relationship between the length and flexibility of the side groups and the extent of the reduction of physical aging.

10.2 Experimental

Purified HiPCO SWCNTs (Bucky Pearls) were supplied by Carbon Nanotechnologies, Inc. (CNI, Houston, TX). Poly(methyl methacrylate) (PMMA) was synthesized by free radical polymerization ($M_n = 355,000$ g/mol, $M_w/M_n = 1.54$, by gel permeation chromatography using universal calibration with PS standards). The probe 4-tricyanovinyl-[N-(2-hydroxyethyl)-N-ethyl]aniline (TC1) was synthesized using procedures reported by Hooker (1996) and McKusick et al. (1958). Following the procedure of Deppe et al. (1996), PMMA was synthesized incorporating a trace of TC1-labeled methacrylate monomer ($M_n = 350,000$ g/mol, $M_w/M_n = 1.60$, by gel permeation chromatography using universal calibration with PS standards). TC1-labeled PMMA contained 0.24 mol% labeled monomer as determined by UV absorbance. Bulk T_g

($T_{g,bulk}$) values were measured by differential scanning calorimetry (DSC) (Mettler-Toledo DSC822, second heat, onset method, 10 °C/min) and also via fluorescence methods and were found to agree within experimental error: PMMA $T_{g,bulk}$ = 393 K by DSC and 391 K by fluorescence, and TC1-labeled PMMA $T_{g,bulk}$ = 393 K by DSC and fluorescence.

Amide-functionalized SWCNTs were prepared through carboxylic acid residues, which were introduced on SWCNT surfaces by a chemical oxidation method, followed by direct coupling of ethylenediamine to obtain SWCNTs functionalized with a (CH₂)₂ side group or 1,12- diaminododecane to obtain SWCNTs functionalized with a (CH₂)₁₂ side group or m-phenylenediamine to obtain SWCNTs functionalized with a phenyl side group. (The details of this method are described elsewhere (Ramanathan et al., 2005a).) A solution evaporation technique was used to prepare the nanocomposites. With this technique, the PMMA was first dissolved in tetrahydrofuran (THF). In another vial, SWCNTs were dispersed in THF by bath sonication for 1 h, added to the polymer solution, and again bath-sonicated for 1 h to disperse the SWCNT in the polymer. The mixture was stirred at 60 °C for 5 h and then cooled to room temperature. The cooled mixture was subsequently poured into stirred methanol and filtered through polytetrafluoroethylene filter paper with a 10 μm pore size. The product was dried at 80 °C under vacuum for 10 h (Ramanathan et al., 2005b). To verify that the PMMA was covalently bonded to the functionalized nanotubes, Fourier transform infrared (FTIR) spectra of the PMMA-SWCNT systems were examined before performing physical aging measurements for all types of nanocomposites. The IR spectra of neat PMMA

and functionalized SWCNTs were compared with the IR spectrum of PMMA-SWCNT structures. The comparison of these spectra provided evidence of the existence of the amide bonds (peak at 1662 cm^{-1}) in the PMMA-SWCNT structures. These bonds are present in the functionalized SWCNTs and are also formed between the free amine groups (NH_2) in the functionalized SWCNTs and the ester groups in PMMA. In addition, the existence of the ester group (peak at 1728 cm^{-1}) in the spectra of the structures, confirmed the presence of PMMA (Ramanathan et al., 2005b).

Films of neat polymer and polymer nanocomposites were prepared by spin-coating (Spangler et al., 1990; Hall et al., 1998b) dilute solutions of polymer with or without nanofiller and dye onto quartz slides. All solutions were made using THF as solvent. Resulting films were at least $1\text{ }\mu\text{m}$ in thickness as determined using a Tencor P10 profilometer. Films were dried for at least 2 days in a chemical fume hood prior to performing fluorescence measurements.

Physical aging was measured using TC1 as the fluorescence dye in bulk polymer and polymer nanocomposite films. Polymer nanocomposites were formed for Systems A, B and C as defined in Figure 10-1. Prior to each aging experiment, the thermal history was erased by annealing above T_g at $150\text{ }^\circ\text{C}$ for 1 h. Films were quenched using a temperature-controlled cell holder preset to the aging temperature. Physical aging was characterized by steady-state fluorescence emission spectra as a function of time using a Photon Technology International fluorimeter with 2.5 mm excitation and emission slits (10 nm and 5 nm band-pass, respectively). Physical aging was monitored by measuring the maximum emission intensity of TC1 (at 560-565 nm for bulk PMMA,

at 582-589 nm for System A, at 573-580 nm for System B and at 568-574 nm for System C) as a function of aging time after quenching the films from the rubbery state above T_g to different aging temperatures. Additional information on the fluorescence technique used to monitor physical aging can be found in chapters 4, 6, 7 and 8.

10.3 Results and Discussion

This study addresses the physical aging characterization of different PMMA-SWCNT nanocomposites by employing fluorescence spectroscopy. Systems A, B and C, as defined in Figure 10-1 were studied. The side groups used to functionalize the SWCNT in these systems are shown in Figure 9-1, the main difference between them is the length of the carbon chain.

The physical aging behaviors of PMMA and PMMA-SWCNT nanocomposites were measured at different temperatures using the increase in fluorescence intensity of the TC1 label as a function of logarithmic aging time. Figure 10-2 illustrates the change in the fluorescence spectrum of TC1 in a bulk PMMA film during physical aging after quenching the temperature from above $T_{g,Bulk}$ to $T_{g,Bulk} - 88$ K. After absorption of light and promotion of an electron to an excited singlet state, TC1 returns to the ground state by internal conversion (energy loss by rotor motions) or by fluorescence. Densification of the material upon aging occurs, suppressing the internal conversion and yielding a major increase in fluorescence intensity.

Figure 10-3 compares the change in TC1 fluorescence intensity during physical aging of bulk PMMA to the changes observed in PMMA-SWCNT nanocomposites after quenching the temperature from above $T_{g,bulk}$ to an aging temperature of 323 K and 295

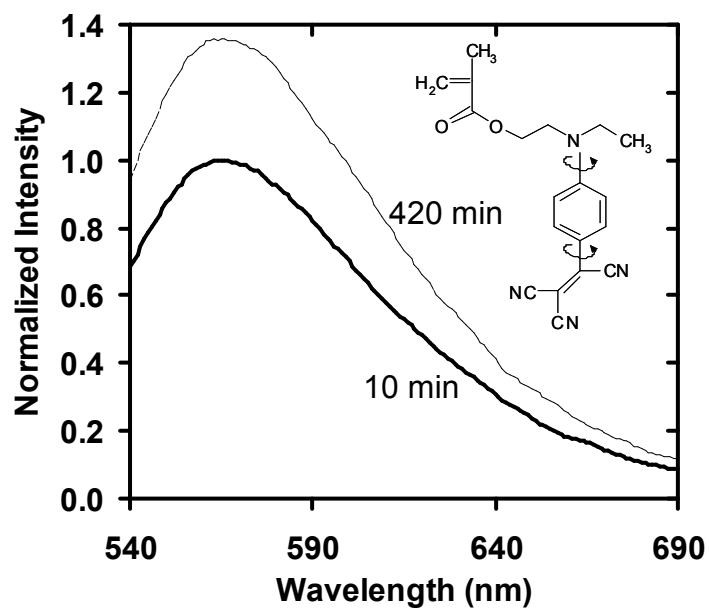


Figure 10-2: Fluorescence emission spectrum of a bulk TC1-labeled PMMA film as a function of physical aging time after a temperature quench from above $T_{g,bulk}$ to $T_{g,bulk} - 88$ K: 10 min (solid line) and 420 min (dashed line). Inset: Molecular structure of TC1-labeled methacrylate monomer.

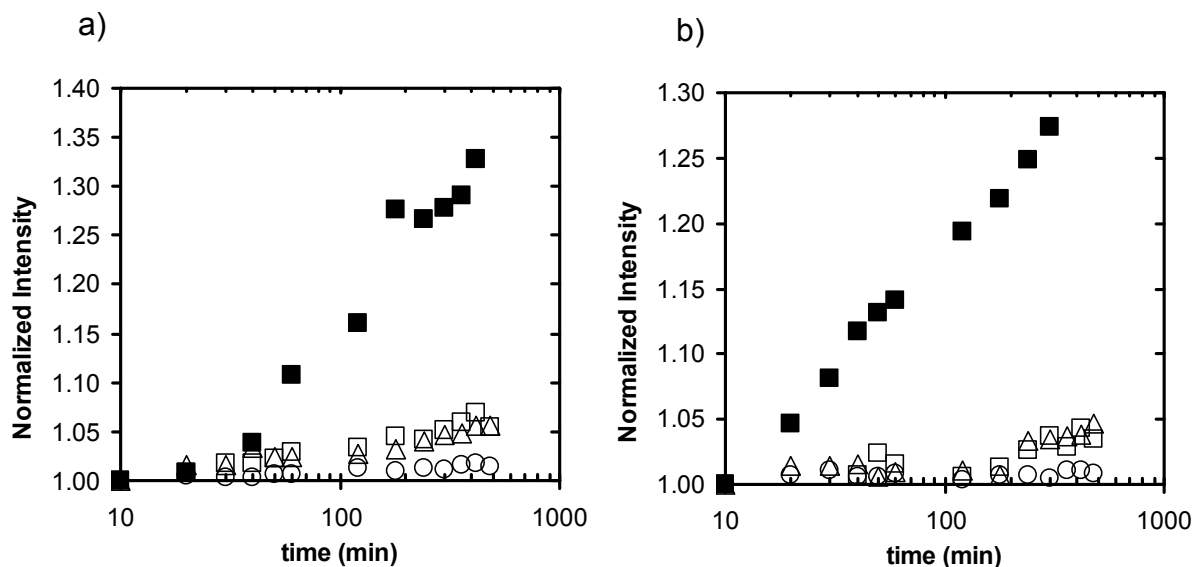


Figure 10-3: a) Normalized fluorescence intensity of TC1 as a function of logarithmic physical aging after quenching from above $T_{g,bulk}$ to 323 K: PMMA ($T_g - 68$ K) (closed squares), system A ($T_g - 71$ K) (open squares), system B ($T_g - 73$ K) (triangles) and system C ($T_g - 76$ K) (circles). b) Normalized fluorescence intensity of TC1 as a function of logarithmic physical aging after quenching from above $T_{g,bulk}$ to 295 K: PMMA ($T_g - 96$ K) (closed squares), system A ($T_g - 99$ K) (open squares), system B ($T_g - 101$ K) (triangles) and system C ($T_g - 104$ K) (circles).

K. When aged at 323 K, the bulk PMMA film shows an approximately 33% increase in fluorescence intensity over 8 h. In contrast, systems A and B exhibit only a 6% increase in intensity over 8 h. The most dramatic suppression of physical aging is observed for system C, which exhibits only a 1% increase in fluorescence intensity over 8 h. With a physical aging temperature of 295 K, the bulk PMMA film exhibits an increment in the intensity of about 27% during 8h, while Systems A and B have an increase of only 4% and System C, within error, exhibits no change in intensity and thus no aging.

In general, covalent bonds between PMMA and SWCNT create strong interfaces that significantly constrain the PMMA segmental mobility and retard the structural relaxation of the polymer. This constrained mobility and relaxations at the interface percolates through the systems. The choice of side group used in the PMMA-SWCNT nanocomposites can lead to major differences in the polymer-nanofiller interface strengths and thereby on the effects in T_g and physical aging. The side group in System C is $(\text{CH}_2)_2$ which is short and rigid, allowing the PMMA chains that are grafted to the SWCNTs through it to be easily attached multiple times to the SWCNT, creating a strong interface. Consequently, the physical aging is severely restricted and the T_g of the system increases greatly (see chapter 9). On the other hand, the side group in System A is $(\text{CH}_2)_{12}$, which is long and flexible and does not allow for the multiple attachments of the PMMA chains to the SWCNTs, thereby creating a weaker interface. Consequently, the physical aging is reduced and the T_g of the system increases to a much smaller extent than in System C (see chapter 9). The side group in System B is a phenyl ring, intermediate in size and flexibility when compared to the two other side

groups. As expected, the T_g for System B falls between those of Systems A and C (see Figure 9-5); however, when the physical aging response for System B is evaluated over relatively short times (8 h), it exhibits glassy state relaxation behavior similar to System A.

In order to compare the effect of aging temperature on the aging rate, r_f , in bulk PMMA and PMMA-SWCNT nanocomposites, equation 4-2 was applied to the fluorescence physical aging data. (Recall that equation 4-2 defines physical aging rate based on changes occurring with logarithmic aging time.) The calculated r_f values are presented in Figure 10-4 for all the systems. It can be observed that bulk PMMA has a maximum aging rate at 305 K. This agrees with the specific volume aging rate (also defined based on logarithmic aging time) of bulk PMMA reported by Greiner and Schwarzl (1984) and with the characterization of r_f using julolidenemalonitrile (JMN) performed by Royal and Torkelson (1993). The aging rates of the PMMA-SWCNT nanocomposites are reduced dramatically in comparison to the bulk material. However, the neat polymer and the nanocomposites exhibit the same trend of r_f with physical aging temperature over the temperatures and times studied. In other words, over the temperature range studied, the maximum aging rate was observed at 305 K and the minimum aging rate was observed at 295 K in neat PMMA and all three PMMA-SWCNT nanocomposite systems. Relative to bulk PMMA, the rate of structural relaxation at 323 K of systems A, B and C are reduced by a factor of 6, 8 and 24, respectively. The changes observed on T_g and presented in chapter 9, together with the physical aging

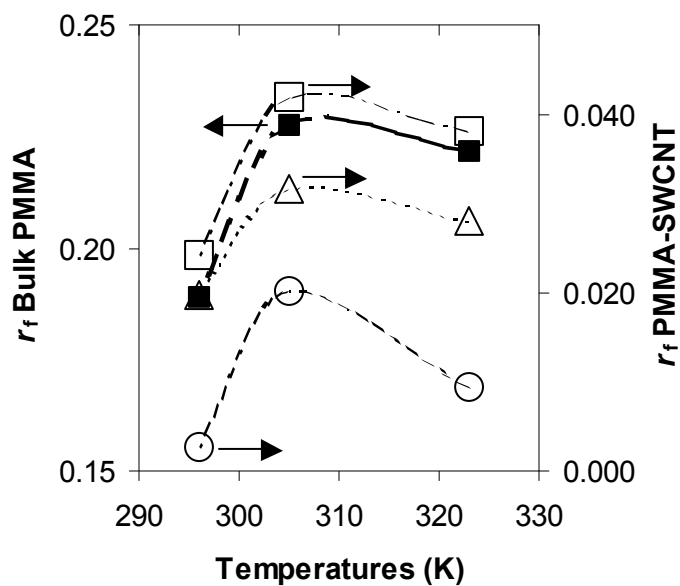


Figure 10-4: Fluorescence aging rate, r_f , as a function of physical aging temperature for PMMA (closed squares), system A (open squares), system B (triangles) and system C (circles). (Fluorescence aging rate is calculated over a physical aging time scale from 10 to 420 min and is based on changes occurring with logarithmic aging time. TC1 was used as the fluorescence label in all systems.)

behavior of the different systems, indicate the existence of a relationship between the length and flexibility of the side groups and these properties.

The extraordinary suppression in aging rate of PMMA-SWCNT observed in this chapter is consistent with previous reports of arrested physical aging in polymer nanocomposites (Lee and Lichtenhan, 1998; Lu and Nutt, 2003a, 2003b; Rittigstein and Torkelson, 2006; Rittigstein et al., 2007; Theneau et al., 2007) and with studies examining the physical aging rates in thin PMMA supported films (Priestley et al., 2005a; Priestley et al., 2005b). In chapter 8 it was shown that when silica nanospheres are added to PMMA the physical aging response of the matrix is reduced. However, by grafting the PMMA to SWCNT a larger suppression is achieved. Another important difference is that the nanocomposites made with silica nanospheres do not follow the same trend of the physical aging rate with temperature that neat PMMA follows. The silica nanocomposites have a maximum aging rate at 360 K not at 305 K, like neat PMMA and PMMA-SWCNT systems.

10.4 Conclusions

Fluorescence spectroscopy has been used to determine the impact of grafting functionalized SWCNT to PMMA on the physical aging behavior of the polymer. Following a temperature quench from above T_g into the glass, isothermal aging was monitored over 8 h at temperatures ranging from 295 K to 323 K. Our results suggest that a small modification in the structure of the functionalized SWCNT may tailor the PMMA-SWCNT interface strength and tune the physical aging behavior of the

nanocomposite leading to strong suppression of physical aging rate deep in the glassy state. As the side group in the functionalized SWCNTs becomes shorter and more rigid, the interface between the PMMA and the SWCNT will be stronger, thereby retarding to a great extent the structural relaxation of the polymer and consequently the physical aging behavior of the nanocomposite.

11 Long-Term Reduction of Enthalpy Relaxation of PMMA-SWCNT Nanocomposites Studied by DSC

11.1 Introduction

When a polymer is cooled from the equilibrium liquid, the transformation to glass occurs at the glass transition temperature (T_g). A material in the glassy state has an excess of thermodynamic quantities such as volume, enthalpy and entropy with respect to equilibrium. Therefore, a glass maintained at a temperature below its T_g , at constant temperature and pressure after its formation history, undergoes a slow and continuous relaxation process toward its thermodynamic equilibrium state. This process is called structural relaxation or physical aging (see chapter 2).

A variety of experimental techniques have been used to study the segmental relaxation behavior of polymers (Donth, 1992; Havriliak and Havriliak, 1997). Among these techniques, differential scanning calorimetry (DSC) is a useful and convenient method to detect the variation in enthalpy during relaxation processes (Bershtein and Egorov, 1994). Numerous studies have used DSC to investigate the enthalpy relaxation of various glassy polymers (Petrie, 1972; Colomer and Gomez Ribelles, 1989; Cowie and Ferguson, 1993; Andreozzi et al., 2002a, 2002b, 2003; Ho and Vu-Khanh, 2003; Lu and Nutt, 2003a, 2003b; Ho and Vu-Khanh, 2004; Andreozzi et al., 2005; Theneau et al., 2007). The common procedure to study isothermal enthalpy relaxation is to subject the sample to different thermal histories that start at a temperature T_0 above T_g , after which the sample is cooled at a constant (rapid) rate to the annealing temperature T_a ,

below T_g , and maintained at this temperature for a time t_a . Next, the sample is cooled to the temperature T_1 far below T_g and subsequently heated to T_0 at a constant rate. The structural relaxation process is usually measured as the recovery of the lost enthalpy associated with the glass transition event during the last heating scan. When an aged glass is heated through T_g to the rubbery state, the lost enthalpy is regained or recovered. This event can be observed as an endothermic peak (in the glass transition region) in the DSC profile, having a strong dependence on the previous thermal history, for example T_a and t_a . The enthalpy recovery in the sample during the isothermal stage at T_a is equal to the area between the heating thermogram measured immediately after the annealing process and the thermogram measured between the same temperatures in a scan without annealing (Petrie, 1972; Colomer and Gomez Ribelles, 1989; Cowie and Ferguson, 1993).

A few studies have aimed at identifying the impact of the addition of nanofillers in the polymeric matrix on the structural relaxation (Lee and Lichtenhan, 1998; Lu and Nutt, 2003a, 2003b; Vlasveld et al., 2005; Rittigstein and Torkelson, 2006; Priestley et al., 2007c; Rittigstein et al., 2007; Theneau et al., 2007). Lee and Lichtenhan (1998) reported that the inclusion of polyhedral oligomeric silsesquioxane (POSS) nanoreinforcements in epoxy by *in situ* polymerization retarded the physical aging rate and the time to reach equilibrium. They proposed that the presence of POSS cages attached to the network chains provides topological constraints to the network junctions, which prevents or severely retards the process of the matrix reaching structural equilibrium. More recently, Lu and Nutt (2003a; 2003b) observed via DSC that

including intercalated clay nanofillers into an epoxy network had a significant effect on the segmental relaxation of the matrix. They found a restricted relaxation behavior with slower overall relaxation rates and a broader distribution of relaxation times in intercalated silicate-epoxy nanocomposites relative to the neat epoxy resin. They concluded that this behavior depends on the extent of exfoliation of the layered silicates and the strength of interaction between the silicate surface and the polymer. Using fluorescence, Rittigstein et al. (Rittigstein and Torkelson, 2006; Rittigstein et al., 2007) recently observed a reduction or suppression of physical aging by adding low levels of well-dispersed silica and alumina nanospheres to PMMA and P2VP, the magnitude of it depend on the interaction between the materials and also on the method of preparation (see chapters 6, 7 and 8).

Very recently, Theneau et al. (2007) used a phenomenological model based on the evolution of the configurational entropy and DSC measurements to study the influence of silica on the kinetics of the structural relaxation process of the poly(2-hydroxyethyl methacrylate) (PHEMA) nanocomposites. They observed a reduction in structural relaxation of PHEMA with increasing silica content. In addition, the presence of silica led to a broadening of the temperature interval in which conformational motions in the glassy state occur over a 200 min time frame. The distribution of the relaxation times also broadens as the silica content increases, as characterized by the decrease of the Kohlrausch-Williams-Watts (KWW) parameter β and the increase of the fragility of the polymer (Kohlrausch, 1847; Williams and Watts, 1970; Williams et al., 1971). In chapter 10, the physical aging behavior of PMMA grafted to different types of functionalized

SWCNT was studied using fluorescence over 8 h. It was found that the covalent bonds between PMMA and SWCNT create stronger interfaces that significantly retard the structural relaxation of the matrix. Also, the results indicated that there is a relationship between the length and flexibility of the side groups in the functionalized SWCNT and the extent of the reduction of physical aging.

In this chapter, the long-term structural relaxation of PMMA chains grafted to functionalized SWCNT is investigated. Differential scanning calorimetry is used to measure the enthalpy relaxation at environmental temperature. The results indicate that grafting 1 wt% SWCNT to PMMA strongly reduces the room-temperature aging relative to neat PMMA. In particular, the enthalpy relaxation experienced over only 4 days by neat PMMA is equal to the enthalpy relaxation of a 99/1 wt% PMMA/SWCNT nanocomposite over 100 days.

11.2 Experimental

Purified HiPCO SWCNTs (Bucky Pearls) were supplied by Carbon Nanotechnologies, Inc. (CNI, Houston, TX). Poly(methyl methacrylate) (PMMA) was synthesized by free radical polymerization ($M_n = 355,000$ g/mol, $M_w/M_n = 1.54$, by gel permeation chromatography using universal calibration with PS standards).

Amide-functionalized SWCNTs were prepared through carboxylic acid residues, which were introduced on SWCNT surfaces by a chemical oxidation method, followed by direct coupling of 1,12-diaminododecane to obtain SWCNTs functionalized with a $(\text{CH}_2)_{12}$ side group (see chapter 9). A solution evaporation technique was used to graft

PMMA to 1 wt% of amide-functionalized SWCNTs with $(\text{CH}_2)_{12}$ side group to form the nanocomposite. In this technique, the PMMA was first dissolved in tetrahydrofuran (THF). In another vial, SWCNTs were dispersed in THF by bath sonication for 1 h, added to the polymer solution, and again bath-sonicated for 1 h to disperse the SWCNT in the polymer. The mixture was stirred at 60 °C for 5 h and then cooled to room temperature. The cooled mixture was subsequently poured into stirred methanol and filtered through polytetrafluoroethylene filter paper with a 10 μm pore size. The product was dried at 80 °C under vacuum for 10 h. To verify that the PMMA was covalently bonded to the functionalized nanotubes, Fourier transform infrared (FTIR) spectrum of the PMMA-SWCNT nanocomposite was examined before performing physical aging measurements. The IR spectra of neat PMMA and functionalized SWCNTs were compared with the IR spectrum of the PMMA-SWCNT nanocomposite. The comparison of these spectra provided evidence of the existence of the amide bonds (peak at 1662 cm^{-1}) in the PMMA-SWCNT nanocomposite. These bonds are present in the functionalized SWCNTs and are also formed between the free amine groups (NH_2) in the functionalized SWCNTs and the ester groups in PMMA. In addition, the existence of the ester group (peak at 1728 cm^{-1}) in the spectra of the structures, confirmed the presence of PMMA (Ramanathan et al., 2005b).

The glass transition temperatures were measured by differential scanning calorimetry (DSC) (Mettler-Toledo DSC822, second heat, onset method, 10 °C/min): PMMA $T_{g,bulk} = 120$ °C and PMMA-SWCNT nanocomposite $T_g = 127$ °C. Differential scanning calorimetry was used to characterize the enthalpy relaxation of PMMA and

PMMA-SWCNT nanocomposites. The calibrations of temperature and enthalpy were performed using an indium standard. Nitrogen purging gas was used in all the experiments. Isothermal annealing experiments were conducted at 22 °C. In order to erase the thermal history, the sample was kept at 150 °C (T_0) during 1 h. Then, the sample was cooled to 22 °C (T_a) at a cooling rate of 40 °C/min and maintained at 22 °C for a specified time ranging between 0 h and 100 days. Next, the sample was cooled to -20 °C (T_1) at a cooling rate of 40 °C/min, and finally heated to T_0 at a heating rate of 10 °C/min. Immediately after each of these experiments, a heating reference scan at 10 °C/min was performed after cooling the sample from the highest to the lowest temperature, from T_0 to T_1 , at 40 °C/min. In this way, the baselines of the DSC corresponding to the annealing and the reference scans are nearly identical, and the position of the sample in the sample holder of the DSC is the same as well. The difference between both scans is zero with great accuracy at the start and at the end of the thermogram.

11.3 Results and Discussion

In this chapter, PMMA is grafted to 1 wt% SWCNT functionalized with a $(\text{CH}_2)_{12}$ side group. The formed nanocomposite presents an increase of 7 °C to 127 °C in the T_g of the polymer as seen for the reference curves in Figure 11-1. This result suggests that the nanotube bundles are well dispersed in PMMA and also that the functionalization of the SWCNTs significantly improves the interaction with the polymer,

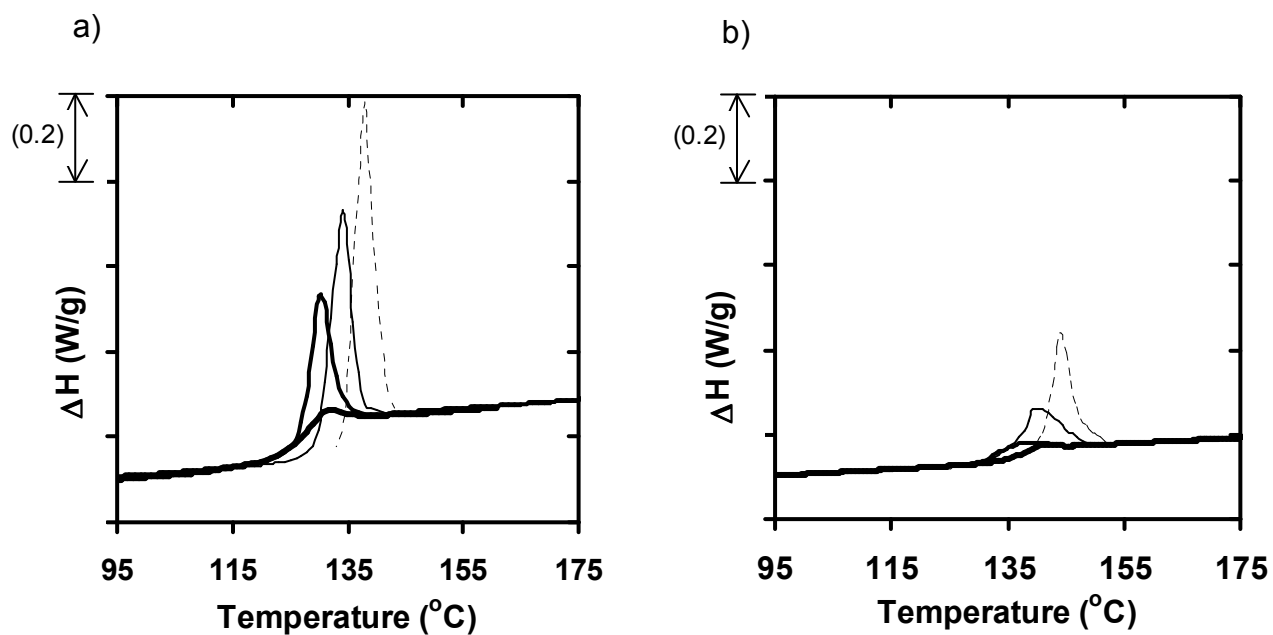


Figure 11-1: Enthalpy recovery curves for: a) neat PMMA and b) PMMA-SWCNT nanocomposite as a function of physical aging time at ambient temperature (20-22 $^{\circ}\text{C}$): 0 h (extra bold line), 48 h (bold line), 17 days (regular line) and 100 days (dashed line).

forming a strong interface that restricts the chain segmental mobility and increases T_g (see chapter 9).

Enthalpy relaxation experiments were conducted at environmental temperature (20-22 °C) over different time frames (between 0 h to 100 days) to determine the effects of SWCNT on restricting the segmental motion in PMMA nanocomposites. Figure 11-1 shows the heating DSC curves (10 °C/min) for neat PMMA and PMMA-SWCNT nanocomposite as a function of isothermal annealing time at environmental temperature. The presence of the aging peak after annealing at a given temperature T_a reveals that some conformational motions are still possible, relaxing the enthalpy during the isothermal period towards its equilibrium value. As expected, the excess enthalpy, represented by the magnitude of the endothermic peak, increases with increasing aging time. The aging time also affects the location of the aging peak. The recovery enthalpy during physical aging depends on the thermal history experienced by the glass and on related experimental variables, such as cooling rate, annealing temperature, annealing time, and heating rate. When these variables are fixed, as in the current study, the smaller recovery enthalpy of the nanocomposites can be ascribed to the slower relaxation rate of the PMMA segments that arises from the restricted mobility associated with the covalent attachment to the SWCNT. A strong reduction and broadening of the enthalpy relaxation peak of PMMA with the incorporation of SWCNT can be observed in Figure 11-1 for all physical aging times. If the temperature interval in which the glass transition takes place is narrow, most of the mass of the material relaxes at the same rate at T_a . On the contrary, a broad glass transition interval reflects the presence of T_g

fluctuations in the material and, as a consequence, at T_a the polymer segments participate in the structural relaxation process differently. Therefore, heterogeneous systems, like polymer nanocomposites, show shorter and broader peaks in the DSC curves.

The enthalpy recovery during the relaxation process can be determined by calculating the area between the heating thermogram measured immediately after the annealing process and the thermogram measured between the same temperatures in a scan without annealing (reference measurement). Figure 11-2 presents the enthalpy recovery of PMMA and PMMA-SWCNT nanocomposite as a function of logarithmic physical aging time at environmental temperature. In accord with enthalpy relaxation studies of neat polymers (Petrie, 1972; Colomer and Gomez Ribelles, 1989; Cowie and Ferguson, 1993), the enthalpy recovery increases roughly linearly with logarithmic physical aging time for both samples. However, as compared with neat PMMA, the polymer nanocomposite exhibits a much reduced segmental relaxation behavior over the 100-day time frame of this physical aging study. The slow relaxation dynamics observed in PMMA-SWCNT nanocomposite can be attributed both to the restricted chain mobility in the interfacial layer in which polymer chains are effectively anchored to the SWCNT surface and to the percolation across the sample. The slopes of the enthalpy recovery lines give the overall relaxation rate (r_δ) for each sample, being ~ 0.515 for neat PMMA and ~ 0.321 for the nanocomposite, illustrating the restriction effect of SWCNT on the segmental relaxation of PMMA. Therefore, grafting just 1 wt%

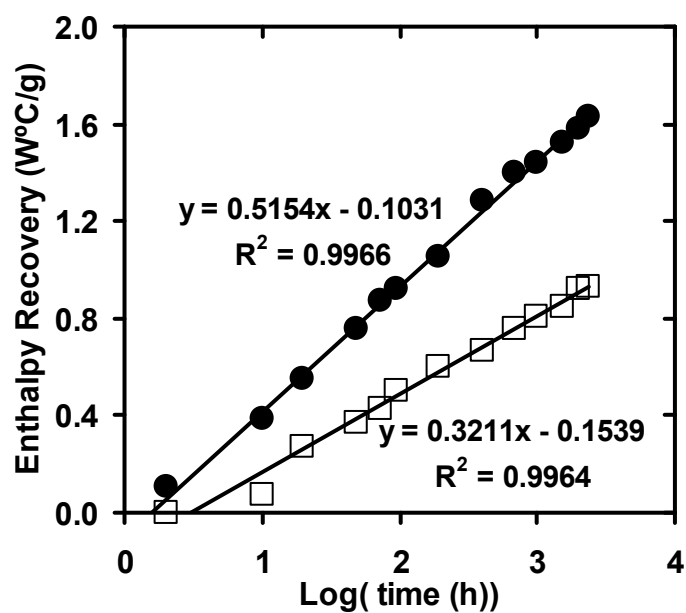


Figure 11-2: Enthalpy recovery as a function of logarithmic physical aging time at environmental temperature for neat PMMA (closed circles) and PMMA-SWCNT nanocomposite (open squares).

of SWCNT functionalized with a $(\text{CH}_2)_{12}$ side group to PMMA reduces the physical aging rate (defined on logarithmic aging time: $r_\delta = dH/d\log t_a$) of the polymer by approximately 40%. Thus, 4 days of aging at 20-22 °C in neat PMMA results in the same relaxation of enthalpy as 100 days of aging in the PMMA-SWCNT nanocomposite. This result suggests a novel application for polymer nanocomposite, because it has produced a non-equilibrium glass with properties that nearly stable during long-term physical aging.

11.4 Conclusions

Compared with neat PMMA, a PMMA-SWCNT nanocomposite formed by grafting PMMA to 1 wt% SWCNT functionalized with a $(\text{CH}_2)_{12}$ side group has a higher glass transition temperature, slower segmental relaxation dynamics, and a slower overall relaxation rate deep in the glassy state. These results are attributed to a complex local environment surrounding the SWCNT, which leads to slow polymer dynamics that percolate across the material.

Structural relaxation is very important technologically, as the long-term changes in properties accompanying aging may be catastrophic. This chapter provides understanding that may contribute to identifying ways to control and even arrest physical aging. The effect of nanofillers in strongly suppressing physical aging deep in the glassy state suggests a new application for polymer nanocomposites as substitutes for glassy polymers in long-term uses.

12 Conclusions and Recommendations

12.1 Conclusions

Nanoconfined polymers are employed in diverse areas and have the potential for many different applications, including chemical sensing (Krasteva et al., 2002; Sarantopoulou et al., 2008), catalysis (Galow et al., 2002; Esumi et al., 2004; Zampieri et al., 2004), drug delivery (Brigger et al., 2002; Wood et al., 2008), energy devices (Croce et al., 1998; Xi et al., 2005; Olivetti et al., 2006; Yildirim et al., 2008), membranes (Merkel et al., 2002; Song et al., 2007), lithographic patterning (Suh and Lee, 2002; Damean et al., 2005), tissue engineering (Griffith and Naughton, 2002; Shi et al., 2007), molecular electronics (Huang et al., 2001; Wang and Park, 2007), microfluidic devices (Therriault et al., 2003; Zhang et al., 2008), and photonic materials (Lin et al., 1998; Andriesh et al., 2007), among others. However, when polymer is confined to the nanoscale, many important properties such as the glass transition temperature (T_g) and physical aging can deviate significantly from bulk behavior. Therefore, it is scientifically and technologically important to understand how confinement alters the physical properties of polymers. Here, a detailed investigation has been performed of the T_g and physical aging behaviors of polymer nanocomposites and polymer thin films and the relationship between these two material systems.

Fluorescence was used to study T_g , physical aging behavior and local polarity of bulk and nanoconfined polymers in chapter 4. For the first time, fluorescence was used to understand the effect of confinement on local polarity in thin polymer films and polymer nanocomposites. In the case of PS systems, confinement by nanocomposite

formation with silica nanoparticles or by formation of ultrathin films on silica can lead to measurable increase in local polarity. However when similar experiments were done using PMMA and P2VP, no changes in the local polarity of the polymers with nanoconfinement was found. The lack of effect in PMMA and P2VP with addition of silica nanospheres is likely associated with the intrinsically polar nature of those two polymers in comparison with the non-polar nature of PS.

Chapter 5 describes the use of a fluorescence/multilayer technique to determine the influence of confinement and interfacial effects on T_g of PMMA films supported on silica. With single-layer PMMA films that are less than 90-nm-thick, T_g increases roughly linearly with decreasing logarithmic thickness. The use of bilayer films reveals that compared to $T_{g,\text{bulk}}$, T_g is reduced at the free surface and increased at the substrate interface, resulting in a T_g -gradient across the film. Measurements of confined bilayer films reveal that the stronger substrate effects percolate across the film to modify the T_g dynamics at the free surface. Thus, with nanoconfinement, the stronger substrate effects dominate the free-surface effects, providing an explanation for the increase in average T_g with decreasing single-layer PMMA film thickness. With extreme confinement, the T_g -gradient across the film thickness is suppressed, with both substrate layer and free-surface layer T_g s exceeding $T_{g,\text{bulk}}$. These results demonstrate that strongly perturbed T_g dynamics at the interfaces propagate across many layers of cooperatively rearranging regions (CRRs) within the films, meaning that configurational changes associated with cooperative segmental dynamics within a CRR do not occur independently of neighboring CRRs. Thus, insight into the fundamental nature of the

glass transition may be gained by measuring the nanoscale distributions of T_g s in confined polymers.

In chapter 6, model PMMA- and P2VP-silica nanocomposites consisting of polymer films confined between silica slides were designed. The dependence of T_g and physical aging on the interlayer distance in model nanocomposites were compared to the dependence on silica nanoparticle content in real nanocomposites. These provide a simple way to gain insight into the effect of interparticle spacing on T_g and to predict the approximate aging response of real nanocomposites. It was found that the model and real nanocomposites with identical T_g deviations yield similar dramatic suppressions of physical aging. The technological importance and significant scientific questions associated with the very long-range, confinement-related enhancements in T_g and the suppression of physical aging observed in polymers undergoing attractive interfacial interactions provide further impetus to study confinement effects in polymer nanocomposites. Model nanocomposites with silica and other substrates yield well-designed systems for such investigations.

In chapter 6 and chapter 7, the effect of confinement on T_g is studied by tuning the polymer-nanofiller interactions in nanocomposites via choice of polymer, nanofiller, or solvent used in the nanocomposite preparation. Nanocomposites containing low levels of nanofiller were used to demonstrate that T_g values could remain unchanged and could also be enhanced or depressed substantially relative to bulk T_g values. In these chapters, the effect of the addition of silica or alumina nanospheres to PS, PMMA and P2VP matrices on T_g was investigated. It was found that wetted interfaces along with

the presence of attractive polymer-nanofiller interactions, for example, in P2VP-alumina and P2VP-silica nanocomposites, increases the T_g relative to neat, bulk polymer. When there are wetted interfaces but no significant attractive interfacial interactions, for example, in PS-alumina and PS-silica nanocomposites, the T_g is equal to neat, bulk T_g . Finally, when the interfaces are non-wetted, that is, when a free surface is present between the polymer and the nanofiller, for example in PMMA-alumina nanocomposites, there is a reduction in T_g relative to neat, bulk T_g . These results are well understood by drawing analogies to studies on confined, ultrathin polymer films. It was also shown how the choice of solvent used to prepare the PMMA-silica nanocomposites can lead to major differences in polymer-nanofiller interactions and in T_g . When the PMMA nanocomposites are prepared using methyl ethyl ketone (MEK), T_g increases with the nanofiller content. However when the polymer nanocomposites are made using acetic acid (AA), there is a sharp decrease in T_g with increasing nanofiller content. Methyl ethyl ketone allows hydrogen bonding between the ester side groups of the PMMA and the hydroxyl groups on the surface of the silica, resulting in a subtle increase in T_g . On the other hand, the acid group of AA prevents or severely reduces this interaction (because the acid group interacts strongly with the PMMA ester side group) leading to the development of free surfaces (free space) between the PMMA and the silica nanofiller. Consequently, a major decrease in T_g is observed.

Using fluorescence, the physical aging responses of P2VP, PMMA and PS with the addition of silica and alumina nanospheres were investigated in chapter 7 and chapter 8. These studies showed that the extent of the reduction of physical aging that can be

obtained depends on the strength of the interaction between the polymer and the nanofiller. For example, in the case of P2VP-alumina nanocomposite, a nearly complete suppression of physical aging was observed, while in the case of P2VP-silica nanocomposites, physical aging was reduced but to a lesser extent. However, no change in physical aging rate was observed upon addition of these nanofillers to PS. In the case of PMMA-silica nanocomposite, we demonstrated that the extent of the reduction of physical aging is affected by the choice of spin coating solvent used to make the polymer nanocomposite. Our results suggest that surface and interface effects in polymer nanocomposites may be tailored to control the structural relaxation of high performance polymeric materials.

In chapter 9 the local and average glass transition temperatures of different PMMA SWCNT nanocomposites were studied. It was shown that fluorescence can be used to measure directly the T_g of the polymer in the vicinity of the nanofiller and also to understand the percolation effect through the whole polymer nanocomposite sample. Different polymer-nanofiller interfacial strengths were studied in order to identify their effect on the local and average glass transition temperatures of the system. With the use of shorter and more rigid side groups in the functionalized SWCNTs, the interface between the PMMA and the SWCNT will be stronger, causing more constraint of the PMMA segmental mobility, thereby increasing the local and average T_g of the system. Higher SWCNT concentrations lead to more polymer-nanofiller interfacial area, increasing the magnitude of the observed effects.

In chapter 10, fluorescence has been used to determine the impact of grafting differently functionalized SWCNTs to PMMA on the initial (8 h) physical aging behavior of the polymer. Our results suggest that a small modification in the structure of the functionalized SWCNT may tailor the PMMA-SWCNT interface strength and tune the physical aging behavior of the nanocomposite. The results indicate that there is a relationship between the length and flexibility of the side groups in the functionalized SWCNT and the extent of the reduction of physical aging.

The long-term structural relaxation of PMMA chains grafted to functionalized SWCNT is investigated in chapter 11. Differential scanning calorimetry is used to measure the enthalpy relaxation at environmental temperature. The results indicate that, in comparison with neat PMMA, the PMMA-SWCNT nanocomposite under study exhibited a slightly higher T_g (by 7 K) but much slower physical aging at 20-22 °C. In particular, the enthalpy relaxation exhibited by neat PMMA over 4 days at 20-22 °C was equal to the enthalpy relaxation exhibited by the PMMA-SWCNT nanocomposite over 100 days at the same aging temperature. These results are attributed to a complex local environment surrounding the SWCNT that is covalently attached to the polymer, which leads to slow polymer dynamics that percolate across the material. Structural relaxation is very important technologically, as the long-term changes in properties accompanying aging may be catastrophic. This chapter provides understanding that may contribute to identifying ways to control and even arrest physical aging. The effect of nanofillers in reducing physical aging suggests a new application for polymer nanocomposites as substitutes for glassy polymers in long-term uses.

12.2 Recommendations for Future Work

More efforts are required to further advance our understanding of the T_g -nanoconfinement effect in polymer nanocomposites and thin polymer films. Some of the ideas investigated in this work can be extended to deepen our understanding of the field. The following paragraphs outline some suggested research directions.

The environmental sensitivity of pyrene was exploited in chapter 4 to study the impact of interfaces with substrates (in the case of films) or nanoparticles (in the case of nanocomposites) on the polarity of a polymeric medium. It would be interesting to extend this to study the influence of confinement and interfacial effects on the local polarity of PS films supported on silica. This can be done following an approach similar to the fluorescence/multilayer technique implemented by Ellison and Torkelson (2003) to study the effect of confinement in the distribution of T_g across the film.

A fluorescence/multilayer method used to determine the effect of nanoconfinement and interfacial interactions on the T_g of PMMA film supported on silica was described on chapter 5. The results indicated that the strongly perturbed T_g dynamics at an interface can propagate over many layers of CRRs. It will be useful to study other systems that would show more dramatic T_g -nanoconfinement effect than PMMA. Poly(2-vinyl pyridine) (P2VP) exhibits large T_g increases of 40-50 K relative to $T_{g,bulk}$ upon nanoconfinement (van Zanten et al., 1996; Park et al., 2004; Roth et al., 2007). Many experiments were attempted to understand the direct effect of the free surface and the substrate on the T_g of P2VP upon confinement by Ellison (2005) employing a variety of

dyes that were unsuccessful. Another option is to study poly(4-vinyl pyridine) (P4VP), because it has a similar molecular structure to P2VP but probably has a stronger nanoconfinement effect than P2VP. This is because the nitrogen atom on the P4VP structure is more accessible for hydrogen bonding interactions.

Chapter 6 and chapter 7 explored in detail the impact of various parameters that tune the T_g -nanoconfinement effect on polymer nanocomposites. The choice of polymer, nanofiller and method of preparation were used to tune the polymer-nanofiller interfacial interaction and to obtain different T_g -nanoconfinement effects. Similar studies in other systems such as P4VP, polyvinylacetate (PVAc), and poly(tert-butyl styrene) (PTBS) with silica, alumina and gold nanoparticles remain to be undertaken. Also, understanding the effect of different sonication strengths on the dispersion of the nanofillers in the matrix, and as a consequence on the T_g of the nanocomposites, would be important. Since the preparation method alters the dispersion and the interfacial interaction between the matrix and the nanofillers, different approaches to make polymer nanocomposites deserve to be studied. Interesting approaches to consider include the *in-situ* formation of the polymer in the presence of the nanofillers (Ash et al., 2002b) and the adsorption of the polymer on the nanofiller surface following the procedure of Blum and coworkers (Xie and Blum, 1996; Porter and Blum, 2000, 2002; Blum et al., 2003; Kulkeratiyut et al., 2006); the effect on T_g in such systems can be observed using fluorescence or differential scanning calorimetry.

Nanofillers are used as nucleating agent and reinforcement in polymer foams, impacting the morphology and the properties of the matrix (Lee et al., 2005; Shen et al.,

2006; Han et al., 2007). Fluorescence can be used to understand the effect of free surface and attractive substrate interactions on the T_g of neat polymer and polymer nanocomposite foams.

Ellison (2005) demonstrated that the temperature dependence of the average decay lifetimes (single exponential decay) of pyrene doped into bulk PS could be employed to identify T_g in a similar manner to that of integrated intensity. This approach can be used to study the T_g s of different polymer nanocomposites and to observe whether a multiexponential decay which would be consistent with the presence of T_g gradients, describes the behavior of the confined material.

Model PMMA- and P2VP-silica nanocomposites consisting of polymer films confined between silica slides were designed and studied in chapter 6. It was found that doubly supported PMMA and P2VP films yield major increases in T_g with confinement at much greater length scales than those observed in films supported by a single substrate. Thus, removing the free surface results in a dramatic increase in the T_g -nanoconfinement effect of polymer that possesses attractive substrate-polymer interactions. Also, model and real nanocomposites with identical T_g deviations yield similar dramatic suppressions of physical aging. A related study using PS, in which T_g decreases with decreasing film thickness in a single supported thin film due to the free surface effect, will be helpful in order to verify that the elimination of the free surface results in no change on T_g upon confinement, as shown by Sharp and Forrest (2003b). On the other hand, a stronger effect upon confinement may be observed if T_g and

physical aging of P4VP model nanocomposites are studied and compared with the real nanocomposites.

The initial (8 h) physical aging responses of P2VP, PMMA and PS with the addition of silica and alumina nanospheres were investigated in chapter 7 and chapter 8 using steady state fluorescence measurements at different temperatures. These studies showed that the extent of the reduction of physical aging depends on the strength of the interaction between the polymer and the nanofiller. Further investigation of these systems can be undertaken using time-resolved fluorescence measurements to determine their long-term physical aging behavior. Also, this approach has the potential to find relationships between the structural relaxation process and the distribution of environments in polymer nanocomposites.

While fluorescence studies on supported PMMA films showed a reduction of the physical aging behavior of the free surface layer (Priestley et al., 2005b), permeability measurements on numerous polymers have shown accelerated physical aging in thin free-standing films compared with much thicker bulk films (Pfromm and Koros, 1995; Dorkenoo and Pfromm, 1999, 2000; McCaig and Paul, 2000; McCaig et al., 2000; Huang and Paul, 2004, 2005; Kim et al., 2006; Huang and Paul, 2007a, 2007b). Since the permeability studies used higher free volume polymers with significantly more rigid backbones than the PMMA, it is important to perform confinement studies of physical aging using fluorescence in those systems. On the other hand, oxygen permeability experiments of PS, PMMA and P2VP thin films as a function of confinement and physical aging time can be done and compared with fluorescence results. Given that

only a very small amount of well-dispersed nanofiller is required to have sufficient polymer/nanofiller-surface interaction to alter T_g (Rittigstein and Torkelson, 2006; Rittigstein et al., 2007), but significantly more nanofiller is required to obtain changes in permeability (Merkel et al., 2002), oxygen permeation studies of different polymer nanocomposites as a function of filler shape, content and aging time would be very interesting. Also, such studies would aid in understanding whether gas transport in permeation studies is sensitive only to the creation of large pockets of free volume between the nanoparticle aggregates (Winberg et al., 2005) or if there are additional dependences.

Chapter 9 described the local and average T_g s of different PMMA SWCNT nanocomposites. It was shown that fluorescence can be used to measure directly the T_g of the polymer in the vicinity of the nanofiller and also to characterize the percolation of the interfacial effect through the whole polymer nanocomposite sample. Also, by modifying the side group in the functionalized SWCNT, different polymer-nanofiller interfaces strengths were studied in order to identify their effect on the local and average glass transition temperatures of the systems. It will be useful to study the effect of different PMMA tacticity in the local and average T_g of the PMMA-SWCNT nanocomposites. Grohens et al. (2002) found that the T_g -confinement effect of PMMA films was a strong function of PMMA tacticity. Their results were explained in terms of a correlation between the observed T_g and the tacticity, the density of the repeat unit and the substrate interactions. By changing the tacticity of the polymer, it is possible that

the strength of the interface between PMMA and SWCNT will be different and therefore their physical properties will also change.

Preliminary work was done in order to observe the miscibility behavior, T_g and width of the transition of PMMA-PVC blends and PMMA grafted to SWCNT-PVC blends using DSC. The initial results indicate that grafting SWCNT to PMMA helps to achieve a more miscible, stable and homogeneous blend. More work employing DSC and fluorescence needs to be done in order to verify and understand the observed trend with the side group in the functionalized SWCNT, PMMA tacticity and blend compositions.

As part of this thesis research, various attempts were made to use reversible addition-fragmentation chain transfer (RAFT) polymerization to synthesize PS chains grafted on silica nanosphere surfaces in a controlled manner. (As a strictly preliminary study, this work is not described in an earlier thesis chapter.) Our results show that two types of PS populations were produced: PS grafted to silica nanospheres and free PS, indicating that the RAFT polymerization employed was not fully controlled. However, the obtained PS grafted to silica nanospheres material showed a very interesting T_g behavior as determined by DSC. Three distinct peaks were observed: bulk T_g and two more peaks corresponding to increments of 20 and 40 K with respect to bulk. These results are very encouraging and illustrate the magnitude of the T_g enhancement that can be achieved. In order to control the polymerization, future attempts should be performed using atom transfer radical polymerization (ATRP). This approach has proven to be a versatile method for incorporating organic polymers of precise molar

mass, composition and functionality onto inorganic substrate surfaces (either flat or curved) leading to well-defined architectures (Pyun and Matyjaszewski, 2001; Davies and Matyjaszewski, 2002; Pyun et al., 2003b). Also, silica nanoparticles possessing covalently bound PS chains prepared by ATRP of styrene from functionalized colloidal surfaces were reported by Savin et al. (2002) and Pyun et al. (2003a). Once PS silica hybrid nanoparticles are made, DSC and fluorescence can be used to study the average T_g and physical aging behavior of the system. The outcomes can be compared with PS silica nanocomposites results (chapter 6 and chapter 8) and with the study by Bansal et al. (2006). The use of a controlled radical technique like ATRP will be instrumental in the selective placement of small amounts of chromophore-labeled monomer (for example 1-butylpyrenyl methacrylate monomer) at special depths in the brush. This procedure might allow the characterization of a discrete distribution of T_g s of the hybrid nanoparticles embedded in a PS matrix via fluorescence. In addition, it may be possible to expand this approach to study the local T_g s of styrene-methyl methacrylate (S/MMA) random copolymer grafted to silica nanospheres as a function of copolymer composition using intrinsic fluorescence.

Chapter 10 and chapter 11 describe the physical aging behavior of PMMA grafted to functionalized SWCNT using steady state fluorescence measurements and DSC, respectively. It was found that PMMA-SWCNT nanocomposites present slow dynamics (initial and long term) compared with bulk PMMA. This can be attributed to the restricted chain mobility in the interfacial layer in which polymer chains are effectively anchored to the SWCNT surface, and then the effect percolates across the sample.

Similar studies in other systems such as PMMA-PVC blends, PMMA grafted to SWCNT-PVC blends and PS silica hybrid nanoparticles remain to be undertaken. Time-resolved fluorescence measurements can also be employed to determine their long-term physical aging behavior.

References

- Adachi, K. and Kotaka, T., 1982. Volume and Enthalpy Relaxation in Polystyrene. *Polym. J.*, 14: 959-970.
- Adam, G. and Gibbs, J.H., 1965. On the Temperature Dependence of Cooperative Relaxation Properties in Glass-Forming Liquids. *J. Chem. Phys.*, 43: 139-146.
- Akabori, K., Tanaka, K., Nagamura, T., Takahara, A. and Kajiyama, T., 2005. Molecular Motion in Ultrathin Polystyrene Films: Dynamic Mechanical Analysis of Surface and Interfacial Effects. *Macromolecules*, 38: 9735-9741.
- Akelah, A. and Moet, A., 1996. Polymer-clay Nanocomposites: Free-radical Grafting of Polystyrene on to Organophilic Montmorillonite Interlayers. *J. Mater. Sci.*, 31: 3589-3596.
- Al-Mulla, A., Mathew, J., Yeh, S.K. and Gupta, R., 2008. Nonisothermal Crystallization Kinetics of PBT Nanocomposites. *Comp. A Appl. Sci. Manuf.*, 39: 204-217.
- Alcoutlabi, M. and McKenna, G.B., 2005. Effects of Confinement on Material Behavior at the Nanometre Size Scale. *J. Phys.: Condens. Matter*, 17: R461-R524.
- Anderson, P., 1995. Through the Glass Lightly: A Collection of Scientists at the Frontier Were Asked What They See in the Future for Science. *Science*, 267: 1615-1616.
- Andreozzi, L., Faetti, M., Giordano, M. and Palazzuoli, D., 2002a. A Calorimetric Study of Structural Relaxation in the Glassy State of a Liquid-Crystal Polymer. *Philos. Mag. B*, 82: 397-407.

- Andreozzi, L., Faetti, M., Giordano, M. and Palazzuoli, D., 2002b. Physical Aging in Side-Chain Liquid Crystal Polymers: A DSC Investigation of the Enthalpy Relaxation. *Macromolecules*, 35: 9049-9056.
- Andreozzi, L., Faetti, M., Giordano, M. and Palazzuoli, D., 2003. Enthalpy Recovery in Low Molecular Weight PMMA. *J. Non-Cryst. Solids*, 332: 229-241.
- Andreozzi, L., Faetti, M., Giordano, M. and Zulli, F., 2005. Molecular-Weight Dependence of Enthalpy Relaxation of PMMA. *Macromolecules*, 38: 6056-6067.
- Andriesh, A., Meshalkin, A., Buzurniuc, S. and Verlan, V., 2007. Some Optical and Recording Properties of Composite Material AS(2)S(3)-PVP. *J. Optoelect. Adv. Mater.*, 9: 3002-3006.
- Angell, C.A., 1991. Relaxation in Liquids, Polymers and Plastic Crystals - Strong Fragile Patterns and Problems. *J. Non-Cryst. Solids*, 131: 13-31.
- Angell, C.A., 1995a. Formation of Glasses from Liquids and Biopolymers. *Science*, 267: 1924-1935.
- Angell, C.A., 1995b. The Old Problems of Glass and the Glass Transition, and the Many Twists. *Proc. Natl. Acad. Sci. USA*, 92: 6675-6682.
- Angell, C.A., 1997. Why $C_1 = 16-17$ in the WLF equation is physical -and the fragility of polymers. *Polymer*, 38: 6261-6266.
- Angell, C.A., Ngai, K.L., McKenna, G.B., McMillan, P.F. and Martin, S.W., 2000. Relaxation in Glass forming Liquids and Amorphous Solids. *J. Appl. Phys.*, 88: 3113-3157.

- Arndt, M., Stannarius, R., Gorbatschow, W. and Kremer, F., 1996. Dielectric Investigations of the Dynamic Glass Transition in Nanopores. *Phys. Rev. E*, 54: 5377-5390.
- Arndt, M., Stannarius, R., Groothues, H., Hempel, E. and Kremer, F., 1997. Length Scale of Cooperativity in the Dynamic Glass Transition. *Phys. Rev. Lett.*, 79: 2077-2080.
- Arrighi, V., McEwen, I.J., Qian, H. and Serrano Prieto, M.B., 2003. The Glass Transition and Interfacial Layer in Styrene-Butadiene Rubber Containing Silica Nanofiller. *Polymer*, 44: 6259-6266.
- Ash, B.J. et al., 2002a. Mechanical Properties of Al₂O₃/polymethylmethacrylate Nanocomposites. *Polym. Comp.*, 23: 1014-1025.
- Ash, B.J., Schadler, L.S. and Siegel, R.W., 2002b. Glass Transition Behavior of Alumina/Polymethylmethacrylate Nanocomposites. *Mater. Lett.*, 55: 83-87.
- Ash, B.J., Siegel, R.W. and Schadler, L.S., 2004. Glass-Transition Temperature Behavior of Alumina/PMMA Nanocomposites. *J. Polym. Sci., Part B: Polym. Phys.*, 42: 4371-4383.
- Badrinarayanan, P. and Simon, S.L., 2007. Origin of the Divergence of the Timescales for Volume and Enthalpy Recovery. *Polymer*, 48: 1464-1470.
- Bair, H.E., Johnson, G.E., Anderson, E.W. and Matsuoka, S., 1981. Non-Equilibrium Annealing Behavior of Polyvinyl Acetate. *Polym. Eng. Sci.*, 21: 930-935.
- Baljon, A.R.C., Billen, J. and Khare, R., 2004. Percolation of Immobil Domains in Supercooled Thin Polymeric Films. *Phys. Rev. Lett.*, 93: 255701 (1-4).

- Bansal, A. et al., 2006. Controlling the Thermomechanical Properties of Polymer Nanocomposites by Tailoring the Polymer-Particle Interface. *J. Polym. Sci., Part B: Polym. Phys.*, 44: 2944-2950.
- Bansal, A. et al., 2005. Quantitative Equivalence Between Polymer Nanocomposites and Thin Polymer Films. *Nat. Mater.*, 4: 693-698.
- Barut, G., Pissis, P., Pelster, R. and Nimtz, G., 1998. Glass Transition in Liquids: Two versus Three-Dimensional Confinement. *Phys. Rev. Lett.*, 80: 3543-3546.
- Baschnagel, J. et al., 2003. Computer Simulation of Polymer Close to Solid Interfaces: Some Selected Topics. *Interf. Sci.*, 11: 159-173.
- Baschnagel, J. and Varnik, F.J., 2005. Computer Simulations of Supercooled Polymer Melts in the Bulk and in Confined Geometry. *J. Phys.: Condens. Matter*, 17: R851-R953.
- Beaucage, G., Composto, R. and Stein, R.S., 1993. Ellipsometric Study of the Glass Transition and Thermal Expansion Coefficients of Thin Polymer Films. *J. Polym. Sci., Part B: Polym. Phys.*, 31: 319-326.
- Bernazzani, P., Simon, S.L., Plazek, D.J. and Ngai, K.L., 2002. Effects of Entanglement Concentration on Tg and Local Segmental Motions. *Eur. Phys. J. E*, 8: 201-207.
- Berriot, J., Montes, H., Lequeux, F., Long, D. and Sotta, P., 2002. Evidence for the Shift of the Glass Transition near the Particles in Silica-Filled Elastomers. *Macromolecules*, 35: 9756-9762.
- Berriot, J., Montes, H., Lequeux, F., Long, D. and Sotta, P., 2003. Gradient of Glass Transition Temperature in Filled Elastomers. *Europhys. Lett.*, 64: 50-56.

- Bershtein, V.A. and Egorov, V.M., 1994. *Differential Scanning Calorimetry of Polymers Physics, Chemistry, Analysis, Technology*, Ellis Hordwood, New York.
- Berthier, L. et al., 2005. Direct Experimental Evidence of Growing Length Scale Accompanying the Glass Transition. *Science*, 310: 1797-1800.
- Bitsanis, I. and Hadziioannou, G., 1990. Molecular Dynamics Simulations of the Structure and Dynamics of Confined Polymer Melts. *J. Chem. Phys.*, 92: 3827-3847.
- Blum, F.D., Lin, W.Y. and Porter, C.E., 2003. Dynamics of Adsorbed Poly(methyl acrylate) and Poly(methyl methacrylate) on Silica. *Coll. Polym. Sci.*, 281: 197-202.
- Blum, F.D., Young, E.N., Smith, G. and Sitton, O.C., 2006. Thermal Analysis of Adsorbed Poly(methyl methacrylate) on Silica. *Langmuir*, 22: 4741-4744.
- Bobiak, J.P. and Koenig, J.L., 2004. Fourier Transform Infrared Imaging of Stereoregular Poly(methyl methacrylate) Dissolution. *Appl. Spectrosc.*, 58: 1141-1146.
- Bohmer, R. and Angell, C.A., 1993. Elastic and Viscoelastic Properties of Amorphous Selenium and Identification of the Phase Transition Between Ring and Chain Structures. *Phys. Rev. B*, 48: 5857-5864.
- Bohmer, R., Ngai, K.L., Angell, C.A. and Plazek, D.J., 1993. Nonexponential Relaxations in Strong and Fragile Glass Formers. *J. Chem. Phys.*, 99: 4201-4209.

- Bower, D.I., 2002. An Introduction to Polymer Physics, Cambridge, UK: Cambridge University Press.
- Brady, R.F. and Charlesworth, J.M., 1993. Influence of Imidazoline Content and Water on the Reaction Between Amidoamine and Epoxy-Resins. *J. Coat. Technol.*, 65: 81-88.
- Brigger, I., Dubernet, C. and Couvreur, P., 2002. Nanoparticles in Cancer Therapy and Diagnosis. *Adv. Drug Delivery Rev.*, 54: 631-651.
- Brown, H.R. and Russell, T.P., 1996. Entanglements at Polymer Surfaces and Interfaces. *Macromolecules*, 29: 798-800.
- Buriak, J.M., 2006. High surface area silicon materials: Fundamentals and New Technology. *Phil. Trans. R. Soc. A*, 364: 217-225.
- Casalini, R., Ngai, K., Robertson, C.G. and Roland, C.M., 2000. α - and β -Relaxations in Neat and Antiplasticized Polybutadiene. *J. Polym. Sci., Part B: Polym. Phys.*, 38: 1841-1847.
- Chang, I. et al., 1994. Translational and Rotational Molecular-Motion in Supercooled Liquids Studied by NMR and Forced Rayleigh-Scattering. *J. Non-Cryst. Solids*, 172: 248-255.
- Chen, H., Guo, Q. and Jhon, M.S., 2007. Effects of Molecular Structure on the Conformation and Dynamics of Perfluoropolyether Nanofilms. *IEEE Trans. Mag.*, 43: 2247-2249.

- Chen, Q., Xu, R. and Yu, D., 2006. Multiwalled Carbon Nanotube/Polybenzoxazine Nanocomposites: Preparation, Characterization and Properties. *Polymer*, 47: 7711-7719.
- Cicerone, M.T., Blackburn, F.R. and Ediger, M.D., 1995. Anomalous Diffusion of Probe Molecules in Polystyrene: Evidence for Spatially Heterogeneous Segmental Dynamics. *Macromolecules*, 28: 8224-8232.
- Cizmecioglu, M., Fedors, R.F., Hong, S.D. and J, M., 1981. Effect of Physical Aging on Stress Relaxation of Poly(methyl Methacrylate). *Polym. Eng. Sci.*, 21: 940-942.
- Cohen, M.H. and Turnbull, D., 1959. Molecular Transport in Liquids and Glasses. *J. Chem. Phys.*, 31: 1164-1169.
- Coll, H. and Searles, C.G., 1988. Solvent Permeation Rates and aging Phenomena in Polymer-Coatings. *Polymer*, 29: 1266-1272.
- Colomer, F.R. and Gomez Ribelles, J.L., 1989. Structural Relaxation of Poly(g-benzyl-L-glutamate). *Polymer*, 30: 849-855.
- Colucci, D.M. et al., 1997. Isochoric and Isobaric Glass Formation: Similarities and Differences. *J. Polym. Sci., Part B: Polym. Phys.*, 35: 1561-1573.
- Cowie, J.M.G. and Ferguson, R., 1993. Physical Ageing of Poly(methyl methacrylate) from Enthalpy Relaxation Measurements. *Polymer*, 34: 2135-2141.
- Cowie, J.M.G., McEwen, I.J. and Matsuda, S., 1998. Stress Relaxation and Physical Ageing in a Blend of Poly(styrene-co-acrylonitrile) and Poly(methyl methacrylate). *J. Chem. Soc., Faraday Trans.*, 94: 3481-3486.

- Croce, F., Appetecchi, G.B., Persi, L. and Scrosati, B., 1998. Nanocomposite Polymer Electrolytes for Lithium Batteries. *Nature*, 394: 456-458.
- Curro, J.J. and Roe, R.-J., 1984. Isothermal Relaxation of Specific Volume and Density Fluctuation in Poly(methyl methacrylate) and Polycarbonate. *Polymer*, 25: 1424-1430.
- D'Amour, J.N., Okoroanyanwu, U. and Frank, C.W., 2004. Influence of Substrate Chemistry on the Properties of Ultrathin Polymer Films. *Microelectron. Eng.*, 73-74: 209-217.
- Dalnoki-Veress, K., Forrest, J.A., Murray, C., Gigault, C. and Dutcher, J.R., 2001. Molecular Weight Dependence of Reductions in the Glass Transition Temperature of Thin, Freely Standing Polymer Films. *Physical Review E*, 63: 031801 (1-10).
- Dalnoki-Veress, K., Nickel, B.G., Roth, C.B. and Dutcher, J.R., 1999. Hole Formation and Growth in Freely Standing Polystyrene Films. *Phys. Rev. E*, 59: 2153-2156.
- Damean, N., Parviz, B.A., Lee, J.N., Odom, T. and Whitesides, G.M., 2005. Composite Ferromagnetic Photoresist for the Fabrication of Microelectromechanical Systems. *J. Micromech. Microeng.*, 15: 29-34.
- Davies, K.A. and Matyjaszewski, K., 2002. Statistical, Gradient, Block, and Graft Copolymers by Controlled/Living Radical Polymerizations. *Adv. Polym. Sci.*, 159.
- de Deus, J.F., Souza, G.P., Corradini, W.A., Atvars, T.D.Z. and Akcelrud, L., 2004. Relaxations of Poly(methyl methacrylate) Probed by Covalently Attached Anthryl Groups. *Macromolecules*, 37: 6938-6944.

- De Gennes, P.G., 2000. Glass Transition in Thin Polymer Films. *Eur. Phys. J. E*, 2: 201-205.
- Debenedetti, P.G. and Stillinger, F.H., 2001. Supercooled Liquids and The Glass Transition. *Nature*, 410: 259-267.
- DeMaggio, G.B., Frieze, W.E. and Gidley, D.W., 1997. Interface and Surface Effects on the Glass Transition in Thin Polystyrene Films. *Phys. Rev. Lett.*, 78: 1524-1527.
- Deppe, D., Dhinojwala, A. and Torkelson, J.M., 1996. Small Molecule Probe Diffusion in Thin Polymer Films Near the Glass Transition: A Novel Approach Using Fluorescence Nonradiative Energy Transfer. *Macromolecules*, 29: 3898-3908.
- Despotopoulou, M.M., Frank, C.W., Miller, R.D. and Rabolt, J.F., 1995. Role of the Restricted Geometry on the Morphology of Ultrathin Poly(di-n-hexylsilane) Films. *Macromolecules*, 28: 6687-6688.
- Despotopoulou, M.M., Frank, C.W., Miller, R.D. and Rabolt, J.F., 1996. Kinetics of Chain Organization in Ultrathin Poly(di-n-hexylsilane) Films. *Macromolecules*, 29: 5797-5804.
- Dhinojwala, A., Wong, G.K. and Torkelson, J.M., 1993. Rotational Reorientation Dynamics of Nonlinear Optical Chromophores in Rubbery and Glassy Polymers: α -Relaxation Dynamics Probed by Second Harmonic Generation and Dielectric Relaxation. *Macromolecules*, 26: 5943-5953.
- Dhinojwala, A., Wong, G.K. and Torkelson, J.M., 1994. Rotational reorientation Dynamics of Disperse Red 1 in Polystyrene: α -Relaxation Dynamics by Second

- Harmonic Generation and Dielectric Relaxation. *J. Chem. Phys.*, 100: 6046-6054.
- Ding, Y. et al., 2007. Poly(methyl methacrylate)-Nanoribbon Nanocomposites with High Thermal Stability and Improvement in the Glass-Transition Temperature. *J. Mater. Res.*, 22: 3316-3323.
- Dixon, P.K., Wu, L. and Nagel, S.R., 1990. Scaling in the Relaxation of Supercooled Liquids. *Phys. Rev. Lett.*, 65: 1108-1111.
- Donati, C. et al., 1998. Stringlike Cooperative Motion in a Supercooled Liquid. *Phys. Rev. Lett.*, 80: 2338-2341.
- Donth, E., 1982. The Size of Cooperatively Rearranging Regions at the Glass Transitions. *J. Non-Cryst. Solids*, 53: 325-330.
- Donth, E., 1984. The Size of Cooperatively Rearranging Regions in Polystyrene and Styrene-Dimethylsiloxane Diblock Copolymers at the Glass Transition Temperature. *Acta Polym.*, 35: 120-123.
- Donth, E., 1992. Relaxation and Thermodynamics in Polymers. Glass Transition, Akademie Verlag, Berlin.
- Donth, E., 1996. Characteristic Length of the Glass Transition. *J. Polym. Sci., Part B: Polym. Phys.*, 34: 2881-2892.
- Donth, E., 1999. Phenomenological Treatment of Dynamic Glass Transition Heterogeneity. *Acta Polymer.*, 50: 240-251.
- Donth, E., 2001. The Glass Transition: Relaxation Dynamics in Liquids and Disordered Materials, Berlin, Springer.

- Doolittle, A.K., 1951. Studies in Newtonian Flow. II. The Dependence of the Viscosity of Liquids on Free-Space. *J. Appl. Phys.*, 22: 1471-1475.
- Doolittle, A.K. and Doolittle, D.B., 1957. Studies in Newtonian Flow. V. Further Verification of the Free-Space Viscosity Equation. *J. Appl. Phys.*, 28: 901-905.
- Dorkenoo, K.D. and Pfromm, P.H., 1999. Experimental Evidence and Theoretical Analysis of Physical Aging in Thin and Thick Amorphous Glassy Polymer Films. *J. Polym. Sci., Part B: Polym. Phys.*, 37: 2239-2251.
- Dorkenoo, K.D. and Pfromm, P.H., 2000. Accelerated Physical Aging of Thin Poly[1-(trimethylsilyl)-1-propyne]. *Macromolecules*, 33: 3747-3751.
- Du, K., Zhang, L., Luo, X. and Yin, Q., 2006. Structure and Properties of PMP Foams Doped with Cu Nanopowders. *J. Appl. Polym. Sci.*, 102: 5627-5632.
- Echeverria, I., Su, P.-C., Simon, S.L. and Plazek, D.J., 1995. Physical Aging of a Polyetherimide: Creep and DSC Measurements. *J. Polym. Sci., Part B: Polym. Phys.*, 33: 2457-2468.
- Ediger, M.D., 2000. Spatially Heterogeneous Dynamics in Supercooled Liquids. *Annu. Rev. Phys. Chem.*, 51: 99-128.
- Ediger, M.D., Angell, C.A. and Nagel, S.R., 1996. Supercooled Liquids and Glasses. *J. Phys. Chem.*, 100: 13200-13212.
- Ellison, C.J., 2005. , Ph.D. Thesis: Probing the Distribution of Glass Transition Temperatures and Related Relaxation Behavior in Thin and Ultrathin Polymer Films Using Novel Fluorescence Approaches, Northwestern University, Evanston.

- Ellison, C.J., Kim, S.D., Hall, D.B. and Torkelson, J.M., 2002. Confinement and Processing Effects on Glass Transition Temperature and Physical Aging in Ultrathin Polymer Film: Novel Fluorescence Measurements. *Eur. Phys. J. E*, 8: 155-166.
- Ellison, C.J., Mundra, M.K. and Torkelson, J.M., 2005. Impacts of Polystyrene Molecular Weight and Modification to the Repeat Unit on the Glass Transition-Nanoconfinement Effect and the Cooperativity Length Scale. *Macromolecules*, 38: 1767-1778.
- Ellison, C.J., Ruszkowski, R.L., Fredin, N.J. and Torkelson, J.M., 2004. Dramatic Reduction of the Effect of Nanoconfinement on the Glass Transition of Polymer Films via Addition of Small-Molecule Diluent. *Phys. Rev. Lett.*, 92: 095702 (1-4).
- Ellison, C.J. and Torkelson, J.M., 2002. Sensing the Glass Transition in Thin and Ultrathin Polymer Films via Fluorescence Probes and Labels. *J. Polym. Sci., Part B: Polym. Phys.*, 40: 2745-2758.
- Ellison, C.J. and Torkelson, J.M., 2003. The Distribution of Glass-Transition Temperature in Nanoscopically Confined Glass Formers. *Nat. Mater.*, 2: 695-700.
- Erwin, B.M. and Colby, R.H., 2002. Temperature Dependence of Relaxation Times and the Length Scale of Cooperative Motion for Glass-Forming Liquids. *J. Non-Cryst. Solids*, 307-310: 225-231.
- Esumi, K., Houdatsu, H. and Yoshimura, T., 2004. Antioxidant Action by Gold-PAMAM Dendrimer Nanocomposites. *Langmuir*, 20: 2536-2538.

- Ferry, J.D., 1980. *Viscoelastic Properties of Polymers*, New York: 3rd ed. Wiley.
- Ferry, J.K., Dong, W.F., Miller, R. and Mohwald, H., 2006. Elastic Moduli of Asymmetric Ultrathin Free-Standing Polyelectrolyte Nanocomposites. *Macromolecules*, 39: 1532-1537.
- Flory, P.J., 1953. *Principles of Polymer Chemistry*, Ithaca, NY: Cornell University Press.
- Forrest, J.A. and Dalnoki-Veress, K., 2001. The Glass Transition in Thin Polymer Films. *Adv. Colloid Interface Sci.*, 94: 167-196.
- Forrest, J.A., Dalnoki-Veress, K. and Dutcher, J.R., 1997. Interface and Chain Confinement Effects on the Glass Transition Temperature of Thin Polymer Films. *Phys. Rev. E*, 56: 5705-5716.
- Forrest, J.A., Dalnoki-Veress, K. and Dutcher, J.R., 1998. Brillouin Light Scattering Studies of the Mechanical Properties of Thin Freely Standing Polystyrene Films. *Physical Review E*, 58: 6109-6114.
- Forrest, J.A., Dalnoki-Veress, K., Stevens, J.R. and Dutcher, J.R., 1996. Effect of Free Surfaces on the Glass Transition Temperature of Thin Polymer Films. *Phys. Rev. Lett.*, 77: 2002-2005.
- Forrest, J.A. and Mattsson, J., 2000. Reductions of the Glass Transition Temperature in Thin Polymer Films: Probing the Length Scale of Cooperative Dynamics. *Phys. Rev. E*, 61: R53-R56.
- Frank, B., Gast, A.P., Russell, T.P., Brown, H.R. and Hawker, C., 1996a. Polymer Mobility in Thin Films. *Macromolecules*, 29: 6531-6534.

- Frank, C.W. et al., 1996b. Structure in Thin and Ultrathin Spin-Cast Polymer Films. *Science*, 273: 912-915.
- Fryer, D.S., Nealey, P.F. and De Pablo, J.J., 2000. Thermal Probe Measurements of the Glass Transition Temperature for Ultrathin Polymer Films as a Function of Thickness. *Macromolecules*, 33: 6439-6447.
- Fryer, D.S. et al., 2001. Dependence of the Glass Transition Temperature of Polymer Films on Interfacial Energy and Thickness. *Macromolecules*, 34: 5627-5634.
- Fukao, K. and Miyamoto, Y., 1999. Glass Transition Temperature and Dynamics of α -Process in Thin Polymer Films. *Europhys. Lett.*, 46: 649-654.
- Fukao, K. and Miyamoto, Y., 2000. Glass Transition and Dynamics in Thin Polymer Films: Dielectric Relaxation of Thin Films of Polystyrene. *Phys. Rev. E*, 61: 1743-1754.
- Fukao, K. and Sakamoto, A., 2005. Aging Phenomena in Poly(methyl methacrylate) Thin Films: Memory and Rejuvenation Effects. *Phys. Rev. E*, 71: 041803 (1-12).
- Fukao, K., Uno, S., Miyamoto, Y., Hoshino, A. and Miyaji, H., 2001. Dynamics of α and β processes in thin polymer films: Poly(vinyl acetate) and poly(methyl methacrylate). *Phys. Rev. E*, 64: 051807 (1-11).
- Fukao, K., Uno, S., Miyamoto, Y., Hoshino, A. and Miyaji, H., 2002. Relaxation Dynamics in Thin Supported Polymer Films. *J. Non-Cryst. Solids*, 307: 517-523.
- Galow, T.H., Drechsler, U., Hanson, J.A. and Rotello, V.M., 2002. Highly Reactive Heterogeneous Heck and Hydrogenation Catalysis Constructed Through 'Bottom-up' Nanoparticle Self-Assembly. *Chem. Commun.*: 1076-1077.

- Ganss, M. et al., 2007. Temperature Dependence of Creep Behavior of PP-MWCNT Nanocomposites. *Macromol. Rapid Commun.*, 28: 1624-1633.
- Giannelis, E.P., 1996. Polymer Layered Silicate Nanocomposites. *Adv. Mater.*, 8: 29-35.
- Gibbs, J.H. and DiMarzio, E.A., 1958. Nature of the Glass Transition and the Glassy State. *J. Chem. Phys.*, 28: 373-383.
- Glotzer, S.C., 2000. Spatially Heterogeneous Dynamics in Liquids: Insights from Simulation. *J. Non-Cryst. Solids*, 274: 342-355.
- Gonzalez-Benito, J. et al., 2000. Fluorescence-Labeled Pyrenesulfonamide Response for Characterizing Polymeric Interfaces in Composite Materials. *J. Fluoresc.*, 10: 141-146.
- Gotze, W. and Sjogren, L., 1992. Relaxation Processes in Supercooled Liquids. *Rep. Prog. Phys.*, 55: 241-376.
- Granick, S. and Hu, H.W., 1994. Nanorheology of Confined Polymer Melts. 1. Linear Shear Response at Strongly Adsorbing Surfaces. *Langmuir*, 10: 3857-3866.
- Greiner, R. and Schwarzl, F.R., 1984. Thermal Contraction and Volume Relaxation of Amorphous Polymers. *Rheol. Acta*, 23: 378-395.
- Greiner, R. and Schwarzl, F.R., 1989. Volume Relaxation and Physical Aging of Amorphous Polymers. 1. Theory of Volume Relaxation After Single Temperature Jumps. *Colloid Polym. Sci.*, 267: 39-47.
- Griffith, L.G. and Naughton, G., 2002. Tissue Engineering-Current Challenges and Expanding Opportunities. *Science*, 295: 1009-1016.

- Grohens, Y., Brogly, M., Labbe, C., David, M.O. and Schultz, J., 1998. Glass Transition of Stereoregular Poly(methyl methacrylate) at Interfaces. *Langmuir*, 14: 2929-2932.
- Grohens, Y., Brogly, M., Labbe, C. and Schultz, J., 1997. Interfacial Conformation Energies of Stereoregular Poly(methyl methacrylate) by Infra-red Reflection Absorption Spectroscopy. *Polymer*, 38: 5913-5920.
- Grohens, Y., Hamon, L., Reiter, G., Soldera, A. and Holl, Y., 2002. Some Relevant Parameters Affecting the Glass Transition of Supported Ultra-thin Polymer Films. *Eur. Phys. J. E*, 8: 217-224.
- Grohens, Y. et al., 2001. Glass Transition of Ultra-thin Films of Modified PVC. *Polymer*, 42: 6419-6423.
- Hall, D.B., Deppe, D., Hamilton, K.E., Dhinojwala, A. and Torkelson, J.M., 1998a. Probe Translational and Rotational Diffusion in Polymers Near T_g : Roles of Probe Size, Shape, and Secondary Bonding in Deviations from Debye-Stokes-Einstein Scaling. *J. Non-Cryst. Solids*, 235: 48-56.
- Hall, D.B., Dhinojwala, A. and Torkelson, J.M., 1997a. Translation-Rotation Paradox for Diffusion in Glass-Forming Polymers: The Role of the Temperature Dependence of the Relaxation Time Distribution. *Phys. Rev. Lett.*, 79: 103-106.
- Hall, D.B., Hooker, J.C. and Torkelson, J.M., 1997b. Ultrathin Polymer Films near the Glass Transition: Effect on the Distribution of α -Relaxation Times As Measured by Second Harmonic Generation. *Macromolecules*, 30: 667-669.

- Hall, D.B. and Torkelson, J.M., 1998. Small Molecule Probe Diffusion in Thin and Ultrathin Supported Polymer Films. *Macromolecules*, 31: 8817-8825.
- Hall, D.B., Underhill, P. and Torkelson, J.M., 1998b. Spin Coating of Thin and Ultrathin Polymer Films. *Polym. Eng. Sci.*, 38: 2039-2045.
- Hampsch, H.L., Yang, J., Wong, G.K. and Torkelson, J.M., 1990. Dopant Orientation Dynamics in Doped Second-Order Nonlinear Optical Amorphous Polymers. 2. Effects of Physical Aging on Poled Films. *Macromolecules*, 23: 3648-3654.
- Han, X., Shen, J., Huang, H., Tomasko, D.L. and Lee, L.J., 2007. CO₂ Foaming Based on Polystyrene/Poly(methyl methacrylate) Blend and Nanoclay. *Polym. Eng. Sci.*, 47: 103-111.
- Hartmann, L., Gorbatschow, W., Hauwede, J. and Kremer, F., 2002. Molecular Dynamics in Thin Films of Isotactic Poly(methyl methacrylate). *Eur. Phys. J. E*, 8: 145-154.
- Havriliak, S. and Havriliak, S.J., 1997. Dielectric and Mechanical Relaxation in Materials: Analysis, Interpretation, and Application to Polymers, Hanser Publishers, Munich.
- Hayashi, Y., Kawada, Y. and Ichimura, k., 1995. Dicyanoanthracene as a Fluorescence Probe for Studies on Silica Surfaces. *Langmuir*, 11: 2077-2082.
- Hayden, L.M. et al., 1990. Second-Order Nonlinear Optical Measurements in Guest-host and Side-chain Polymers. *J. Appl. Phys.*, 68: 456-465.

- Hempel, E., Hempel, G., Hensel, A., Schick, C. and Donth, E., 2000. Characteristic Length of Dynamic Glass Transition Near T_g for a Wide Assortment of Glass-Forming Substances. *J. Phys. Chem. B*, 104: 2460-2466.
- Hergeth, W.D., Steinau, U.J., Bittrich, H.J., Simon, G. and Schmutzler, K., 1989. Polymerization in the Presence of Seeds. Part IV: Emulsion Polymers Containing Inorganic Filler Particles. *Polymer*, 30: 254-258.
- Herminghaus, S., Seemann, R. and Landfester, K., 2004. Polymer Surfaces Melting Mediated by Capillary Waves. *Phys. Rev. Lett.*, 93: 017801 (1-4).
- Ho, C.H. and Vu-Khanh, T., 2003. Effects of Time and Temperature on Physical Aging of Polycarbonate. *Theor. Appl. Fracture Mech.*, 39: 107-116.
- Ho, C.H. and Vu-Khanh, T., 2004. Physical Aging and Time-Temperature Behavior Concerning Fracture Performance of Polycarbonate. *Theor. Appl. Fracture Mech.*, 41: 103-114.
- Hodge, I.M., 1987. Effects of Annealing and Prior History on Enthalpy Relaxation in Glassy Polymers. 6. Adam-Gibbs Formulation of Nonlinearity. *Macromolecules*, 20: 2897-2908.
- Hodge, I.M., 1995. Physical Aging in Polymer Glasses. *Science*, 267: 1945-1947.
- Hofstraat, J.W., Veurink, J., Gebben, B., Verheij, H.J. and Verhoeven, J.W., 1998. Charge-Transfer Fluorescent Probes Applied to the Characterization of Thermal and Mechanical Properties of Polymers. *J. Fluoresc.*, 8: 335-342.

- Hong, P.D., Chuang, W.T., Yeh, W.J. and Lin, T.L., 2002. Effect of Rigid Amorphous Phase on Glass Transition Behavior of Poly(trimethylene terephthalate). *Polymer*, 43: 6879-6886.
- Hong, R.Y., Qian, J.Z. and Cao, J.X., 2006. Synthesis and Characterization of PMMA Grafted ZnO Nanoparticles. *Powder Technol.*, 163: 160-168.
- Hooker, J.C., 1996. Ph.D. Thesis, Northwestern University.
- Hu, H.W. and Granick, S., 1992. Viscoelastic Dynamics of Confined Polymer Melts. *Science*, 238: 1339-1342.
- Huang, Y., Duan, X., Wei, Q. and Lieber, C.M., 2001. Directed Assembly of One-Dimensional Nanostructures into Functional Networks. *Science*, 291: 630-633.
- Huang, Y. and Paul, D.R., 2004. Physical Aging of Thin Glassy Polymer Films Monitored by Gas Permeability. *Polymer*, 45: 8377-8393.
- Huang, Y. and Paul, D.R., 2005. Effect of Temperature on Physical Aging of Thin Glassy Polymer Films. *Macromolecules*, 38: 10148-10154.
- Huang, Y. and Paul, D.R., 2006. Physical Aging of Thin Glassy Polymer Films Monitored by Optical Properties. *Macromolecules*, 39: 1554-1559.
- Huang, Y. and Paul, D.R., 2007a. Effect of Film Thickness on the Glass-Permeation Characteristics of Glassy Polymer Membranes. *Ind. Eng. Chem. Res.*, 46: 2342-2347.
- Huang, Y. and Paul, D.R., 2007b. Effect of Molecular Weight and Temperature on Physical Aging of Thin Glassy Poly(2,6-dimethyl-1,4-phenylene oxide) films. *J. Polym. Sci., Part B: Polym. Phys.*, 45: 1390-1398.

- Huang, Y.M., Uppalapati, M., Hancock, W.O. and Jackson, T.N., 2005. Microfabricated Capped Channels for Biomolecular Motor-Based Transport. *IEEE Trans. Adv. Pack.*, 28: 564-570.
- Hub, C., Harton, S.E., Hunt, M.A., Fink, R. and Ade, H., 2007. Influence of Sample Preparation and Processing on Observed Glass Transition Temperatures of Polymer Nanocomposites. *J. Polym. Sci., Part B: Polym. Phys.*, 45: 2270-2276.
- Huguenard, C. and Pefferkorn, E., 1994. Rate of Adsorption of Diblock Copolymers from Micellar Solutions on Solid-Liquid Interfaces. *Macromolecules*, 27: 5271-5276.
- Hutchinson, J.M., 1995. Physical Aging of Polymers. *Prog. Polym. Sci.*, 20: 703-760.
- Hwang, Y., Inoue, T., Wagner, P.A. and Ediger, M.D., 2000. Molecular Motion during Physical Aging in Polystyrene Investigation Using Probe Reorientation. *J. Polym. Sci., Part B: Polym. Phys.*, 38: 68-79.
- Ilsaka, K. and Shibayama, K., 1978. Mechanical α -Dispersion and Interaction in Filled Polystyrene and Polymethylmethacrylate. *J. Appl. Polym. Sci.*, 22: 3135-3143.
- Imans, F., Viaene, L., van Der Auweraer, M. and De Schryver, F.C., 1996. Local Properties of Adsorption Sites Probed by the Emission of Fluorophores of Different Size and Shape. *Chem. Phys. Lett.*, 262: 583-588.
- Jackson, C.L. and McKenna, G.B., 1991. The Glass Transition of Organic Liquids Confined to Small Pores. *Journal of Non-Crystalline Solids*, 131: 221-224.
- Jackson, C.L. and McKenna, G.B., 1996. Vitrification and Crystallization of Organic Liquids Confined to Nanoscale Pores. *Chem. Mater.*, 8: 2128-2137.

- Jager, W.F., Van den Berg, O. and Picken, S.J., 2005. Novel Color-Shifted Mobility Sensitive Fluorescent Probes for Polymer Characterization. *Macromol. Symp.*, 230: 11-19.
- Jain, T.S. and De Pablo, J.J., 2004. Investigation of Transition States in Bulk and Freestanding Film Polymer Glasses. *Phys. Rev. Lett.*, 92: 155505 (1-4).
- Jean, Y.C., Zhang, R., Cao, H., Yuan, J.P. and Huang, C.M., 1997. Glass Transition of Polystyrene Near the Surface Studied by Slow-Positron-Annihilation Spectroscopy. *Phys. Rev. E*, 56: R8459-R8462.
- Jerome, B. and Commandeur, J., 1997. Dynamics of Glasses Below the Glass Transition. *Nature*, 386: 589-592.
- Jiang, Q., Shi, H.X. and Li, J.C., 1999. Finite Size Effect on Glass Transition Temperatures. *Thin Solid Films*, 354: 283-286.
- Jones, R.L., Kumar, S.K., Ho, D.L., Bridger, R.M. and Russell, T.P., 1999. Chain Conformation in Ultrathin Polymer Films. *Nature*, 400: 146-149.
- Kajiyama, T., Tanaka, K. and Takahara, A., 1997. Surface Molecular Motion of the Monodisperse Polystyrene Films. *Macromolecules*, 30: 280-285.
- Kalyanasundaram, K., 1987. *Photochemistry in Microheterogeneous Systems*, Academic Press: New York.
- Kalyanasundaram, K. and Thomas, J.K., 1977. Environmental Effects on Vibronic Band Intensities in Pyrene Monomer Fluorescence and Their Application in Studies of Micellar. *J. Am. Chem. Soc.*, 99: 2039-2044.

- Kanaya, T. et al., 2003. Annealing Effects on Thickness of Polystyrene Thin Films as Studied by Neutron Reflectivity. *Polymer*, 44: 3769-3773.
- Karpovich, D.S. and Blanchard, G.J., 1995. Relating the Polarity-Dependent Fluorescence Response of Pyrene to Vibronic Coupling Achieving a Fundamental Understanding of the Py Polarity Scale. *J. Phys. Chem.*, 99: 3951-3958.
- Kaufman, S., Slichter, W.P. and Davis, D.D., 1971. Nuclear Magnetic Resonance Study of Rubber-Carbon Black Interactions. *J. Polym. Sci., Part A-2*, 9: 829-839.
- Kauzmann, W., 1948. The Nature of the Glassy State and the Behavior of Liquids at Low Temperatures. *Chem. Rev.*, 43: 219-256.
- Kawaguchi, D., Tanaka, K., Kajiyama, T., Takahara, A. and Tasaki, S., 2003. Mobility Gradient in Surface Region of Monodisperse Polystyrene Films. *Macromolecules*, 36: 1235-1240.
- Kawana, S. and Jones, R.A.L., 2001. Character of the Glass Transition in Thin Supported Polymer Films. *Phys. Rev. E*, 63: 021501 (1-6).
- Kawana, S. and Jones, R.A.L., 2003. Effect of Physical Ageing in Thin Glassy Polymer Films. *Eur. Phys. J. E*, 10: 223-230.
- Ke, Y., Long, C. and Qi, Z., 1999. Crystallization, Properties, and Crystal and Nanoscale Morphology of PET-Clay Nanocomposites. *J. Appl. Polym. Sci.*, 71: 1139-1146.
- Keddie, J.L. and Jones, R.A.L., 1995. Glass Transition Behavior in Ultra-Thin Polystyrene Films. *Israel J. Chem.*, 35: 21-26.

- Keddie, J.L., Jones, R.A.L. and Cory, R.A., 1994a. Interface and Surface Effects on the Glass-transition Temperature in Thin Polymer Films. *Faraday Discuss.*, 98: 219-230.
- Keddie, J.L., Jones, R.A.L. and Cory, R.A., 1994b. Size-Dependent Depression of the Glass Transition Temperature in Polymer Films. *Europhys. Lett.*, 27: 59-64.
- Kim, J.H. and Jang, J., 2002. Thickness and Composition Dependence of the Glass Transition Temperature in Thin Homogeneous Polymer Blend Films. *Macromolecules*, 35: 311-313.
- Kim, J.H., Jang, J. and Zin, W.C., 2000. Estimation of the Thickness Dependence of the Glass Transition Temperature in Various Thin Polymer Films. *Langmuir*, 16: 4064-4067.
- Kim, J.H., Jang, J. and Zin, W.C., 2001. Thickness Dependence of the Glass Transition Temperature in Thin Polymer Films. *Langmuir*, 17: 2703-2710.
- Kim, J.H., Koros, W.J. and Paul, D.R., 2006. Physical Aging of Thin 6FDA-based Polyimide Membranes Containing Carboxyl Acid Groups. Part I. Transport Properties. *Polymer*, 47: 3094-3103.
- Kobayashi, Y. et al., 1989. Free Volume and Physical Aging of Poly(vinyl acetate) Studies by Positron Annihilation. *Macromolecules*, 22: 2302-2306.
- Kohlrausch, R., 1847. *Ann. Phys. (Leipzig)*, 72: 353.
- Kojima, Y. et al., 1993. Mechanical-Properties of Nylon 6-Clay Hybrid. *J. Mater. Res.*, 8: 1185-1189.

- Korus, J., Hempel, E., Breiner, M., S, K. and Donth, E., 1997. Temperature Dependence of a Glass Transition Cooperativity. *Acta Polymer.*, 48: 369-378.
- Kotsilkova, R., Fragiadakis, D. and Pissis, P., 2005. Reinforcement Effect of Carbon Nanofillers in a Epoxy Resin System: Rheology, Molecular Dynamics, and Mechanical Studies. *J. Polym. Sci., Part B: Polym. Phys.*, 43: 522-533.
- Kovacs, A.J., 1981. A Multiparameter Approach for Structural Recovery of Glasses and Its Implication for Their Physical Properties In: J.M. O'Reilly and M. Goldstein (Editors), *Structure and Mobility in Molecular and Atomic Glasses*, New York: The New York Academy of Sciences.
- Kovacs, A.J., Aklonis, J.J., Hutchinson, J.M. and Ramos, A.R., 1979. Isobaric Volume and Enthalpy Recovery of Glasses. 2. Transparent Multi-Parameter Theory. *J. Polym. Sci., Part B: Polym. Phys.*, 17: 1097.
- Krasteva, N. et al., 2002. Self-Assembled Gold Nanoparticle/Dendrimer Composite Films for Vapor Sensing Applications. *Nano Lett.*, 2: 551-555.
- Kraus, J., Muller-Buschbaum, P., Kuhlmann, T., Schubert, D.W. and Stamm, M., 2000. Confinement Effects on the Chain Conformation in Thin Polymer Films. *Europhys. Lett.*, 49: 210-216.
- Krausch, G., Dai, C.A., Kramer, E.J. and Marko, J.F., 1993. Interference of Spinodal Waves in Thin Polymer Films. *Macromolecules*, 26: 5566-5571.
- Krishnamoorti, R. and Vaia, R.A., 2002. *Polymer Nanocomposites: Synthesis, Characterization, and Modeling*, ACS Symp. Ser. 804: Washington, D.C.

- Kropka, J.M., Putz, K.W., Pryamitsyn, V., Ganesan, V. and Green, P., 2007. Origin of Dynamical Properties in PMMA-C60 Nanocomposites. *Macromolecules*, 40: 5424-5432.
- Kuhlmann, T., Kraus, J., Muller-Buschbaum, P., Schubert, D.W. and Stamm, M., 1998. Effects of Confined Geometry and Substrate Interaction on the Initial Stages of Interdiffusion in Polystyrene Films. *J. Non-Cryst. Solids*, 235-237: 457-463.
- Kulkeratiyut, S., Kulkeratiyut, S. and Blum, F.D., 2006. Bound Carbonyls in PMMA Adsorbed on Silica Using Transmission FTIR. *J. Polym. Sci., Part B: Polym. Phys.*, 44: 2071-2078.
- Lakowicz, J.R., 1999. *Principles of Fluorescence Spectroscopy*, Plenum: New York.
- Lamarre, L. and Sung, C.S.P., 1983. Studies of Physical Aging and Molecular Motion by Azochromophoric Labels Attached to the Main Chains of Amorphous Polymers. *Macromolecules*, 16: 1729-1736.
- Law, K.Y. and Loutfy, R.O., 1983. Fluorescence Probe for Microenvironments on the Fluorescence Properties of Para-N,N-Dialkylaminobenzylidenemalononitrile in Polymer Matrices. *Polymer*, 24: 439-442.
- Lee, A. and Lichtenhan, J.D., 1998. Viscoelastic Responses of Polyhedral Oligosilsesquioxane Reinforced Epoxy Systems. *Macromolecules*, 31: 4970-4974.
- Lee, J.Y. et al., 2007a. Impact of Surface-Modified Nanoparticles on Glass Transition Temperature and Elastic Modulus of Polymer Thin Films. *Macromolecules*, 40: 7755-7757.

- Lee, K.J., Lee, D.K., Kim, Y.W., Choe, W.-S. and Kim, J.H., 2007b. Theoretical Consideration on the Glass Transition Behavior of Polymer Nanocomposites. *J. Polym. Sci., Part B: Polym. Phys.*, 45: 2232-2238.
- Lee, L.J. et al., 2005. Polymer Nanocomposite Foams. *Compos. Sci. Technol.*, 65: 2344-2363.
- Lenhart, J.L., Van Zanten, J.H., Dunkers, J.P. and Parnas, R.S., 2001. Studying the Buried Interfacial Region with an Immobilized Fluorescence Probe. *Macromolecules*, 34: 2225-2231.
- Lenhart, J.L. and Wu, W.L., 2002. Deviations in the Thermal Properties of Ultrathin Polymer Network Films. *Macromolecules*, 35: 5145-5152.
- Lenhart, J.L. and Wu, W.L., 2003. Influence of Cross-Link Density on the Thermal Properties of Thin Polymer Network Films. *Langmuir*, 19: 4863-4865.
- Levita, G. and Smith, T.L., 1981. Effect of Tensile Strain, Time, and Temperature on Gas Transport in Biaxially Oriented Polystyrene. *Polym. Eng. Sci.*, 21: 936-939.
- Li, G., Du, W.M., Sakai, A. and Cummins, H.Z., 1992. Light-scattering Investigation of α and β Relaxation Near the Liquid-glass Transition of the Molecular Glass Salol. *Phys. Rev. A*, 46: 3343-3356.
- Liem, H., Cabanillas-Gonzalez, J., Etchegoin, P. and Bradley, D.D.C., 2004. Glass Transition Temperatures of Polymer Thin Films Monitored by Raman Scattering. *J. Phys.: Condens. Matter*, 16: 721-728.
- Lin, S.Y. et al., 1998. A Three-Dimensional Photonic Crystal Operating at Infrared Wavelengths. *Nature*, 394.

- Liu, F.K., Hsieh, S.Y., Ko, F.H. and Chu, T.C., 2003. Synthesis of Gold/Poly(methyl methacrylate) Hybrid Nanocomposites. *Colloids Surf., A*, 231: 31-38.
- Liu, T., Ozisik, R. and Siegel, R.W., 2006. Pore Structure and Glass Transition Temperature of Nanoporous Poly(ether imide). *J. Polym. Sci., Part B: Polym. Phys.*, 44: 3546-3552.
- Long, D. and Lequeux, F., 2001. Heterogeneous Dynamics at the Glass Transition in van der Waals Liquids, in the Bulk and in Thin Films. *Eur. Phys. J. E*, 4: 371-387.
- Loutfy, R.O., 1981. High-Conversion Polymerization Fluorescence Probes. 1. Polymerization of Methyl Methacrylate. *Macromolecules*, 14: 270-275.
- Loutfy, R.O., 1986. Fluorescence Probes for Polymer Free-Volume. *Pure Appl. Chem.*, 58: 1239-1248.
- Loutfy, R.O. and Arnold, B.A., 1982. Effect of Viscosity and Temperature on Torsional Relaxation of Molecular Rotors. *J. Phys. Chem.*, 86: 4205-4211.
- Loutfy, R.O. and Teegarden, D.M., 1983. Effect of Polymer Chain Tacticity on the Fluorescence of Molecular Rotors. *Macromolecules*, 16: 452-456.
- Lu, H. and Nutt, S., 2003a. Enthalpy Relaxation of Layered Silicate-Epoxy Nanocomposites. *Macromol. Chem. Phys.*, 204: 1832-1841.
- Lu, H. and Nutt, S., 2003b. Restricted Relaxation in Polymer Nanocomposites near the Glass Transition. *Macromolecules*, 36: 4010-4016.
- Majeste, J.C., Montfort, J.P., Allal, A. and Marin, G., 1998. Viscoelasticity of Low Molecular Weight Polymers and the Transition to the Entangled Regime. *Rheol. Acta*, 37: 486-499.

- Mark, J. et al., 2004. *Physical Properties of Polymers*. Cambridge University Press: Cambridge.
- Marsh, R.A., Groves, C. and Greenham, N.C., 2007. A Microscopic Model for the Behavior of Nanostructured Organic Photovoltaic Devices. *J. Appl. Phys.*, 101: 083509 (1-7).
- Marshall, A.S. and Petrie, S.E.B., 1975. Rate-determining Factors for Enthalpy Relaxation of Glassy Polymers; Molecular Weight. *J. Appl. Phys.*, 46: 4223-4230.
- Martins, T.D., Gulmine, J.V., Akcelrud, L., Weiss, R.G. and Atvars, T.D.Z., 2006. Dependence of Relaxation Process in a Low-density Polyethylene with Different Crosslink Densities Investigated by Fluorescence Spectroscopy. *Polymer*, 47: 7414-7424.
- Masson, J.L. and Green, P.F., 2002. Viscosity of Entangled Polystyrene Thin Film Melts: Film Thickness Dependence. *Phys. Rev. E*, 65: 031806 (1-5).
- Matsuoka, S., 1986. Free Volume, Entropy, and Relaxation Phenomena. *J. Rheol.*, 30: 869-876.
- Matsuoka, S., Williams, G., Johnson, G.E., Anderson, E.W. and Furukawa, T., 1985. Phenomenological Relationship between Dielectric Relaxation and Thermodynamic Recovery Processes near the Glass Transition. *Macromolecules*, 18: 2652-2663.
- Mattsson, J., Forrest, J.A. and Borjesson, L., 2000. Quantifying Glass Transition Behavior in Ultrathin Free-Standing Polymer Films. *Phys. Rev. E*, 62: 5187-5200.

- Mayes, A.M., 1994. Glass Transition of Amorphous Polymer Surfaces. *Macromolecules*, 27: 3114-3115.
- Mbhele, Z.H. et al., 2003. Fabrication and Characterization of Silver-Polyvinyl Alcohol Nanocomposites. *Chem. Mater.*, 15: 5019-5024.
- McCafferty, E. and Wightman, J.P., 1998. Determination of the Concentration of Surface Hydroxyl Groups on Metal Oxide Films by a Quantitative XPS Method. *Surf. Interface Anal.*, 26: 549-564.
- McCaig, M.S. and Paul, D.R., 2000. Effect of Film Thickness on the Changes in Gas Permeability of a Glassy Polyarylate due to Physical Aging Part I. Experimental Observations. *Polymer*, 41: 629-637.
- McCaig, M.S., Paul, D.R. and Barlow, J.W., 2000. Effect of Film Thickness on the Changes in Gas Permeability of a Glassy Polyarylate due to Physical Aging Part II. Mathematical Model. *Polymer*, 41: 639-648.
- McCoy, J.D. and Curro, J.G., 2002. Conjectures on the Glass Transition of Polymers in Confined Geometries. *J. Chem. Phys.*, 116: 9154-9157.
- McCrum, N.G., Read, B.E. and Williams, G., 1991. *Anelastic and Dielectric Effect in Polymeric Solids*, New York: Dover Publications, Inc.
- McKenna, G.B., 1989. Glass Formation and Glassy Behavior. In: C. Booth and C. Price (Editors), *Comprehensive Polymer Science*, Oxford: Pergamon, pp. 311-362.
- McKenna, G.B., 2000. Size and Confinement Effects in Glass Forming Liquids: Perspectives on Bulk and Nano-scale Behaviors. *J. Phys. IV*, 10: 53-57.

- McKenna, G.B. and Simon, S.L., 2002. The Glass Transition: Its Measurements and Underlying Physics. In: S.Z.D. Cheng (Editor), Handbook of Thermal Analysis and Calorimetry, New York: Elsevier.
- McKusick, B.C., Heckert, R.E., Cairns, T.L., Coffman, D.D. and Mower, H.F., 1958. Cyanocarbon Chemistry. VI. Tricyanovinylamines. J. Am. Chem. Soc., 80: 2806-2815.
- Melnichenko, Y.B., Schuller, J., Richert, R. and Ewen, B., 1995. Dynamics of Hydrogen-bonded Liquids Confined to Mesopores: A Dielectric and Neutron Spectroscopy Study. J. Chem. Phys., 103: 2016-2014.
- Merabia, S., Sotta, P. and Long, D., 2004. Heterogeneous Nature of the Dynamics and Glass Transition in Thin Polymer Films. Eur. Phys. J. E, 15: 189-210.
- Merkel, T.C. et al., 2002. Ultrapermeable, Reverse-Selective Nanocomposite Membranes. Science, 296: 519-522.
- Merolle, M., Garrahan, J.P. and Chandler, D., 2005. Space-time Thermodynamics of the Glass Transition. Proc. Natl. Acad. Sci. USA, 102: 10837-10840.
- Messersmith, P.B. and Giannelis, E.P., 1995. Synthesis and Barrier Properties of Poly(ϵ -Caprolactone)-Layered Silicate nanocomposites. J. Polym. Sci., Part A: Polym. Chem., 33: 1047-1057.
- Meyer, E.F. et al., 1990. Free-Volume Changes in Poly(vinyl acetate) Measured by Fluorescence Spectroscopy. Polymer, 31: 243-247.

- Miyazaki, T., Inoue, T., Nishida, K. and Kanaya, T., 2007. X-ray Reflectivity Studies on Glass Transition of Free Standing Polystyrene thin Film. *Eur. Phys. J. Special Topics*, 141: 203-206.
- Miyazaki, T., Nishida, K. and Kanaya, T., 2004. Thermal Expansion behavior of Ultrathin Polymer Films Supported on Silicon Substrate. *Phys. Rev. E*, 69: 061803 (1-6).
- Muller, M., 2002. Chain Conformations and Correlations in Thin Polymer Films: A Monte Carlo Study. *J. Chem. Phys.*, 116: 9930-9938.
- Mundra, M.K., Donthu, S.K., Dravid, V.P. and Torkelson, J.M., 2007a. Effect of Spatial Confinement on the Glass Transition Temperature of Patterned Polymer Nanostructures. *Nano Lett.*, 7: 713-718.
- Mundra, M.K., Ellison, C.J., Behling, R. and Torkelson, J.M., 2006. Confinement, Composition, and Spin-coating Effects on the Glass Transition and Stress Relaxation of Thin Films of Polystyrene and Styrene-containing Random Copolymers: Sensing by Intrinsic Fluorescence. *Polymer*, 47: 7747-7759.
- Mundra, M.K., Ellison, C.J., Rittigstein, P. and Torkelson, J.M., 2007b. Fluorescence Studies of Confinement in Polymer Films and Nanocomposites: Glass Transition Temperature, Plasticizer Effects, and Sensitivity to Stress Relaxation and Local Polarity. *Eur. Phys. J. Special Topics*, 141: 143-151.
- Nakajima, A., 1971. Solvent Effect on Vibrational Structures of Fluorescence and Absorption-Spectra of Pyrene. *Bull. Chem. Soc. Jpn.*, 44: 3272-3277.
- Nakajima, A., 1974. Solvent Enhancement in First Singlet-Singlet Transition of Pyrene-D10. *Spectrochim. Acta, Part A*, 30: 860-862.

- Nakajima, A., 1976a. Effects of Isomeric Solvents on Vibronic Band Intensities in Fluorescence-Spectrum of Pyrene. *J. Mol. Spectrosc.*, 61: 467-469.
- Nakajima, A., 1976b. Fluorescence-Spectra of Pyrene in Chlorinated Aromatic Solvents. *J. Lumin.*, 11: 429-432.
- Narayanan, R. et al., 2006. Dynamics and Internal Stress at the Nanoscale Related to Unique Thermomechanical Behavior in Polymer Nanocomposites. *Phys. Rev. Lett.*, 97: 075505 (1-4).
- Ngai, K.L., 1998. Relation Between Some Secondary Relaxations and the α Relaxations in Glass-forming Materials According to the Coupling Model. *J. Chem. Phys.*, 109: 6982-6994.
- Ngai, K.L., 2000. Effects of Confinement on Relaxation in Glass-formers: Magnitude, Trends and Dependence on the Kohrausch Exponent. *J. Phys. IV*, 10: 21-26.
- Ngai, K.L., 2006. Interpreting the Dynamics of Nano-Confined Glass Formers and Thin Polymer Films: Importance of Starting from Viable Theory for the Bulk. *J. Polym. Sci., Part B: Polym. Phys.*, 44: 2980-2995.
- Ngai, K.L., 2007. Why the Glass Transition Problem Remains Unsolved? *J. Non-Cryst. Solids*, 353: 709-718.
- Ngai, K.L., Rizo, A.K. and Plazek, D.J., 1998. Reduction of the Glass Temperature of Thin Freely Standing Polymer Films Caused by the Decrease of the Coupling Parameter in the Coupling Model. *J. Non-Cryst. Solids*, 235-237: 435-443.
- Ngai, K.L. and Roland, C.M., 1993. Chemical Structure and Intermolecular Cooperativity: Dielectric Relaxation Results. *Macromolecules*, 26: 6824-6830.

- O'Connell, P.A. and McKenna, G.B., 2006. Dramatic Stiffening of Ultrathin Polymer Films in the Rubbery Regime. *Eur. Phys. J. E*, 20: 143-150.
- Olivetti, E.A., Kim, J.H., Sadoway, D.R., Asatekin, A. and Mayes, A.M., 2006. Sol-Gel Synthesis of Vanadium Oxide within a Block Copolymer Matrix. *Chem. Mater.*, 18: 2828-2833.
- Orts, W.J., Van Zanten, J.H., Wu, W.L. and Satija, S.K., 1993. Observation of Temperature Dependent Thicknesses in Ultrathin Polystyrene Films on Silicon. *Phys. Rev. Lett.*, 71: 867-870.
- Papakonstantopoulos, G., Yoshimoto, K., Doxastakis, M., Nealey, P.F. and De Pablo, J.J., 2005. Local Mechanical Properties of Polymeric Nanocomposites. *Phys. Rev. E*, 72: 031801 (1-6).
- Park, C.H. et al., 2004. Thickness and Composition Dependence of The Glass Transition Temperature in Thin Random Copolymer Films. *Polymer*, 45: 4507-4513.
- Parsonage, E., Tirrell, M., Watanabe, H. and Nuzzo, R.G., 1991. Adsorption of Poly(2-vinylpyridine)-Poly(styrene) Block Copolymers from Toluene Solutions. *Macromolecules*, 24: 1987-1995.
- Pathmanathan, K., Johari, G.P., Faivre, J.P. and Monnerie, L., 1986. A Dielectric Study of Secondary Relaxations and "Memory Effect" in Two Compatible Polystyrene Blends. *J. Polym. Sci., Part B: Polym. Phys.*, 24: 1587-1595.

- Patterson, G.D., Jue, P.K. and Stevens, J.R., 1990. Rayleigh-Brillouin Spectroscopy of Syndiotactic Poly(n-butyl methacrylate) Near the Glass Transition. *J. Polym. Sci., Part B: Polym. Phys.*, 28: 481-504.
- Peter, C.J., Alvarez, V.A., Mondragon, I. and Vazquez, A., 2008. Water Uptake Behavior of Layered Silicate/Starch-Polycaprolactone Blend Nanocomposites. *Polym. Int.*, 57: 247-253.
- Peter, S., Meyer, H. and Baschnagel, J., 2006. Thickness-Dependent Reduction of the Glass-Transition Temperature in Thin Polymer Films with a Free Surface. *J. Polym. Sci., Part B: Polym. Phys.*, 44: 2951-2967.
- Petrie, S.E.B., 1972. Thermal Behavior of Annealed Organic Glasses. *J. Polym. Sci., Part A-2*, 10: 1255-1272.
- Pfromm, P.H. and Koros, W.J., 1995. Accelerated Physical Aging of Thin Glassy Polymer Films: Evidence from Gas Transport Measurements. *Polymer*, 36: 2379-2387.
- Pham, J.Q. and Green, P.F., 2002. The Glass Transition of Thin Film Polymer/Polymer Blends: Interfacial Interactions and Confinement. *J. Chem. Phys.*, 116: 5801-5806.
- Pham, J.Q. and Green, P.F., 2003. Effective T_g of Confined Polymer-Polymer Mixtures. Influence of Molecular Size. *Macromolecules*, 36: 1665-1669.
- Pham, J.Q. et al., 2003. Glass Transition of Polymer/Single-Walled Carbon Nanotube Composite Films. *J. Polym. Sci., Part B: Polym. Phys.*, 41: 3339-3345.

- Pochan, D.J., Lin, E.K., Satija, S.K. and Wu, W.L., 2001. Thermal Expansion of Supported Thin Polymer Films: A Direct Comparison of Free Surface vs Total Confinement. *Macromolecules*, 34: 3041-3045.
- Porter, C.E. and Blum, F.D., 2000. Thermal Characterization of PMMA Thin Films Using Modulated Differential Scanning Calorimetry. *Macromolecules*, 33: 7016-7020.
- Porter, C.E. and Blum, F.D., 2002. Thermal Characterization of Adsorbed Polystyrene Using Modulated Differential Scanning Calorimetry. *Macromolecules*, 35: 7448-7452.
- Priestley, R.D., Broadbelt, L.J. and Torkelson, J.M., 2005a. Physical Aging of Ultrathin Polymer Films above and below the Bulk Glass Transition Temperature: Effects of Attractive vs Neutral Polymer-Substrate Interactions Measured Fluorescence. *Macromolecules*, 38: 654-657.
- Priestley, R.D., Broadbelt, L.J., Torkelson, J.M. and Fukao, K., 2007a. Glass Transition and α -relaxation Dynamics in Thin Films of Labeled Polystyrene. *Phys. Rev. E*, 75: 061806 (1-10).
- Priestley, R.D., Ellison, C.J., Broadbelt, L.J. and Torkelson, J.M., 2005b. Structural Relaxation of Polymer Glasses at Surfaces, Interfaces, and In Between. *Science*, 309: 456-459.
- Priestley, R.D., Mundra, M.K., Barnett, N., Broadbelt, L.J. and Torkelson, J.M., 2007b. Effects of Nanoscale Confinement and Interfaces on the Glass Transition Temperature of a Series of Poly(n-methacrylate) Films. *Aust. J. Chem.*, 60: 765-771.

- Priestley, R.D., Rittigstein, P., Broadbelt, L.J., Fukao, K. and Torkelson, J.M., 2007c. Evidence for the Molecular-scale Origin of the Suppression of Physical Ageing in Confined Polymer: Fluorescence and Dielectric Spectroscopy Studies of Polymer-Silica Nanocomposites. *J. Phys.: Condens. Matter*, 19: 205120 (1-12).
- Prucker, O. et al., 1998. On the Glass Transition in Ultrathin Polymer Films of Different Molecular Architecture. *Macromol. Chem. Phys.*, 199: 1435-1444.
- Pu, Y. et al., 2001a. Mobility of Polymer Chains Confined at a Free Surface. *Phys. Rev. Lett.*, 87: 206101 (1-4).
- Pu, Y. et al., 2001b. Probe Diffusion in Thin PS Free-Standing Films. *Macromolecules*, 34: 8518-8522.
- Pyun, J., Jia, S., Kowalewski, T., Patterson, G.D. and Matyjaszewski, K., 2003a. Synthesis and Characterization of Organic/Inorganic Hybrid Nanoparticles: Kinetics of Surface-Initiated Atom Transfer Radical Polymerization and Morphology of Hybrid Nanoparticle Ultrathin Films. *Macromolecules*, 36: 5094-5104.
- Pyun, J., Kowalewski, T. and Matyjaszewski, K., 2003b. Synthesis of Polymer Brushes using Atom Transfer Radical Polymerization. *Macromolecular Rapid Communications*, 24: 1043-1059.
- Pyun, J. and Matyjaszewski, K., 2001. Synthesis of Nanocomposite Organic/Inorganic Hybrid Materials Using Controlled/"Living" Radical Polymerization. *Chemistry of Materials*, 13: 3436-3448.

- Qiu, X. and Ediger, M.D., 2003. Length Scale of Dynamic Heterogeneity in Supercooled D-Sorbitol: Comparison to Model Predictions. *J. Phys. Chem. B*, 107: 459-464.
- Quake, S.R. and Scherer, A., 2000. From Micro- to Nanofabrication with Soft Materials. *Science*, 290: 1536-1540.
- Ramanathan, T., Fisher, F.T., Ruoff, R.S. and Brinson, L.C., 2005a. Amino-Functionalized Carbon Nanotubes for Binding to Polymers and Biological Systems. *Chem. Mater.*, 17: 1290-1295.
- Ramanathan, T., Liu, H. and Brinson, L.C., 2005b. Functionalized SWNT/Polymer Nanocomposites for Dramatic Property Improvement. *J. Polym. Sci., Part B: Polym. Phys.*, 43: 2269-2279.
- Reinsberg, S.A., Qiu, X.H., Wilhelm, M., Spiess, H.W. and Ediger, M.D., 2001. Length Scale of Dynamic Heterogeneity in Supercooled Glycerol Near T_g. *J. Chem. Phys.*, 114: 7299-7302.
- Reiter, G., 1992. Dewetting of Thin Polymer Films. *Phys. Rev. Lett.*, 68: 75-78.
- Reiter, G., 1993. Mobility of Polymers in Films Thinner Than Their Unperturbed Size. *Europhys. Lett.*, 23: 579-584.
- Richert, R., 1996. Geometrical Confinement and Cooperativity in Supercooled Liquids Studied by Solvation Dynamics. *Phys. Rev. B*, 54: 15762-15766.
- Richert, R., 2000. Triplet State Solvation Dynamics: Basics and Applications. *J. Chem. Phys.*, 113: 8404-8429.

- Riggleman, R.A., Yoshimoto, K., Douglas, J.F. and de Pablo, J.J., 2006. Induce of Confinement on the Fragility of Antiplasticized and Pure Polymer Films. *Phys. Rev. Lett.*, 97: 045502 (1-4).
- Rittigstein, P., Priestley, R.D., Broadbelt, L.J. and Torkelson, J.M., 2007. Model Polymer Nanocomposites Provide an Understanding of Confinement Effects in Real Nanocomposites. *Nat. Mater.*, 7: 278-282.
- Rittigstein, P. and Torkelson, J.M., 2006. Polymer-Nanoparticle Interfacial Interactions in Polymer Nanocomposites: Confinement Effects on Glass Transition Temperature and Supression of Physical Aging. *J. Polym. Sci., Part B: Polym. Phys.*, 44: 2935-2943.
- Rizos, A.K. and Ngai, K.L., 1999. Experimental Determination of the Cooperative Length Scale of a Glass-forming Liquid near the Glass Transition Temperature. *Phys. Rev. E*, 59: 612-617.
- Robertson, C.G. and Wang, X., 2004. Nanoscale Cooperative Length of Local Segmental Motion in Polybutadiene. *Macromolecules*, 37: 4266-4270.
- Roe, R.-J. and Curro, J.J., 1983. Small-Angle X-ray Scattering Study of Density Fluctuation in Polystyrene Annealed below the Glass Transition Temperature. *Macromolecules*, 16: 428-434.
- Roe, R.-J. and Song, H.-H., 1985. Isothermal Relaxation of Volume and Density Fluctuation of Polystyrene Glass Prepared under Elevated Pressure. *Macromolecules*, 18: 1603-1609.

- Roland, C.M., 1992. Terminal and Segmental Relaxations in Epoxidized Polyisoprene. *Macromolecules*, 25: 7031-7036.
- Roland, C.M., 1994. Constraints on Local Segmental Motion in Poly(vinylethylene) Networks. *Macromolecules*, 27: 4242-4247.
- Roland, C.M. and Casalini, R., 2003. Temperature Dependence of Local Segmental Motion in Polystyrene and its Variation with Molecular Weight. *J. Chem. Phys.*, 119: 1838-1842.
- Roland, C.M. and Ngai, K.L., 1991. Segmental Relaxation and Molecular Structure in Polybutadienes and Polyisoprene. *Macromolecules*, 24: 5315-5319.
- Roland, C.M., Santangelo, P.G., Ngai, K.L. and Meier, G., 1993. Relaxation Dynamics in Poly(methylphenylsiloxane), 1,1-Bis(p-methoxyphenyl)cyclohexane, and their Mixtures. *Macromolecules*, 26: 6164-6170.
- Roth, C.B. and Dutcher, J.R., 2003. Glass Transition Temperature of Freely-Standing Films of Atactic Poly(methyl methacrylate). *Eur. Polym. J. E*, 12: S103-S107.
- Roth, C.B. and Dutcher, J.R., 2005. Glass Transition and Chain Mobility in Thin Polymer Films. *J. Electroanal. Chem.*, 584: 13-22.
- Roth, C.B., McNerny, K.L., Jager, W.F. and Torkelson, J.M., 2007. Eliminating the Enhanced Mobility at the Free Surface of polystyrene: Fluorescence Studies of the Glass Transition Temperature in Thin Bilayer Films of Immiscible Polymers. *Macromolecules*, 40: 2568-2574.

- Roth, C.B. and Torkelson, J.M., 2007. Selective Probing the Glass Transition Temperature in Multilayer Polymer Films: Equivalence of Block Copolymers and Multilayer Films of Different Homopolymer. *Macromolecules*, 40: 3328-3336.
- Royal, J.S. and Torkelson, J.M., 1990. Monitoring the Molecular Scale Effects of Physical Aging in Polymer Glasses with Fluorescence Probes. *Macromolecules*, 23: 3536-3538.
- Royal, J.S. and Torkelson, J.M., 1992. Molecular-Scale Asymmetry and Memory Behavior in Poly(vinyl acetate) Monitored with Mobility-Sensitive Fluorescent Molecules. *Macromolecules*, 25: 1705-1710.
- Royal, J.S. and Torkelson, J.M., 1993. Physical Aging Effects on Molecular-Scale Polymer Relaxations Monitored with Mobility-Sensitive Fluorescent Molecules. *Macromolecules*, 26: 5331-5335.
- Royal, J.S., Victor, J.G. and Torkelson, J.M., 1992. Photocromic and Fluorescent Probe Studies in Glassy Polymer Matrices. 4. Effects of Physical Aging on Poly(methyl methacrylate) as Sensed by a Size Distribution of Photocromic Probes. *Macromolecules*, 25: 729-734.
- Russell, E.V. and Israeloff, N.E., 2000. Direct Observation of Molecular Cooperativity Near the Glass Transition. *Nature*, 408: 695-698.
- Sanchez, C., Julian, B., Belleville, P. and Popall, M., 2005. Applications of Hybrid Organic-Inorganic Nanocomposites. *J. Mater. Chem.*, 15: 3559-3592.

- Santangelo, P.G., Ngai, K.L. and Roland, C.M., 1994a. Anomalous Relaxation in Polychlorinated Biphenyl/Polybutadiene Mixtures. *Macromolecules*, 27: 3859-3863.
- Santangelo, P.G., Roland, C.M., Ngai, K.L., Rizos, A.K. and Katerinopoulos, H., 1994b. Dielectric and Mechanical Relaxation in PMPS, BMC and Their Mixtures. *J. Non-Cryst. Solids*, 172-174: 1084-1093.
- Sarantopoulou, E. et al., 2008. Surface Nano/micro Functionalization of PMMA Thin Films by 157 nm Irradiation for Sensing Applications. *Appl. Surf. Sci.*, 254: 1710-1719.
- Sargsyan, A., Tonoyan, A., Davtyan, S. and Schick, C., 2007. The Amount of Immobilized Polymer in PMMA SiO₂ Nanocomposites Determined from Calorimetric Data. *Eur. Polym. J.*, 43: 3113-3127.
- Savin, D.A., Pyun, J., Patterson, G.D., Kowalewski, T. and Matyjaszewski, K., 2002. Synthesis and Characterization of Silica-grafted-Polystyrene Hybrid Nanoparticles: Effect of Constraint on the Glass-Transition Temperature of Spherical Polymer Brushes. *J. Polym. Sci., Part B: Polym. Phys.*, 40: 2667-2676.
- Schadler, L.S., Brinson, L.C. and Sawyer, W.G., 2007a. Polymer Nanocomposites: A Small Part of the Story. *JOM*, 59: 53-60.
- Schadler, L.S., Kumar, S.K., Benicewicz, B.C., Lewis, S.L. and Harton, S.E., 2007b. Designed Interfaces in Polymer Nanocomposites: A Fundamental Viewpoint. *MRS Bull.*, 32: 335-340.

- Schiener, B., Bohmer, R., Loidl, A. and Chamberlin, R.V., 1996. Nonresonant Spectral Hole Burning in the Slow Dielectric Response of Supercooled Liquids. *Science*, 274: 752-754.
- Schmidt-Rohr, K. and Spiess, H.W., 1991. Nature of Nonexponential Loss of Correlation above the Glass Transition Investigated by Multidimensional NMR. *Phys. Rev. Lett.*, 66: 3020-3023.
- Schonhals, A., Goering, H. and Schick, C., 2002. Segmental and Chain Dynamics of Polymers: From the Bulk to the Confined State. *J. Non-Cryst. Solids*, 305: 140-149.
- Schulman, S.G., 1977. *Fluorescence and Phosphorescence Spectroscopy: Physicochemical Principles and Practice*, New York: Pergamon Press.
- Schwab, S.D., Agra, D.M.G., Kim, J.H., Kumar, S. and Dhinojwala, A., 2000. Surface Dynamics in Rubbed Polymer Thin Films Probed with Optical Birefringence Measurement. *Macromolecules*, 33: 4903-4909.
- Schwab, S.D. and Levy, R.L., 1990. Free-Volume-Dependent Fluorescence Probes of Physical Aging in Polymers. *ACS Symp. Ser.*, 227: 397-408.
- Sen, S. et al., 2007. Equivalence Between Polymer Nanocomposites and Thin Films: Effect of Processing Conditions and Molecular Origins of Observed Behavior. *Eur. Phys. J. Special Topics*, 141: 161-165.
- Sharma, A. and Schulman, S.G., 1999. *Introduction to Fluorescence Spectroscopy*, Wiley-Interscience Publication: New York.

- Sharp, J.S. and Forrest, J.A., 2003a. Dielectric and Ellipsometric Studies of the Dynamics in Thin Films of Isotactic Poly(methylmethacrylate) with One Free Surface. *Phys. Rev. E*, 67: 031805 (1-9).
- Sharp, J.S. and Forrest, J.A., 2003b. Free Surfaces Cause Reductions in the Glass Transition Temperature of Thin Polystyrene Films. *Phys. Rev. Lett.*, 91: 235701 (1-4).
- Sharp, J.S. and Forrest, J.A., 2003c. Thickness Dependence of the Dynamics in Thin Films of Isotactic Poly(methylmethacrylate). *Eur. Phys. J. E*, 12: S97-S101.
- Shearmur, T.E., Clough, A.S., Drew, D.W., van der Grinten, M.G.D. and Jones, R.A.L., 1998. Interdiffusion of Deuterated and Protonated Poly(methyl methacrylate). *Polymer*, 39: 2155-2159.
- Shen, J., Han, X. and Lee, L.J., 2006. Nanoscaled Reinforcement of Polystyrene Foams Using Carbon Nanofibers. *J. Cell. Plast.*, 42: 105-126.
- Shi, X.F. et al., 2007. Fabrication of Porous Ultra-short Single-walled Carbon Nanotube Nanocomposite Scaffolds for Bone Tissue Engineering. *Biomaterials*, 28: 4078-4090.
- Sidebottom, D., Bergman, R., Borjesson, L. and Torell, L.M., 1993. Two-Step Relaxation Decay in a Strong Glass Former. *Phys. Rev. Lett.*, 71: 2260-2263.
- Sillescu, H., 1999. Heterogeneity at the Glass Transition: A Review. *J. Non-Cryst. Solids*, 243: 81-108.
- Simon, S.L., 2002. Physical Aging. In: J. Krouchovitz (Editor), *Encyclopedia of Polymer Science and Technology*. John Wiley and Sons, pp. 290-318.

- Simon, S.L., Park, J.Y. and McKenna, G.B., 2002. Enthalpy Recovery of a Glass-forming Liquid Constrained in a Nanoporous Matrix: Negative Pressure Effects. *Eur. Phys. J. E*, 8: 209-216.
- Singh, L., Ludovice, P.J. and Henderson, C.L., 2004. Influence of Molecular Weight and Film Thickness on the Glass Transition Temperature and Coefficient of Thermal Expansion of Supported Ultrathin Polymer Films. *Thin Solid Films*, 449: 231-241.
- Smith, G.D., Bedrov, D. and Borodin, O., 2003. Structural Relaxation and Dynamic Heterogeneity in a Polymer Melt at Attractive Surfaces. *Phys. Rev. Lett.*, 90: 226103 (1-4).
- Smith, G.D., Bedrov, D., Li, L. and Bytner, O., 2002. A Molecular Dynamics Simulation Study of the Viscoelastic Properties of Polymer Nanocomposites. *J. Chem. Phys.*, 117: 9478-9489.
- Soles, C.L., Douglas, J.F., Jones, R.L. and Wu, W.L., 2004a. Unusual Expansion and Contraction in Ultrathin Glassy Polycarbonate Films. *Macromolecules*, 37: 2901-2908.
- Soles, C.L., Douglas, J.F., Wu, W.L., Peng, H. and Gidley, D.W., 2004b. Comparative Specular X-ray Reflectivity, Positron Annihilation Lifetime Spectroscopy, and Incoherent Neutron Scattering Measurements of the Dynamics in Thin Polycarbonate Films. *Macromolecules*, 37: 2890-2900.
- Solunov, C.A., 1999. Cooperative Molecular Dynamics and Strong/Fragile Behavior of Polymer. *Eur. Polym. J.*, 35: 1543-1556.

- Song, H.-H. and Roe, R.-J., 1987. Structural Change Accompanying Volume Change in Amorphous Polystyrene as Studied by Small and Intermediate Angle X-ray Scattering. *Macromolecules*, 20: 2723-2732.
- Song, S., Khang, D.Y., Kim, M.J., Park, J.E. and Lee, H.H., 2007. Asymmetric Porous Thin Film Preparation by Controlled Solvent Absorption Using PDMS. *J. Membr. Sci.*, 305: 5-12.
- Spange, S., Vilsmeier, E. and Zimmermann, Y., 2000. Probing the Surface Polarity of Various Silicas and other Moderately Strong Acids by Means of Different Genuine Solvatochromic Dyes. *J. Phys. Chem. B*, 104: 6417-6428.
- Spangler, L., Torkelson, J.M. and Royal, J.S., 1990. Influence of Solvent and Molecular Weight on Thickness and Surface Topography of Spin-Coated Polymer Films. *Polym. Eng. Sci.*, 30: 644-653.
- Sperling, L.H., 1992. *Introduction of Physical Polymer Science*, Wiley: New York.
- Spiess, H.W., 1983. Molecular Dynamics of Solid Polymers as Revealed by Deuteron NMR. *Coll. Polym. Sci.*, 261-209: 193-209.
- Srivastava, S. and Basu, J.K., 2007a. Experimental Evidence for a New Parameter to Control the Glass Transition of Confined Polymers. *Phys. Rev. Lett.*, 98: 165701 (1-4).
- Srivastava, S. and Basu, J.K., 2007b. Influence of Nanoparticles on Glass Transition of Polymers. *J. Nanosci. Nanotechnol.*, 7: 2101-2104.

- Srivatsan, S., Babu, J.R., Riffle, J.S. and Wilkes, G.L., 1997. Crystallization and Morphology of Poly(Arylene Ether Ether Sulfide)s: Dual Spherulitic Morphology. *J. Macromol. Sci.-Phys.*, B36: 455-474.
- Stahlberg, J. and Almgren, M., 1985. Polarity of Chemically Modified Silica Surfaces and Its Dependence on Mobile-Phase Composition by Fluorescence Spectrometry. *Anal. Chem.*, 57: 817-821.
- Starr, F.W., Schroder, T.B. and Glotzer, S.C., 2001. Effects of a Nanoscopic Filler on the Structure and Dynamics of a Simulated Polymer Melt and the Relationship to Ultrathin Films. *Phys. Rev. E*, 64: 021802.
- Starr, F.W., Schroder, T.B. and Glotzer, S.C., 2002. Molecular Dynamics Simulations of a Polymer Melt with a Nanoscopic Particle. *Macromolecules*, 35: 4481-4492.
- Stevenson, J.D., Schmalian, J. and Wolynes, P.G., 2006. The Shape of Cooperatively Rearranging Regions in Glass-forming Liquids. *Nature Phys.*, 2: 268-274.
- Stickel, F., Fischer, E.W. and Richert, R., 1996. Dynamics of Glass-forming Liquids. II. Detailed Comparison of Dielectric Relaxation, dc-Conductivity, and Viscosity Data. *J. Chem. Phys.*, 104: 2043-2055.
- Strehmel, B., Strehmel, V. and Younes, M., 1999. Fluorescence Probes for Investigation of Epoxy Systems and Monitoring of Crosslinking Processes. *J. Polym. Sci., Part B: Polym. Phys.*, 37: 1367-1386.
- Struik, L.C.E., 1978. *Physical Aging in Amorphous Polymers and Other Materials*, Elsevier: Amsterdam.

- Struik, L.C.E., 1987. The Mechanical and Physical Ageing of Semicrystalline Polymers: 1. *Polymer*, 28: 1521-1533.
- Suh, K.Y. and Lee, H.H., 2002. Capillary Force Lithography: Large-area Patterning, Self-organization, and Anisotropic Dewetting. *Adv. Funct. Mater.*, 12: 405-413.
- Sun, Y.Y., Zhang, Z., Moon, K.S. and Wong, C.P., 2004. Glass Transition and Relaxation Behavior of Epoxy Nanocomposites. *J. Polym. Sci., Part B: Polym. Phys.*, 42: 3849-3858.
- Sung, L., Karim, A., Douglas, J.F. and Han, C.C., 1996. Dimensional Crossover in the Phase Separation Kinetics of Thin Polymer Blend Films. *Phys. Rev. Lett.*, 76: 4368-4371.
- Sutton, S.J., Izumi, K., Miyaji, H., Miyamoto, Y. and Miyashita, S., 1997. The Morphology of Isotactic Polystyrene Crystals Grown in Thin Films: The Effect of Substrate Material. *J. Mater. Sci.*, 32: 5621-5627.
- Tanaka, K., Yoon, J.S., Takahara, A. and Kajiyama, T., 1995. Ultrathinning-Induced Surface Phase Separation of Polystyrene/Poly(vinyl methyl ether) Blend Film. *Macromolecules*, 28: 934-938.
- Tant, M.R. and Wilkes, G.L., 1981. An Overview of the Nonequilibrium Behavior of Polymer Glasses. *Polym. Eng. Sci.*, 21: 874-895.
- Tate, R.S. et al., 2001. Extraordinary Elevation of the Glass Transition Temperature of Thin Polymer Films Grafted to Silicon Oxide Substrates. *J. Chem. Phys.*, 115: 9982-9990.

- Theneau, C. et al., 2007. The Kinetics of the Structural Relaxation Process in PHEMA-Silica Nanocomposites Based on an Equation for the Configurational Entropy. *Eur. Phys. J. E*, 24: 69-77.
- Therriault, D., White, S.R. and Lewis, J.A., 2003. Chaotic Mixing in Three-dimensional Microvascular Networks Fabricated by Direct-write Assembly. *Nat. Mater.*, 2: 265-271.
- Thureau, C.T. and Ediger, M.D., 2002a. Influence of Spatially Heterogeneous Dynamics on Physical Aging of Polystyrene. *J. Chem. Phys.*, 116: 9089-9099.
- Thureau, C.T. and Ediger, M.D., 2002b. Spatially Heterogeneous Dynamics During Physical Aging Far Below the glass Transition Temperature. *J. Polym. Sci., Part B: Polym. Phys.*, 40: 2463-2472.
- Torres, J.A., Nealey, P.F. and De Pablo, J.J., 2000. Molecular Simulation of Ultrathin Polymeric Films near the Glass Transition. *Phys. Rev. Lett.*, 85: 3221-3224.
- Tracht, U. et al., 1998. Length Scale of Dynamic Heterogeneities at the Glass Transition Determined by Multidimensional Nuclear Magnetic Resonance. *Phys. Rev. Lett.*, 81: 2727-2730.
- Tribone, J.J., O'Reilly, J.M. and Greener, J., 1986. Analysis of Enthalpy Relaxation in Poly(methyl methacrylate): Effects of Tacticity, Deuteration, and Thermal History. *Macromolecules*, 19: 1732-1739.
- Tsagaropoulos, G. and Eisenberg, A., 1995. Dynamic Mechanical Study of the Factors Affecting the Two Glass Transition Behavior of Filled Polymers. Similarities and Differences with Random Ionomers. *Macromolecules*, 28: 6067-6077.

- Tsay, F.D. and Gupta, A., 1987. Studies of Magnetic Resonance Phenomena in Polymers. II. Molecular Motions in Poly(methyl methacrylate) as Studied by Spin-Probe and Spin-Label Methods. *J. Polym. Sci., Part B: Polym. Phys.*, 25: 855-881.
- Tsay, F.D., Hong, S.D., Moacanin, J. and Gupta, A., 1982. Studies of Magnetic-Resonance Phenomena in Polymers. 1. The Effects of Free-Volume and Segmental Mobility on the Motion of Nitroxide Spin Probes and Labels in Poly(Methyl Methacrylate). *J. Polym. Sci., Part B: Polym. Phys.*, 20: 763-772.
- Tsui, O.K.C., Russell, T.P. and Hawker, C.J., 2001. Effect of Interfacial Interactions on the Glass Transition of Polymer Thin Films. *Macromolecules*, 34: 5535-5539.
- Tsui, O.K.C. and Zhang, H.F., 2001. Effects of Chain Ends and Chain Entanglement on the Glass Transition Temperature of Polymer Thin Film. *Macromolecules*, 34: 9139-9142.
- Turrion, S.G., Olmos, D., Ekizoglou, N. and Gonzalez-Benito, J., 2005. Fluorescence Response from Anthracene-Labeled Polystyrene to Study its Thermal Transition. *Polymer*, 46: 4023-4031.
- Vacatello, M., 2001. Monte Carlo Simulations of Polymer Melts Filled with Solid Nanoparticles. *Macromolecules*, 34: 1946-1952.
- Vacatello, M., 2002. Molecular Arrangements in Polymer-Based Nanocomposites. *Macromol. Theory Simul.*, 11: 757-765.
- Vaia, R.A. and Giannelis, E.P., 2001. Polymer Nanocomposites: Status and Opportunities. *Mater. Res. Soc. Bull.*, 26: 394-401.

- Valeur, B., 2002. *Molecular Fluorescence*, Wiley-VCH: Weinheim.
- van den Berg, O. et al., 2006. A Wavelength-Shifting Fluorescence Probe for Investigating Physical Aging. *Macromolecules*, 39: 224-231.
- Van Workum, K. and De Pablo, J.J., 2003. Computer Simulation of the Mechanical Properties of Amorphous Polymer Nanostructures. *Nano Lett.*, 3: 1405-1410.
- van Zanten, J.H., Wallace, W.E. and Wu, W.L., 1996. Effect of Strongly Favorable Interactions on the Thermal Properties of Ultrathin Polymer Films. *Phys. Rev. E*, 53: R2053-R2056.
- Varnik, F., Baschnagel, J. and Binder, K., 2002. Glassy Dynamics in Thin Polymer Films: Recent MD Results. *J. Non-Cryst. Solids*, 307-310: 524-531.
- Victor, J.G. and Torkelson, J.M., 1988. Photochromic and Fluorescence Probe Studies in Glassy Polymer Matrices. 3. Effects of Physical Aging and Molar Weight on the Size Distribution of Local Free Volume in Polystyrene. *Macromolecules*, 21: 3490-3497.
- Vlasveld, D.P.N., Bersee, H.E.N. and Picken, S.J., 2005. Creep and Physical Aging Behavior of PA6 Nanocomposites. *Polymer*, 46: 12539-12545.
- Vleeshouwers, S., Jamieson, A.M. and Simha, R., 1989. Effect of Physical Aging on Tensile Stress Relaxation and Tensile Creep of Cured EPON 828/ Epoxy Adhesives in the Linear Viscoelastic Region. *Polym. Eng. Sci.*, 29: 662-670.
- Vyazovkin, S. and Dranca, I., 2004. A DSC of α - and β -Relaxations in PS-Clay System. *J. Phys. Chem B*, 108: 11981-11987.

- Wallace, W.E., Fischer, D.A., Efimenko, K., Wu, W.L. and Genzer, J., 2001. Polymer Chain Relaxation: Surface Outpaces Bulk. *Macromolecules*, 34: 5081-5082.
- Wang, C.Y. and Ediger, M.D., 1997. Enhanced Translational Diffusion of 9,10-Bis(phenylethynyl)anthracene (BPEA) in Polystyrene. *Macromolecules*, 30: 4770-4771.
- Wang, C.Y. and Ediger, M.D., 2000. Lifetime of Spatially Heterogeneous Dynamic Domains in Polystyrene Melts. *J. Chem. Phys.*, 112: 6933-6937.
- Wang, L.M., He, F. and Richert, R., 2004. Intramicellar Glass Transition and Liquid Dynamics in Soft Confinement. *Phys. Rev. Lett.*, 92: 095701 (1-4).
- Wang, S.J. and Park, H.H., 2007. Study of PEDOT: PSS-SnO₂ Nanocomposite Film as an Anode for Polymer Electronics. *J. Electroceram.*, 18: 161-165.
- Wang, X., Liu, H. and Qiu, L., 2007. Cationic polymerization of tetrahydrofuran from multiple-walled carbon nanotubes: Preparation and glass transition kinetics. *Mater. Lett.*, 61: 2350-2353.
- Wang, Y.T., Chang, T.C., Hong, Y.S. and Chen, H.B., 2003. Effect of the Interfacial Structure on the Thermal Stability of Poly(methyl methacrylate)-silica Hybrids. *Thermochimica Acta*, 397: 219-226.
- Weeks, E.R., Crocker, J.C., Levitt, A.C., Schofield, A. and Weitz, D.A., 2000. Three-dimensional Direct Imaging of Structural Relaxation near the Colloidal Glass Transition. *Science*, 287: 627-631.

- Weldon, M.K. et al., 1996. Infrared Spectroscopy as a Probe of Fundamental Processes in Microelectronics: Silicon Wafer Cleaning and Bonding. *Surf. Sci.*, 368: 163-178.
- White, C.C., Migler, K.B. and Wu, L.W., 2001. Measuring Tg in Ultra-Thin Polymer Films with an Excimer Fluorescence Technique. *Polym. Eng. Sci.*, 41: 1497-1505.
- Williams, G. and Watts, D.C., 1970. Non-Symmetrical Dielectric Relaxation Behavior Arising from a Simple Empirical Decay Function. *Trans. Faraday Soc*, 66: 80-85.
- Williams, G., Watts, D.C., Dev, S.B. and North, A.M., 1971. Further Considerations of Non Symmetrical Dielectric Relaxation Behavior Arising from a Simple Empirical Decay Function. *Trans. Faraday Soc*, 67: 1323-1335.
- Williams, M.L., Landel, R.F. and Ferry, J.D., 1955. The Temperature Dependence of Relaxation Mechanism in Amorphous Polymers and Other Glass-forming Liquids. *J. Am. Chem. Soc.*, 77: 3701-3707.
- Winberg, P. et al., 2005. Free Volume and Interstitial Mesopores in Silica Filled Poly(1-trimethylsilyl-1-propyne) Nanocomposites. *Macromolecules*, 38: 3776-3782.
- Winnik, M.A., 1986. *Photophysical and Photochemical tools in Polymer Science*, Reidel Pub Co: San Miniato, Italy.
- Wood, K.C. et al., 2008. Electroactive Controlled Release Thin Films. *Proc. Natl. Acad. Sci. USA*, 105: 2280-2285.
- Wubbenhorst, M., Murray, C. and Dutcher, J.R., 2003. Dielectric Relaxations in Ultrathin Isotactic PMMA Films and PS-PMMA-PS Trilayer Films. *Eur. Phys. J. E*, 12: S109-S112.

- Xi, J. et al., 2005. Composite Polymer Electrolyte Doped with Mesoporous Silica SBA-15 for Lithium Polymer Battery. *Solid State Ionics*, 176: 1249-1260.
- Xie, M. and Blum, F.D., 1996. Adsorption and Dynamics of Low Molecular Weight Poly(styrene-*b*-2-vinylpyridine) on Silica and Alumina in Toluene. *Langmuir*, 12: 5669-5673.
- Yamamoto, S., Tsujii, Y. and Fakuda, T., 2002. Glass Transition Temperature of High-Density Poly(methyl methacrylate) Brushes. *Macromolecules*, 35: 6077-6079.
- Yano, K., Usuki, A., Okada, A., Kurauchi, T. and Kamigaito, O., 1993. Synthesis and Properties of Polyimide-Clay Hybrid. *J. Polym. Sci., Part B: Polym. Phys.*, 31: 2493-2498.
- Yildirim, F.A. et al., 2008. Gate Insulators and Interface Effects in Organic Thin-Film Transistors. *Org. Electron.*, 9: 70-76.
- Yu, W.C., Sung, C.S.P. and Robertson, R.E., 1988. Site-Specific Labeling and the Distribution of Free Volume in Glassy Polystyrene. *Macromolecules*, 21: 355-364.
- Zampieri, A. et al., 2004. Zeolite Coatings on Microcellular Ceramic Foams: A Novel Route to Microreactor and Microseparator Devices. *Adv. Mater.*, 16: 819-823.
- Zhang, B. and Blum, F.D., 2003. Modulated Differential Scanning Calorimetry of Ultrathin Adsorbed PS-*r*-PMMA Copolymers on Silica. *Macromolecules*, 36: 8522-8527.

- Zhang, Q., Xu, J.J., Liu, Y. and Chen, H.Y., 2008. In-situ Synthesis of Poly(dimethylsiloxane)-gold Nanoparticles Composite Films and its Application in Microfluidic Systems. *Lab on a Chip*, 8: 352-357.
- Zheng, X., Rafailovich, M.H., Sokolov, J., Strzhemechny, Y. and Schwarz, S.A., 1997. Long-Range Effects on Polymer Diffusion Induced by a Bounding Interface. *Phys. Rev. Lett.*, 79: 241-244.
- Zhou, C., Chung, T.S., Wang, R. and Goh, S.H., 2004. A Governing Equation for Physical Aging of Thick and Thin Fluoropolyimide Films. *J. Appl. Polym. Sci.*, 92: 1758-1764.